

MULTIPARTON PRODUCTION AT  
HADRON COLLIDERS

J.G.M. Kuijf

24 APR. 1991

BIBLIOTHEEK  
INSTITUUT-LORENTZ  
voor theoretische natuurkunde  
Postbus 9506 - 2300 RA Leiden  
Nederland

Kast dissertaties

# MULTIPARTON PRODUCTION AT HADRON COLLIDERS

PROEFSCHRIFT

VOOR DE GRAAD VAN DOCTOR AAN  
DE UNIVERSITEIT TE LEIDEN, OP GEZAG VAN  
DE HOOR WAARDIGEN DR. J.M. DEKRAKER,  
RECTOR-MAGISTRUS IN DE FACULTEIT DER WISKUNDE EN  
NATUURKUNDE, VOLLENS BESLUIT VAN  
HET COLLEGE VAN DERZELVEN TE VERDEDIGEN OP  
DINSDAG 12 FEBRUARI 1983 TE KLOKKE 15.35 UUR

DOOR

JHANNES GERARDIJS MARINUS KUIJF

GEBOREN TE UTRECHT IN 1962

MULTIPARTON PRODUCTION AT  
HADRON COLLIDERS

First character

# MULTIPARTON PRODUCTION AT HADRON COLLIDERS

## Contents

### PROEFSCHRIFT

TER VERKRIJGING VAN DE GRAAD VAN DOCTOR AAN  
DE RIJSUNIVERSITEIT TE LEIDEN, OP GEZAG VAN  
DE RECTOR MAGNIFICUS DR. J.J.M. BEENAKKER,  
HOGLERAAR IN DE FACULTEIT DER WISKUNDE EN  
NATUURWETENSCHAPPEN, VOLGENS BESLUIT VAN  
HET COLLEGE VAN DEKANEN TE VERDEDIGEN OP  
WOENSDAG 20 FEBRUARI 1991 TE KLOKKE 15.15 UUR

DOOR

**JOHANNES GERARDUS MARINUS KUIJF**

GEBOREN TE UTRECHT IN 1962

MULTIPARTON PRODUCTION AT  
HADRON COLLIDERS

Promotiecommissie :

- Promotor : prof. dr. F.A. Berends
- Referent : dr. W.L.G.A.M. van Neerven
- Overige leden : prof. dr. K.J.F. Gaemers  
prof. dr. C.J.N. van den Meijdenberg  
prof. dr. R.H. Terwiel

PROFSCHRIFT

TER VERVOLGING VAN DE GRAAD VAN DOCTOR AAN  
DE RIJKSUNIVERSITEIT TE LEIDEN, OP GEZAG VAN  
DE RECTOR MAGISTRUS DR. L.M. BEZEMER,  
HOOGLEERAAR IN DE FACULTEIT DER WETENSCHAPEN  
NATUURWETENSCHAPPEN, VOLGENS BESLUIT VAN  
HET COLLEGE VAN DOZENTEN TE VONDENEN OP  
WOENSDAG 20 FEBRUARI 1982 TE KIJKKE 10.15 UUR

DOOR

JOHANNES GERARDUS MARINUS KUIJF

GEBOREN TE OTRICHT IN 1940

# Contents

|     |                                                          |    |
|-----|----------------------------------------------------------|----|
| 1   | Introduction and Outline                                 | 1  |
| 2   | QCD and collider physics                                 | 4  |
| 2.1 | Introduction                                             | 4  |
| 2.2 | The multiparton phase space                              | 7  |
| 2.3 | Parton density functions                                 | 11 |
| 2.4 | Collider and detector properties                         | 15 |
| 3   | Computational techniques                                 | 19 |
| 3.1 | Introduction                                             | 19 |
| 3.2 | Weyl-van der Waerden spinors                             | 21 |
| 3.3 | Spin- $\frac{1}{2}$ particles                            | 25 |
| 3.4 | Bosonic particles                                        | 30 |
| 3.5 | Matrix elements in QCD                                   | 34 |
| 3.6 | Examples of Weyl-van der Waerden spinor calculus         | 40 |
| 3.7 | Numerical implementation of Weyl-van der Waerden spinors | 50 |
| 4   | Zero quark processes                                     | 53 |
| 4.1 | Introduction                                             | 53 |
| 4.2 | The zero quark process                                   | 54 |
| 4.3 | Properties of $C$ -functions                             | 56 |
| 4.4 | Exact and approximate colour treatment                   | 59 |
| 4.5 | The LCA in processes with zero quarks                    | 63 |
| 4.6 | Cross sections and distributions                         | 65 |
| 5   | Two quark processes                                      | 71 |
| 5.1 | The two quark process                                    | 71 |
| 5.2 | The LCA in processes with two quarks                     | 74 |
| 6   | Four quark processes                                     | 76 |
| 6.1 | The four quark process, part I                           | 76 |
| 6.2 | The four quark process, part II                          | 80 |
| 6.3 | The LCA in processes with four quarks                    | 84 |

|      |                                                |     |
|------|------------------------------------------------|-----|
| 7    | Six quark processes                            | 85  |
| 7.1  | The six quark process                          | 85  |
| 7.2  | The six quark process with gluons              | 88  |
| 7.3  | Six quark processes and experiment             | 90  |
| 8    | QCD and experiment                             | 92  |
| 8.1  | Introduction                                   | 92  |
| 8.2  | Four jets at the CERN collider                 | 92  |
| 8.3  | Jets at the LHC                                | 95  |
| 8.4  | Jet cross sections                             | 109 |
| 9    | Enumeration techniques                         | 115 |
| 9.1  | Enumeration of externally labelled tree graphs | 115 |
| 9.2  | Enumeration in QCD                             | 123 |
| 10   | QCD matrix elements                            | 127 |
| 10.1 | Introduction                                   | 127 |
| 10.2 | Four parton matrix elements                    | 129 |
| 10.3 | Five parton matrix elements                    | 130 |
| 10.4 | Six parton matrix elements                     | 132 |
| 10.5 | Seven parton matrix elements                   | 140 |
| 10.6 | Special helicity configurations                | 144 |
| A    | Matrix elements and computers                  | 146 |
|      | Samenvatting                                   | 148 |
|      | Curriculum vitae                               | 150 |
|      | List of publications                           | 151 |

# Chapter 1

## Introduction and Outline

*Can one tell QCD from a hole in the ground?*

- A. de Rujula et al. [1]

It is generally believed that the strong interaction force which acts between the constituents of the proton and the neutron, is described by the theory of Quantum Chromodynamics (QCD). The two kinds of constituents, also called partons, are presented by the quarks and gluons which correspond to matter and force carriers respectively. There are indications that QCD explains the experimental observation that quarks and gluons only appear as confined states (hadrons) and do not occur as free particles. QCD is a non-abelian gauge field theory where the quarks and gluons carry a colour charge. The massless gauge fields, the gluons, are put in an SU(3) octet and the quarks are represented by a colour triplet. The latter is often indicated by the colours green, red and blue. The fact that hadrons are observed instead of quarks and gluons, is theoretically explained by the principle of colour confinement: only colourless objects occur in nature. For instance a green, a red and a blue quark can together form a colourless hadron. Predictions in QCD can in principle only be obtained by a non-perturbative treatment which turns out to be very hard. However under specific conditions it is possible to compute some quantities by means of perturbative methods. This approach is justified by asymptotic freedom, a property non-abelian gauge field theories are expected to possess. With this property and renormalization group techniques one can define a running coupling constant  $\alpha_S(Q^2)$  which becomes zero in the limit  $Q^2 \rightarrow \infty$ . This limit allows us to make a perturbative expansion in  $\alpha_S(Q^2)$  provided the partons are energetic enough to make  $Q$  large and hence  $\alpha_S(Q^2)$  small. This situation is for instance realized in large hadron-hadron colliders like the SppS at CERN and the Tevatron at Fermilab. The perturbative approach can be even more accurately tested when the Large Hadron Collider and the Superconducting Super Collider become operational.

Theoretically a hadron-hadron collision is described by the QCD improved parton model. In this model the actual collision takes place between partons and not between the hadrons themselves. The contents of hadrons, in terms of quark and gluon densities is given by the parton density function. The product of two such functions predicts the probability of having a quark-quark, a quark-gluon, etc. collision. We are interested in

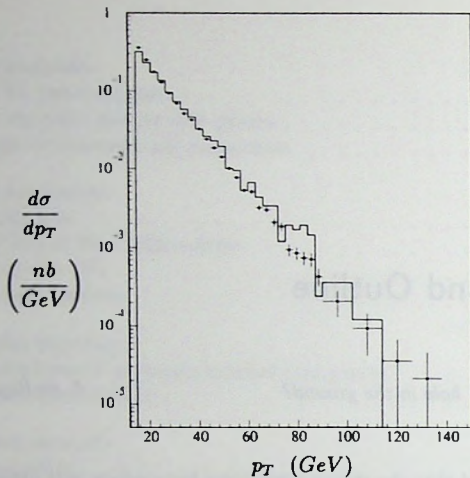


Fig. 1.1. Comparison of the theoretical prediction with the experimental four jet inclusive  $p_T$  spectrum. The measurement was done at the CERN SppS collider.

those parton-parton collisions after which all outgoing partons emerge from the interaction area with large momenta transverse to the direction of the incoming partons. Only then the above-mentioned perturbative expansion can be expected to be valid. Every final state parton is detected as a spray of newly formed hadrons, a jet, moving more or less in the direction of the parton. In view of colour confinement, the formation of jets is a necessity to get locally colourless objects. The formation of jets is described by a hadronization function. Both the production of the initial state partons and the hadronization of the final state partons are described by functions that can only be derived within the framework of non-perturbative QCD. Since this has not yet been achieved, both functions have to be extracted from other experiments. For the description of the scattering process between the two partons, perturbative QCD is used. It involves the calculation of the transition probability for finding a particular final state, given the initial state. This rather technical calculation is the subject of this thesis. In particular we study multiparton production, specifically four and five parton production, for which one has to evaluate the complicated scattering amplitudes describing  $2 \rightarrow 4$  and  $2 \rightarrow 5$  parton reactions. In this respect we note that in the experimental situation the parton momentum can be reconstructed from the jet contents which implies that a jet and a final state parton can be identified in many situations. Therefore it will not be necessary for us to consider any hadronization effect. Since we consider processes where only quarks and gluons are involved, the study of jet production will shed some light on the applicability of perturbative methods in QCD.

To give an impression of the accuracy of perturbative QCD a plot of the inclusive transverse momentum spectrum is given in fig. 1.1. It shows a comparison of the experimental measurement, of four jet production made by the UA2 group at CERN, with the

theoretical predictions based on the scattering amplitudes calculated in this thesis. The agreement is very good over many orders of magnitude. The analysis of five and six jet production can not be carried out at this point in view of the poor experimental statistics. This will certainly be improved on in the near future. For more details, see chapter 8.

The outline of this thesis is as follows. In chapter 2 a general but brief introduction is given on theoretical aspects of collider physics. The computational tools needed to evaluate predictions for measurable quantities in hadron-hadron collisions are discussed. In particular attention is paid to methods which enable us to calculate the total cross section for  $m$ -jet production ( $2 \leq m \leq 5$ ). The mathematics that is used to calculate scattering amplitudes is explained in chapter 3. In a number of examples it is shown that the use of Weyl-van der Waerden spinor techniques simplifies the calculations to a large extent. The examples also show that the techniques are applicable outside the framework of QCD calculations. In chapters 4-7 the techniques of chapter 3 are used to calculate parton processes involving 0, 2, 4 and 6 quarks, respectively, accompanied by an arbitrary number of gluons. By introducing recursion in the number of gluons, starting with a predefined number of quarks we are able to calculate any QCD scattering amplitude with at most six quarks but in principle with an arbitrary number of gluons. The results of chapters 4-7 are sufficient to determine the total cross section and any differential cross section for up to five jet production. Chapter 8 contains three practical applications of the results. Firstly, a comparison between theory and experiment is made for the CERN Sp $\bar{p}$ S collider. Secondly, predictions are given for multijet production at the planned CERN LHC. Approximations proposed to replace the exact matrix elements are examined and their usefulness will be discussed. In view of the complicated exact matrix elements such approximations are needed to speed up the calculation. It is shown in chapter 8 that some of them can be used, as they give predictions close to those obtained from the exact calculation. And thirdly, for the four major hadron-hadron colliders the jet production rates are calculated. In chapter 9 various quantities, related with the subject of this thesis are enumerated. For example, we calculate the number of Feynman diagrams that correspond to scattering processes in a certain class of field theories, among which QCD, and the number of hard parton subprocesses that contribute to a hadron-hadron collision. In chapter 10 the tree level QCD matrix elements (the lowest order in the perturbation series) for which exact analytical results are known will be presented in the form most suitable for numerical applications.

To obtain numerical results the algorithms and methods of chapters 2-10 have been implemented in NJETS, a computer program based on Monte Carlo techniques to study multiparton production.

## References

- [1] A. de Rujula, J. Ellis, R. Petronzio, G. Preparata and W. Scott in: Proceedings of the 1979 International School on Point-like Structures Inside and Outside Hadrons, Erice, 1979.

## Chapter 2

### QCD and collider physics

*Several topics that are of importance if one wants to evaluate predictions for hadron-hadron collisions will be introduced. In particular we are interested in how to calculate quantities like the total cross section and differential cross sections for multiparton production using the QCD improved parton model. In this context computational tools like RAMBO and VEGAS are described.*

#### 2.1 Introduction

Multijet events have been frequently observed at both the CERN and the FERMILAB  $p\bar{p}$  colliders and hence the predictions of perturbative QCD can be tested. Understanding multijet processes is important since many processes containing new physics like top quark or Higgs production, have multijet final states as the dominant decay mode. A major problem in this respect is that jet backgrounds are dominating any interesting signal. Therefore multijet events should be studied to get a better quantitative understanding of perturbative QCD, for instance by examining scale choices and the reliability of parton density functions. In this chapter we introduce basic computational techniques that are of interest if one wants to evaluate predictions in perturbative QCD. For an introduction to phenomenological perturbative QCD we refer to the many review articles and books that have been written on this subject, a short list is given in ref. [1].

We first discuss the parton model [2] in more detail than was done in chapter 1. According to the QCD improved parton model the hadrons are built of constituents called partons. The contents of the hadron is characterized by the parton density function,  $f_i^H(x, Q^2)$ . The parton density function is the probability density for finding a parton  $i$ , carrying a momentum fraction  $x$  of the hadron  $H$ . The  $i$  can either be a quark or a gluon. Naive parton scaling predicts that  $f_i^H(x, Q^2)$  is independent of the QCD scale  $Q$  (Bjorken scaling). This result is not true in a renormalizable quantum field theory. A second mass scale  $\mu$  to remove the ultra-violet divergencies has to be introduced and dimensionless quantities will depend on the ratio  $Q/\mu$ . By assumption  $Q$  must be bigger than all other dimensionful parameters like the masses of the hadrons. In fig. 2.1 a schematic plot is given of a hadron-hadron collision. From each of the two hadrons  $H_1$  and  $H_2$  only one constituent collides. The  $m$  partons produced in this collision are detected as jets

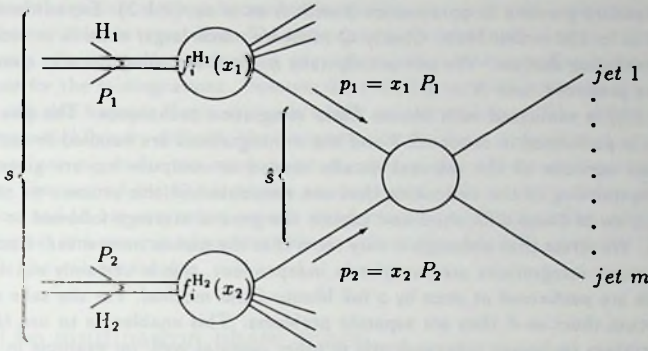


Fig. 2.1. A hadron-hadron collision according to the parton model.

of hadrons. In this thesis the hadronization process is not given any attention and in all predictions final state partons and jets will be identified. In fig. 2.1,  $s$  is the centre-of-mass energy squared on the hadron level and  $\hat{s} = x_1 x_2 s$  the centre-of-mass energy squared on the parton level.

The quantity of interest is  $\sigma_m$ , the total cross section for  $m$ -jet production in hadron-hadron colliders. It is given by

$$\sigma_m(s) = \sum_{final} \sum_{i,j} \int \cdots \int d\Phi_m dx_1 dx_2 \quad (2.1.1)$$

$$\left\{ f_i^{H_1}(x_1, Q^2) f_j^{H_2}(x_2, Q^2) \left( \frac{d\hat{\sigma}_m(x_1 x_2 s)}{d\Phi_m} \right)_{i,j,final} \right\},$$

where the partonic cross section  $\hat{\sigma}_m(\hat{s})$  contains among other things the spin ( $\lambda$ ) and colour ( $c$ ) summed matrix element squared,  $\sum_{c,\lambda} |\mathcal{M}_n|^2$ . Here we introduce the convention that the number of jets  $m \equiv n - 2$ , where  $n$  is the total number of partons in the hard scattering process. The integrals in eq. (2.1.1) are performed over the parton momentum fractions  $x_1$  and  $x_2$  and over the accessible phase space,  $\Phi_m$  at a given  $\hat{s}$ . The  $\sum_{final}$  and  $\sum_{i,j}$  represent the sum over all possible parton processes, conservation of charge and flavour is implicitly understood. One important assumption of the parton model is that the partons inside hadrons do not interact with each other. This assumption is implied by the incoherent sum  $\sum_{i,j}$ . The  $\sum_{c,\lambda} |\mathcal{M}_n|^2$  contains a factor  $g^{2m}$ , where  $g$  is the running coupling constant. In first order, the QCD perturbation parameter is given by

$$\alpha_S(Q^2) \equiv \frac{g^2(Q^2)}{4\pi} = \frac{12\pi}{(11N - 2n_f) \log(Q^2/\Lambda^2)}, \quad (2.1.2)$$

where  $n_f$  is the number of quark flavours,  $N$  the number of colours and  $\Lambda$  determines the scale at which  $\alpha_S(Q^2)$  becomes large (strong coupling). Perturbative QCD tells us

how  $\alpha_S(Q^2)$  scales but does not tell us its size. The latter is obtained from experiment and it is standard practice to parametrize it with  $\Lambda$  as in eq. (2.1.2). Experimentally it is found that  $\Lambda \simeq 100 - 200$  MeV. Clearly  $Q$  must be much larger than  $\Lambda$  in order to be in the perturbative domain. We will usually take  $n_f = 5$  assuming the top quark is too heavy to be produced, and  $N = 3$ .

Eq. (2.1.1) is evaluated with Monte Carlo integration techniques. The phase space integration is performed in section 2.2 and the  $x$ -integrations are handled in section 2.3. In these two sections all the relevant details needed to compute  $\sigma_m$  are given. For a better understanding of the difficulties that one encounters in this process we start with a brief overview of these difficulties and explain the general strategy followed to evaluate eq. (2.1.1). We stress that although it may seem that the parton momentum fraction and the phase space integrations are completely independent, this is certainly not the case. All integrals are performed at once by a full Monte Carlo method. For the sake of clarity we will discuss them as if they are separate problems. This enables us to use the phase space integration technique independently in other cases as well, for example in  $e^+e^- \rightarrow$  hadrons.

There are many sources of uncertainties, both theoretical and experimental, and consequently multijet production rates are hard to predict. Restricting ourselves to the theoretical problems the difficulties can be summarized as follows:

- The uncertainty in the parton density functions. The energies of future colliders are much higher than the CERN and FERMILAB energies and very low values of the momentum fractions  $x$  occur, for which the density functions may be unreliable. At this moment it is not even clear how the low  $x$  behaviour of the gluon looks like, see section 2.3.1. It is conceivable that HERA will provide measurements to improve on this situation.
- The scale choice  $Q$  in the strong coupling constant and related to it, the higher order corrections in QCD. This is especially a problem in multijet physics since an error of 10% in  $\alpha_S(Q^2)$  leads to a systematic error of 50% in the prediction for five jet production.
- The calculation of the complicated exact matrix element in perturbative QCD. On tree level all parton processes with at most five partons in the final state have now been calculated. In spite of this achievement there remains a practical problem because the numerical evaluation of multiparton processes is time consuming.
- The pole structure of  $\sum_{c,\lambda} |\mathcal{M}_n|^2$  leads to extreme peaks in some regions of the phase space. Therefore it is hard to obtain reliable numbers using Monte Carlo integration techniques.

Although our investigations mostly concerns the third point we note that the last two points are closely related. The numerical problems with  $\sum_{c,\lambda} |\mathcal{M}_n|^2$  are such that one must choose between two Monte Carlo methods of performing the phase space integration as analytically evaluating the multidimensional phase space integrals is out of the

question. The first method is to parametrize the phase space in such a way that the pole structure of the matrix element becomes transparent, i.e. each pole is expressed in as few integration variables as is possible. Then one can use various techniques to improve on the convergence. For example by applying the adaptive stratified sampling technique which we will use for the  $x$ -integrations. However for multidimensional processes this method is not very suitable because if one succeeds in the parametrization of the phase space with some cuts, which is very difficult, the integration in the  $3n - 4$  variables is impossible to optimize as one needs far too many points to analyze the pole structure of  $\sum_{c,\lambda} |\mathcal{M}_n|^2$  in detail. The second method is to use an event generator to perform the phase space integration and to use very many points, which requires a fast evaluation of  $\sum_{c,\lambda} |\mathcal{M}_n|^2$ . In this respect one can use approximations to replace the exact  $\sum_{c,\lambda} |\mathcal{M}_n|^2$ . This second method is the one we employ.

## 2.2 The multiparton phase space

In this section we discuss the integration over the phase space for  $m$  partons. The Monte Carlo integration technique we employ is described in subsection 2.2.1. This technique allows us to put constraints (cuts) on the phase space volume integrated over. These cuts are necessary for two reasons. Firstly, without cuts the result of the integration will be infinite as the integrand of eq. (2.1.1) becomes infinite in some regions of phase space. Secondly, detector properties can be simulated by imposing cuts on the phase space points (events) so that only observable events are integrated over. To this end we discuss the detector cuts that are most commonly used in subsection 2.2.2.

### 2.2.1 Phase space integration

The parton density functions in eq. (2.1.1) are multiplied by the result for the partonic cross section

$$\left( \frac{d\hat{\sigma}_m(\hat{s})}{d\Phi_m} \right)_{i,j,final} = \frac{(2\pi)^{4-3m}}{8\hat{s}} \Phi_m(\hat{s}) F_c F_s \sum_{c,\lambda} |\mathcal{M}_n|^2, \quad (2.2.1)$$

which takes into account the spin ( $1/4$ ) and colour average ( $F_c; 1/N$  for a quark and  $1/(N^2 - 1)$  for a gluon) over the incoming partons, and the Bose-Einstein symmetry ( $F_s$ ) of the  $m$  outgoing partons as well as the flux factor ( $1/(2\hat{s})$ ). The summation of  $|\mathcal{M}_n|^2$  runs over all colours ( $c$ ) and helicities ( $\lambda$ ). The factor  $\Phi_m(\hat{s})$  is the total phase space volume for a final state of  $m$  massless particles with invariant mass squared  $\hat{s}$  [3]

$$\Phi_m(\hat{s}) = \frac{(\pi/2)^{m-1} \hat{s}^{m-2}}{(m-1)! (m-2)!}. \quad (2.2.2)$$

The phase space integration element is given by

$$d\Phi_m = \frac{1}{\Phi_m(\hat{s})} \delta^{(4)} \left( \sum_{total} K_i \right) \prod_{final} \left( \frac{d^3 \mathbf{K}_i}{2K_i^0} \right) \quad (2.2.3)$$

and is normalized to unity, which is the reason for separating the  $(2\pi)^{4-3m}$  factor in eq. (2.2.1). This is convenient for the Monte Carlo integration, which we discuss below. The  $\delta^{(4)}$  in eq. (2.2.3) denotes momentum conservation of  $n$  partons with momenta  $K_i$ . The *total* and *final* in eq. (2.2.3) let  $i$  run over all partons and final state partons respectively.

Because of the multidimensionality of our problem and the complicated character of the phase space cuts that have to be applied, integration of the cross section by Monte Carlo methods is the only feasible approach. We refer to ref. [4, 5] for a general introduction on Monte Carlo integration techniques and to ref. [6] for a more applied discussion. Our treatment is essentially the following: with the two parton momenta  $x_1$  and  $x_2$  the  $\hat{s}$  is determined by  $\hat{s} = x_1 x_2 s$ . Then we construct the centre-of-mass frame of the incoming partons, and generate the momenta of the outgoing partons. Since  $\sum_{c,\lambda} |\mathcal{M}_n|^2$  is a complicated function of momenta and the phase space cuts tend to be such that peaks in  $\sum_{c,\lambda} |\mathcal{M}_n|^2$  are eliminated (by putting  $d\hat{\sigma} = 0$  by hand if the cuts are not satisfied), we have made no attempt to optimize the generation of the momenta. Instead we rely on the phase space routine RAMBO [7] which generates momentum configurations with a strictly uniform phase space density. This has the added advantage of providing us with an estimate of the volume of phase space that is allowed by the cuts. The estimate for the differential partonic cross section is based on only one RAMBO event (and equals 0 when the event does not pass the cuts). During the Monte Carlo integration many values of  $x_1$  and  $x_2$  result in approximately the same  $\hat{s}$  value and therefore we get a reliable estimate for the phase space integration in eq. (2.1.1). The fact that this method is not very efficient when the partonic cross section has a very peaky behaviour can not be avoided. Due to the techniques outlined in section 2.3.3 the partonic cross section will be most accurately evaluated where it is largest.

Since all cuts have to be applied to all final state partons in an event, the volume of the allowed phase space tends to be a small part of the total volume for  $m \geq 4$ . This observation is important for two reasons. Firstly, as has already been pointed out, the multijet final state will figure as an important background for the hadronic modes of various new-physics processes. One might try to suppress this background by imposing tight cuts on the jets but then the signal will also tend to be suppressed by a factor of the same order. Secondly, and more importantly, qualitative assumptions about the global behaviour of the cross section can not be argued to be valid under cuts that single out a small part of the phase space. This invalidates practically all assumptions that underlie any approximate expression for the exact matrix element and throws us back on empirical testing, which we shall do in chapters 4 and 8.

With respect to approximations an additional remark on the Monte Carlo integration technique is in order. Computing the exact cross section is so time-consuming that our event samples have limited statistics. Hence the Monte Carlo errors on the various results may not be negligible, and in fact are larger than the difference between the exact result and the one for the approximation. The standard solution in such cases is to use control variates [5]. One makes sure that the results for exact and approximate expressions are as much positively correlated as is possible. This we do by employing *exactly the same*

events several times: once we use them to evaluate the exact cross section, and the other times for the approximations. In this way the statistical fluctuations in the result for the total cross section are removed in the difference as much as possible. Of course it would even be better to perform a regression analysis, using more than one event sample for each set of cuts: due to limitations on computer power this is not always feasible.

As a last remark we note that the method described in this section can be very easily extended to allow for massive final state partons.

## 2.2.2 Phase space cuts

In this section we review the basic concepts of detector simulation in hadronic collisions. From the point of view of a theoretical physicist detector simulation is something that ought to be left to the experimentalist. The exact properties of a detector like dead angles, response time, etc., make it hard, if not impossible, for him to predict any definite results for a collider experiment. To be able to make any predictions at all quantities are introduced to mimic the detector properties. What follows here is just what is needed to define a detector theoretically: we do not go into the details of how a detector functions and how jets are detected.

In the detector the partons emerging from a collision are seen as jets. The jet's four momentum is reconstructed by adding all the hadrons that arrive in a certain cone. An immediate consequence of this is that two fairly collinear jets cannot be separated. Likewise a jet cannot be observed when it is close to the beam. A last important feature of detectors is that a minimum amount of transverse energy must be deposited before a stream of hadrons can be accepted as a jet. Note in this respect that we identify final state partons and jets. The actual formation of jets out of partons is described by the fragmentation functions but this complicated aspect will not be discussed here.

A collider simulation consists of two main parts, the production of partons from the colliding hadrons and the integration over the available phase space. To mimic the detector properties we impose constraints on the phase space points we integrate over. The most commonly used constraints are discussed below.

The available centre-of-mass energy on the parton level is  $\sqrt{\hat{s}} = \sqrt{x_1 x_2 s}$ . In the lab-frame we have the following reaction on the parton level:

$$p_p + p_p \rightarrow p_1 + p_2 + \dots + p_m. \quad (2.2.4)$$

We take the incoming momenta aligned with the  $z$ -axis:  $p_p = (x_1 \sqrt{s}/2, 0, 0, x_1 \sqrt{s}/2)$  and  $p_{\bar{p}} = (x_2 \sqrt{s}/2, 0, 0, -x_2 \sqrt{s}/2)$ , i.e. the colliding beams enter the interaction point as coming from the positive and negative  $z$ -direction. The transverse momentum of an outgoing parton with momentum  $p = (p_0, p_x, p_y, p_z)$  is given by

$$p_T = |\vec{p}| \sin \theta = \sqrt{p_x^2 + p_y^2}. \quad (2.2.5)$$

The angle  $\theta$  is the angle between the parton and the positive  $z$ -axis. Requiring a minimum  $p_T$  for each parton

$$p_T > p_{T \min}, \quad (2.2.6)$$

guarantees they are energetic enough to be distinguished from the ever present low- $p_T$  background for which perturbative QCD can not be used. Consequently  $\sum_{c,\lambda} |\mathcal{M}_n|^2$  can be expected not to suffer numerically from soft parton divergencies in the part of the phase space integrated over.

To have well separated partons we define a minimum separation angle between the outgoing partons  $i$  and  $j$ :

$$\theta_{ij} = \angle(\vec{p}_i, \vec{p}_j) \geq \theta_{min}. \quad (2.2.7)$$

The separation of the partons and the beam can be controlled by the rapidity:

$$y \equiv \frac{1}{2} \ln \left( \frac{p_0 + p_z}{p_0 - p_z} \right) \quad (2.2.8)$$

or equivalently for massless partons by the pseudo-rapidity:

$$\eta = -\ln \tan \frac{\theta}{2}. \quad (2.2.9)$$

The pseudo-rapidity constraint on the event is given by

$$|\eta| \leq \eta_{max}. \quad (2.2.10)$$

The pseudo-rapidity can be regarded as the angle of the parton with the beam. It has the advantage over a normal angle of being additive under a Lorentz boost along the  $z$ -axis. The values  $\eta_{max} = 1, 2, 3$  correspond to separation angles between the parton and the beam direction of 40.4, 15.4 and 5.7 degrees respectively. Like the  $p_T$  constraint the angles keep  $\sum_{c,\lambda} |\mathcal{M}_n|^2$  away from the divergent regions.

Eq. (2.2.7) is sometimes replaced by

$$\Delta R_{ij} = \sqrt{(\Phi_i - \Phi_j)^2 + (\eta_i - \eta_j)^2} = \sqrt{\Delta\Phi_{ij}^2 + \Delta\eta_{ij}^2} > \Delta R_{min}, \quad (2.2.11)$$

with  $\Phi$  the azimuthal angle,

$$\Delta\Phi_{ij} = \arccos \left( \frac{p_{xi}p_{xj} + p_{yi}p_{yj}}{p_{Ti}p_{Tj}} \right). \quad (2.2.12)$$

A last cut sometimes used is a minimum for the total transverse energy,  $E_T^{tot}$  produced in the event.

$$E_T^{tot} = \sum_i E_{Ti} > E_T^{min}. \quad (2.2.13)$$

$E_T^{tot}$  is automatically bounded from below by  $mp_{Tmin}$  and it can serve as an experimental event trigger.  $E_T^{tot}$  can be used to stay away from the uncertain regions of the parton density functions.

## 2.3 Parton density functions

In this section we discuss a method to integrate out the parton momentum fractions  $x_1$  and  $x_2$  that occur in eq. (2.1.1). These variables are integrated over using the VEGAS integration routine of which the basic principles are outlined in subsection 2.3.2. In order to get a better understanding of the integrand we first examine some properties of the parton density functions in subsection 2.3.1. The details of the integration over  $x_1$  and  $x_2$  can be found in subsection 2.3.3.

### 2.3.1 Parton density functions

As was mentioned in the introduction of this chapter, the contents of a hadron, in terms of quarks and gluons, is given by the parton density function, also referred to as the structure function. In this section we will briefly describe how these functions are parametrized. For details about the way they are obtained from experiment and the theoretical input used in that process we refer to ref. [1], in particular to lecture 3 and reviews 5 and 6.

The  $f_i(x, Q^2)$  are parametrized by similar functions for quarks and gluons. However as the quark densities can be measured more directly the constraints are more severe for the quark densities than they are for the gluon density.

In deep inelastic experiments the quark densities are measured over a broad range of  $x$ -values up to  $Q = 15$  GeV. Knowing  $\Lambda_{\overline{MS}}$ , these values can be evolved to higher  $Q$ -values using the Altarelli-Parisi equations and subsequently used in collider phenomenology. In numerical applications it is faster to use a parametrization instead of using the Altarelli-Parisi equation for each  $x$  and  $Q$ . The one most frequently used is the Duke and Owens parametrization [8], which reads

$$f(x, Q^2) = Ax^a(1+cx)(1-x)^b \quad (2.3.1)$$

$$A = A_0 + A_1s + A_2s^2 + \dots \quad (2.3.2)$$

$$s = \ln \left( \frac{\ln(Q^2/\Lambda^2)}{\ln(Q_0^2/\Lambda^2)} \right) > 0, \quad (2.3.3)$$

where  $Q_0$  is some reference value and  $a$ ,  $b$  and  $c$  are polynomials in  $s$ . The parameters  $A_0, A_1, \dots$  are fitted to an exact leading order evolution to give an accuracy of a few percent.

Because deep inelastic scattering does not significantly constrain the gluon densities, more theoretical input is needed. Most parametrizations are based on eq. (2.3.1). Some recent examples are [9]

$$f_g(x, Q^2) = Ax^{-1}(1-x)^5 \quad \Lambda_{\overline{MS}} = 107 \text{ MeV soft gluon}, \quad (2.3.4)$$

$$f_g(x, Q^2) = Ax^{-1}(1+9x)(1-x)^4 \quad \Lambda_{\overline{MS}} = 250 \text{ MeV hard gluon}, \quad (2.3.5)$$

$$f_g(x, Q^2) = Ax^{-1.5}(1+9x)(1-x)^4 \quad \Lambda_{\overline{MS}} = 178 \text{ MeV } \sqrt{x} \text{ gluon}. \quad (2.3.6)$$

The hard gluon seems to be ruled out by fixed-target experiments [9]. The fact that the soft gluon and the  $\sqrt{x}$  gluon both fit the data shows that the  $x$ -values have a limited range ( $0.1 \leq x \leq 0.3$ ) in which the  $f_g(x, Q^2)$  is really accurate.

The most recent parton density functions for the gluon use eq. (2.3.1) and are called the HMRS-parametrizations. For the values  $a = -1/2$  (valence-like),  $a = -1$  (standard gluon) and  $a = -3/2$  (singular gluon), the best values for  $b$ ,  $c$  and  $A$  were determined [10] based on  $\Lambda_{\overline{MS}} = 100$  MeV. The standard gluon choice resulted in  $b = 4.4$  and  $c = 0$ . The validity range of the HMRS-parametrizations is:  $10^{-5} < x < 1$  and  $5 < Q^2 < 1.3 \cdot 10^6$ .

The three different choices of  $a$  in the HMRS-sets will result in different predictions once low  $x$ -values occur as will be the case for the LHC and the SSC. This situation is not satisfactory, see chapter 8 and hopefully HERA will put more constraints on the possible parametrizations of  $f_g(x, Q^2)$ .

### 2.3.2 Adaptive stratified sampling

In this section the adaptive stratified sampling technique to improve on the speed of convergence in a Monte Carlo integration is explained. We will pay special attention to an integration routine VEGAS [11, 12] which is based on this technique. Clearly this is not the place to discuss the theoretical aspects of Monte Carlo integration techniques in general [4]. Therefore we merely outline the principles of adaptive stratified sampling and discuss some of its consequences. We note the existence of other numerical integration routines of a similar nature [13].

Although the number of  $x$ -integrations in the integrand of eq. (2.1.1) is only two, we consider the more general  $n$ -dimensional case

$$I = \int_V d^n \vec{x} f(\vec{x}), \quad (2.3.7)$$

with  $f(\vec{x})$  a finite function, not necessarily smooth and  $V$  a finite volume for which we take the unit hypercube:  $x_i \in [0, 1]$  for  $i = 1, \dots, n$ . Under these condition  $I$  exists and the most simple Monte Carlo method one can think of to estimate  $I$  is to generate random values for  $\vec{x}$  and evaluate the corresponding function  $f(\vec{x})$ . An estimate  $\tilde{I}$  for  $I$  is then given by

$$\tilde{I} = \frac{1}{N} \sum_{j=1}^N f(\vec{x}_j). \quad (2.3.8)$$

In the limit  $N \rightarrow \infty$  this leads to  $\tilde{I} = I$ . This method has already been used in section 2.2.1 to determine the phase space integral. The error on  $\tilde{I}$  behaves as  $O(1/\sqrt{N})$  irrespective of the dimensionality. We write this error as  $c(N)/\sqrt{N}$ , where  $c(N)$  depends on  $f(\vec{x})$  and on the dimensionality. It goes to a constant for large  $N$ . We will try to reduce  $c(N)$  for small  $N$ -values by a better handling of the  $x$ -integrations.

To reduce  $c(N)$  we apply stratified sampling. The integration volume is divided into subvolumes and in each subvolume  $f(\vec{x})$  is evaluated the same number of times. This way the random points are more evenly distributed over  $V$  which has the effect of reducing  $c(N)$  for small values of  $N$ . A second improvement is to let the integration learn from the results already obtained, i.e. an adaptive integration. The idea is to make the

size of the subvolumes depend on the behaviour of  $f(\vec{x})$ , say  $|f(\vec{x})|$  or  $|f'(\vec{x})|$ , in that part of  $V$ . By integrating in a number of iterations and redividing or combining the subvolumes, the distribution of the subvolumes will eventually reflect the behaviour of  $f(\vec{x})$ . What happens is that a mapping of the  $x$ -integration variables to new variables is introduced (a very complicated mapping and generally impossible to parametrize) such that the integral becomes a 'constant', that is the contribution of each subvolume to  $I$  is the same. However in practice it is not possible to have an infinitely refined grid of subvolumes and after a few iterations the grid will not change much anymore as it then optimally corresponds with the behaviour of the integrand, given the number of subvolumes. Therefore it is a good idea to compose the final estimate for  $I$  out of the results for each iteration: a weighted average over all intermediate results. In general a weighted average looks like

$$I = \left( \sum_{i=1}^{N_i} \rho_i \bar{I}_i \right) / \left( \sum_{i=1}^{N_i} \rho_i \right), \quad (2.3.9)$$

where  $\rho_i$  is the weight with which to add the  $i$ -th estimator  $\bar{I}_i$  to the final estimate  $\bar{I}$  and  $N_i$  is the number of iterations. A possible choice for  $\rho_i$  is

$$\rho_i = 1/\sigma_i^2 \quad (2.3.10)$$

with  $\sigma_i$  the standard deviation of the  $i$ -th estimator. Later iterations will have smaller  $\sigma_i$ 's and thus are more important. The choice VEGAS uses is

$$\rho_i = \bar{I}_i^2 / \sigma_i^2. \quad (2.3.11)$$

This choice is motivated by the observation that when  $f(\vec{x})$  has narrow peaks they will not be found in the first few iterations but the corresponding  $\sigma$ 's can still be small compared to later  $\sigma$ 's and thus those specific iterations become relatively too important. By including the result of the iteration in  $\rho_i$  this effect is somewhat weakened. Therefore eq. (2.3.11) is presumably a better choice than eq. (2.3.10).

The technique of adaptive stratified sampling optimizes the integration over the pariton momentum fractions. A direct consequence is that the phase space integral in the integrand is most accurately determined for that value of  $\hat{s}$  where it is largest. This again shows that the  $x$ -integrations and the  $\Phi_m$ -integrations are not independent.

There exists a variety of tests to check whether the estimators  $\bar{I}_i$  are consistent with each other. VEGAS uses an analogue of the  $\chi^2$ -test. Corresponding with eq. (2.3.10) we define  $\chi^2/\text{dof}$  as follows

$$\frac{\chi^2}{\text{dof}} = \frac{1}{N_i - 1} \sum_{i=1}^{N_i} \frac{(\bar{I}_i - \bar{I})^2}{\sigma_i^2}, \quad (2.3.12)$$

where dof denotes the number of degrees of freedom. For eq. (2.3.11) it becomes

$$\frac{\chi^2}{\text{dof}} = \frac{1}{N_i - 1} \sum_{i=1}^{N_i} \frac{(\bar{I}_i - \bar{I})^2}{\sigma_i^2} \left( \frac{\bar{I}_i}{\bar{I}} \right)^2. \quad (2.3.13)$$

For  $\bar{I}$  VEGAS uses the estimate for the integral based on the previous  $(i-1)$ -iterations. The expectation value for  $\chi^2/\text{dof} = 1$  in both cases. In practice this has the following consequences:  $\chi^2/\text{dof} \ll 1$  means that the values for  $\bar{I}_i$  differ much less than could be expected on grounds of the standard deviations and  $\chi^2/\text{dof} \gg 1$  means the opposite, i.e. the  $\sigma_i$  are very small compared to the range of  $\bar{I}_i$  values.

We conclude with two remarks that are of interest when VEGAS is used.

- The first remark concerns the way to subdivide the integration volume. It is very difficult to parametrize the multidimensional volume in such a way that it corresponds exactly with the behaviour of the integrand. In VEGAS the subdivisions are hypercubes, i.e. the subdivisions are obtained by making intervals in the integration variables. A direct consequence of this is that the integration routine is not sensitive to extrema in  $f(\vec{x})$  that are not parallel, or equivalently can not be mapped to lie parallel, to an integration axis. For the integrand in eq. (2.1.1) the above means that we must introduce a mapping for  $x_1$  and  $x_2$  to enable VEGAS to find the extremum in the partonic cross section, see section 2.3.3.
- Using VEGAS to plot the functional behaviour of the integrand in a straightforward way by taking the value for  $f(\vec{x})$  and using  $\vec{x}$  to make the histogram, is not a correct procedure. Points from different iterations normally contribute to the integral with a different weight. Therefore, adding contributions in a simple way by putting them unweighted in the histogram, will lead to an incorrect distribution. Provided the results of the iterations are not too far apart it is better from a practical point of view to accept this error in the distributions than to try to include the VEGAS weights in the histograms.

### 2.3.3 Integration over the parton momentum fractions.

In this section we look at the two integrations over the parton momentum fractions,  $x_1$  and  $x_2$ . In a simplified notation the integral in eq. (2.1.1) can be written as

$$I = \int_{x_{1-}}^1 dx_1 \int_{x_{2-}}^1 dx_2 f_i(x_1) f_j(x_2) M_m(x_1 x_2 s), \quad (2.3.14)$$

where  $f_i(x_1)$  and  $f_j(x_2)$  are the parton density functions and  $M_m(x_1 x_2 s \equiv \hat{s})$  denotes the phase space integration for  $m$  final state partons. Two problems of numerical nature arise when eq. (2.3.14) is evaluated with the aid of an adaptive integration program. The first problem is that a minimum for  $\hat{s}$  is required to produce  $m$  jets and thus the lower limits  $x_{1-}$  and  $x_{2-}$  of the integral (2.3.14) are related by

$$x_{1-} x_{2-} = \frac{(m E_{\min})^2}{s} \equiv \epsilon, \quad (2.3.15)$$

with  $E_{\min}$  the minimum energy required for each parton (a result of the phase space cuts). The parameter  $\sqrt{\epsilon}$  denotes the fraction of the hadronic centre-of-mass energy minimally

required on the parton level. Of course  $E_{min}$  can be set to zero, and hence  $x_{1-}$  and  $x_{2-}$ , at the cost of some efficiency during the integration. The second, more severe, problem is that  $M_m(\hat{s})$  is peaked around a certain value  $\hat{s}'$ . In the integrand of eq. (2.3.14) the peak lies along the two-dimensional curve  $x_1 x_2 = \hat{s}'/s$ . As explained, VEGAS cannot optimally integrate functions that have peaks not parallel to a coordinate axis.

Both problems are solved by introducing a mapping of  $x_1$  and  $x_2$  to  $\hat{x}_1$  and  $\hat{x}_2$ :

$$\begin{cases} x_1 = \epsilon^{\hat{x}_1 \hat{x}_2} \\ x_2 = \epsilon^{\hat{x}_2(1-\hat{x}_1)} \end{cases} \quad (2.3.16)$$

Inserting eq. (2.3.16) into eq. (2.3.14) results in

$$\bar{l} = \int_0^1 d\hat{x}_1 \int_0^1 d\hat{x}_2 J(x_1, x_2; \hat{x}_1, \hat{x}_2) f_i(x_1) f_j(x_2) M_m(\epsilon^{\hat{x}_2 s}), \quad (2.3.17)$$

where eq. (2.3.16) is used to simplify the notation. The Jacobian in (2.3.17) is given by

$$J(x_1, x_2; \hat{x}_1, \hat{x}_2) = \hat{x}_2 \epsilon^{\hat{x}_2} \log^2(\epsilon) \quad (2.3.18)$$

The result of the above mapping is that both integrations run from 0 to 1 and that the minimum energy on the parton level is automatically  $\sqrt{\epsilon s}$ . Furthermore  $M_m(\epsilon^{\hat{x}_2 s})$  is a function in one variable and VEGAS can easily find its extrema and optimize the integration accordingly. Another effect of the coordinate transformation eq. (2.3.16) is that it favours low values for  $x_1$  and  $x_2$ . This is exactly the behaviour of the integrand and therefore increases the efficiency.

## 2.4 Collider and detector properties

In this section we review some properties of four important hadron-hadron colliders. These colliders are the Super proton-antiproton Synchrotron (Sp $\bar{p}$ S), the Tevatron, the planned Large Hadron Collider (LHC) and the proposed Superconducting Super Collider (SSC). The facts and properties in table 2.1 are of a general nature and are meant to picture the physical size of the present (and future) colliders. The luminosities can be used to calculate the expected number of multijet events with

$$\text{number of } m\text{-jet events} = \sigma_m \int L(t) dt, \quad (2.4.1)$$

and the results for  $\sigma_m$  as given in section 8.4.

Of the four hadron-hadron colliders, the Sp $\bar{p}$ S and the Tevatron are the only two in operation. The main difference between them is that it is still possible to find the top quark at Fermilab while for the Sp $\bar{p}$ S the top quark is already too heavy to be found ( $m_{top} > 89$  GeV. [14]). Many jet related quantities such as ratios of cross sections, etc., do not vary much between these two colliders. Likewise this is the case for the LHC in comparison with the SSC. For more information on collider properties we refer to ref. [15].

| Collider                                             | SppS        | Tevatron             | LHC    | SSC     |
|------------------------------------------------------|-------------|----------------------|--------|---------|
| Location                                             | CERN        | Fermilab             | CERN   | USA     |
| Operational                                          | 1981        | 1987                 | 1996   | 1999    |
| Circumference (km)                                   | 6.911       | 6.28                 | 26.559 | 87.12   |
| Colliding particles                                  | $p \bar{p}$ | $p \bar{p}$          | $p p$  | $p p$   |
| $\sqrt{s}$ (GeV)                                     | 630         | 1800                 | 16000  | 40000   |
| Luminosity<br>$10^{30} \text{cm}^{-2} \text{s}^{-1}$ | 3           | 2 (1989)<br>7 (1991) | 40000  | 55-1000 |

Table 2.1. Collider properties.

| Collider | $\sqrt{s}$ (GeV) | $p_T$ (GeV) | $\theta^\circ$ | $ \eta $ | $\Delta R$ |
|----------|------------------|-------------|----------------|----------|------------|
| SppS     | 630              | 12          | 30             | 2.5      | -          |
| Tevatron | 1800             | 25          | -              | 3.5      | 0.8        |
| LHC      | 16000            | 60          | 40             | 2.0      | -          |
| SSC      | 40000            | 100         | 40             | 2.0      | -          |

Table 2.2. Phase space cuts to mimic detector properties.

Of more interest to us are the phase space cuts that have to be used to simulate detector properties, see table 2.2. For a description of the variables we refer to section 2.2.2. For the two operational colliders the cuts most frequently used by the experimentalists are quoted. For the LHC and the SSC the cuts have been chosen such that the accessible phase space volume (or the fraction of events that pass the phase space cuts) is about the same for all four colliders. The results obtained with these cuts will surely be typical for what can be expected.

## References

- [1] Below a list of literature is presented that can serve as an introduction to QCD phenomenology and collider physics. [x] denotes the number of references.

Books:

1. *Hadron Interactions*, P.D.B. Collins and A.D. Martin  
Adam Hilger Ltd, 1984.
2. *Foundations of Quantum Chromodynamics*, T. Muta  
World Scientific, 1987.
3. *QCD Hard Hadronic processes* edited by B. Cox  
NATO ASI Series B: Physics Vol. 197, Plenum press 1988.

## Lectures:

1. *Topics in Modern Phenomenology*, W.J. Stirling [55]  
Lecture Notes - HEP Summer school, Rutherford Appleton Laboratory 1987.
2. *Lectures on perturbative QCD, Jets and the Standard Model: Collider phenomenology*, S.D. Ellis [59]  
preprint: 40423-01-P8 / NSF-ITP-88-55, 1987.
3. *Problems in Hadronization physics*, B. Andersson [41]  
preprint: LU TP 88-2, March 1988.

## Reviews:

1. *Gauge theories*, E.S. Abers and B.W. Lee  
Phys. Rep. 9 (1973) 1.
  2. *Asymptotic freedom in deep inelastic processes in the leading order and beyond*, A.J. Buras, Rev. Mod. Phys. 52 (1980) 199.
  3. *Perturbative QCD at high energies*, A.H. Mueller [109]  
Phys. Rep. 73 (1981) 237.
  4. *Partons in Quantum Chromo Dynamics*, G.A. Altarelli [434]  
Phys. Rep. 81 (1982) 1.
  5. *Physics with matter-antimatter colliders*, G. Salvini and A. Silverman [527]  
Phys. Rep. 171 (1988) 231.
  6. *QCD and Collider Physics*, R.K. Ellis and W.J. Stirling [103]  
preprint: FERMILAB-Conf-90/164-T, August 14, 1990.
- [2] R.P. Feynman, Phys. Rev. Lett. 23 (1969) 1415.
- [3] *Particle kinematics*, E. Byckling and K. Kajantie, John Wiley, 1973.
- [4] F. James, Rep. Prog. Phys. 43 (1980) 1145, and the refs. quoted there.
- [5] *Monte Carlo methods*, J.M. Hammersley and D.C. Handscomb, Methuen, 1967.
- [6] R.H.P. Kleiss, Monte Carlo simulation of radiative processes in electron-positron scattering, thesis, Leiden, 1982.
- [7] S.D. Ellis, R. Kleiss and W.J. Stirling, Comp. Phys. Comm. 40 (1986) 359.
- [8] D.W. Duke and J.F. Owens, Phys. Rev. D30 (1984) 49.
- [9] A.D. Martin, R.G. Roberts and W.J. Stirling, Phys. Rev. D37 (1988) 1161; Mod. Phys. Lett. A4 (1989) 1135.
- [10] P. N. Harriman, A. D. Martin, R. G. Roberts and W. J. Stirling, Phys. Lett. 243B (1990) 421.

- [11] G.P. Lepage, J. Comp. Phys 27 (1978) 192;  
G.P. Lepage, Cornell preprint CLNS-80/447 (1980).
- [12] *A critical review of VEGAS*, H. Kuijf and S.C. van der Marck, Leiden, unpublished.
- [13] Some other adaptive integration programs are:  
RIWAD by B. Lautrup, Proc. 2<sup>nd</sup> colloquium on advanced  
computing methods in theoretical physics, Marseille (1971) I-58.  
DIVONNE2 by J. Friedman, SLAC Computation Research Group  
Technical Memo CGTM 188 (1971).
- [14] F. Abe et al., Phys. Lett. 64B (1990) 147;  
G.P. Yeh, FERMILAB-CONF-90/138-E to be published in the proceedings of *Les  
Rencontres de Physique de la Vallée d'Aoste*, edited by M. Greco, Editions Frontiers,  
1990.
- [15] *Review of Particle Properties*, Phys. Lett. B239 (1990).

## Chapter 3

# Computational techniques

*The basic techniques needed for the calculation of QCD matrix elements are introduced. A translation procedure from Dirac spinors and Minkowski vectors to Weyl-van der Waerden spinors is worked out. In a number of examples the use of these spinors is demonstrated.*

### 3.1 Introduction

We start with an introduction how one arrives at the use of Weyl-van der Waerden (WvdW) spinors to calculate matrix elements. Given an interaction Lagrangian one can determine the Feynman rules and use the Feynman diagram technique to write down the matrix element  $\mathcal{M}$  for every possible scattering process. The standard way to obtain the transition probability is to square  $\mathcal{M}$  using the spin sums [1]

$$\sum_s u_s(p)\bar{u}_s(p) = \not{p} + m \quad \text{and} \quad \sum_s v_s(p)\bar{v}_s(p) = \not{p} - m \quad (3.1.1)$$

for spin- $\frac{1}{2}$  (anti)-particles and

$$\sum_\lambda \epsilon_\lambda^\mu(k)\epsilon_\lambda^{\nu*}(k) = -g^{\mu\nu} + \frac{k^\mu n^\nu + k^\nu n^\mu}{(k \cdot n)} - \frac{(n \cdot n)k^\mu k^\nu}{(k \cdot n)^2} \quad (3.1.2)$$

for massless spin-1 particles,  $n^\mu$  is arbitrary but not parallel to  $k^\mu$ . In eq. (3.1.2) the freedom  $n^\mu$  disappears for massive particles and must be replaced by  $k^\mu$ . In QCD, the theory of our interest, one also has to perform the colour sums. After the appropriate colour and spin sums we arrive at the matrix element squared, colour and spin summed:  $\sum_{c,\lambda} |\mathcal{M}_n|^2$ . This approach has some advantages. Firstly, it is straightforward and secondly the gauge freedom  $n^\mu$  can be used as a check on the calculation. In case the spin-1 particles are photons the right-hand side of eq. (3.1.2) can be replaced by  $-g^{\mu\nu}$ . Then the calculation simplifies but the check is lost. An obvious disadvantage of the above method is that a lot of trace algebra and in QCD also a lot of colour algebra, has to be performed before  $\sum_{c,\lambda} |\mathcal{M}_n|^2$  is obtained. Furthermore the final expressions can become very large and although they are expressed in terms of inner products of Minkowski vectors it is hard to use momentum conservation to simplify them. In fact the method sketched above already fails for many six parton processes. This is the case in spite of the availability of

algebraic computation programs, see ref. [2]. Here we only refer to the ones developed for calculations in high energy physics.

We shall illustrate the disadvantages of the standard method described above with two examples. The first one concerns the two to three gluon scattering processes in QCD, where the original expressions were presented in several tables and long formulae [3]. With the better techniques described below, the expressions are rewritten in a more compact and systematic form [4], see section 3.6.2. The second example concerns the two to two graviton scattering process [5]. Ultimately a short expression was found but only after using many hours of computer time. This calculation becomes trivial, see section 3.6.3, when the techniques described in subsequent sections are used.

New tricks have to be introduced before one can start calculating processes with many particles. An important improvement is the idea to evaluate helicity amplitudes instead of  $\sum_{e,\lambda} |\mathcal{M}_n|^2$ . By introducing orthogonal helicity states for all particles, the evaluation goes as follows. Instead of explicitly carrying out the spin sums using eqs. (3.1.1) and (3.1.2), the amplitude  $\mathcal{M}$  is evaluated for every possible combination of the helicity states. These amplitudes will from now on be denoted by the term *helicity amplitudes*. Because the helicity states are orthogonal,  $\sum_{e,\lambda} |\mathcal{M}_n|^2$  is the sum over all helicity amplitudes squared. Although the expressions for  $\mathcal{M}$  are more compact one has to evaluate up to  $2^n$  helicity amplitudes for a process with  $n$  massless spin carrying particles. So at first sight it does not appear to be an improvement. It turns out that parity conservation, charge conjugation and other symmetries which we will encounter later on, substantially lower this number  $2^n$ . More importantly the gauge freedom  $n^\mu$  of eq. (3.1.2) results in a freedom of choosing the helicity vectors for massless spin-1 particles, which can be used in such a way that many Feynman diagrams immediately vanish. This method of using the gauge freedom is crucial in the CALKUL method [6]. The helicity vectors still have awkward appearances and the correlation with the vector  $n^\mu$  in eq. (3.1.2) is not always obvious. The CALKUL method was slowly refined and improved on. The  $n^\mu$  became an explicit parameter in the helicity vectors of spin-1 particles [7] and ultimately it lead to

$$e_{\lambda}^{\mu}(k) = \frac{1}{\sqrt{2}} \frac{\bar{u}_{\lambda}(k) \gamma^{\mu} u_{\lambda}(n)}{\bar{u}_{-\lambda}(n) u_{\lambda}(k)}. \quad (3.1.3)$$

for massless spin-1 particles [8]. By choosing  $n^\mu$  equal to one of the other external momenta, say  $p^\mu$ , the calculation simplifies because terms with  $\bar{u}(p)u(p)$  and  $\not{p}u(p)$  vanish. For a complete description of the CALKUL method we refer to [9].

Another improvement is the use of two-dimensional complex WvdW spinors [10, 11] and the related spinor calculus [11]. One of the main problems of the improved CALKUL method is that the  $\gamma$ -matrix algebra still exists. Connected with this problem is the fact that Dirac spinors and Minkowski vectors are treated as different objects. The use of WvdW spinors removes the  $\gamma$ -algebra altogether and translates Dirac spinors and Minkowski vectors to the same kind of objects, WvdW spinors. As a side effect the helicity vectors for massless bosons get an elegant form and the gauge freedom can be fully exploited in calculations. Especially in numerical applications the WvdW spinor formalism turns out to be extremely useful. This is the present status of tree level matrix element calculations.

The outline of this chapter is as follows. In the next section we introduce WvdW spinors. In sections 3.3 and 3.4 translation schemes for fermions and bosons are presented. Furthermore explicit representations for both massive and massless particles in terms of WvdW spinors will be derived. In section 3.5 the consequences for QCD are discussed and the Feynman rules for this theory in terms of WvdW spinors are given. In this section we also introduce techniques to handle the colour structures in QCD. The spinor techniques are applied to calculate a number of scattering processes in section 3.6. In section 3.7 we conclude with a discussion on the numerical implementation of WvdW spinors.

## 3.2 Weyl-van der Waerden spinors

In this section we introduce WvdW spinors [12, 13] and the related spinor calculus. Furthermore we relate the spinors to Minkowski vectors by giving a translation scheme.

The WvdW spinor,  $\Psi_A$  is a two dimensional complex spinor and  $\Psi_{\dot{A}}$  is its complex conjugate, indicated by the dotted index. The complex conjugated spinor will sometimes be referred to as the dotted spinor. In components the spinors read

$$\Psi_A = \begin{pmatrix} c_1 \\ c_2 \end{pmatrix}, \quad \Psi_{\dot{A}} = \begin{pmatrix} c_1^* \\ c_2^* \end{pmatrix}, \quad (3.2.1)$$

with  $c_1$  and  $c_2$  ordinary complex numbers. The spinors in eq. (3.2.1) could be called covariant spinors. The spinor index is raised and lowered with the spinor metric  $\epsilon^{AB}$ :

$$\epsilon^{AB} = \begin{pmatrix} 0 & 1 \\ -1 & 0 \end{pmatrix} = \epsilon_{AB} = \epsilon^{\dot{A}\dot{B}} = \epsilon_{\dot{A}\dot{B}}. \quad (3.2.2)$$

Eq. (3.2.2) implies that  $\epsilon^{AB} = -\epsilon^{BA}$ , therefore it is necessary to raise the indices in a well defined order. This is in contrast with raising Lorentz indices using the symmetric Minkowski metric  $g^{\mu\nu}$ , for which we use the  $(+, -, -, -)$  signature. We raise spinor indices with the so-called south-west rule. The spinor index to be raised (lowered) must be placed directly south-west (north-east) of the corresponding index in the spinor metric  $\epsilon^{AB}$  ( $\epsilon_{AB}$ ). For instance

$$\Psi^B = \Psi_A \epsilon^{AB}, \quad \Psi_{\dot{A}} = \epsilon_{\dot{A}\dot{B}} \Psi^{\dot{B}}. \quad (3.2.3)$$

Some direct consequences of eqs. (3.2.2) and (3.2.3) are

$$\epsilon^A_B = \begin{pmatrix} 1 & 0 \\ 0 & 1 \end{pmatrix}, \quad \epsilon_{\dot{A}}^{\dot{B}} = \begin{pmatrix} -1 & 0 \\ 0 & -1 \end{pmatrix}, \quad \epsilon^A_A = 2. \quad (3.2.4)$$

$$\Psi_A = \begin{pmatrix} c_1 \\ c_2 \end{pmatrix} \Rightarrow \Psi^A = \begin{pmatrix} -c_2 \\ c_1 \end{pmatrix}. \quad (3.2.5)$$

The spinorial inner product between two WvdW spinors is defined by

$$\langle \Psi_1 \Psi_2 \rangle \equiv \Psi_{1A} \Psi_2^A, \quad \langle \Psi_1 \Psi_2 \rangle^* \equiv \Psi_{1\dot{A}} \Psi_2^{\dot{A}}. \quad (3.2.6)$$

A number of relations between WvdW spinors can be derived. From the definition of the inner product it follows that

$$\langle \Psi_1 \Psi_2 \rangle = -\langle \Psi_2 \Psi_1 \rangle, \quad (3.2.7)$$

and in particular that

$$\langle \Psi \Psi \rangle = 0. \quad (3.2.8)$$

The spinor metric  $\epsilon^{AB}$  satisfies the Schouten-identity

$$\epsilon^{AB} \epsilon^{CD} + \epsilon^{AC} \epsilon^{DB} + \epsilon^{AD} \epsilon^{BC} = 0. \quad (3.2.9)$$

Multiplying eq. (3.2.9) from the left and right with some spinors yields two very important rules for spinor calculus.

$$\times \Psi_{1B} \Psi_{2C} \Psi_{3D} \Rightarrow \langle \Psi_1 \Psi_2 \rangle \Psi_3^A + \langle \Psi_2 \Psi_3 \rangle \Psi_1^A + \langle \Psi_3 \Psi_1 \rangle \Psi_2^A = 0. \quad (3.2.10)$$

$$\times \Psi_{1C} \Psi_{2D} \Rightarrow \Psi_1^A \Psi_2^B - \Psi_2^A \Psi_1^B = \langle \Psi_2 \Psi_1 \rangle \epsilon^{AB}. \quad (3.2.11)$$

Of course similar relations exist for dotted spinors. With eqs. (3.2.10) and (3.2.11) complicated relations between spinors can be derived, one nice example is

$$\frac{1}{\langle ab \rangle \langle bc \rangle \langle cd \rangle} + \frac{1}{\langle ac \rangle \langle cb \rangle \langle bd \rangle} = \frac{\langle ad \rangle}{\langle ab \rangle \langle bd \rangle} \frac{1}{\langle ac \rangle \langle cd \rangle}, \quad (3.2.12)$$

with  $a$ ,  $b$ ,  $c$  and  $d$  arbitrary spinors. More complicated objects like  $\Psi^{AB}{}_C$ ,  $\Psi^A{}^{BC}{}_D$ ,  $\Psi_{\dot{A}\dot{B}}$  will also be used. Especially the last object is relevant as we are going to relate it to Minkowski vectors. The translation of Minkowski vectors into WvdW spinors (and vice versa) uses the  $\sigma$ -matrices to map the vectors onto the two dimensional complex spinors. We choose the following representation of the Pauli-Dirac matrices

$$\sigma^0 = \begin{pmatrix} 1 & 0 \\ 0 & 1 \end{pmatrix}, \quad \sigma^1 = \begin{pmatrix} 0 & -1 \\ -1 & 0 \end{pmatrix}, \quad \sigma^2 = \begin{pmatrix} 0 & i \\ -i & 0 \end{pmatrix}, \quad \sigma^3 = \begin{pmatrix} -1 & 0 \\ 0 & 1 \end{pmatrix}. \quad (3.2.13)$$

The *spin-tensor*  $\sigma^{\mu\dot{A}B}$ , an object with both Lorentz and spinor indices is defined as

$$\sigma^{\mu\dot{A}B} \equiv \sigma^\mu = (\sigma^0, \sigma^1, \sigma^2, \sigma^3) = (\sigma^0, \vec{\sigma}), \quad (3.2.14)$$

where  $\dot{A}B$  replace the spin indices of the  $\sigma$ -matrix. In the following the dotted index denotes the row and the undotted the column of the matrix. With  $g_{\mu\nu}$  and  $\epsilon_{AB}$  to lower indices we find

$$\sigma_{\dot{A}B}^\mu = (\sigma^0, -\vec{\sigma}^*), \quad \sigma_{\mu\dot{A}B} = (\sigma_0, -\vec{\sigma}^*). \quad (3.2.15)$$

A number of relations can be derived for spin-tensors. The most useful ones are

$$(\sigma_{\mu\dot{A}B})^* = \sigma_{\mu\dot{B}A}, \quad (3.2.16)$$

$$\sigma_{\mu\dot{A}B} \sigma_{\nu\dot{C}D}^{\dot{A}B} = 2g_{\mu\nu}, \quad (3.2.17)$$

$$\sigma_{\mu\dot{A}B} \sigma_{\dot{C}D}^\mu = 2\epsilon_{\dot{A}\dot{C}} \epsilon_{B\dot{D}}, \quad (3.2.18)$$

$$\sigma_{\mu\dot{A}E} \sigma_{\nu\dot{C}}^{\dot{A}C} + \sigma_{\nu\dot{A}B} \sigma_{\dot{C}}^{\dot{A}C} = 2g_{\mu\nu} \epsilon^C{}_B. \quad (3.2.19)$$

With the spin-tensor, Minkowski four vectors  $K^\mu$  and spinor objects  $K^{\dot{A}B}$  can be related as follows. Given the Minkowski vectors

$$K^\mu = (K^0, K^1, K^2, K^3) = (K^0, \vec{K}) \text{ and } K_\mu = (K_0, K_1, K_2, K_3) \quad (3.2.20)$$

where  $K^0 = K_0$  is the energy component and  $\vec{K}$  the momentum part, the momentum in spinor language,  $K^{\dot{A}B}$  is defined by

$$K^{\dot{A}B} \equiv \sigma^{\mu\dot{A}B} K_\mu = \sigma_\mu^{\dot{A}B} K^\mu = \begin{pmatrix} K_0 - K_3 & -K_1 + iK_2 \\ -K_1 - iK_2 & K_0 + K_3 \end{pmatrix} \quad (3.2.21)$$

and equivalently

$$K_{\dot{A}B} \equiv \sigma_{\mu\dot{A}B} K^\mu = \sigma_{\dot{A}B}^\mu K_\mu = \begin{pmatrix} K_0 + K_3 & K_1 + iK_2 \\ K_1 - iK_2 & K_0 - K_3 \end{pmatrix}. \quad (3.2.22)$$

The  $K_{\dot{A}B}$  and  $K^{\dot{A}B}$  are related by  $K_{\dot{A}B} = \epsilon_{\dot{A}C} \epsilon_{BD} K^{\dot{C}D}$  or in components:

$$K^{\dot{A}B} = \begin{pmatrix} K^{11} & K^{12} \\ K^{21} & K^{22} \end{pmatrix} \Rightarrow K_{\dot{A}B} = \begin{pmatrix} K^{22} & -K^{21} \\ -K^{12} & K^{11} \end{pmatrix}. \quad (3.2.23)$$

From eq. (3.2.21) and eq. (3.2.17) the inverse translation is found to be

$$\sigma_{\nu\dot{A}B} K^{\dot{A}B} = \sigma_{\nu\dot{A}B} \sigma_\mu^{\dot{A}B} K^\mu = 2g_{\mu\nu} K^\mu = 2K_\nu \quad (3.2.24)$$

and thus

$$K^\mu = \frac{1}{2} \sigma_{\dot{A}B}^\mu K^{\dot{A}B} = \frac{1}{2} \sigma^{\mu\dot{A}B} K_{\dot{A}B}. \quad (3.2.25)$$

An example of a translated object is the Minkowski inner product

$$(K \cdot P) = K^\mu P_\mu = \frac{1}{2} \sigma_{\dot{A}B}^\mu K^{\dot{A}B} \frac{1}{2} \sigma_{\mu\dot{C}D} P^{\dot{C}D} = \frac{1}{2} K^{\dot{A}B} P_{\dot{A}B} \equiv \frac{1}{2} (K, P), \quad (3.2.26)$$

which serves as the definition of  $\{K, P\}$ , the inner product of two momenta in spinor language. Another example is the metric  $g_{\mu\nu}$  which is translated as

$$g_{\mu\nu} = \frac{1}{2} \sigma_{\mu\dot{A}B} \sigma_{\nu\dot{C}D} \epsilon^{\dot{A}C} \epsilon^{BD}. \quad (3.2.27)$$

So far  $K^\mu$  is a general four vector with real components and the only property of  $K^{\dot{A}B}$  is hermiticity by virtue of eq. (3.2.16).

$$K_{\dot{A}B} = (K_{\dot{B}A})^*. \quad (3.2.28)$$

In most practical situations we deal with light-cone vectors,  $K^2 = 0 = \{K, K\}$ . This has important consequences for the  $K_{\dot{A}B}$  because from

$$K_{\dot{A}B} K^{\dot{A}B} = 2(K_{11} K_{22} - K_{12} K_{21}) = 0 \quad (3.2.29)$$

it follows that  $K_{\dot{A}B}$  has  $\det(K_{\dot{A}B})=0$  and therefore can be written as a dyad of the eigenspinor which corresponds to the non-zero eigenvalue. Based on the property of hermitian matrices,  $K_{\dot{A}B}$  can be written as

$$K_{\dot{A}B} = \sum_n \lambda_n l_{n\dot{A}} l_{nB}, \quad (3.2.30)$$

with  $\lambda_n$  the eigenvalues and  $(l_n)^*$  the corresponding normalized eigenvectors. The eigenvalues of  $K_{\dot{A}B}$  are  $\lambda_{1,2} = 0, 2K_0$  and with  $k_A = \sqrt{2K_0} l_{2A}$  we have

$$K_{\dot{A}B} = k_{\dot{A}} k_B. \quad (3.2.31)$$

A spinor  $k_A$  corresponding to a light-cone momentum  $K_\mu$ , is called a *momentum spinor*. The general convention is that capitals denote space-time momenta, possibly in spinor language, and lower case characters the corresponding momentum spinors. E.g.  $K_{\dot{A}B}$  corresponds with a particle momentum and  $k_A$  with the spinor as defined by eq. (3.2.31). The normalized eigenvector  $k_A$  reads

$$k_A = e^{i\theta} \begin{pmatrix} \sqrt{K_0 + K_3} \left( \frac{K_1 - iK_2}{K_1 + iK_2} \right)^{1/4} \\ -\sqrt{K_0 - K_3} \left( \frac{K_1 + iK_2}{K_1 - iK_2} \right)^{1/4} \end{pmatrix}, \quad (3.2.32)$$

with  $\theta$  arbitrary.  $k_A$  is well defined for all  $K_\mu$ , in particular for  $K_1 = K_2 = 0$ . With the restriction that  $K_0 \neq K_3$ ,  $k_A$  can be rewritten in a more convenient form

$$k_A = \begin{pmatrix} K_1 - iK_2 / \sqrt{K_0 - K_3} \\ \sqrt{K_0 - K_3} \end{pmatrix}. \quad (3.2.33)$$

With the momentum spinor, the Minkowski inner product of two light-cone vectors  $K_\mu$  and  $P_\mu$  can be expressed as

$$(K \cdot P) = \frac{1}{2} \{K, P\} = \frac{1}{2} K_{\dot{A}B} P^{\dot{A}B} = \frac{1}{2} k_B P^B k_{\dot{A}} P^{\dot{A}} = \frac{1}{2} \langle kP \rangle \langle kP \rangle^* = \frac{1}{2} |\langle kP \rangle|^2. \quad (3.2.34)$$

Considering the Minkowski inner product from this point of view it appears that spinor inner products are more fundamental quantities. It turns out that matrix elements do indeed get a more compact form when expressed in terms of spinor inner products.

The above holds for light-cone vectors. Now consider an on-shell massive particle that has momentum  $P_\mu$  with  $P^2 = M_V^2$ . It is possible to find the decomposition in eigenspinors using eq. (3.2.30). However in practice it is better to decompose  $P_\mu$  in two light-cone vectors  $K_\mu$  and  $M_\mu$  as follows:  $P_\mu = K_\mu + \alpha M_\mu$ , or in spinor language:

$$P_{\dot{A}B} = K_{\dot{A}B} + \alpha M_{\dot{A}B} = k_{\dot{A}} k_B + \alpha m_{\dot{A}} m_B \quad (3.2.35)$$

with the restriction that

$$\alpha \langle km \rangle \langle km \rangle^* = M_V^2. \quad (3.2.36)$$

The momentum  $M_\mu$  (and thus  $m_A$ ) can be chosen completely arbitrary. Every particular choice fixes  $\alpha$  and  $K_\mu$ . The  $M_V \rightarrow 0$  limit can be obtained with  $\alpha \rightarrow 0$ . The decomposition eq. (3.2.35) can be used to express all momenta in momentum spinors at the cost of introducing new momenta. As the spinors  $k_A$  and  $m_A$  appear in the spin-state solutions as well as in the decomposition above is the only worthwhile decomposition as the freedom in choosing  $m$  is important. The decomposition based on eigenspinors does not have this advantage.

### 3.3 Spin- $\frac{1}{2}$ particles

Within the framework of WvdW spinors we examine spinor representations for fermionic spin- $\frac{1}{2}$  particles. The outline of this section is as follows: after defining  $\gamma$ -matrices and Dirac-spinors in the WvdW formalism, the Dirac-Lagrangian is translated into WvdW spinor language and the Dirac equation is solved for massless particles. This procedure leads to a set of helicity states for the fermions in terms of momentum spinors. At the end of this section an extension to massive fermions is discussed and the spin-state solutions that can be used in calculations are derived.

Using the spin-tensor, see eq. (3.2.14), the  $\gamma$ -matrices in the Weyl-representation can be put in the form

$$(\gamma^\mu)^a_b = \begin{pmatrix} 0 & \sigma^{\mu}_{\dot{B}A} \\ \sigma^{\mu AB} & 0 \end{pmatrix}. \quad (3.3.1)$$

With this definition the commutation rule for  $\gamma$ -matrices

$$(\gamma^\mu)^a_b (\gamma^\nu)^b_c + (\gamma^\nu)^a_b (\gamma^\mu)^b_c = 2g^{\mu\nu} (I)^a_c \quad (3.3.2)$$

with  $I$  the unit  $4 \times 4$  matrix, is seen to be satisfied when eq. (3.2.19) is used after eq. (3.3.1) has been substituted. With the explicit representation of  $\sigma^{\mu AB}$ , see eq. (3.2.13), we arrive at the following representation for the  $\gamma$ -matrices

$$(\gamma^0)^a_b = \begin{pmatrix} 0 & \sigma^0 \\ \sigma^0 & 0 \end{pmatrix}, \quad (\gamma^i)^a_b = \begin{pmatrix} 0 & -\sigma^i \\ \sigma^i & 0 \end{pmatrix}, \quad (3.3.3)$$

with  $i = 1, 2$  or  $3$ . In this Weyl-representation  $\gamma^5$  reads

$$\gamma^5 = \gamma_5 = i\gamma^0\gamma^1\gamma^2\gamma^3 = \begin{pmatrix} I & 0 \\ 0 & -I \end{pmatrix}. \quad (3.3.4)$$

Note that there is some arbitrariness in the definition of the Weyl-representation in the literature; one can define  $(\gamma^\mu)^a_b$  differently while keeping  $\gamma_5$  the same. The representation of the  $\gamma_5$  determines whether it is a Weyl-representation or not.

With eqs. (3.3.1)-(3.3.4) one can derive the following translation rules for traces of  $\gamma$ -matrices, with  $n$  even

$$\begin{aligned} \text{Tr}(\gamma^{\mu_1} \dots \gamma^{\mu_n}) &= \sigma^{\mu_1 \dot{A}B} \sigma^{\mu_2 \dot{C}D} \sigma^{\mu_3 \dot{E}F} \dots \sigma^{\mu_n \dot{K}L} + \sigma^{\mu_1 \dot{B}A} \sigma^{\mu_2 \dot{D}C} \sigma^{\mu_3 \dot{F}E} \dots \sigma^{\mu_n \dot{L}K} \\ &= \sigma^{\mu_1 \dot{A}B} \sigma^{\mu_2 \dot{C}D} \sigma^{\mu_3 \dot{E}F} \dots \sigma^{\mu_n \dot{K}L} + c.c. \end{aligned} \quad (3.3.5)$$

and

$$\begin{aligned} \text{Tr}(\gamma^{\mu_1} \dots \gamma^{\mu_n} \gamma^5) &= \sigma^{\mu_1 \dot{B}A} \sigma^{\mu_2 \dot{D}C} \sigma^{\mu_3 \dot{F}E} \dots \sigma^{\mu_n \dot{L}K} - \sigma^{\mu_1 \dot{A}B} \sigma^{\mu_2 \dot{C}D} \sigma^{\mu_3 \dot{E}F} \dots \sigma^{\mu_n \dot{K}L} \\ &= \sigma^{\mu_1 \dot{B}A} \sigma^{\mu_2 \dot{D}C} \sigma^{\mu_3 \dot{F}E} \dots \sigma^{\mu_n \dot{L}K} - c.c. \end{aligned} \quad (3.3.6)$$

In particular from eq. (3.2.17) it follows that

$$\text{Tr}(\gamma^\mu \gamma^\nu) = \sigma^\mu_{\dot{A}B} \sigma^{\nu\dot{A}B} + \sigma^{\mu\dot{B}A} \sigma^\nu_{\dot{B}A} = 4g^{\mu\nu}. \quad (3.3.7)$$

Contraction of eq. (3.3.5) with  $n$  massless particle momenta  $p_{1\mu_1}, \dots, p_{n\mu_n}$  results in

$$\text{Tr}(\not{p}_1 \dots \not{p}_n) = \langle p_1 p_2 \rangle \langle p_3 p_2 \rangle^* \langle p_3 p_4 \rangle \dots \langle p_1 p_n \rangle^* + \text{c.c.} \quad (3.3.8)$$

and the Levi-Civita tensor

$$\mathcal{E}(p_1, p_2, p_3, p_4) \equiv \mathcal{E}_{\mu\nu\rho\sigma} p_1^\mu p_2^\nu p_3^\rho p_4^\sigma, \quad (3.3.9)$$

with  $\mathcal{E}_{0123} = 1$ , is translated as

$$4i\mathcal{E}(p_1, p_2, p_3, p_4) = \langle 12 \rangle^* \langle 23 \rangle \langle 34 \rangle^* \langle 41 \rangle - \text{c.c.} \quad (3.3.10)$$

This demonstrates the enormous simplification of the trace algebra when one uses WvdW spinors. There is simply no trace algebra left.

In the Weyl-representation the Dirac-spinor reads

$$\Psi^a = \begin{pmatrix} \Psi_R \\ \Psi_L \end{pmatrix} \equiv \begin{pmatrix} \Psi_A \\ \Phi^{\dot{A}} \end{pmatrix} = \begin{pmatrix} \Psi_1 \\ \Psi_2 \\ \Phi^{\dot{1}} \\ \Phi^{\dot{2}} \end{pmatrix}, \quad (3.3.11)$$

where  $\Psi_R$  and  $\Psi_L$  correspond with the physical right and left-handed spin states. The spinor index  $a$  is frequently omitted as it will be clear from the context what is meant. For the Dirac-spinor we take a form that expresses the 4-spinor in terms of one covariant spinor  $\Psi_A$  and one contravariant spinor  $\Phi^{\dot{A}}$ . These two WvdW spinors correspond with the two helicity states of massless fermions

$$\Psi_R = \Psi_+ = \frac{1}{2}(1 + \gamma_5)\Psi = \begin{pmatrix} \Psi_A \\ 0 \end{pmatrix} \quad (3.3.12)$$

$$\Psi_L = \Psi_- = \frac{1}{2}(1 - \gamma_5)\Psi = \begin{pmatrix} 0 \\ \Phi^{\dot{B}} \end{pmatrix}. \quad (3.3.13)$$

We will prove that the  $\Psi_\pm$  are indeed the helicity states once we have explicit solutions for them. The adjoint spinor  $\bar{\Psi}$  is given by

$$\bar{\Psi} = \Psi^\dagger \gamma^0 = (\Psi_L^*, \Psi_R^*) = (\Phi^{\dot{A}T}, \Psi_A^T) = (\Phi^{\dot{1}}, \Phi^{\dot{2}}, \Psi_1, \Psi_2), \quad (3.3.14)$$

where  $T$  denotes transposition. The Dirac-Lagrangian

$$\mathcal{L} = \frac{i}{2} (\bar{\Psi} \gamma^\mu (\partial_\mu \Psi) - (\partial_\mu \bar{\Psi}) \gamma^\mu \Psi) - M \bar{\Psi} \Psi, \quad (3.3.15)$$

where  $M$  is the mass of the fermion, translated into its WvdW analogue reads

$$\begin{aligned} \mathcal{L} = & + \frac{i}{2} (\Psi_A \partial^{\dot{A}B} \Psi_B - \Psi_B \partial^{\dot{A}B} \Psi_A) \\ & + \frac{i}{2} (\Phi^{\dot{B}} \partial_{\dot{A}B} \Phi^{\dot{A}} - \Phi^{\dot{A}} \partial_{\dot{A}B} \Phi^{\dot{B}}) \\ & - M (\langle \Psi \Phi \rangle + \langle \Psi \Phi \rangle^*) \end{aligned} \quad (3.3.16)$$

where we have used that

$$\bar{\Psi}\Psi = \Psi_A\Phi^A + \Psi_A\Phi^{\dot{A}} = \langle\Psi\Phi\rangle + \langle\Psi\Phi\rangle^* \quad (3.3.17)$$

$$\bar{\Psi}\gamma^\mu\Psi = \Psi_{\dot{A}}\Psi_B\sigma^{\mu\dot{A}B} + \Phi^A\Phi_{\dot{B}A}\sigma_{\dot{B}A}^\mu. \quad (3.3.18)$$

Setting  $M = 0$  in eq. (3.3.16) results in two uncoupled equations of motion

$$\begin{cases} \partial^{\dot{A}B}\Psi_B = 0 \\ \partial_{\dot{A}B}\Phi^{\dot{A}} = 0 \end{cases} \quad (3.3.19)$$

Transforming  $\Psi_B$  to momentum space, eq. (3.3.19) becomes very simple, for instance

$$K^{\dot{A}B}\tilde{\Psi}_B = k^{\dot{A}}k^B\tilde{\Psi}_B = 0, \quad (3.3.20)$$

with  $K^{\dot{A}B}$  the four-momentum of the fermion,  $\{K, K\} = 0$  and  $k_A$  its momentum spinor. The  $\tilde{\Psi}_B$  denotes the Fourier transform of  $\Psi_B$ . Eq. (3.3.20) leads to the following solution for the spin states in momentum space

$$u(\vec{K}) = \tilde{\Psi} = \begin{pmatrix} \tilde{\Psi}_A \\ \tilde{\Phi}^{\dot{A}} \end{pmatrix} = \begin{pmatrix} \alpha_+ e^{i\theta_+} k_A \\ \alpha_- e^{i\theta_-} k^{\dot{A}} \end{pmatrix}, \quad (3.3.21)$$

and for the two helicity states

$$u_+(\vec{K}) = \begin{pmatrix} \alpha_+ e^{i\theta_+} k_A \\ 0 \end{pmatrix} \quad \text{and} \quad u_-(\vec{K}) = \begin{pmatrix} 0 \\ \alpha_- e^{i\theta_-} k^{\dot{A}} \end{pmatrix}. \quad (3.3.22)$$

Similarly for the adjoint spinors

$$\bar{u}_+(\vec{K}) = (0, \alpha_+ e^{-i\theta_+} k_A) \quad \text{and} \quad \bar{u}_-(\vec{K}) = (\alpha_- e^{-i\theta_-} k^{\dot{A}}, 0). \quad (3.3.23)$$

The  $u_+$  and  $u_-$  are two orthogonal spin states, i.e. with  $\lambda_1 = \pm$  and  $\lambda_2 = \pm$  we have

$$u_{\lambda_1}^* u_{\lambda_2} = 2K_0 \delta_{\lambda_1 \lambda_2} \quad (3.3.24)$$

Furthermore we have the real parameters  $\alpha_+ > 0, \alpha_- > 0$  and  $\theta_+, \theta_-$  arbitrary. The  $\alpha$ 's are determined by the completeness relation or the spin sum condition

$$\sum_\lambda u_\lambda(\vec{K}) \bar{u}_\lambda(\vec{K}) = \gamma^\mu K_\mu \quad \text{or} \quad \begin{pmatrix} 0 & \alpha_+^2 K_{\dot{B}A} \\ \alpha_-^2 K^{\dot{A}B} & 0 \end{pmatrix} = \begin{pmatrix} 0 & K_{\dot{B}A} \\ K^{\dot{A}B} & 0 \end{pmatrix}, \quad (3.3.25)$$

which leads to  $\alpha_+ = 1$  and  $\alpha_- = 1$ . Setting both phase factors equal to one we arrive at

$$u_+(\vec{K}) = \begin{pmatrix} k_A \\ 0 \end{pmatrix} \quad \text{and} \quad u_-(\vec{K}) = \begin{pmatrix} 0 \\ k^{\dot{A}} \end{pmatrix}. \quad (3.3.26)$$

That  $u_+$  and  $u_-$  correspond with the  $+$  and  $-$  helicity states can be checked by using the explicit representations for  $k_A$  and  $k^{\dot{A}}$  and verifying that  $u_+$  and  $u_-$  have the correct eigenvalues for the helicity operator  $\vec{\Sigma} \cdot \vec{K}$

$$\vec{\Sigma} \cdot \vec{K} u_\lambda = \frac{1}{|\vec{K}|} \begin{pmatrix} \vec{\sigma} \cdot \vec{K} & 0 \\ 0 & \vec{\sigma} \cdot \vec{K} \end{pmatrix} u_\lambda = \lambda u_\lambda, \quad (3.3.27)$$

for  $\lambda = \pm$ .

The solutions of the Dirac equation  $u$  and  $\bar{u}$  describe the creation and annihilation of fermions. The solution for anti-fermions can be constructed from  $u$  and  $\bar{u}$  by means of the charge conjugation relation

$$Cv_{\pm} = -\bar{u}_{\pm}^T. \quad (3.3.28)$$

Here the  $T$  again denotes the transposed spinor and  $C = -i\gamma^2\gamma^0$ . For massless spinors this definition of  $C$  gives the same result as the following argument. As both the momentum and the spin are reversed the helicity remains the same. In other words we can interchange the  $+$  and the  $-$  solutions of the particles to get the solutions of the anti-particles. Thus

$$v_{-}(\vec{K}) = u_{+}(\vec{K}), \quad v_{+}(\vec{K}) = u_{-}(\vec{K}). \quad (3.3.29)$$

are the helicity states for anti-fermions. The  $v_{\lambda}$  corresponds to the annihilation of an anti-fermion.

Now we turn to massive fermions. The equations of motion derived from eq. (3.3.16) in momentum space read

$$\begin{cases} P^{\dot{A}B}\tilde{\Psi}_B = M\tilde{\Phi}^{\dot{A}} \\ P_{\dot{A}B}\tilde{\Phi}^{\dot{A}} = M\tilde{\Psi}_B \end{cases} \quad (3.3.30)$$

with  $P_{\dot{A}B}$  the four-momentum of the massive fermion,  $\{P, P\} = 2M^2$ . As noted in section 3.2 we can decompose the momentum  $P^{\dot{A}B}$  in two light-cone momenta  $K^{\dot{A}B}$  and  $M^{\dot{A}B}$  with

$$P^{\dot{A}B} = K^{\dot{A}B} + \alpha M^{\dot{A}B} = k^{\dot{A}}k^B + \alpha m^{\dot{A}}m^B. \quad (3.3.31)$$

The notation is such that in the  $M \rightarrow 0$  or equivalently  $\alpha \rightarrow 0$  limit,  $P^{\dot{A}B} \rightarrow K^{\dot{A}B}$ . In eq. (3.3.31) the spinor  $m_A$  is arbitrary but  $m_A \neq k_A$  and  $\langle km \rangle$  is given by

$$\alpha \langle km \rangle \langle km \rangle^* = M^2, \quad \alpha \epsilon R^+. \quad (3.3.32)$$

or

$$\langle km \rangle = e^{i\theta} M / \sqrt{\alpha} \quad (3.3.33)$$

Using eqs. (3.3.31) and (3.3.33) the following relations can be derived

$$P_{\dot{A}B}k^B = \alpha m_{\dot{A}} \langle mk \rangle = -\sqrt{\alpha} e^{i\theta} M m_{\dot{A}} \quad (3.3.34)$$

$$P_{\dot{A}B}m^B = \langle km \rangle k_{\dot{A}} = e^{i\theta} M / \sqrt{\alpha} k_{\dot{A}} \quad (3.3.35)$$

We try as solutions of (3.3.30)

$$\begin{cases} \tilde{\Psi}_B = k_B + \sqrt{\alpha} m_B \\ \tilde{\Phi}^{\dot{A}} = k^{\dot{A}} - \sqrt{\alpha} m^{\dot{A}} \end{cases} \quad (3.3.36)$$

and similarly

$$\begin{cases} \tilde{\Psi}_B = k_B - \sqrt{\alpha} m_B \\ \tilde{\Phi}^A = -k^A - \sqrt{\alpha} m^A \end{cases} \quad (3.3.37)$$

Substituting  $\tilde{\Psi}_B$  and  $\tilde{\Phi}^A$  in eq. (3.3.30) gives  $\theta = \pi$ . From these solutions we construct two spin states for the fermion. These spin states are based on the massive case and in the  $M \rightarrow 0$  limit the spin states transform in the corresponding massless states. The complete set of solutions for both fermions and anti-fermions is given by

$$\begin{aligned} u_+(\vec{P}) &= \begin{pmatrix} k_A \\ -\sqrt{\alpha} m^A \end{pmatrix}, & u_-(\vec{P}) &= \begin{pmatrix} \sqrt{\alpha} m_A \\ k^A \end{pmatrix}, \\ \bar{u}_+(\vec{P}) &= \begin{pmatrix} -\sqrt{\alpha} m^A & k_A \end{pmatrix}, & \bar{u}_-(\vec{P}) &= \begin{pmatrix} k^A & \sqrt{\alpha} m_A \end{pmatrix}, \\ v_+(\vec{P}) &= \begin{pmatrix} -\sqrt{\alpha} m_A \\ k^A \end{pmatrix}, & v_-(\vec{P}) &= \begin{pmatrix} k_A \\ \sqrt{\alpha} m^A \end{pmatrix}, \\ \bar{v}_+(\vec{P}) &= \begin{pmatrix} k^A & -\sqrt{\alpha} m_A \end{pmatrix}, & \bar{v}_-(\vec{P}) &= \begin{pmatrix} \sqrt{\alpha} m^A & k_A \end{pmatrix}. \end{aligned} \quad (3.3.38)$$

The solutions for the anti-particles can again be obtained by means of the charge conjugation relation in eq. (3.3.28). Notice that we do not have  $v_+ = u_-$  and  $v_- = u_+$ . With the solution eqs. (3.3.38) the completeness relations and the standard normalization for massive fermions can be checked.

$$\sum_{\lambda} u_{\lambda}(\vec{P}) \bar{u}_{\lambda}(\vec{P}) = \gamma^{\mu} P_{\mu} + M I = \begin{pmatrix} M \epsilon^{B A} & P_{B A} \\ P^{A B} & M \epsilon^A_B \end{pmatrix}, \quad (3.3.39)$$

$$\sum_{\lambda} v_{\lambda}(\vec{P}) \bar{v}_{\lambda}(\vec{P}) = \gamma^{\mu} P_{\mu} - M I = \begin{pmatrix} -M \epsilon^{B A} & P_{B A} \\ P^{A B} & -M \epsilon^A_B \end{pmatrix}, \quad (3.3.40)$$

$$\bar{u}_{\lambda_1} u_{\lambda_2} = 2M \delta_{\lambda_1 \lambda_2}, \quad (3.3.41)$$

$$\bar{v}_{\lambda_1} v_{\lambda_2} = -2M \delta_{\lambda_1 \lambda_2}. \quad (3.3.42)$$

The solutions for particles and anti-particles are also orthogonal

$$\bar{u}_{\lambda_1}(\vec{P}) v_{\lambda_2}(\vec{P}) = \bar{v}_{\lambda_1}(\vec{P}) u_{\lambda_2}(\vec{P}) = 0. \quad (3.3.43)$$

Note that the solutions in eq. (3.3.38) do not correspond to helicity states, i.e. they are not eigenstates of the helicity operator. As a last point we note that the freedom of choosing  $m_A$  can be used to simplify calculations with massive fermions.

### 3.4 Bosonic particles

Having considered the translation of Dirac spinors in WvdW spinors we turn to bosons. We give a detailed derivation of the explicit representation of helicity vectors corresponding to free bosonic particles. As will be clear from the many examples in section 3.6 it is not important whether the particle carries colour, so photons and gluons can be treated on equal footing. We use vectors and spinors alongside each other; the equations are put in the language that is most convenient.

The equation of motion for a free massless spin-1 particle in the Lorentz gauge

$$\partial \cdot A = 0. \quad (3.4.1)$$

reads

$$\square A^\mu = 0. \quad (3.4.2)$$

The general solution can be written as a plane wave solution

$$A^\mu(x) = \int d^4k (\epsilon^\mu(k)e^{ikx} + \epsilon^{*\mu}(k)e^{-ikx}). \quad (3.4.3)$$

In general there would be four independent  $\epsilon^\mu(k)$ 's but the Lorentz condition (3.4.1), reduces this to three. Furthermore we can change  $A^\mu$  by a gauge transformation, which implies that the  $\epsilon^\mu$  still have the gauge freedom:

$$\epsilon'^\mu = \epsilon^\mu + \xi K^\mu. \quad (3.4.4)$$

The massless spin-1 field has two degrees of freedom, represented by the right- and left-handed complex helicity vectors,  $\epsilon_\lambda^\mu$  with  $\lambda = \pm$ . In spinor language the orientation and normalization of the polarization vectors can be chosen such that the  $\epsilon_\lambda^\mu$  are determined by the following set of relations:

$$\{K, K\} = 0 \quad (3.4.5)$$

$$\{\epsilon_\lambda, K\} = 0 \quad (3.4.6)$$

$$\{\epsilon_\lambda, \epsilon_\lambda\} = 0 \quad (3.4.7)$$

$$\epsilon_\lambda^{\dot{B}A} = (\epsilon_{-\lambda}^{\dot{A}B})^* \quad (3.4.8)$$

$$\{\epsilon_\lambda, \epsilon_{-\lambda}\} = -2 \quad (3.4.9)$$

with  $K^{\dot{A}B}$  the momentum of the particle. Note that eq. (3.4.7) does not imply that  $\epsilon_\lambda^{\dot{A}B} = e^{\dot{A}} e^B$  for some spinor  $e^{\dot{A}}$ , see eq. (3.2.30), because the components of  $\epsilon_\lambda^\mu$  are complex. For transverse vectors there is the extra condition that

$$\vec{\epsilon}_\lambda \cdot \vec{K} = 0. \quad (3.4.10)$$

This relation can be satisfied by a redefinition of  $\epsilon$  by means of eq. (3.4.4). With these relations we find that the helicity vectors can be written as

$$\epsilon_+^{AB} = \sqrt{2} e^{i\alpha} \frac{k^A b^B}{\langle kb \rangle} \quad (3.4.11)$$

$$\epsilon_-^{AB} = \sqrt{2} e^{-i\alpha} \frac{b^A k^B}{\langle kb \rangle^*} \quad (3.4.12)$$

with  $b^A$  an arbitrary spinor not proportional to  $k^A$ . The phase factor  $e^{i\alpha}$  is just an overall rotation of the two helicity vectors around the direction of propagation of the boson. We set  $\alpha = 0$ . The gauge freedom of the helicity vectors is manifestly present in spinor language. That is, if  $\epsilon_\lambda^\mu$  is a solution then

$$\epsilon'_\lambda{}^\mu = \epsilon_\lambda^\mu + \xi K^\mu, \quad (3.4.13)$$

with  $\xi$  arbitrary, is also a solution. It corresponds with two different choices for  $b^A$ . For example, using (3.2.10)

$$\epsilon_+^{AB} = \sqrt{2} \frac{k^A k^B}{\langle kb \rangle} = \sqrt{2} \frac{k^A c^B}{\langle kc \rangle} + \sqrt{2} \frac{k^A k^B \langle bc \rangle}{\langle kb \rangle \langle kc \rangle} = \epsilon_+^{AB} + \xi K^{AB}. \quad (3.4.14)$$

The easiest way to show that  $\epsilon_+^{AB}$  corresponds to the right-handed helicity state is to define the boson to propagate along the z-axis with  $K^\mu = (K^0, 0, 0, K^0)$ . Using eq. (3.2.33) we find that

$$k_A = \begin{pmatrix} 0 \\ 2 K_0 \end{pmatrix}. \quad (3.4.15)$$

Together with the definition of the momentum spinor

$$b_A \equiv \begin{pmatrix} b_1 \\ b_2 \end{pmatrix}, \quad (3.4.16)$$

based on  $B^\mu = (B^0, B^1, B^2, B^3)$  with  $B^2 = 0$ , it follows that

$$\epsilon_{+AB} = \frac{\sqrt{2}}{\langle kb \rangle} \begin{pmatrix} 0 & 0 \\ 2 K_0 b_1 & 2 K_0 b_2 \end{pmatrix}. \quad (3.4.17)$$

Using  $\epsilon_+^\mu = \frac{1}{2} \sigma^{\mu AB} \epsilon_{+AB}$  and eq. (3.4.4) to remove the component parallel to  $K^\mu$  gives

$$\epsilon_+^\mu = \beta_+(0, (-B^0 - B^3 - B^1 + iB^2), i(-B^0 - B^3 - B^1 + iB^2), 0), \quad (3.4.18)$$

with  $\beta_+$  some function of inner products with  $K^\mu$ 's and  $B^\mu$ 's. With the definition that the helicity vectors transform under a rotation over an angle  $\theta$  as

$$R_\nu^\mu(\theta) \epsilon_\lambda^\nu = \begin{pmatrix} 1 & 0 & 0 & 0 \\ 0 & \cos \theta & \sin \theta & 0 \\ 0 & -\sin \theta & \cos \theta & 0 \\ 0 & 0 & 0 & 1 \end{pmatrix} \epsilon_\lambda^\nu = e^{i\lambda\theta} \epsilon_\lambda^\nu, \quad (3.4.19)$$

the right-handedness of  $\epsilon_+^\mu$  can easily be established.

As a last check we compute the sum over helicities

$$\sum_\lambda \epsilon_\lambda^\mu (\epsilon_\lambda^\nu)^* = -g^{\mu\nu} + \frac{K^\mu B^\nu + K^\nu B^\mu}{(K \cdot B)} \quad (3.4.20)$$

with  $B^\mu = 1/2 \sigma_{AB}^\mu b^A b^B$  and  $B^\mu$  not parallel to  $K^\mu$ . Eq. (3.4.20) is the spin sum in the light-like axial gauge and confirms that our spin-1 particles are physical. That we still have the axial gauge freedom is important. We will set the  $b^A$  equal to other momenta spinors present in a scattering process. This leads to enormous simplifications as will be shown in section 3.6.

We consider two extensions of free massless spin-1 particles. First we increase the spin. Massless spin- $n$  particles have two physical degrees of freedom and we will show that the helicity vectors can be chosen such that they are a direct generalization of spin-1 helicity vectors. For convenience we specialize to  $n = 2$ . In the de Donder gauge

$$\partial_\mu h_\nu^\mu = 1/2 \partial_\nu h_\mu^\mu, \quad (3.4.21)$$

the equation of motion is the Fierz-Pauli equation, which reads

$$\square h^{\mu\nu} = 0. \quad (3.4.22)$$

The symmetric field  $h^{\mu\nu}$  has a priori 10 degrees of freedom, two of which we want to remain. The general solution in plane waves reads

$$h^{\mu\nu}(x) = \int d^4 k (\epsilon^{\mu\nu}(k) e^{ikx} + \epsilon^{*\mu\nu}(k) e^{-ikx}). \quad (3.4.23)$$

Using a general coordinate transformation one can formulate another set of gauge fixing conditions [14] such that two degrees of freedom remain. The resulting form for  $\epsilon^{\mu\nu}(k)$  is not very suitable for our purposes. It is better to choose the gauge fixing relations such that the polarization tensor fulfils the following conditions

$$\epsilon_\lambda^{\mu\nu} = \epsilon_\lambda^\mu \epsilon_\lambda^\nu, \quad (3.4.24)$$

$$(\epsilon_\lambda \cdot K) = 0, \quad (3.4.25)$$

$$(\epsilon_\lambda \cdot B) = 0. \quad (3.4.26)$$

Next choose an orthogonal basis for the two remaining vectors

$$(\epsilon_\lambda \cdot \epsilon_\lambda) = 0. \quad (3.4.27)$$

$$(\epsilon_\lambda \cdot \epsilon_{-\lambda}) = -1. \quad (3.4.28)$$

This set of relations satisfies eq. (3.4.21) and furthermore we have the analogue of the Lorentz gauge (3.4.25) and the axial gauge (3.4.26). This means that the helicity vectors are physical and that we do not have to consider the ghost sector. So the spin-2 helicity tensor is written as a dyad of two spin-1 helicity vectors and we still have the axial gauge

freedom at our disposal to simplify expressions. It also means that the field  $h^{\mu\nu}$  is traceless. In the example section the properties of the solution, eqs. (3.4.24)-(3.4.28) will be used.

The second extension is to give mass to the spin-1 bosons. The extra degree of freedom of massive bosons emerges as a longitudinal polarization vector  $\epsilon_0$ . We start with the Proca field equation and find the equivalent set of equations

$$\square\Phi^\mu + M_b^2\Phi^\mu = 0 \quad (3.4.29)$$

$$\partial \cdot \Phi = 0 \quad (3.4.30)$$

In spinor language the polarization vectors can be chosen such that they satisfy

$$\{Q, Q\} = 2M_b^2 \quad (3.4.31)$$

$$\{\epsilon_\lambda, Q\} = \{\epsilon_0, Q\} = 0 \quad (3.4.32)$$

$$\{\epsilon_\lambda, \epsilon_\lambda\} = \{\epsilon_0, \epsilon_\lambda\} = 0 \quad (3.4.33)$$

$$\epsilon_\lambda^{\dot{A}B} = (\epsilon_{-\lambda}^{\dot{A}B})^* \quad (3.4.34)$$

$$\epsilon_0^{\dot{A}B} = (\epsilon_0^{\dot{A}B})^* \quad (3.4.35)$$

$$\{\epsilon_\lambda, \epsilon_{-\lambda}\} = \{\epsilon_0, \epsilon_0\} = -2 \quad (3.4.36)$$

where  $Q^\mu$  is the momentum of the vector boson and  $Q^2 = M_b^2$ . As has been shown in section 3.2 we can decompose the momentum  $Q^\mu$  into two massless momenta

$$Q^\mu = K^\mu + \alpha M^\mu \Leftrightarrow Q^{\dot{A}B} = K^{\dot{A}B} + \alpha M^{\dot{A}B} = k^{\dot{A}B} + \alpha m^{\dot{A}B}. \quad (3.4.37)$$

A solution for the polarization vectors then becomes

$$\epsilon_+^{\dot{A}B} = \sqrt{2} \frac{k^{\dot{A}B} m^B}{(km)} \quad (3.4.38)$$

$$\epsilon_-^{\dot{A}B} = \sqrt{2} \frac{m^{\dot{A}B} k^B}{(km)^*} \quad (3.4.39)$$

$$\epsilon_0^{\dot{A}B} = \frac{K^{\dot{A}B} - \alpha M^{\dot{A}B}}{M_b}. \quad (3.4.40)$$

The polarization states in eqs. (3.4.38) and (3.4.39) are suggestively denoted by  $\epsilon_+$  and  $\epsilon_-$ . However they do not satisfy the transversality condition eq. (3.4.10). The polarization vectors are put in this form for two reasons. Firstly, the vectors  $\epsilon_\pm$  can directly be identified with the massless solution in eqs. (3.4.11) and (3.4.12). Secondly, the + and - solutions are each others complex conjugate, a useful property in calculations. Because  $m_A$  is arbitrary we can use it to simplify expressions. Replacing  $B^\mu$  in eq. (3.4.20) by  $\alpha M^\mu$  and adding  $\epsilon_0^\mu (\epsilon_0^\mu)^*$  to it, results in

$$\sum_{\alpha=\lambda,0} \epsilon_\alpha^\mu (\epsilon_\alpha^\nu)^* = -g^{\mu\nu} + \frac{Q^\mu Q^\nu}{M_b^2}. \quad (3.4.41)$$

## 3.5 Matrix elements in QCD

This section consists of two parts. In the first part the Feynman rules for QCD are presented, in the standard notation as well as in the WvdW spinor notation. The second part serves as an introduction to subsequent chapters. We discuss the colour decomposition techniques in QCD. This leads to colourless Feynman rules with which the calculation of scattering amplitudes in QCD simplifies.

### 3.5.1 QCD Feynman rules

We are interested in the calculation of scattering amplitudes on tree level. To get the gluon propagator in its simplest form we work in the 't Hooft-Feynman gauge. The QCD Lagrangian reads

$$\mathcal{L}_{QCD} = \bar{\Psi}_i \gamma^\mu D_\mu \Psi_j - m \bar{\Psi}_i \Psi_i - \frac{1}{4} \mathcal{F}^{a\mu\nu} \mathcal{F}_{\mu\nu}^a + \frac{1}{2} (\partial_\mu A^{a\mu})^2, \quad (3.5.1)$$

where  $m$  denotes the mass of the quark and  $i, j$  and  $a$  are colour labels. The Fadeev-Popov Lagrangian is not needed here because we work at tree level. Furthermore we used the definitions

$$D_\mu = i\partial_\mu \delta_{ij} - g(T^a)_{ij} A_\mu^a, \quad (3.5.2)$$

$$\mathcal{F}_{\mu\nu}^a = \partial_\mu A_\nu^a - \partial_\nu A_\mu^a - g f^{abc} A_\mu^b A_\nu^c. \quad (3.5.3)$$

Here the  $f^{abc}$  are the real structure constants of the  $SU(N)$  colour gauge group with  $N$  the number of colours. The fundamental representation matrices  $(T^a)_{ij}$  satisfy the following relations

$$[T^a, T^b]_{ij} = i f^{abc} (T^c)_{ij}, \quad (3.5.4)$$

$$f^{a_1 a_2 a_3} = -2i \{ \text{Tr}(T^{a_1} T^{a_2} T^{a_3}) - \text{Tr}(T^{a_3} T^{a_2} T^{a_1}) \}. \quad (3.5.5)$$

The structure constants satisfy the Jacobi-identity

$$f^{abx} f^{xcd} + f^{cbx} f^{xda} + f^{dbx} f^{xac} = 0. \quad (3.5.6)$$

Some useful relations to perform colour sums are

$$(T^a)_{ij} (T^a)_{kl} = 1/2 \left[ \delta_{il} \delta_{kj} - \frac{1}{N} \delta_{ij} \delta_{kl} \right], \quad (3.5.7)$$

$$\text{Tr}(T^{a_1} T^{a_2}) = 1/2 \delta^{a_1 a_2}, \quad (3.5.8)$$

$$\delta^{aa} = N^2 - 1 \text{ and } \delta_{ii} = N. \quad (3.5.9)$$

We frequently work with traces of  $T^a$ 's, therefore the shorthand notations

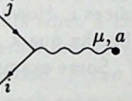
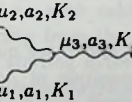
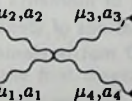
|                                                                                    |                                                                                                                                                                                                                                                                                                                                                                                                                                                                                                                                                                                                 |
|------------------------------------------------------------------------------------|-------------------------------------------------------------------------------------------------------------------------------------------------------------------------------------------------------------------------------------------------------------------------------------------------------------------------------------------------------------------------------------------------------------------------------------------------------------------------------------------------------------------------------------------------------------------------------------------------|
|    | <p>Creation of a quark with momentum <math>P</math> and colour <math>i</math>.</p> <ul style="list-style-type: none"> <li>- Standard notation: <math>\bar{u}_i(P)</math></li> <li>- WvdW, <math>m = 0</math>: <math>+ \rightarrow p_{i\dot{\lambda}}</math> and <math>- \rightarrow p_{\dot{\lambda}i}</math></li> <li>- WvdW, <math>m \neq 0</math>: <math>'+' \rightarrow (-\sqrt{\alpha} p_{2\dot{\lambda}}^A p_{1\dot{\lambda}})</math> and <math>'-' \rightarrow (p_{1\dot{\lambda}}^A \sqrt{\alpha} p_{2\dot{\lambda}})</math></li> </ul>                                                 |
|    | <p>Creation of an antiquark with momentum <math>P</math> and colour <math>j</math>.</p> <ul style="list-style-type: none"> <li>- Standard notation: <math>v_j(P)</math></li> <li>- WvdW, <math>m = 0</math>: <math>+ \rightarrow p_{\dot{\lambda}B}</math> and <math>- \rightarrow p_{B\dot{\lambda}}</math></li> <li>- WvdW, <math>m \neq 0</math>: <math>'+' \rightarrow \begin{pmatrix} -\sqrt{\alpha} p_{2B} \\ p_{1\dot{\lambda}}^B \end{pmatrix}</math> and <math>'-' \rightarrow \begin{pmatrix} p_{1B} \\ \sqrt{\alpha} p_{2\dot{\lambda}}^B \end{pmatrix}</math></li> </ul>            |
|    | <p>Creation of a gluon with momentum <math>K</math> and colour <math>a</math>.</p> <ul style="list-style-type: none"> <li>- Standard notation: <math>\epsilon_\mu^a(K)</math></li> <li>- WvdW: <math>+ \rightarrow \frac{1}{2} \sigma_{\mu\dot{\lambda}B} \sqrt{2} \frac{k^A b^B}{\langle kb \rangle}</math> and <math>- \rightarrow \frac{1}{2} \sigma_{\mu\dot{\lambda}B} \sqrt{2} \frac{k^B b^A}{\langle kb \rangle^*}</math></li> </ul>                                                                                                                                                     |
|    | <p>Quark propagator.</p> <ul style="list-style-type: none"> <li>- Standard notation: <math>i(P + mI)\delta_{ij}/(P^2 - m^2)</math></li> <li>- WvdW: <math>\frac{i\delta_{ij}}{P^2 - m^2} \begin{pmatrix} m\epsilon_{\dot{\lambda}A}^B &amp; P_{\dot{\lambda}A}^B \\ P^{AB} &amp; m\epsilon_{\dot{\lambda}B}^A \end{pmatrix}</math></li> <li>- WvdW, <math>m = 0</math>: <math>i</math>-side + helicity: <math>iP^{AB}\delta_{ij}/P^2</math></li> <li>- WvdW, <math>m = 0</math>: <math>i</math>-side - helicity: <math>iP_{\dot{\lambda}A}^B\delta_{ij}/P^2</math></li> </ul>                   |
|    | <p>Gluon propagator.</p> <ul style="list-style-type: none"> <li>- Standard notation: <math>-ig_{\mu\nu}\delta_{ab}/K^2</math></li> <li>- WvdW: <math>-ic^{\dot{\lambda}C} \epsilon_{\dot{\lambda}AB}^D \sigma_{\mu\dot{\lambda}B} \sigma_{\nu\dot{\lambda}C} D / \{K, K\}</math></li> </ul>                                                                                                                                                                                                                                                                                                     |
|    | <p>Interaction between a quark, an antiquark and a gluon.</p> <ul style="list-style-type: none"> <li>- Standard notation: <math>ig(T^a)_{ij}\gamma^\mu</math></li> <li>- WvdW: <math>ig(T^a)_{ij} \begin{pmatrix} 0 &amp; \sigma_{\dot{\lambda}A}^B \\ \sigma_{\mu\dot{\lambda}B} &amp; 0 \end{pmatrix}</math></li> <li>- WvdW, <math>i</math>-side + helicity: <math>ig(T^a)_{ij}\sigma^{\mu\dot{\lambda}B}</math></li> <li>- WvdW, <math>i</math>-side - helicity: <math>ig(T^a)_{ij}\sigma_{\dot{\lambda}B}^\mu</math></li> </ul>                                                            |
|   | <p>Interaction between three gluons.</p> <ul style="list-style-type: none"> <li>- Standard notation: <math>-gf^{a_1 a_2 a_3} V^{\mu_1 \mu_2 \mu_3}(K_1, K_2, K_3)</math></li> <li>- <math>V^{\mu_1 \mu_2 \mu_3}(K_1, K_2, K_3) = \sum_C(123)(K_1 - K_2)^{\mu_3} g^{\mu_1 \mu_2}</math></li> <li>- WvdW: <math>-gf^{a_1 a_2 a_3} \frac{1}{8} \sigma_{\dot{\lambda}AB}^{\mu_1} \sigma_{\dot{\lambda}CD}^{\mu_2} \sigma_{\dot{\lambda}EF}^{\mu_3} V^{\dot{\lambda}ABCDEF}(K_1, K_2, K_3)</math></li> </ul>                                                                                         |
|  | <p>Interaction between four gluons.</p> <ul style="list-style-type: none"> <li>- Standard notation: <math>-ig^2 W^{\mu_1 \mu_2 \mu_3 \mu_4}_{a_1 a_2 a_3 a_4}</math></li> <li>- <math>W^{\mu_1 \mu_2 \mu_3 \mu_4}_{a_1 a_2 a_3 a_4} = \sum_C(123) f^{a_1 a_2 z} f^{z a_3 a_4} (g^{\mu_1 \mu_3} g^{\mu_2 \mu_4} - g^{\mu_1 \mu_4} g^{\mu_2 \mu_3})</math></li> <li>- WvdW: <math>-ig^2 \frac{1}{16} \sigma_{\dot{\lambda}AB}^{\mu_1} \sigma_{\dot{\lambda}CD}^{\mu_2} \sigma_{\dot{\lambda}EF}^{\mu_3} \sigma_{\dot{\lambda}GH}^{\mu_4} W^{\dot{\lambda}ABCDEF\dot{\lambda}GH}</math></li> </ul> |

Table 3.1. Feynman rules for QCD

$$\text{Tr}(T^{a_1} T^{a_2} \dots T^{a_n}) \equiv (a_1 a_2 \dots a_n) \quad (3.5.10)$$

$$(T^{a_1} T^{a_2} \dots T^{a_n})_{ij} \equiv (a_1 a_2 \dots a_n)_{ij} \quad (3.5.11)$$

are used to clarify the expressions.

From eq. (3.5.1) the Feynman rules can be derived. In table 3.1 they are given in the standard notation as well as in the WvdW notation. The following remarks clarify the contents of the table. The momenta of massive particles are decomposed in light-cone momenta with  $P = P_1 + \alpha P_2$ , and all particles are outgoing. The colour labels are omitted in the explicit representation of the free field solutions. The spinor labels are omitted in the standard notation. In the WvdW notation the outgoing quark has spinor labels  $A$  and  $\bar{A}$ , while the outgoing antiquark has labels  $B$  and  $\bar{B}$ . In the Feynman rules in the WvdW language the helicities are specified. From the list one can deduce the Feynman rules for QED without any problem.

### 3.5.2 Colour decomposition in QCD

A general method to separate the colour structure part and the dynamical part in QCD processes is discussed in detail. The amplitude for a scattering process can be written as a sum of gauge invariant functions, containing the space-time dynamics, each with a certain colour structure:

$$\mathcal{M}_n(P) = ig^{n-2} \sum_{\text{perms}} F(T^a, i, N) K_F(P). \quad (3.5.12)$$

The matrix element depends on a phase space point  $P$ , a set of  $n$  particle momenta and helicities. The strong coupling constant  $g$  is separated from the dynamics. The function  $F(T^a, i, N)$  is built up from representation matrices  $(a)_{xy}$  and colour indices  $i$ . However, the open indices of the fundamental representation matrices can only be the quark and antiquark colour indices. Furthermore  $F$  can be an explicit function of  $N$ . Some examples are

$$\frac{1}{N} (a_1 a_2 a_3)_{ij} (a_4)_{kl} \quad \text{and} \quad (a_1 a_2 a_3 a_4)_{ij},$$

which are  $F$ 's for a four and a two quark process respectively ( $i, j, k$  and  $l$  are quark colour indices). This set of  $F$ 's is independent. Therefore the decomposition of  $\mathcal{M}$  in terms of  $F$ 's with eq. (3.5.12) leads to a set of gauge invariant expressions  $K_F(P)$  in a unique way. These  $K_F(P)$  we call *subamplitudes*. They are a function of momenta and helicities only and not of the colours. The  $\sum_{\text{perms}}$  runs over all permutations of identical particles which change  $F$ . With eq. (3.3.31) it is found that the QCD matrix elements squared are given by

$$\sum_{c, \lambda} |\mathcal{M}_n|^2 = g^{2n-4} \sum_{c, \lambda} \left| \sum_{\text{perms}} F(T^a, N, i) K_F(P) \right|^2. \quad (3.5.13)$$

Evaluating the square and summing over all colours  $c$  results in a  $N_P \times N_P$  colour matrix, where  $N_P$  is the above mentioned number of permutations. The  $\sum_\lambda$  denotes the sum over all possible helicity configurations  $\lambda$ .

To obtain the decomposition (3.5.12) in a calculation one could rewrite every diagram in terms of  $F$ 's using eqs. (3.5.4)-(3.5.7), ending with colour expressions like in eqs. (3.5.10) and (3.5.11). However, this is a tedious task and errors are likely to slip in. Below we discuss an alternative method.

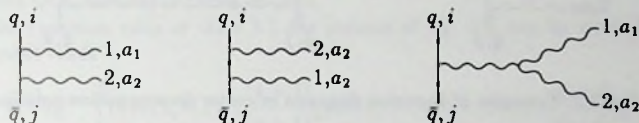


Fig. 3.1. The Feynman diagrams contributing to  $\emptyset \rightarrow q\bar{q}gg$ .

The decomposition of  $\mathcal{M}$  into subamplitudes raises two questions. Do all the possible  $F$ 's show up in an actual calculation? Is it possible to predict in advance which Feynman diagrams contribute to a certain  $F$ ? These two questions are answered by introducing a new concept: Colour flow. With this concept we are able to determine to which  $F$ 's a Feynman diagram contributes. The contribution itself is called the dynamic part of the diagram. Of course this colour flow concept is nothing else than a clever way of applying the QCD Feynman rules.

The first step is to read  $F$  from a Feynman diagram. For this purpose the Feynman diagrams for the process  $\emptyset \rightarrow q\bar{q}gg$  have been drawn in fig. 3.1. We start by defining a *chain* as an object of the form  $(a_1 \dots a_n)_{ij}$ . Notice that  $\delta_{ij}$  is also a chain. A trace occurs when a chain is closed with  $i = j$ . In a Feynman diagram the colour flows from external line to external line in a predefined direction for which we take the clockwise direction.  $F$  can be constructed as follows. A chain is started at a random external line. For each external particle encountered a colour object is added to the chain. This object is a  $\delta_{iR}$  for a quark with colour  $i$ , a  $\delta_{iL}$  for an antiquark with colour  $j$  and a  $(a)_{i_L i_R}$  for a gluon with colour  $a$ . The  $i_L$  and  $i_R$  will be contracted with colour indices  $i_R$  and  $i_L$  coming from the previous and the next colour objects. This procedure is repeated until the starting external line is encountered. To illustrate this way of constructing  $F$ 's from Feynman diagrams we apply it to the first diagram in fig. 3.1. Start at gluon 1 and go round in clockwise direction. The colour structure develops as

$$(a_1)_{i_L i_R} \rightarrow (a_1 a_2)_{i_L i_R} \rightarrow (a_1 a_2)_{i_L j} \rightarrow (a_1 a_2)_{ij}. \quad (3.5.14)$$

So the first diagram contributes to  $F(T^a, N, i) = (a_1 a_2)_{ij}$ . Treating the third diagram this way we find the colour structure to be the same. However the two gluons can be interchanged which changes the colour structure to  $(a_2 a_1)_{ij}$ . This means that the third diagram contributes to both  $(a_1 a_2)_{ij}$  and  $(a_2 a_1)_{ij}$ . However not with the same  $K_F(P)$

as will be shown below. The claim is that no other colour structures exist for the process in fig. 3.1. For instance  $(a_1 a_2) \delta_{ij}$  does not exist or equivalently, has a  $K_F(P)$  which is zero. Before continuing with this example we look more closely at the way the Feynman diagrams have to be drawn so that the corresponding  $F$  can be read.

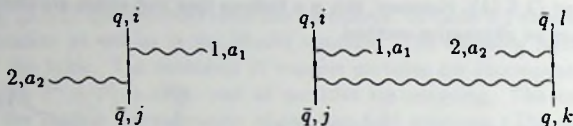


Fig. 3.2. Examples of Feynman diagrams in colour decomposition notation.

The Feynman diagrams must be drawn in the normal way with two restrictions

- The moment a chain is closed from the right, i.e. when an antiquark is encountered, a new chain must be started from a quark line. This implies that no external gluons should be in between an antiquark and the next quark. The first diagram in fig. 3.2 is therefore an illegal way of drawing a diagram.
- Because a chain ultimately starts with a quark colour index and ends with an antiquark index we must take care to encounter them alternately. In the second graph in fig. 3.2 an example is given how to draw a diagram with more quark pairs.

The rules given so far do not produce explicit  $N$  dependent colour structures which are known to appear in processes with more than one quark pair. The  $N$  are generated by an additional trick: removing some internal gluon lines in processes with more than one quark pair. Removal of a gluon propagator which connects two quark lines divides the diagram in two parts. On the level of colour structures this corresponds to performing the colour sum over the  $T^a$ 's occurring at both sides of the gluon propagator. A factor  $-1/N$  is added to the product of the colour structures of each of the two parts. These colour structures are again obtained with the method sketched above, applied to the separate parts. The propagator to be removed should not be connected to other particles than the two quark lines mentioned. This method of removing gluon propagators must be applied recursively to the separated parts.

As an example we look at the second diagram in fig. 3.2. As it is drawn the colour structure reads:  $(a_1 a_2)_{ij} \delta_{kj}$ . Leaving out the propagator gives:  $-1/N (a_1)_{ij} (a_2)_{kl}$ . The way of drawing the diagram has not changed and therefore the dynamical contribution to both  $F$ 's is the same. This example shows that sometimes more  $F$ 's are obtained from the same diagram without rearranging particles.

The method sketched above answers the first question raised in the beginning of this section: Not all possible  $F$ 's occur. The reason for this is both simple and complicated. The dynamical contributions to other kinds of colour structures add up to zero. In

chapter 4 this will be shown for purely gluonic processes. Here it suffices to note that from the same diagram with 1 and 2 interchanged one also gets an  $\frac{1}{N} \delta_{ij}(a_1 a_2)$ , but with a dynamical part that is the same except for the sign. These two contributions cancel because  $(a_1 a_2) = (a_2 a_1)$ . Notice that interchanging 1 and 2 is not part of the  $\sum_{\text{perms}}$  in eq. (3.5.12). It is just drawing the same diagram in a different way.

Having introduced a way to read the colour structure from a diagram, we need to adapt the Feynman rules. The new rules will be called colourless Feynman rules. We derive them using the example in fig. 3.1 and by rewriting the colour structures that appear in the QCD vertices in terms of  $(a)$ 's.

With the Feynman rules of table 3.1 the process of fig. 3.1 can be evaluated. The matrix element reads

$$\mathcal{M} = -ig^2 \left\{ (a_1 a_2)_{ij} \bar{u}(q) \not{\epsilon}_1 \frac{(\not{q} + \not{1})}{(q+1)^2} \not{\epsilon}_2 v(\bar{q}) + (a_2 a_1)_{ij} \bar{u}(q) \not{\epsilon}_2 \frac{(\not{q} + \not{2})}{(q+2)^2} \not{\epsilon}_1 v(\bar{q}) - i f^{a_1 a_2 a} (a)_{ij} \frac{\bar{u}(q) \gamma_\mu v(\bar{q})}{(q+\bar{q})^2} V^{\epsilon_1 \epsilon_2 \mu}(1, 2, -1-2) \right\} \quad (3.5.15)$$

where the gluon momenta are denoted by 1 and 2. With eqs. (3.5.5) and (3.5.7), it follows that

$$f^{a_1 a_2 a} (a)_{ij} = -i \{ (a_1 a_2)_{ij} - (a_2 a_1)_{ij} \}. \quad (3.5.16)$$

Therefore the third term contributes to both  $(a_1 a_2)_{ij}$  and  $(a_2 a_1)_{ij}$  as has been indicated above. The function  $V^{\mu_1 \mu_2 \mu_3}(1, 2, -1-2)$  is independent of the colour structure. It has the correct symmetry when gluons 1 and 2 are interchanged. From this example the following colourless Feynman rules can be inferred: The quark-gluon vertex remains the same, stripped from its colour part.

Looking in more detail at the gauge boson vertices and using eq. (3.5.5) one finds for the three-gluon vertex

$$-ig f^{a_1 a_2 a_3} V^{\mu_1 \mu_2 \mu_3}(1, 2, 3) = 2g \sum_{P(12)} (a_1 a_2 a_3) \hat{V}^{\mu_1 \mu_2 \mu_3}(1, 2, 3), \quad (3.5.17)$$

with the colourless Feynman rule for the three-gluon vertex given by

$$\hat{V}^{\mu_1 \mu_2 \mu_3}(1, 2, 3) = ig V^{\mu_1 \mu_2 \mu_3}(1, 2, 3). \quad (3.5.18)$$

One sees that a three-gluon vertex contributes to two different sets of  $F$ 's, corresponding with the two possible ways to draw this vertex. The factor 2 in eq. (3.5.17) must be kept with the colour part. In case one of the colour labels is internal this factor 2 cancels the  $\frac{1}{2}$  that arises from the use eq. (3.5.7). The four-gluon vertex is treated in the same manner. We find that

$$-ig^2 W_{a_1 a_2 a_3 a_4}^{\mu_1 \mu_2 \mu_3 \mu_4} = 2g^2 \sum_{P(123)} (a_1 a_2 a_3 a_4) \hat{W}^{\mu_1 \mu_2 \mu_3 \mu_4}, \quad (3.5.19)$$

with

$$\hat{W}^{\mu_1 \mu_2 \mu_3 \mu_4} = i \{ 2g^{\mu_1 \mu_3} g^{\mu_2 \mu_4} - g^{\mu_1 \mu_2} g^{\mu_3 \mu_4} - g^{\mu_1 \mu_4} g^{\mu_2 \mu_3} \}. \quad (3.5.20)$$

From eq. (3.5.19) it follows that the four-gluon vertex contributes to six different sets of  $F$ 's but with different contributions. They correspond to the six ways this vertex can be drawn.

Analyzing the colour structure in detail shows that a factor  $(\frac{1}{2})^{l-1}$ , with  $l$  the number of quark pairs, remains when the summation over all internal colour labels is carried out. Finally we also leave out all  $i$ 's that appear in the colourless Feynman rules and in the gluon-propagator the  $-$  sign too. The result for each diagram must then be multiplied with  $(i)^{n_q}$ , with  $n_q$  the number of quark-propagators. This rule is based on the fact that for every gluon-vertex, which has an  $i$ , there is an corresponding gluon-propagator which has a  $-i$ .

A summary of the colourless Feynman rules for QCD.

- The matrix element is decomposed in colour structures  $F(T^a, i, N)$  and subamplitudes  $K_F(P)$  as in eq. (3.5.12).
- To which  $F$ 's a diagram contributes can be determined by the method sketched in this section.
- The  $K_F(P)$  is obtained by applying the colourless Feynman rules to the Feynman diagrams drawn accordingly the rules described above, using the modified versions of eqs. (3.5.18) and (3.5.20) and the modified propagators and adding all contributions to the same  $F(T^a, i, N)$ .

The colourless Feynman rules are the basic building blocks of the recursion relation techniques in chapter 4. What the recursion relations actually do is adding up directly those diagrams that contribute to the same  $F(T^a, i, N)$ .

## 3.6 Examples of Weyl-van der Waerden spinor calculus

Before we calculate a number of elementary particle scattering processes in WvdW spinor language, we look at gauge spinor choices in a more general way. In particular how the helicity vectors show up in Feynman diagrams and how they are contracted with other vectors and spinors. To this end processes with only massless particles are examined, mainly because they illustrate the possibilities the best. When masses come into play the expressions become more involved and the simplifications that arise because of clever spinor choices are more modest. But even in those cases the spinor techniques work very well, see section 3.6.4. An important remark which holds for all the examples in this section is that most of the time physical scattering processes are examined but in the calculations all the particles are taken to be outgoing.

We distinguish between processes with and without fermions. As an example of the first group the process  $e^+e^- \rightarrow \gamma\gamma$  is calculated in section 3.6.1. Here we just have a look at the vertex at the positron side, which schematically reads  $\not{\epsilon}(k)v(p) \equiv e^{AB} p_B$  when the

positron has negative helicity. By making use of the explicit representation of the helicity vectors of the photon, see eqs. (3.4.11) and (3.4.12) and setting  $b = p$  results in

$$\sqrt{2} \frac{k^A p^B}{(kp)} p_B = 0 \quad \text{for the } + \text{ helicity.} \quad (3.6.1)$$

$$\sqrt{2} \frac{p^A k^B}{(kp)^*} p_B = -\sqrt{2} p^A \frac{(kp)}{(kp)^*}. \quad \text{for the } - \text{ helicity.} \quad (3.6.2)$$

So with the choice  $b = p$  some diagrams vanish. This immediately implies that the helicity configurations where all photons have the + helicity are zero. Of course equivalent choices hold for  $e^- \gamma$ -vertex and for other helicity configurations. From this experience we conclude: in processes with fermions and bosons it is a good choice to set the gauge spinor equal to the momentum spinor of one of the fermions, see section 3.6.1

The examples in sections 3.6.2 and 3.6.3 deal with processes where only bosons are present. We start with a general analysis of such processes [15]. Write down the Feynman diagrams and apply the relevant Feynman rules. Without the presence of  $\gamma$ -matrices only three types of terms can appear in the numerator, these are  $(K_i \cdot K_j)$ ,  $(K_i \cdot \epsilon_j)$  and  $(\epsilon_i \cdot \epsilon_j)$ . For spin- $m$  particles the polarization vectors can be rewritten as dyads of  $m$  spin-1 polarization vectors. The expressions are simplified by using the gauge spinors in such a way that as many inner products as possible vanish. The particular choices of gauge spinors that accomplish this we call *minimal gauge* choices. This choice depends on the helicity configuration but is always easy to find. Without loss of generality the  $n$  particles are ordered in such a way that particles 1 through  $l$  have positive helicity and that particles  $l+1$  through  $n$  have negative helicity.

$$e_i^{AB} = \sqrt{2} \frac{k_i^A b_i^B}{(k_i b_i)} \quad (i \leq l) \quad e_i^{AB} = \sqrt{2} \frac{k_i^B b_i^A}{(k_i b_i)^*} \quad (i > l). \quad (3.6.3)$$

Setting all  $b_i = k_n$  for  $i \leq l$  and  $b_i = k_1$  for  $i > l$  is a minimal gauge choice. In case  $l < 2$  or  $l \geq n-1$  this choice results in all  $(\epsilon_i \cdot \epsilon_j) = 0$ , as can be easily checked. Notice that also  $(K_1 \cdot \epsilon_i) = 0$  for  $i > l$  and  $(K_n \cdot \epsilon_i) = 0$  for  $i \leq l$ . For other values of  $l$  there are non-zero inner products between helicity vectors. For example  $l = 2$  results in  $(\epsilon_2 \cdot \epsilon_3) \neq 0, \dots, (\epsilon_2 \cdot \epsilon_{n-1}) \neq 0$ . So for  $n = 4$  just one inner product is non-zero.

Next we look at a scattering process. The number of momenta that appear in the numerator is important. The amount of  $K$ 's depends on the interaction theory one considers and on the number of propagators in the Feynman diagram. Let us suppose that the three point coupling in spin- $m$  theories contains  $m$  momenta. The dimensionality is corrected by giving the coupling constant a dimension. Examples are:  $m = 1$  for Yang-Mills and  $m = 2$  for linearized gravitation. The terms with the fewest  $(\epsilon_i \cdot \epsilon_j)$  combinations have the most  $K$ 's. Looking for the diagrams with the most momenta in the numerator we find them to be diagrams with three vertices only. The numerators then contain  $m(n-2)$  momenta and  $nm$  helicity vectors. So at least  $m$   $(\epsilon_i \cdot \epsilon_j)$ 's are present in every expression. According to the minimal gauge choice this implies that the amplitude is zero when at most one helicity is different from all the others.

Replacing two three-vertices by one four-vertex changes the amount of  $K$ 's in the numerator to  $m(n-2) - 2$  resulting in at least  $m+1$   $(\epsilon_i \cdot \epsilon_j)$ 's in every term. In a minimal gauge choice this means that these diagrams only contribute when there are at least 3 particles with plus and 3 particles with minus helicity are available. Therefore in processes with  $n < 6$  the diagrams with four-vertices can be gauged away.

In subsequent sections we apply the results above. In more elaborate processes with all kind of particles, possibly massive, it is not always clear which choice for the gauge spinors is the best. However when it is not possible to get a lot of terms equal to zero, experience leads us to believe that the choice of spinors that simplifies the calculation the most is the choice where the normalization of the helicity vectors contains a physical pole.

### 3.6.1 The process $\emptyset \rightarrow e^+e^-\gamma\gamma$

The process

$$\emptyset \rightarrow e^+(P_+) e^-(P_-) \gamma(K_1) \gamma(K_2) \quad (3.6.4)$$

serves as an illustration that simple calculations become even simpler in the WvdW spinor formalism. By working out process (3.6.4) many aspects of the WvdW formalism will show up. The  $\emptyset$  in (3.6.4) denotes the vacuum and implies that all momenta are outgoing. We start by writing down the two Feynman diagrams in fig. 3.3.

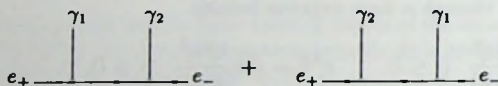


Fig. 3.3. The Feynman diagrams for  $\emptyset \rightarrow e^+e^-\gamma_1\gamma_2$ .

The matrix element becomes

$$\mathcal{M} = -ie^2 \left\{ \bar{u}(P_-) \not{\epsilon}_2 \frac{(\not{P}_- + \not{K}_2)}{(P_- + K_2)^2} \not{\epsilon}_1 v(P_+) + \bar{u}(P_-) \not{\epsilon}_1 \frac{(\not{P}_- + \not{K}_1)}{(P_- + K_1)^2} \not{\epsilon}_2 v(P_+) \right\} \quad (3.6.5)$$

Parity conservation allows us to fix the helicities of the fermions. Taking the + helicity for the electron and using the explicit representation for all particles  $\mathcal{M}$  is translated in WvdW spinor language with

$$\mathcal{M} = -ie^2 \left\{ p_{-\dot{A}} \epsilon_2^{\dot{A}B} \frac{(P_- + K_2)_{CB}}{\{P_-, K_2\}} \epsilon_1^{CD} p_{+D} + p_{-\dot{A}} \epsilon_1^{\dot{A}B} \frac{(P_- + K_1)_{CB}}{\{P_-, K_1\}} \epsilon_2^{CD} p_{+D} \right\} \quad (3.6.6)$$

In table 3.2 the results for all four different helicity combinations of the photons are presented.

| $(\lambda_1, \lambda_2)$ | $\epsilon_1^{AB}$                          | $\epsilon_2^{AB}$                          | $\mathcal{M}$                                   |
|--------------------------|--------------------------------------------|--------------------------------------------|-------------------------------------------------|
| (+, +)                   | $\sqrt{2} \frac{k_1^A p_+^B}{(k_1 p_+)}$   | $\sqrt{2} \frac{k_2^A p_+^B}{(k_2 p_+)}$   | 0                                               |
| (+, -)                   | $\sqrt{2} \frac{k_1^A p_+^B}{(k_1 p_+)}$   | $\sqrt{2} \frac{p_+^A k_2^B}{(k_2 p_-)^*}$ | $-2ie^2 \frac{(k_2 p_+)^2}{(p_+ k_1)(k_1 p_-)}$ |
| (-, +)                   | $\sqrt{2} \frac{p_-^A k_1^B}{(k_1 p_-)^*}$ | $\sqrt{2} \frac{k_2^A p_+^B}{(k_2 p_+)}$   | $-2ie^2 \frac{(k_1 p_+)^2}{(p_+ k_2)(k_2 p_-)}$ |
| (-, -)                   | $\sqrt{2} \frac{p_-^A k_1^B}{(k_1 p_-)^*}$ | $\sqrt{2} \frac{p_+^A k_2^B}{(k_2 p_-)^*}$ | 0                                               |

Table 3.2. The four possible helicity configurations of the two photons.

As was shown in the introduction, the (+, +) and the (-, -) combinations vanish. The explicit representation for the helicity vectors is given as well. The spin summed matrix element squared,  $\sum_{\lambda} |\mathcal{M}|^2$  is trivially computed from the results in table 3.2 and reads

$$\sum_{\lambda} |\mathcal{M}|^2 = 8e^4 \left[ \frac{(K_2 \cdot P_+)^2 + (K_1 \cdot P_+)^2}{(P_+ \cdot K_1)(K_2 \cdot P_+)} \right] \quad (3.6.7)$$

which is the familiar result for process (3.6.4).

### 3.6.2 Four and five gluon scattering amplitudes

With the Feynman rules from section 3.5 we can compute all the helicity amplitudes for four and five gluon scattering. For simplicity we restrict ourselves to the evaluation of a few subamplitudes only. Recall that QCD amplitudes can be decomposed with eq. (3.3.31). In the case of purely gluonic processes the  $K_F(P)$  are denoted by  $\mathcal{C}$ -functions. These  $\mathcal{C}$ -functions are built up from the contribution of every diagram to a specific colour structure. Using the relations that exist between  $\mathcal{C}$ -functions, see chapter 4, we need to evaluate just two helicity combinations for both  $\mathcal{C}(1234)$  and  $\mathcal{C}(12345)$  to be able to obtain  $\sum_{c,\lambda} |\mathcal{M}_n|^2$  for  $n = 4$  and  $n = 5$ .

#### 3.6.2.1 $\mathcal{C}(1234)$

The subamplitude  $\mathcal{C}(1234)$  corresponds to the colour structure  $(a_1 a_2 a_3 a_4)$  and receives a contribution from the three diagrams in fig. 3.4. The third diagram has exactly two  $(\epsilon_i \cdot \epsilon_j)$ 's in every term. Therefore it vanishes in a minimal gauge choice, as was shown in the introduction of this section. Using colourless Feynman rules, see eqs. (3.5.18) and (3.5.20), the contribution of the first two diagrams to the colour structure  $(a_1 a_2 a_3 a_4)$  reads

$$\begin{aligned} \mathcal{C}(1234) = & \hat{V}_{\epsilon_1 \epsilon_2 \alpha} (K_1, K_2, -K_1 - K_2) \frac{g^{\alpha\beta}}{2(K_1 \cdot K_2)} \hat{V}_{\epsilon_3 \epsilon_4 \beta} (K_3, K_4, -K_3 - K_4) \\ & + \hat{V}_{\epsilon_4 \epsilon_1 \alpha} (K_4, K_1, -K_1 - K_4) \frac{g^{\alpha\beta}}{2(K_4 \cdot K_1)} \hat{V}_{\epsilon_2 \epsilon_3 \beta} (K_2, K_3, -K_2 - K_3) \end{aligned} \quad (3.6.8)$$

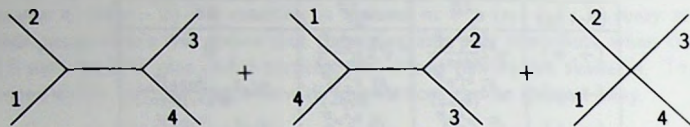


Fig. 3.4. The Feynman diagrams contributing to the  $C(1234)$ -function.

After substituting eq. (3.5.18) in eq. (3.6.8) and using that  $(K_i \cdot \epsilon_i) = 0$  a lot of terms remain. However because we are in a minimal gauge choice most of these terms vanish. Utilizing the relations between the  $C$ -functions we only need to evaluate the  $C(++--)$  and the  $C(+--+)$  helicity combinations, where the helicities correspond to the particles 1, 2, 3 and 4. For both cases  $b_+ = k_4$  and  $b_- = k_1$  is a minimal gauge choice. Expressions that have a  $(\epsilon_2 \cdot \epsilon_3)$  remain, all the other terms are directly zero. Expression (3.6.8) simplifies enormously and becomes

$$C(1234) = -2(\epsilon_2 \cdot \epsilon_3) \frac{(\epsilon_1 \cdot K_2)(\epsilon_4 \cdot K_3)}{(K_1 \cdot K_2)} \quad (3.6.9)$$

Translation of eq. (3.6.9) into spinor language is easy using the following representation of the minimal gauge choices. For  $C(++--)$  we have

$$\epsilon_1^{AB} = \sqrt{2} \frac{1^A 4^B}{\langle 14 \rangle} \quad \epsilon_2^{AB} = \sqrt{2} \frac{2^A 4^B}{\langle 24 \rangle} \quad \epsilon_3^{AB} = \sqrt{2} \frac{1^A 3^B}{\langle 31 \rangle} \quad \epsilon_4^{AB} = \sqrt{2} \frac{1^A 4^B}{\langle 41 \rangle} \quad (3.6.10)$$

and for  $C(+--+)$

$$\epsilon_1^{AB} = \sqrt{2} \frac{1^A 4^B}{\langle 14 \rangle} \quad \epsilon_2^{AB} = \sqrt{2} \frac{1^A 2^B}{\langle 21 \rangle} \quad \epsilon_3^{AB} = \sqrt{2} \frac{3^A 4^B}{\langle 34 \rangle} \quad \epsilon_4^{AB} = \sqrt{2} \frac{1^A 4^B}{\langle 41 \rangle} \quad (3.6.11)$$

The use of these representations and the use of momentum conservation, for instance  $\langle 21 \rangle \langle 32 \rangle = -\langle 14 \rangle \langle 43 \rangle$ , results in

$$C(++--) = \frac{(\sqrt{2})^4}{2} \frac{\langle 34 \rangle^4}{\langle 12 \rangle \langle 23 \rangle \langle 34 \rangle \langle 41 \rangle} = \frac{(\sqrt{2})^4}{2} \frac{\langle 12 \rangle^{\bullet 4}}{\langle 12 \rangle^{\bullet} \langle 23 \rangle^{\bullet} \langle 34 \rangle^{\bullet} \langle 41 \rangle^{\bullet}} \quad (3.6.12)$$

$$C(+--+)= \frac{(\sqrt{2})^4}{2} \frac{\langle 24 \rangle^4}{\langle 12 \rangle \langle 23 \rangle \langle 34 \rangle \langle 41 \rangle} = \frac{(\sqrt{2})^4}{2} \frac{\langle 13 \rangle^{\bullet 4}}{\langle 12 \rangle^{\bullet} \langle 23 \rangle^{\bullet} \langle 34 \rangle^{\bullet} \langle 41 \rangle^{\bullet}} \quad (3.6.13)$$

We will soon see that these elegant expressions for the  $C$ -functions have a simple generalization for processes with more gluons. The  $|\sum_{c,\lambda} \mathcal{M}_4|^2$  reads

$$\sum_{c,\lambda} |\mathcal{M}_4|^2 = \sum_{hcls} \left| 2g^2 \sum_{P(234)} \text{Tr}(T^{a_1} T^{a_2} T^{a_3} T^{a_4}) C(1234) \right|^2. \quad (3.6.14)$$

With eq. (3.6.14), using colour sum rules, one finds that the contribution of non-leading order terms in the colour polynomials cancel and that the result is

$$\sum_{c,\lambda} |\mathcal{M}_4|^2 = g^4 N^2 (N^2 - 1) \times \left( \sum_{i=1}^3 \sum_{j=i+1}^4 (i \cdot j)^4 \right) \times \left( \sum_{P(234)} \frac{1}{(1 \cdot 2)(2 \cdot 3)(3 \cdot 4)(4 \cdot 1)} \right) \quad (3.6.15)$$

### 3.6.2.2 $\mathcal{C}(12345)$

The  $\mathcal{C}(12345)$ -function is build up from the 10 diagrams in fig. 3.5. The sum contains

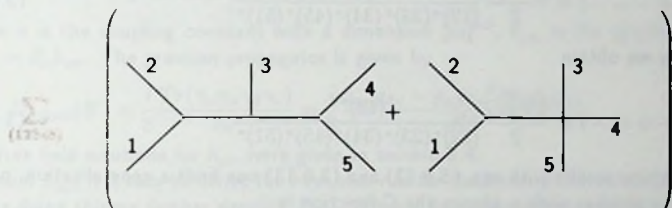


Fig. 3.5. The Feynman diagrams contributing to the  $\mathcal{C}(12345)$ -function.

the five cyclic permutations of (12345). The diagrams with the four-vertex result in expressions that contain 1 momentum and 5 helicity vectors in the numerator, therefore at least two  $(\epsilon_i \cdot \epsilon_j)$ 's are present and these diagrams do not contribute in a minimal gauge choice. The  $\mathcal{C}$ -function in terms of colourless Feynman rules is given by

$$\mathcal{C}(12345) = \sum_{C(12345)} \left\{ \hat{V}_{\epsilon_1 \epsilon_2 \alpha}(K_1, K_2, -K_1 - K_2) \frac{g^{\alpha\beta}}{2(K_1 \cdot K_2)} \times \hat{V}_{\epsilon_3 \gamma}(K_1 + K_2, K_3, K_4 + K_5) \frac{g^{\gamma\delta}}{2(K_4 \cdot K_5)} \hat{V}_{\epsilon_4 \epsilon_5 \delta}(K_4, K_5, -K_4 - K_5) \right\}. \quad (3.6.16)$$

We only have to evaluate two helicity combinations:  $\mathcal{C}(+ + - - -)$  and  $\mathcal{C}(+ - + - -)$ . All other  $\mathcal{C}$ -functions can be obtained by parity conservation and other properties of  $\mathcal{C}$ -functions. We take for a minimal gauge choice:  $b_+ = k_5$  and  $b_- = k_1$ . This leads to  $(\epsilon_2 \cdot \epsilon_3) \neq 0$  and  $(\epsilon_2 \cdot \epsilon_4) \neq 0$  for  $\mathcal{C}(+ + - - -)$  and equivalently the only non-zero inner products for  $\mathcal{C}(+ - + - -)$  are  $(\epsilon_2 \cdot \epsilon_3)$  and  $(\epsilon_3 \cdot \epsilon_4)$ . In this minimal gauge choice eq. (3.6.16) immediately leads to

$$\mathcal{C}(+ + - - -) = \frac{+2(\epsilon_1 \cdot K_2)}{(K_1 \cdot K_2)(K_4 \cdot K_5)} \times \quad (3.6.17)$$

$$\begin{aligned}
& [+(\epsilon_2 \cdot \epsilon_3)(\epsilon_4 \cdot K_3)(\epsilon_5 \cdot K_4) - (\epsilon_2 \cdot \epsilon_3)(\epsilon_4 \cdot K_5)(\epsilon_5 \cdot K_3) + (\epsilon_2 \cdot \epsilon_4)(\epsilon_3 \cdot K_2)(\epsilon_5 \cdot K_4)] \\
& \quad \frac{+2(\epsilon_1 \cdot K_2)}{(K_1 \cdot K_2)(K_3 \cdot K_4)} \times \\
& [- (\epsilon_2 \cdot \epsilon_3)(\epsilon_4 \cdot K_3)(\epsilon_5 \cdot K_2) + (\epsilon_2 \cdot \epsilon_4)(\epsilon_3 \cdot K_4)(\epsilon_5 \cdot K_2)] \\
& \quad \frac{+2(\epsilon_1 \cdot K_4)}{(K_2 \cdot K_3)(K_4 \cdot K_5)} \times \\
& [- (\epsilon_2 \cdot \epsilon_3)(\epsilon_4 \cdot K_3)(\epsilon_5 \cdot K_4) + (\epsilon_2 \cdot \epsilon_3)(\epsilon_4 \cdot K_5)(\epsilon_5 \cdot K_3) - (\epsilon_2 \cdot \epsilon_4)(\epsilon_3 \cdot K_2)(\epsilon_5 \cdot K_4)]
\end{aligned}$$

With the explicit representation of the helicity vectors, the analogue of eq. (3.6.10), momentum conservation and the use of eqs. (3.2.10) and (3.2.11) one quickly arrives at

$$C(+ + - - -) = \frac{(\sqrt{2})^5}{2} \frac{\langle 12 \rangle^{*4}}{\langle 12 \rangle^* \langle 23 \rangle^* \langle 34 \rangle^* \langle 45 \rangle^* \langle 51 \rangle^*}, \quad (3.6.18)$$

and similarly we obtain

$$C(+ - + - -) = \frac{(\sqrt{2})^5}{2} \frac{\langle 13 \rangle^{*4}}{\langle 12 \rangle^* \langle 23 \rangle^* \langle 34 \rangle^* \langle 45 \rangle^* \langle 51 \rangle^*}, \quad (3.6.19)$$

Comparing these results with eqs. (3.6.12) and (3.6.13) one finds a generalization, proven in [16]. For a process with  $n$  gluons the  $C$ -function is

$$C(12 \dots n) = \frac{(\sqrt{2})^n}{2} \frac{\langle ij \rangle^{*4}}{\langle 12 \rangle^* \langle 23 \rangle^* \dots \langle n1 \rangle^*}, \quad (3.6.20)$$

where gluons  $i$  and  $j$  have the plus helicity. With this general form it follows that

$$\begin{aligned}
\sum_{\epsilon, \lambda} |\mathcal{M}_S|^2 &= g^6 N^3 (N^2 - 1) \times \\
& \left( \sum_{i=1}^4 \sum_{j=i+1}^5 (i \cdot j)^4 \right) \times \left( \sum_{P(2345)} \frac{1}{(1 \cdot 2)(2 \cdot 3)(3 \cdot 4)(4 \cdot 5)(5 \cdot 1)} \right)
\end{aligned} \quad (3.6.21)$$

Again only the leading order terms in the colour matrix remain. For  $n = 6$  this is no longer the case, see chapter 10.

### 3.6.3 Graviton scattering amplitudes

In this example we discuss  $2 \rightarrow 2, 3, 4$  graviton scattering. For our purpose it is not relevant whether the spin-2 particle of linearized gravitation corresponds to the carrier of the gravitational force. What we want to demonstrate is that the use of WvdW spinor calculus simplifies the calculation of scattering processes with gravitons. To this end we start by discussing the interaction Lagrangian,  $L_{222}$ , and subsequently calculate the  $2 \rightarrow 2$  graviton process. Then we give results for  $2 \rightarrow 3, 4$  graviton scattering when two particles have the  $+$  and the others have the  $-$  helicity. Finally the collinear limit of these amplitudes is examined. For clarity all Lorentz indices are lowered.

### 3.6.3.1 Interaction Lagrangian for linearized gravitation

Since we perform the calculation in a minimal gauge choice for two helicities equal and the rest opposite, it is sufficient to know the interaction Lagrangian between three gravitons. Diagrams with four-vertices result in too many inner products between helicity vectors: some of them must be zero. The  $L_{222}$  is given in [5, 17]. A detailed derivation of the gravitational interaction Lagrangian can be found in [18].

$$\begin{aligned}
 L_{222} = & \kappa \left[ +h_{\mu\nu,\nu}h_{\mu\rho,\rho}h_{\sigma\sigma} - \frac{3}{2}h_{\mu\nu,\rho}h_{\mu\rho,\nu}h_{\sigma\sigma} + \frac{1}{4}h_{\mu\nu,\rho}h_{\mu\nu,\rho}h_{\sigma\sigma} \right. \\
 & + \frac{1}{2}h_{\mu\nu,\nu}h_{\rho\rho,\mu}h_{\sigma\sigma} - \frac{1}{4}h_{\nu\nu,\mu}h_{\rho\rho,\mu}h_{\sigma\sigma} - 2h_{\nu\nu,\mu}h_{\mu\rho,\sigma}h_{\rho\sigma} + h_{\mu\nu}h_{\mu\sigma,\rho}h_{\nu\rho,\sigma} \\
 & + 2h_{\mu\nu}h_{\nu\rho,\sigma}h_{\rho\sigma,\mu} - h_{\mu\nu}h_{\mu\rho,\sigma}h_{\nu\rho,\sigma} - \frac{1}{2}h_{\mu\nu}h_{\rho\sigma,\mu}h_{\rho\sigma,\nu} \\
 & \left. + \frac{1}{2}h_{\mu\nu}h_{\sigma\sigma,\mu}h_{\rho\rho,\nu} - h_{\nu\mu,\nu}h_{\rho\sigma,\mu}h_{\rho\sigma} + h_{\nu\nu,\mu}h_{\rho\sigma,\mu}h_{\rho\sigma} \right], \quad (3.6.22)
 \end{aligned}$$

where  $\kappa$  is the coupling constant with a dimension  $[m]^{-1}$ ,  $h_{\mu\nu}$  is the graviton field and  $h_{\rho\sigma,\mu} = \partial_\mu h_{\rho\sigma}$ . The graviton-propagator is given by

$$D_{\alpha\beta\gamma\delta}(\vec{k}) = \frac{i}{8} \frac{\text{Tr}(\gamma_\alpha \gamma_\mu \gamma_\beta \gamma_\nu)}{K^2} = \frac{i}{2} \frac{g_{\alpha\mu}g_{\beta\nu} - g_{\alpha\beta}g_{\mu\nu} + g_{\alpha\nu}g_{\beta\mu}}{K^2}. \quad (3.6.23)$$

The free field solutions for  $h_{\mu\nu}$  were given in section 3.4.

From  $L_{222}$  it is easy to derive the Feynman rule for the three-graviton vertex. However, before doing this we further simplify  $L_{222}$ . When a  $h_{\mu\mu}$  corresponds with an internal field it leads to the formation of  $(\epsilon_i \cdot \epsilon_j)$ 's that are zero. For a similar reason interaction terms with  $h_{\mu\nu,\nu}$  can be dropped. From eq. (3.6.22) the following terms remain in  $L_{222}^{\text{mgc}}$ , the interaction Lagrangian in a minimal gauge choice.

$$\begin{aligned}
 L_{222}^{\text{mgc}} = & \kappa \left[ +h_{\mu\nu}h_{\mu\sigma,\rho}h_{\nu\rho,\sigma} + 2h_{\mu\nu}h_{\nu\rho,\sigma}h_{\rho\sigma,\mu} \right. \\
 & \left. - h_{\mu\nu}h_{\mu\rho,\sigma}h_{\nu\rho,\sigma} - \frac{1}{2}h_{\mu\nu}h_{\rho\sigma,\mu}h_{\rho\sigma,\nu} \right]. \quad (3.6.24)
 \end{aligned}$$

The corresponding vertex reads

$$\begin{aligned}
 V_{\mu_1\nu_1;\mu_2\nu_2;\mu_3\nu_3}^{\text{mgc}}(K_1, K_2, K_3) = & \quad (3.6.25) \\
 -i\kappa \sum_{P(123)} & \left[ +g_{\mu_1\nu_1}g_{\nu_1\mu_2}K_{2\nu_2}K_{3\nu_2} - g_{\mu_1\nu_2}g_{\nu_1\mu_3}g_{\nu_2\nu_3}(K_2 \cdot K_3) \right. \\
 & \left. + 2g_{\nu_1\nu_2}g_{\nu_2\nu_3}K_{2\nu_2}K_{3\nu_1} - \frac{1}{2}g_{\mu_2\nu_2}g_{\nu_2\nu_3}K_{2\nu_1}K_{3\nu_1} \right],
 \end{aligned}$$

where  $K_1, K_2$  and  $K_3$  are outgoing momenta and use has been made of  $h_{\mu\nu} = h_{\nu\mu}$ .

### 3.6.3.2 The process: $\emptyset \rightarrow 4$ gravitons.

With eqs. (3.6.23) and (3.6.24) we evaluate the four graviton scattering process. Denoting the amplitudes by  $G(+ + \dots)$  we only need to determine the  $G(+ + \dots)$  helicity combination. Other helicity combinations can either be obtained by renumbering the gravitons or are zero. In the minimal gauge choice of eq. (3.6.10) the three possible diagram with two three-graviton vertices give the following contributions

$$G(+ + \dots)|_{\text{o-channel}} = -i\kappa^2 \frac{(\epsilon_2 \cdot \epsilon_3)^2 (\epsilon_1 \cdot K_2)^2 (\epsilon_4 \cdot K_3)^2}{2(K_1 \cdot K_2)}, \quad (3.6.26)$$

$$G(+ + \dots) |_{t\text{-channel}} = -i\kappa^2 \frac{(\epsilon_2 \cdot \epsilon_3)^2 (\epsilon_1 \cdot K_3)^2 (\epsilon_4 \cdot K_2)^2}{2(K_1 \cdot K_3)}, \quad (3.6.27)$$

$$G(+ + \dots) |_{u\text{-channel}} = 0. \quad (3.6.28)$$

Using the explicit representation for the helicity vectors we find

$$G(+ + \dots) = -i \left(\frac{\kappa}{2}\right)^2 \frac{\langle 12 \rangle^{*8}}{N^*(4)} \frac{\langle 12 \rangle^*}{\langle 34 \rangle^*}, \quad (3.6.29)$$

with

$$N(n) = \prod_{1 \leq i < j \leq n} \frac{1}{\langle ij \rangle}, \quad (3.6.30)$$

and  $N^*(n)$  its complex conjugate. Other helicity combinations follow from renumbering.

### 3.6.3.3 The processes: $\emptyset \rightarrow 5, 6$ gravitons.

Application of the method of the previous subsection to processes with more gravitons result in the following expressions for  $G(+ + (n-2)-)$

$$G(+ + \dots) = 4 \left(\frac{\kappa}{2}\right)^3 \frac{\langle 12 \rangle^{*8}}{N^*(5)} \mathcal{E}(1, 2, 3, 4) \quad (3.6.31)$$

$$G(+ + \dots) = 4 \left(\frac{\kappa}{2}\right)^4 \frac{\langle 12 \rangle^{*8}}{N^*(6)} \times \quad (3.6.32)$$

$$\begin{aligned} & [+ \langle 12 \rangle \langle 13 \rangle^* \langle 14 \rangle^* \langle 25 \rangle^* \langle 26 \rangle^* \mathcal{E}(2, 3, 4, 6) \\ & + \langle 26 \rangle \langle 12 \rangle^* \langle 25 \rangle^* \langle 36 \rangle^* \langle 46 \rangle^* \mathcal{E}(1, 2, 3, 4) \\ & + \langle 12 \rangle \langle 15 \rangle^* \langle 16 \rangle^* \langle 23 \rangle^* \langle 24 \rangle^* \mathcal{E}(1, 3, 4, 6) \\ & + \langle 23 \rangle \langle 12 \rangle^* \langle 24 \rangle^* \langle 35 \rangle^* \langle 36 \rangle^* \mathcal{E}(1, 3, 4, 6) ], \end{aligned}$$

with  $\mathcal{E}(1, 2, 3, 4)$  as defined in eq. (3.3.10). The minimal gauge choices that have been used are straightforward extensions of eq. (3.6.10). Comparing the various  $G(+ + (n-2)-)$ 's leads to the following generalization

$$G(+ + (n-2)-) = -i \left(\frac{\kappa}{2}\right)^{n-2} \frac{\langle 12 \rangle^{*8}}{N^*(n)} A(1, \dots, n). \quad (3.6.33)$$

Here  $A(1, \dots, n)$  is antisymmetric in all argument interchanges. However  $A$  becomes rapidly more complex for larger  $n$  [19].

### 3.6.3.4 Collinear gravitons.

In expressions (3.6.31) and (3.6.32) one can look at the case when two gravitons become collinear. The resulting expression has to be finite because collinear divergencies are not cancelled. The finiteness in this limit can easily be demonstrated by using eq. (3.3.10).

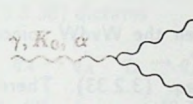
The soft graviton limit,  $E_5 \rightarrow 0$ , can be inferred. From eqs. (3.6.29) and (3.6.31) follows that

$$|G(++----)|^2 = \left(\frac{\kappa}{2}\right)^2 |G(++---)|^2 \frac{(34)^{\circ}}{(12)^{\circ}} \left[ \left( \sum_{1 \leq i < j \leq 4} \frac{(i \cdot j)^2}{(5 \cdot i)(j \cdot 5)} \right) - 3 \right] \quad (3.6.34)$$

Expression (3.6.34) can be derived on general quantum mechanical grounds [20]. In [21] it was shown that soft divergency cancels against virtual corrections.

### 3.6.4 Massive vector bosons

As an example how the residual freedom of polarization choice for massive vectors bosons, i.e. the freedom to choose  $M^\mu$ , can be used to simplify calculations we examine the non-abelian three boson vertex in the Standard Model. To be more specific, we look at the  $\gamma W^+ W^-$  vertex with the  $W$ 's on-shell. With all momenta outgoing this vertex reads



$$W^+, K_+, \mu \equiv A^{\alpha\mu\nu} = ie \{ +g^{\mu\alpha} (K_0 - K_+)^{\nu} + g^{\alpha\nu} (K_- - K_0)^{\mu} + g^{\nu\mu} (K_+ - K_-)^{\alpha} \}, \quad (3.6.35)$$

Contraction of  $A^{\alpha\mu\nu}$  with the polarization vectors,  $\epsilon_{\mu\lambda_+}(+)$  for the  $W^+$  and  $\epsilon_{\nu\lambda_-}(-)$  for the  $W^-$  and translation of  $A^\alpha$  into spinor language with  $A^\alpha = \frac{1}{2} \sigma_{\dot{A}B}^\alpha A^{\dot{A}B}$  we find for  $A^{\dot{A}B}$ :

$$A^{\dot{A}B}(\lambda_+, \lambda_-) = \frac{ie}{2} \left( -2\epsilon_{\lambda_+}^{\dot{A}B}(+) \{ \epsilon_{\lambda_-}(-), K_+ \} + 2\epsilon_{\lambda_-}^{\dot{A}B}(-) \{ \epsilon_{\lambda_+}(+), K_- \} + (K_+ - K_-)^{\dot{A}B} \{ \epsilon_{\lambda_+}(+), \epsilon_{\lambda_-}(-) \} \right). \quad (3.6.36)$$

Where we have used that  $\{ \epsilon_{\lambda_+}(+), K_+ \} = \{ \epsilon_{\lambda_-}(-), K_- \} = 0$  and  $K_0^\mu = -K_+^\mu - K_-^\mu$ . For the decomposition of  $K_+^{\dot{A}B}$  and  $K_-^{\dot{A}B}$  in massless vectors, see eqs. (3.2.35) and (3.4.37), we use the primary momentum of the other vector boson as choice for  $M^\mu$ . This results in

$$\begin{cases} K_+^{\dot{A}B} = K_1^{\dot{A}B} + \alpha_1 K_2^{\dot{A}B} \\ K_-^{\dot{A}B} = K_2^{\dot{A}B} + \alpha_2 K_1^{\dot{A}B} \end{cases} \quad (3.6.37)$$

When the masses of the  $W$ 's are both equal to  $M_W$  we have  $\alpha_1 = \alpha_2 = \alpha$ . This leads to the following polarization states, see eqs. (3.4.38)-(3.4.40).

$$\begin{aligned} \epsilon_+^{\dot{A}B}(+) &= \sqrt{2} \frac{k_1^{\dot{A}} k_2^{\dot{B}}}{\langle k_1 k_2 \rangle} & \epsilon_+^{\dot{A}B}(-) &= \sqrt{2} \frac{k_2^{\dot{A}} k_1^{\dot{B}}}{\langle k_2 k_1 \rangle} \\ \epsilon_-^{\dot{A}B}(+) &= \sqrt{2} \frac{k_2^{\dot{A}} k_1^{\dot{B}}}{\langle k_1 k_2 \rangle} & \epsilon_-^{\dot{A}B}(-) &= \sqrt{2} \frac{k_1^{\dot{A}} k_2^{\dot{B}}}{\langle k_2 k_1 \rangle} \\ \epsilon_0^{\dot{A}B}(+) &= \frac{k_1^{\dot{A}} k_1^{\dot{B}} - \alpha k_2^{\dot{A}} k_2^{\dot{B}}}{M_W} & \epsilon_0^{\dot{A}B}(-) &= \frac{k_2^{\dot{A}} k_2^{\dot{B}} - \alpha k_1^{\dot{A}} k_1^{\dot{B}}}{M_W} \end{aligned} \quad (3.6.38)$$

This results in most of the inner products being zero, a complete list involves

$$\begin{aligned}
 \{K_+, \epsilon_{\pm}(-)\} &= 0 & \{\epsilon_{\mp}(+), \epsilon_{\pm}(-)\} &= 0 \\
 \{K_-, \epsilon_{\pm}(+)\} &= 0 & \{\epsilon_{\pm}(+), \epsilon_0(-)\} &= 0 \\
 \{\epsilon_{\pm}(-), \epsilon_0(+)\} &= 0 & \{\epsilon_0(+), \epsilon_0(-)\} &= (1 + \alpha^2)/\alpha \\
 \{\epsilon_+(+), \epsilon_+(-)\} &= 2\langle km \rangle^* / \langle km \rangle & \{\epsilon_-(+), \epsilon_-(-)\} &= 2\langle km \rangle / \langle km \rangle^* \\
 \{K_+, \epsilon_0(-)\} &= M_W(1 - \alpha^2)/\alpha & \{K_-, \epsilon_0(+)\} &= M_W(1 - \alpha^2)/\alpha
 \end{aligned} \quad (3.6.39)$$

Substituting eq. (3.6.39) in eq. (3.6.36) results in short expressions for all  $A^{\hat{A}B}(\lambda_+, \lambda_-)$ 's. Two of them are zero:  $A^{\hat{A}B}(+, -)$  and  $A^{\hat{A}B}(-, +)$ .

### 3.7 Numerical implementation of Weyl-van der Waerden spinors

In this section we briefly discuss two problems that arise when the WvdW spinors of section 3.3 are used in a numerical application.

The first problem concerns the representation of  $k_A$ , see eq. (3.2.33). There is a unphysical pole at  $K_0 = K_3$ . In a Monte Carlo simulation this would not pose a problem because no events with exactly this property would be evaluated. However it is standard practice to have the beam parallel to the 3- or z-axis. Therefore this pole must be removed. A solution is to rotate the space by means of  $x \rightarrow y \rightarrow z \rightarrow x$ . This preserves the right- and left-handedness of the particles.

The second problem is that when scattering processes are calculated, this is done with all momenta outgoing. This can pose a problem when explicit results are used for helicity states and one has to cross one or more partons from outgoing to incoming.

When the parton is an outgoing gluon it is characterized by a momentum  $K$  and polarization vector  $\epsilon_{\lambda}$ . The matrix element is a function  $\mathcal{M}(K, \epsilon_{\lambda}(K))$  and in spinor language a function  $\mathcal{M}(k_A, k_{\dot{A}})$ . When the gluon is incoming with momentum  $K'$  and helicity  $-\lambda$  the matrix element is obtained from the previous one by taking  $\mathcal{M}(-K', \epsilon_{\lambda}(-K')) = \mathcal{M}(-K', \epsilon_{-\lambda}(K'))$ . The spinors  $k_A$  and  $k_{\dot{A}}$  are related to the corresponding momentum by eq. (3.2.33) and the complex conjugated equation. The amplitude for the process with an incoming gluon takes the form  $\mathcal{M}(ik'_A, ik'_{\dot{A}})$ . For the spinors arising from momenta this prescription is obviously correct. For the spinors arising from the polarization vectors this is also the case, since under the replacement

$$k_A \rightarrow ik'_A, \quad k_{\dot{A}} \rightarrow ik'_{\dot{A}} \quad (3.7.1)$$

and consequently

$$\langle pk \rangle \rightarrow i\langle pk' \rangle, \quad \langle pk \rangle^* \rightarrow i\langle pk' \rangle^*, \quad (3.7.2)$$

we have according to eqs. (3.4.11) and (3.4.12)

$$\epsilon_{+\hat{A}B}(K) \rightarrow \sqrt{2} \frac{k'_{\hat{A}} g_B}{\langle g k' \rangle} = \epsilon_{-\hat{A}B}(K'), \quad (3.7.3)$$

$$\epsilon_{-\dot{A}B}(K) \rightarrow \sqrt{2} \frac{g_A k'_B}{(g k')^*} = \epsilon_{+\dot{A}B}(K'). \quad (3.7.4)$$

For the quarks one can use a similar replacement as in eq. (3.7.1) i.e.

$$q_A \rightarrow i q'_A, \quad q_{\dot{A}} \rightarrow i q'_{\dot{A}}, \quad (3.7.5)$$

when the incoming antiquark has a physical momentum  $Q'$ , whereas the outgoing quark had momentum  $Q$ . Denoting the known amplitude by  $\mathcal{M}(Q, \bar{v}_\lambda(Q))$  we have as amplitude for the crossed process  $\mathcal{M}(-Q', \bar{v}_\lambda(Q'))$ . For the substitution  $Q \rightarrow -Q'$  eq. (3.7.5) is adequate, however when we make the replacement

$$\bar{u}_\lambda(Q) \rightarrow \bar{v}_{-\lambda}(Q') \quad (3.7.6)$$

eq. (3.3.36) dictates

$$q_A \rightarrow q'_A, \quad q_{\dot{A}} \rightarrow q'_{\dot{A}} \quad (3.7.7)$$

which differ from eq. (3.7.5) by a factor  $i$ . Thus one can apply the replacements (3.7.5) for quarks when at the same time one multiplies the amplitude with a factor  $(-i)^{n_q}$ , where  $n_q$  is the number of crossed quarks. The reason that we don't want the occurrence of a complex phase factor is that in the evaluation of matrix elements we sometimes use complex conjugation which would lead to incorrect relative phases in amplitudes with crossed quarks. For instance we have the replacement

$$\widetilde{\mathcal{M}}(q_A, q_{\dot{A}}) \rightarrow -i \widetilde{\mathcal{M}}(i q_A, i q_{\dot{A}}) \quad (3.7.8)$$

if we make an outgoing quark (antiquark) an incoming antiquark (quark).

## References

- [1] H. Casimir, *Helvetica Physica Acta* **6**, (1933) 287.
- [2] FORM by J. Vermaseren, REDUCE by A.C. Hearn and SCHOONSCHIP by M. Veltman, are the algebraic programs most frequently used for matrix element calculations.
- [3] T. Gottschalk and D. Sivers, *Phys. Rev.* **D21** (1980) 102; J. Kripfganz and A. Schiller, *Phys. Lett.* **79B** (1978) 317; A. Schiller, *J. Phys.* **G5** (1979) 1329; C.J. Maxwell, *Nucl. Phys.* **B149** (1979) 61; Z. Kunszt and E. Pietarinen, *Nucl. Phys.* **B164** (1980) 45.
- [4] F.A. Berends, R. Kleiss, P. de Causmaecker, R. Gastmans and T.T. Wu, *Phys. Lett.* **103B** (1981) 124.
- [5] F. A. Berends and R. Gastmans, *Nucl. Phys.* **B88** (1975) 99.

- [6] D. Danckaert, P. de Causmaecker, R. Gastmans, W. Troost and T.T. Wu, Phys. Lett. 114B(1982) 203;  
F.A. Berends, R. Kleiss, P. de Causmaecker, R. Gastmans, W. Troost and T.T. Wu, Nucl. Phys. B206 (1982) 53; Nucl. Phys. B206 (1982) 61; Nucl. Phys. B239 (1984) 382; Nucl. Phys. B239 (1984) 395; Nucl. Phys. B264 (1986) 243; Nucl. Phys. B264 (1986) 265.  
P. de Causmaecker, Fotonen en gluonon bij hoge energie, thesis, Leuven, 1983.
- [7] R. Kleiss, Nucl. Phys. B241 (1984) 129;  
R. Kleiss and W. J. Stirling, Nucl. Phys. B262 (1985) 235;  
J.F. Gunion and Z. Kunszt, Phys. Lett. 161B (1985) 333.
- [8] Z. Xu, D-H Zhang and L. Chang, Nucl. Phys. B291 (1987) 392.
- [9] *The Ubiquitous Photon: Helicity Method for QED and QCD*, R. Gastmans and T.T. Wu, Clarendon press, 1990.
- [10] G. Farrar and F. Neri, Phys. Lett. 130B (1983) 109;  
K. Hagiwara and D. Zeppenfeld, Nucl. Phys. B274 (1986) 1.
- [11] A. Kersch and F. Scheck, Nucl. Phys. B263 (1986) 475;  
F.A. Berends and W.T. Giele, Nucl. Phys. B294 (1987) 700.
- [12] H. Weyl, Zeit. Phys. 56 (1929), 330;  
B.L. van der Waerden, Goettinger Nachrichten (1929) 100.
- [13] *Introduction to tensors, spinors and relativistic wave equations*, E. M. Corson, Blackie, 1953.
- [14] *Gravitation and Cosmology, Principles and applications of the general theory of relativity*, S. Weinberg, John Wiley & Sons, 1972.
- [15] W.T. Giele, masters thesis, Leiden, 1986; H. Kuijf, masters thesis, Leiden, 1986;  
F.A. Berends and W.T. Giele, Nucl. Phys. B294 (1987) 700.
- [16] W.T. Giele, Properties and calculations of multiparton processes, thesis, Leiden, 1989;  
F.A. Berends and W.T. Giele, Nucl. Phys. B313 (1989) 595.
- [17] B.S. DeWitt, Phys. Rev. 162 (1967) 1239.
- [18] G.J.H. Burgers, On the construction of field theories for higher spin massless particles, thesis, Leiden, 1985;  
*Quantum theory of gravitation*, lectures given by M. Veltman, Les Houches, 1975.
- [19] F.A. Berends, W.T. Giele and H. Kuijf, Phys. Lett. 232B (1989) 266.
- [20] S. Weinberg, Phys. Lett. 9 (1964) 357.
- [21] S. Weinberg, Phys. Rev. 140 (1965), B516.

## Chapter 4

### Zero quark processes

*Calculational methods and results are given for QCD processes without quarks. A systematic method is discussed to evaluate multigluon matrix elements. Special attention is paid to the properties of the subamplitudes. In view of the numerical importance of this subprocess a detailed study is presented. In particular the exact results are compared with a number of approximations.*

#### 4.1 Introduction

The QCD scattering process without quarks received a lot of attention during the last decade [1]. It is not only considered to be the most complex QCD process on tree level, it also dominates over other parton subprocesses. Firstly because  $\sum_{c,\lambda} |\mathcal{M}_n|^2$  is generally larger for the multigluon process and secondly the behaviour of the parton density function is such that the gluon initial state is favoured. A historical sketch of multigluon calculations through the years can be found in [2, 3]. We concentrate on the systematic calculation of the multigluon process and on the consequences of some approximations.

The plan of this chapter is as follows. In the next section a general method to calculate the multigluon matrix element is given. The method is based on the colour decomposition techniques to obtain subamplitudes, see section 3.5. The various contributions to a particular colour structure are added by means of a recursion relation technique. Only a few explicit results will be given in this chapter, more can be found in chapter 10. In section 4.3 the properties of the subamplitudes are discussed in detail. These properties play an important role in section 4.4 where a method is developed to handle the colour structure of the multigluon process which involves the manipulation of very large matrices. In section 4.5 the colour matrix is approximated by neglecting all non leading terms in  $N$ . This reduces the colour matrix to a diagonal matrix and therefore greatly simplifies the computation of  $\sum_{c,\lambda} |\mathcal{M}_n|^2$ . Finally in section 4.6 we present results for 4, 5 and 6 jet production at the Tevatron collider based on the gluonic process only. Furthermore the exact result is compared with a number of approximations. More predictions, including other subprocesses can be found in chapter 8.

## 4.2 The zero quark process

In this section we review a systematic method to calculate the multigluon subprocess. The method uses the colour decomposition technique as described in section 3.5 and adds the various parts that contribute to a subamplitude by means of a recursion relation for gluon currents [4]. The process with all gluons outgoing reads

$$0 \rightarrow g(K_1) + \dots + g(K_n). \quad (4.2.1)$$

The gluons carry colour  $a_1 \dots a_n$ . The helicity amplitude for process (4.2.1) reads

$$\mathcal{M}(1 \dots n) = 2 i g^{n-2} \sum_{P(1 \dots n-1)} (a_1 \dots a_n) \mathcal{C}(1 \dots n), \quad (4.2.2)$$

where  $(a_1 \dots a_n)$  represents a trace of generators of the  $SU(N)$  gauge group in the fundamental representation. The sum runs over all the permutations of  $(1 \dots n-1)$ . Note that for clarity the notation has been simplified in some ways; the colours, helicities and momenta are implicitly understood and superfluous commas between function arguments are omitted too. The colour matrix that arises during the computation of  $\sum_{c,\lambda} |\mathcal{M}_n|^2$  is dealt with in section 4.4. Here we discuss the computation of the subamplitudes.

Consider a current  $\hat{J}_\mu^a(1 \dots n)$  with  $n$  on-shell gluons, where  $a$  is the colour index and  $\mu$  the Lorentz index of the current. This vector current receives contributions from all the Feynman diagrams of a process with  $n+1$  gluons where gluon  $n+1$  represents the off-shell current gluon.  $\hat{J}_\mu^a(1 \dots n)$  is a conserved current, i.e.

$$\kappa(1, n)^\mu \hat{J}_\mu^a(1 \dots n) = 0 \quad \text{with} \quad \kappa(1, n)^\mu \equiv \sum_{i=1}^n K_i^\mu. \quad (4.2.3)$$

Using colour decomposition techniques  $\hat{J}_\mu^a(1 \dots n)$  can be written as

$$\hat{J}_\mu^a(1 \dots n) = 2 g^{n-1} \sum_{P(1 \dots n)} (a_1 \dots a_n a) J_\mu(1 \dots n). \quad (4.2.4)$$

where  $J_\mu(1 \dots n)$  is a colourless, but still conserved, current. Contrary to  $\hat{J}_\mu^a(1 \dots n)$  the ordering of indices is important in  $J_\mu(1 \dots n)$ . The following recursion relation can be derived for  $J_\mu(1 \dots n)$ :

$$J_\mu(1 \dots n) = \frac{1}{\kappa(1, n)^2} \left( \sum_{m=1}^{n-1} [J(1 \dots m), J(m+1 \dots n)]_\mu \right. \\ \left. + \sum_{m=1}^{n-2} \sum_{k=m+1}^{n-1} \{J(1 \dots m), J(m+1 \dots k), J(k+1 \dots n)\}_\mu \right), \quad (4.2.5)$$

with

$$[J(1 \dots m), J(m+1 \dots n)]_\mu = \quad (4.2.6) \\ + 2 \kappa(m+1, n) \cdot J(1 \dots m) J_\mu(m+1 \dots n) \\ - 2 \kappa(1, m) \cdot J(m+1 \dots n) J_\mu(1 \dots m) \\ + J(1 \dots m) \cdot J(m+1 \dots n) [\kappa(1, m) - \kappa(m+1, n)]_\mu,$$

$$\begin{aligned}
& \{J(1 \dots m), J(m+1 \dots k), J(k+1 \dots n)\}_\mu = \\
& +2 J(1 \dots m) \cdot J(k+1 \dots n) J_\mu(m+1 \dots k) \\
& - J(1 \dots m) \cdot J(m+1 \dots k) J_\mu(k+1 \dots n) \\
& - J(m+1 \dots k) \cdot J(k+1 \dots n) J_\mu(1 \dots m).
\end{aligned} \tag{4.2.7}$$

The boundary or stopping condition reads,  $J_\mu(i) = e_{i\mu}$ : the polarization vector for gluon  $i$ . Eq. (4.2.5) contains a sum over all colourless QCD vertices, where the ordering of the gluons corresponds with the colour structure. Furthermore in eq. (4.2.6) all the gluons are on-shell. With the multigluon current  $\hat{J}_\mu^a(1 \dots n)$  the matrix element is obtained with

$$\mathcal{M}(1 \dots n) = \hat{J}_\mu^a(1 \dots n-1) \hat{J}^{a\mu}(n) i\kappa^2(1, n-1)|_{\kappa(1,n)=0}. \tag{4.2.8}$$

The  $n-1$  gluon current is contracted with a polarization vector under the condition that momentum is conserved. The  $i\kappa^2(1, n-1)$  removes the unphysical propagator included in  $\hat{J}_\mu^a(1 \dots n-1)$ . From eqs. (4.2.2) and (4.2.8) we find that the subamplitude is given by

$$\mathcal{C}(1 \dots n) = J_\mu(1 \dots n-1) J^\mu(n) \kappa^2(1, n-1)|_{\kappa(1,n)=0}. \tag{4.2.9}$$

Eqs. (4.2.2)-(4.2.9) are sufficient to calculate the multigluon process (4.2.1) for any number of gluons. It is interesting to see this simple algorithm in the light of the time and effort spent on multigluon calculations. Still, in a numerical application it is better to have analytical expressions for the  $\mathcal{C}$ -functions. With the aid of eq. (4.2.9) and the refinements described in [5] we have accomplished this for  $n \leq 7$ , see chapter 10. For  $n > 7$  the above method must be used to compute  $\sum_{e,\lambda} |\mathcal{M}_n|^2$ .

The advantages of the above method to calculate multigluon amplitudes are twofold. Firstly, the gauge invariance of the gluons can be used to check the result. Varying the gluon polarization vectors by choosing different gauge spinors  $b^A$ , see eq. (3.4.11), does not change  $\mathcal{C}(1 \dots n)$ . Secondly the method enables us to calculate  $\sum_{e,\lambda} |\mathcal{M}_n|^2$  for any  $n$ . For testing approximations this is clearly useful.

For some helicity combinations a short analytical form is known for  $\mathcal{C}$ -functions for general  $n$ . When all gluons or all but one have the same helicity the subamplitude vanishes:

$$\mathcal{C}(1 \dots n) = 0. \tag{4.2.10}$$

When gluons  $i$  and  $j$  have helicity  $-$  and all other gluons helicity  $+$  it reads

$$\mathcal{C}(12 \dots n) = \frac{(\sqrt{2})^n}{2} \frac{\langle ij \rangle^4}{\langle 12 \rangle \langle 23 \rangle \dots \langle n-1n \rangle \langle n1 \rangle}, \tag{4.2.11}$$

In a numerical situation one of course wants to exploit as many symmetries as possible. From eq. (4.2.9) is clear that  $\mathcal{C}(1 \dots n) = \mathcal{C}(2 \dots n1)$ . The symmetry properties of the  $\mathcal{C}$ -functions are discussed in the next section. In this respect we shall show that eq. (4.2.9) together with properties of  $\mathcal{C}$ -functions enables us to calculate all  $n!$   $J_\mu(1 \dots n)$ 's from the  $(n-1)!$   $J_\mu(12 \dots n)$ 's where gluon 1 is fixed.

### 4.3 Properties of $C$ -functions

The  $n!$  gauge invariant  $C$ -functions of multigluon scattering are not independent. There are many, mostly non-linear, relations between  $C$ -functions. We are interested in to what extent the  $n!$   $C$ -functions are linearly independent. We follow the historical line of research [6] which ultimately leads to eq. (4.3.7), an important relation in many proofs of theorems concerning multigluon relations [2].

The real problem in computing multigluon scattering is not the number of helicity configurations but rather the number of diagrams, or equivalently the number of different  $C$ -functions. Since this grows as  $n!$  any simple relation between  $C$ -functions is welcome. Several such relations exist in the literature. First of all, the  $C$ -functions are *cyclic* in their momenta

$$C(123 \dots n) = C(23 \dots n1) \quad (4.3.1)$$

and this property has in fact already been used in the construction of the matrix element for multigluon scattering, see eq. (4.2.2). Moreover we have the *reflection* property

$$C(12 \dots n-1 n) = (-1)^n C(n n-1 \dots 21), \quad (4.3.2)$$

and the so-called *subcyclic* property:

$$\sum_{P_C(2 \dots n)} C(1i_2 \dots i_n) = 0, \quad (4.3.3)$$

where  $P_C(2 \dots n)$  stands for the set of all *cyclic* permutations of  $(2 \dots n)$ . Notice that the subcyclic property cannot be used directly in eq. (4.2.2) because there the  $C$ -functions all occur with different colour factors.

With the above relations, it is possible to compute a basis of  $C$ -functions. All other  $C$ -functions can be obtained by expressing them in this basis using eqs. (4.3.1), (4.3.2) and (4.3.3).

It has been thought for some time that these identities were enough to express all  $C$ -functions in terms of the so-called 1,2-basis, which consists of all  $(n-2)!$   $C$ -functions of the form  $C(12i_3 \dots i_n)$ . For  $n = 4, 5$  and  $6$  this is indeed the case, but for  $n > 6$  it no longer holds. In the latter case we need more than the  $(n-2)!$   $C$ -functions of the 1,2-basis. The proof of this statement is given in [6]. It shows in detail why for  $n = 6$  the 1,2-basis suffices and why for  $n = 7$  it does not. Therefore, using only the identities (4.3.1)-(4.3.3), the 1,2-basis is not large enough to specify uniquely all  $C$ -functions. In fact, when we enlarge the basis, which has 120 elements for  $n = 7$ , to 121 elements by also giving, e.g.  $C(1342567)$ , all other  $C$ -functions do follow uniquely. For  $n = 8$ , it appears necessary to supplement the 720-element 1,2-basis with an additional 109  $C$ -functions before the solution is unique. Clearly, this is an unsatisfactory situation, since the number of extra  $C$ -functions can only be determined empirically for a given  $n$ . Expressing all other  $C$ -functions in this set calls for some quite complicated combinations of identities. Moreover, not every choice of the extra  $C$ -functions yields a basis from which all the other  $C$ -functions can be derived. Since the number of additional necessary  $C$ -functions

has been found by an experimental search, it is possible that the strict minimum is in fact a bit lower. This will turn out to be irrelevant.

At this point we need a new linear relation between  $C$ -functions to accomplish that the elements in the 1,2-basis can generate all  $C$ -functions. Besides aesthetical and practical arguments there are also theoretical motivations, for instance look at the  $q\bar{q}(n-2)g$  process. Supersymmetry relates this process with  $(n-2)!$  linearly independent  $D$ -functions, see chapter 5, to the multigluon  $C$ -functions.

In studying the colour structure of the 7-gluon process we found another linear relation, which does reduce all  $C$ -functions to the 1,2-basis, and which can be described as follows. First we introduce the notion of *merging*. Consider two ordered lists of elements  $\{x_1 x_2 \dots x_p\}$  and  $\{y_1 y_2 \dots y_q\}$ . We define a merging  $M(\{x_1 \dots x_p\} \{y_1 \dots y_q\})$  of these two lists to be any permutation of the set  $(x_1 \dots x_p y_1 \dots y_q)$  which leaves the ordering of the sublists  $x_i$  and  $y_i$  invariant; there are  $(p+q)!/p!q!$  of such permutations. Two examples illustrate this merging mechanism

$$M(\{1\}\{23\}) = \{(123), (213), (231)\}, \quad (4.3.4)$$

$$M(\{12\}\{34\}) = \{(1234), (1324), (1342), (3124), (3142), (3412)\}. \quad (4.3.5)$$

The new identity can be written as follows

$$C(1x_1 \dots x_p 2y_1 \dots y_q) = (-1)^p \sum_M C(12M(\{x_p x_{p-1} \dots x_1\} \{y_1 y_2 \dots y_q\})), \quad (4.3.6)$$

where the sum runs over all mergings of the two lists. Note the reversal of the order of the  $x$ 's on the right-hand side. In those cases where the  $C$ -function was already uniquely given the identity (4.3.6) coincides with known ones. Setting  $q = 0$  in eq. (4.3.6) results in eq. (4.3.2) and  $q = 1$  results in eq. (4.3.3). With the notion of merging sets one is able to derive an equivalent formulation of (4.3.6) [7].

$$\sum_M C(1M(\{x_1 \dots x_p\} \{y_1 \dots y_q\})) = 0. \quad (4.3.7)$$

Eq. (4.3.7) appears to be completely different from eq. (4.3.6) although they both contain mergings. They are however equivalent. Before proving this statement we stress that eq. (4.3.6) is computationally more attractive since it expresses any  $C$ -function in the 1,2-basis in a very direct manner. Eq. (4.3.7) turned out to be a very powerful tool for proving various multigluon current relations. Extending eq. (4.3.7) to merge more groups of gluons

$$\sum_M C(1M(\{x_1 \dots x_p\} \{y_1 \dots y_q\} \dots \{z_1 \dots z_r\})) = 0, \quad (4.3.8)$$

does not contain any new relation. This can most easily be seen by merging the groups  $y$  through  $z$  and considering each merging to be a version of eq. (4.3.7).

We now prove that relations (4.3.6) and (4.3.7) are equivalent.

To show the equivalence we must prove that the two arrows in (4.3.6)  $\Leftrightarrow$  (4.3.7) hold. The  $\Leftarrow$  side of the proof uses a special form of (4.3.7)

$$\sum_M C(1M(\{2x_p \dots x_1\}\{y_1 \dots y_q\})) = 0. \quad (4.3.9)$$

to rewrite eq. (4.3.6) into

$$\sum_M C(12M(\{x_p \dots x_1\}\{y_1 \dots y_q\})) = \quad (4.3.10)$$

$$- \sum_M C(1y_1 M(\{2x_p \dots x_1\}\{y_2 \dots y_q\})).$$

After applying eq. (4.3.9) another  $q - 1$  times we arrive at

$$\sum_M C(12M(\{x_p \dots x_1\}\{y_1 \dots y_q\})) = \quad (4.3.11)$$

$$(-1)^q \sum_M C(1y_q M(\{y_{q-1} \dots y_1 2x_p \dots x_1\}\{\})) =$$

$$(-1)^q C(1y_q \dots y_1 2x_1 \dots x_p) = (-1)^p C(1x_1 \dots x_p 2y_1 \dots y_q)$$

which concludes the first part of the proof. In the last step we used eq. (4.3.2).

The  $\Rightarrow$  side of the proof is more involved and we start by observing that

$$\sum_{j=0}^q \sum_M (-1)^j M(\{y_j \dots y_1\}\{y_{j+1} \dots y_q\}) = 0. \quad (4.3.12)$$

Each value  $j = k$  results in a set of terms which are completely cancelled by terms coming from  $j = k - 1$  and  $j = k + 1$ . Together with the fact that the terms for  $j = k$  do not occur for other values of  $j$  besides the two mentioned, the sum must be zero.

Without loss of generality take  $x_i = 2$  in eq. (4.3.7). Substitution of eq. (4.3.6) for each term in eq. (4.3.7) leads to

$$\sum_M C(1M(\{x_1 \dots x_{i-1} 2x_{i+1} \dots x_p\}\{y_1 \dots y_q\})) = \quad (4.3.13)$$

$$\sum_{j=0M, M'}^q \sum (-1)^{i-1+j} C(12M(\{x_{i-1} \dots x_1\}\{y_j \dots y_1\})M'(\{x_{i+1} \dots x_p\}\{y_{j+1} \dots y_q\})) =$$

$$\sum_{j=0}^q \sum_M (-1)^{i-1+j} C(12M(\{x_{i-1} \dots x_1\}\{y_j \dots y_1\}\{x_{i+1} \dots x_p\}\{y_{j+1} \dots y_q\})) =$$

$$\sum_{j=0}^q \sum_M (-1)^{i-1+j} C(12M(\{x_{i-1} \dots x_1\}\{x_{i+1} \dots x_p\}\{y_j \dots y_1\}\{y_{j+1} \dots y_q\})) = 0,$$

where we have used that a product of mergings is just a new merging with more lists and that lists inside a merging can be interchanged. For the last step eq. (4.3.12) was used.

By showing the equivalence we established the validity of eq. (4.3.6), since eq. (4.3.7) was proven in [7].

It is our belief that eq. (4.3.6) contains all the linear relations between  $C$ -functions. Of course there are non-linear relations. As an example we give [9]

$$\sum_{P(234)} \{1,2\}\{4,5\} C(123456) \times \quad (4.3.14)$$

$$[+\{3,5\} C(215346) + (\{3,4\} + \{3,5\}) C(215436)$$

$$-\{1,3\} C(231546) - (\{1,3\} + \{2,3\}) C(321546)] = 0.$$

For more external particles the expression becomes lengthier but can be derived from ref. [10]. Eq. (4.3.14) can easily be verified for special helicity configurations. However it is too complicated to be of any practical relevance.

## 4.4 Exact and approximate colour treatment

The expression for the matrix element (4.2.2) can be written in different ways

$$\mathcal{M}(1 \dots n) = 2 i g^{n-2} \sum_{P(2 \dots n)} (a_1 \dots a_n) \mathcal{C}(1 \dots n) \quad (4.4.1)$$

$$= i g^{n-2} \sum_P [(a_1 P(a_2 \dots a_n)) + (-1)^n (a_1 P^T(a_2 \dots a_n))] \mathcal{C}(1 \dots n) \quad (4.4.2)$$

$$\equiv i g^{n-2} \sum_P \{a_1 P(a_2 \dots a_n)\} \mathcal{C}(1 \dots n). \quad (4.4.3)$$

In eq. (4.4.2) use has been made of the reflective property (4.3.1) of the subamplitudes.  $P^T(a_2 \dots a_n)$  is  $P(a_2 \dots a_n)$  in the reversed order. The sum runs over all  $(n-1)!$  permutations  $P$  of  $(2 \dots n)$ . In eq. (4.4.3) a shorthand notation has been introduced.

For the matrix element squared we find

$$\sum_{c, \lambda} |\mathcal{M}_n|^2 = g^{2n-4} \sum_{\lambda} \sum_{i, j} c_{ij} C_i C_j^* \quad (4.4.4)$$

with

$$c_{ij} = \sum_{\text{colours}} \{a_1 P_i(a_2 \dots a_n)\} \{a_1 P_j(a_2 \dots a_n)\}^* \equiv c(P_i, P_j). \quad (4.4.5)$$

Again  $i, j = 1, 2, \dots, (n-1)!$  in eq. (4.4.4). The explicit assignment of permutations to the label  $i$  will be discussed below.

For  $n > 6$  a numerical evaluation of  $c_{ij}$  becomes unavoidable. The natural way is to perform this calculation first and store the result, after which the actual multiplication with  $C_i C_j^*$  can be carried out. This procedure quickly runs into a storage problem for the matrix  $c_{ij}$ . The solution to this problem is to exploit the symmetries of  $c_{ij}$ , such that a limited number of elements have to be stored. The others can then be obtained when needed in the multiplication by a simple algorithm. Although in principle all rows of  $c_{ij}$  can be obtained from the first row, the algorithm for this is quite complicated. We shall choose for the evaluation of a number of rows and then apply a simple substitution rule based on the symmetry of the matrix to obtain the other rows.

Besides these remarks about the general strategy another fact should be stressed. From the previous section we know that the basis of linearly independent  $C_i$  contains really  $(n-2)!$  elements instead of  $(n-1)!$ . Eventually we shall use a basis of  $(n-2)!$  elements and a corresponding matrix  $\tilde{c}_{ij}$ . Although the matrix  $c_{ij}$  as defined by eq. (4.4.5) is unique, there is an infinite set of matrices  $c_{ij}$  which leads to the same  $\tilde{c}_{ij}$ . The latter matrix gives the essential information like e.g. the real  $N$  dependence whereas  $c_{ij}$  only gives an apparent  $N$  dependence of the cross section.

We first focus on the evaluation of  $c_{ij}$  according to the definition (4.4.5). In the treatment we discuss the symmetry of  $c_{ij}$ . Although  $c_{ij}$  is an  $(n-1)! \times (n-1)!$  matrix the actual matrix elements depend on a smaller number of polynomials in  $N$ , which show up in a systematic way. A suitable labelling of the permutations makes the symmetries visible. A convenient labelling uses cyclic permutations. Let us illustrate this for  $n = 5$ , from which the general case becomes clear.

The permutations  $P_1, P_2, \dots, P_{24}$  transform the set [12345] into the sets

$$\begin{aligned} & [12345], [12354], [12453], [12435], [12534], [12543], \\ & [13452], [13425], [13524], [13542], [13245], [13254], \\ & [14523], [14532], [14235], [14253], [14352], [14325], \\ & [15234], [15243], [15342], [15324], [15423], [15432]. \end{aligned}$$

The permutations  $P_2, P_3$  and  $P_7$  are the cyclic permutations (45), (345), (2345), where  $(i_1 i_2 \dots i_m)$  means  $i_1 \rightarrow i_2, i_2 \rightarrow i_3, \dots, i_m \rightarrow i_1$ . The above labelling means the

$$P_i = P_7^l P_3^m P_2^q \quad (4.4.6)$$

with  $l = 0, 1, 2, 3, m = 0, 1, 2, q = 0, 1$  and  $i = 6l + 2m + q + 1$ . For  $n = 6$  the cyclic permutations are (56), (456), (3456), (23456) and

$$P_i = P_{25}^k P_7^l P_3^m P_2^q \quad (4.4.7)$$

with  $k = 0, 1, 2, 3, 4$  and  $i = 24k + 6l + 2m + q + 1$ . This generalizes to arbitrary  $n$ .

The labelling gives the matrix  $c_{ij}$  a form with some special symmetry. This symmetry generates the whole matrix from the first  $\frac{1}{2}(n-2)!$  rows. The element  $c_{ij}$  is given by

$$c_{ij} = c(P_i, P_j) = c(P_i, P_i^{-1} P_j), \quad (4.4.8)$$

where the sum over all colours has allowed us to rename  $[P_i 2, P_i 3, \dots, P_i n]$  as  $[2, \dots, n]$ . In this fashion every row can in principle be obtained from the first row by evaluating  $P_i^{-1} P_j$ . In general this is involved, but comparing the first  $(n-2)!$  rows with the second  $(n-2)!$  rows we see that in the case of  $n = 5$  we have to compare  $(P_3^m P_2^q)^{-1} P_j$  with  $(P_7 P_3^m P_2^q)^{-1} P_j$  or in other words with  $(P_3^m P_2^q)^{-1} P_7^{-1} P_j = (P_3^m P_2^q)^{-1} P_7^3 P_j$ . Thus the second  $(n-2)!$  rows are obtained from the first  $(n-2)!$  rows by a shift. This becomes clear from the  $n = 5$  case, where  $c_{ij}$  takes the form

$$c_{ij} = \begin{pmatrix} A & B & C & D \\ D & A & B & C \\ C & D & A & B \\ B & C & D & A \end{pmatrix} \quad (4.4.9)$$

with  $6 \times 6$  submatrices  $A, B, C, D$ . For  $n = 6$  we similarly have five  $24 \times 24$  submatrices which build up the full matrix  $c_{ij}$ .

Within the first  $(n-2)!$  rows the first  $\frac{1}{2}(n-2)!$  determine the second set in another way. This is seen from the structure

$$(A B C D) = \begin{pmatrix} c_{1,1} & c_{1,2} & c_{1,3} & \dots & c_{1,24} \\ c_{2,1} & c_{2,2} & c_{2,3} & \dots & c_{2,24} \\ c_{3,1} & c_{3,2} & c_{3,3} & \dots & c_{3,24} \\ c_{3,6} & c_{3,5} & c_{3,4} & \dots & c_{3,7} \\ c_{2,6} & c_{2,5} & c_{2,4} & \dots & c_{2,7} \\ c_{1,6} & c_{1,5} & c_{1,4} & \dots & c_{1,7} \end{pmatrix} \quad (4.4.10)$$

The bottom half is in the reverse order and shifted.

In general, one has to evaluate  $\frac{1}{2}(n-2)!$  rows. In practice they are also obtained from the first row by exploiting eq. (4.4.8). However the relations are more involved than the patterns of eqs. (4.4.9) and (4.4.10).

Next we turn to the evaluation of the first row. Many elements of this row are the same, since one has several relations. The first one reads

$$\begin{aligned} \sum_{\text{colours}} \{a_1 a_2 \dots a_n\} \{a_1 a_{i_2} \dots a_{i_n}\} &= \sum_{\text{colours}} \{a_1 a_2 \dots a_n\} \{a_2 a_{i_2}' \dots a_{i_n}'\} \\ &= \sum_{\text{colours}} \{a_1 a_2 \dots a_n\} \{a_{i_2}' a_{i_2+1}' \dots a_{i_2-1}'\}. \end{aligned} \quad (4.4.11)$$

The labels  $i_m$  follow from  $i_m$  by a cyclic permutation  $s$

$$i_{m+1} = s i_m \quad (4.4.12)$$

with  $s = (1 \dots n)$ . The label  $i_1'$  is the one which takes the value 1. The relation (4.4.11) is based on the cyclic invariance of both factors and the possibility of renaming the colour labels. The relation also holds with  $s^2, s^3, \dots, s^{n-1}$ . As an example, for  $n = 5$  one finds amongst others

$$c_{1,2} = c_{1,19} = c_{1,4} = c_{1,11} = c_{1,7}. \quad (4.4.13)$$

Thus sets of  $c_{ij}$  can be shown to be equal. From eq. (4.4.11) it follows that every element is equal to one of the set

$$\{c_{1,1}, c_{1,2}, c_{1,3}, c_{1,6}, c_{1,9}, c_{1,10}, c_{1,16}, c_{1,24}\}. \quad (4.4.14)$$

Another relation follows from the reflective property of  $c_{ij}$

$$\begin{aligned} \sum_{\text{colours}} \{a_1 a_2 \dots a_n\} \{a_1 a_{i_2} \dots a_{i_n}\} &= \sum_{\text{colours}} \{a_1 a_n \dots a_2\} \{a_1 a_{i_n} \dots a_{i_2}\} \\ &= \sum_{\text{colours}} \{a_1 a_2 \dots a_n\} \{a_1 a_{i_n}' \dots a_{i_2}'\} \end{aligned} \quad (4.4.15)$$

with  $i_m' = T i_m$ , where  $T$  is the permutation which reverses the order of  $(2 \dots n)$ . For the  $n = 5$  case this relation does not further reduce the set (4.4.14).

A similar relation reverses the order only in one factor giving

$$\sum_{\text{colours}} \{a_1 a_2 \dots a_n\} \{a_1 a_{i_2} \dots a_{i_n}\} = (-1)^n \sum_{\text{colours}} \{a_1 a_2 \dots a_n\} \{a_1 a_{i_n} \dots a_{i_2}\}. \quad (4.4.16)$$

Using eqs. (4.4.11) and (4.4.16) gives for  $n = 5$

$$c_{1,1} = -c_{1,24}, \quad c_{1,2} = -c_{1,6}, \quad c_{1,3} = -c_{1,10}, \quad c_{1,9} = -c_{1,16}, \quad (4.4.17)$$

which leaves us in essence with four elements. A final property is

$$c(P_1, P_j) = c(P_j, P_1) = c(P_1, P_j^{-1}) \quad (4.4.18)$$

which gives together with (4.4.11) just one new relation for  $n = 5$

$$c_{1,9} = c_{1,16}. \quad (4.4.19)$$

The four different entries in the first row are calculated by performing the sum over colours. We find polynomials in  $N$ .

$$\begin{aligned} c_{1,1} &= \frac{1}{2^4} N^3 (N^2 - 1) \left( \frac{10}{N^4} - \frac{4}{N^2} + 1 \right) \\ c_{1,2} &= \frac{1}{2^4} N^3 (N^2 - 1) \left( \frac{4}{N^4} - \frac{2}{N^2} \right) \\ c_{1,3} &= \frac{1}{2^4} N^3 (N^2 - 1) \frac{2}{N^4} \\ c_{1,9} &= 0 \end{aligned}$$

The last result also directly follows from eqs. (4.4.17) and (4.4.19).

A similar procedure for  $n = 6, 7, 8$  and  $9$  leads to 10, 28, 127 and 686 polynomials. The polynomials have the form

$$R = \frac{1}{2^{n-1}} N^{n-2} (N^2 - 1) \left( \alpha_0 + \sum_{i=1}^{2\lfloor \frac{n}{2} - 1 \rfloor} \frac{\alpha_i}{N^{2i}} \right), \quad (4.4.20)$$

where  $[a]$  is the entier of  $a$  and  $\alpha_i$  is an integer.

So far, we have used the linearly dependent basis  $\mathcal{C}(1P(2, \dots, n))$  containing  $(n-1)!$  elements. As was shown in the previous section, it is possible to introduce a basis of  $(n-2)!$  elements by using eq. (4.3.6). The reduced  $(n-2)! \times (n-2)!$  matrix  $\bar{c}_{ij}$  still possesses the earlier stated symmetries. This is due to the fact that for all permutations  $\Pi$  of the set  $(x_1, \dots, x_p, 2, y_1, \dots, y_q)$  which do not affect the label 2 we have

$$\mathcal{C}(1\Pi(x_1 \dots x_p 2 y_1 \dots y_q)) = (-1)^p \sum_M \mathcal{C}(12M(\Pi(x_p \dots x_1 y_1 \dots y_q))). \quad (4.4.21)$$

The symmetries of the  $(n-1)! \times (n-1)!$  matrix  $c_{ij}$  involve the cyclic permutations  $(23 \dots n)$ , but the  $(n-2)! \times (n-2)!$  submatrix  $c_{ij}$ ,  $i, j = 1, \dots, (n-2)!$  possesses symmetries which depend on the permutations  $(3 \dots n)$  and shorter cyclic permutations and do not affect label 2. The reduced matrix  $\bar{c}_{ij}$  therefore has the symmetry of the  $(n-2)! \times (n-2)!$  submatrix  $c_{ij}$ . For the  $n = 6$  case the reduced  $24 \times 24$  matrix has the symmetries of eqs. (4.4.9) and (4.4.10).

The reduced matrix for  $n = 5$  is given in chapter 10. The  $1/N^2$  terms disappear, which means that the leading colour result is exact, i.e. the  $O(N^{-2})$  terms in

$$\sum_c |\mathcal{M}_3|^2 = \left( \frac{g^2 N}{2} \right)^3 (N^2 - 1) \left( \sum_{P(2 \dots 5)} |\mathcal{C}(1 \dots 5)|^2 + O(N^{-2}) \right), \quad (4.4.22)$$

are absent. In other words, the diagonal  $4! \times 4!$  colour matrix with diagonal element  $(N/2)^3(N^2 - 1)$  is equivalent with  $c_{ij}$ . For  $n = 6, 7$  the  $1/N^2$  terms survive in the reduced matrix, but higher powers of  $1/N^2$  vanish, for  $n = 8, 9$  the  $1/N^4$  term remains but higher powers drop out. This suggests a general pattern for higher  $n$  values, which has an interesting consequence for collinear gluons. In the case where two gluons are collinear we have

$$|\mathcal{M}(1, \dots, n+1)|^2 = P |\mathcal{M}(1, \dots, n)|^2, \quad (4.4.23)$$

with  $P$  a function related to the splitting function. Since  $P \sim N$ , the  $1/N^2$  term is collinear finite for  $n = 6$ , but not for  $n = 7$ . Similarly the  $1/N^4$  is collinear finite for  $n = 8$ , but not for  $n = 9$ .

For  $n = 6$  the reduced matrix is equivalent with a simple interference pattern in the original basis. For  $n = 7$  the number of interference terms increases. Some results are collected in chapter 10.

## 4.5 The LCA in processes with zero quarks

In this section we examine the consequences of neglecting all  $O(1/N^2)$  terms in the colour matrix. This so-called leading order in colour approximation, abbreviated by LCA, is used in many approximations for multiparton matrix elements, see chapter 8 and section 4.6.

To establish the influence of the non-leading order terms we carried out the following program, see also sections 5.2 and 6.3. Determine the differential cross sections for the exact matrix element as well as for the LCA. In the latter  $\sum_{c,\lambda} |\mathcal{M}_n|^2$  is given by

$$\sum_{c,\lambda} |\mathcal{M}(1 \dots n)|^2 = g^{2n-4}(N^2 - 1) \left(\frac{N}{2}\right)^{n-2} \sum_{\lambda} \sum_{P(2 \dots n)} |\mathcal{C}(1 \dots n)|^2. \quad (4.5.1)$$

The LCA colour factor follows from the relations

$$(x a_1 \dots a_n)(x a_1 \dots a_n)^* = \frac{1}{2}(a_1 \dots a_n a_n \dots a_1) - \frac{1}{2N}(a_1 \dots a_n)(a_1 \dots a_n)^*, \quad (4.5.2)$$

and

$$(a_1 \dots a_n x x a_n \dots a_1) = \frac{N^2 - 1}{2N}(a_1 \dots a_n a_n \dots a_1), \quad (4.5.3)$$

where repeated indices imply summation. Eq. (3.5.7) has been used in both (4.5.2) and (4.5.3). The colour products on the diagonal of eq. (4.4.4) produce the highest order in  $N$ , they become

$$(a_1 \dots a_n)(a_1 \dots a_n)^* = \sum_{j=0}^n (-1)^j \left(\frac{N^2 - 1}{2N}\right)^{n-j}. \quad (4.5.4)$$

Taking into account the factor 2 that appears in eq. (4.4.1) leads to the given LCA colour factor. The LCA is exact for  $n = 4$  and  $n = 5$ . The linear dependence of the  $\mathcal{C}$ -functions

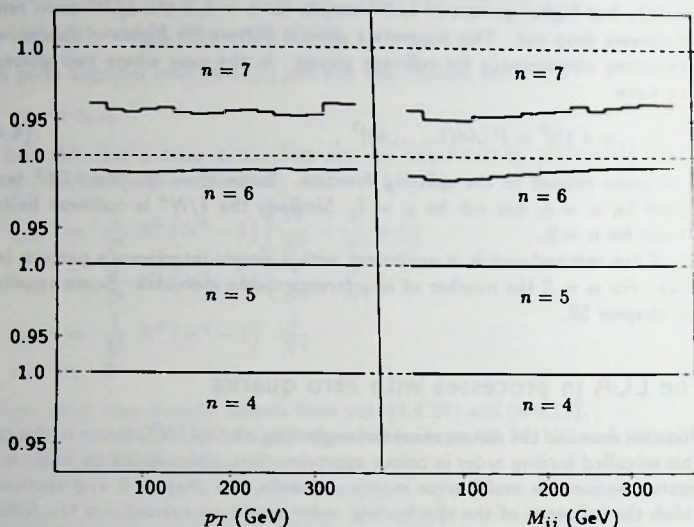


Fig. 4.1. Ratio LCA/exact for the  $p_T$  and  $M_{ij}$  distributions.

can be used to diagonalize the colour matrix as we have already seen in the previous section. This is the motivation to have the  $(N^2 - 1)$  instead of simply  $N^2$ .

In the numerical calculation the distributions for both the exact and the LCA are based on the same Monte Carlo integration points. This positive correlation of the distributions reduces among others the statistical errors, the influence of scale choices, etc. when the ratio LCA/exact is considered. Two distributions, the transverse momentum  $p_T$  and the dijet invariant mass  $M_{ij}$  are plotted in fig. 4.1. The parameters used are those for the LHC;  $p_T > 50$  GeV,  $\theta > 40^\circ$  and  $|\eta| < 2$  (for the definition of these quantities we refer to chapter 2). The influence of the parton density function on the ratio turned out to be negligible.

As can be seen from fig. 4.1 the LCA is exact for  $n = 4$  and  $n = 5$ . For  $n = 6$  and  $n = 7$  this is no longer so, however the deviation from the exact result is small and approximately a constant for a whole range of  $p_T$  and  $M_{ij}$  values. This is important because it means that the LCA only affects the normalization of the distributions which is not well known anyway. The increase in the error from  $n = 6$  to  $n = 7$  is so small that the LCA is expected to be relevant for  $n = 8$ . An explicit exact calculation [11] confirms this. A more detailed study of the LCA can be found in [5]

## 4.6 Cross sections and distributions

The analytical formulae from section 4.2 together with the colour matrix techniques, explained in section 4.4, are used to determine the total cross section rates for  $n = 6, 7$  and 8. Due to the new techniques which speed up the calculation, we are also able to present differential cross sections. For  $n = 6$  and 7 the analytical results for the  $\mathcal{C}$ -functions are given in chapter 10. We compare the exact results with various approximations proposed in the literature. A short description of the essential points of these approximations is included for completeness.

- The first approximation is the LCA as defined in the previous section. It replaces  $\sum_{c,\lambda} |\mathcal{M}_n|^2$  by

$$\sum_{c,\lambda} |\mathcal{M}_n|^2 = g^{2n-4} (N^2 - 1) \left(\frac{N}{2}\right)^{n-2} \sum_{\lambda} \sum_{P(2..n)} |\mathcal{C}(1 \dots n)|^2. \quad (4.6.1)$$

This simplification of the colour matrix does not substantially speed up the calculation, only by a factor two or so. Most of the effort now goes into evaluating the  $\mathcal{C}$ -functions.

- The second method is the Kunszt-Stirling (KS) approximation [12]. This method assumes that all non-zero helicity amplitudes contribute equally to the matrix element squared. The KS method calculates those helicity combinations for which a short analytical form is known. These are the so-called Parke-Taylor (PT) helicity combinations which have the property that all but two helicities are the same. These  $\mathcal{C}$ -functions are given in eq. (4.2.11). All other non-zero amplitudes are accounted for by introduction of a simple combinatorial factor

$$S_n \equiv \frac{\text{Number of non-zero amplitudes}}{\text{Number of PT amplitudes}} = \frac{2^n - 2(n+1)}{n(n-1)}. \quad (4.6.2)$$

In the KS method the colour matrix is treated in leading order too. Together this leads to the following expression for  $\sum_{c,\lambda} |\mathcal{M}_n|^2$

$$\sum_{c,\lambda} |\mathcal{M}_n|_{KS}^2 = 2S_n g^{2n-4} (N^2 - 1) N^{n-2} \sum_{\lambda} \sum_{P(2..n)} \frac{\sum_{1 < i < j < n} \{i,j\}^4}{\{1,2\}\{2,3\} \dots \{n,1\}}. \quad (4.6.3)$$

Note that the KS method is a part of the more general SPHEL approximation, which will be described in detail in chapter 8.

- The third and last approximation we examine is the one proposed by Maxwell (MW) [13]. His method is based on a reduction scheme in which the pair of most collinear gluons is replaced by a single on-shell gluon and some collinearity factor. This process continues until only 5 gluons are left for which the exact result is used. Effectively the MW method amounts to

$$\sum_{c,\lambda} |\mathcal{M}_n|_{MW}^2 = G_n \sum_{c,\lambda} |\mathcal{M}_n|_{KS}^2, \quad (4.6.4)$$

where  $G_n$  depends on the event instead of being a constant as in eq. (4.6.2).

For comparison of these approximations with the exact matrix elements squared, we did the Monte Carlo integrations with the same events in each case. The results are thus positively correlated, enabling us to draw conclusions beyond the precision of the integration. However, the obtained accuracy is such that this correlation is not strictly necessary. The calculations are done at the Tevatron 1800 GeV centre-of-mass energy, using the parton density functions of Duke and Owens with  $\Lambda = 0.2$  GeV [14]. For the QCD scale  $Q$  we took the average  $p_T$  of the event and  $\alpha_S$  was used in first order with  $n_f = 5$ . We note that the correctness of the approximations is insensitive to variations in  $\alpha_S$  and the centre-of-mass energy. Furthermore we used the cuts as defined in table 2.2.

| Method | $gg \rightarrow gggg$ | $gg \rightarrow ggggg$ | $gg \rightarrow gggggg$ |
|--------|-----------------------|------------------------|-------------------------|
| Exact  | $15.8 \pm 0.2$        | $0.91 \pm 0.03$        | $0.059 \pm 0.004$       |
| LCA    | $15.6 \pm 0.2$        | $0.87 \pm 0.03$        | $0.054 \pm 0.003$       |
| KS     | $19.1 \pm 0.3$        | $1.33 \pm 0.04$        | $0.102 \pm 0.006$       |
| MW     | $15.0 \pm 0.2$        | $0.81 \pm 0.03$        | $0.048 \pm 0.003$       |

Table 4.1. Total cross sections in nb for  $n = 6, 7$  and  $8$  for the Tevatron.

The total cross section rates for  $gg \rightarrow gggg$ ,  $gg \rightarrow ggggg$  and  $gg \rightarrow gggggg$  scattering are listed in table 4.1. The KS result is too large, indicating that the PT amplitudes are larger than the other amplitudes. Both LCA and MW are reliable approximations for the total cross section rates. It is interesting to note that for  $n = 7$  each approximation is doing worse compared to the  $n = 6$  case. Likewise for  $n = 8$  compared with  $n = 7$ . For the MW reduction method the error increases from 5% for  $n = 6$  to 12% for  $n = 7$  and 23% for  $n = 8$ , making it dangerous to say something about the correctness for  $n > 8$ . To indicate the effort necessary to obtain the plots note that 100000 accepted events were used for  $n = 6$ , 20000 for  $n = 7$  and 11000 for  $n = 8$ . This  $n = 7$  number is to be compared with the 1000 events used in [6].

To examine the approximations further we plotted two differential cross sections in figures 4.2, 4.3 and 4.4, each having four distributions a, b, c and d. The question is how good the shapes are, since we already know the differences in normalization. The LCA approximation is not included in any of the plots, because the LCA distributions resemble the exact distributions very much (as could be expected from the previous section). In a we show the  $\frac{d\sigma}{dp_T}$  for finding a jet with transverse momentum  $p_T$ . The  $n = 6$  case is in good agreement with the plot in [15]. The MW approximate method gives qualitatively the right shape of this distribution. The KS method overestimates the low  $p_T$  events relatively more than the high  $p_T$  events. About 20% for  $p_T = 40$  GeV and 10% for

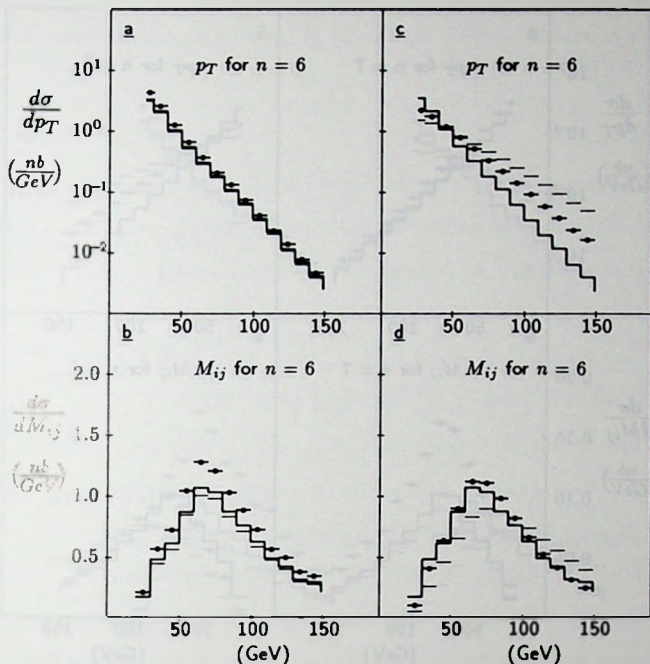


Fig. 4.2. Distributions for the  $n = 6$  process, see text for details.

$p_T = 150$  GeV. Unlike the total cross section the approximations are not worse for  $n = 7$  and  $n = 8$  than for  $n = 6$ . The shape of the LCA and the MW distributions are as good as for  $n = 6$ , while the KS is slightly worse. Again the low  $p_T$  events are relatively overestimated, the error varies from 45% for  $p_T = 40$  GeV to 30% for  $p_T = 150$  GeV. The KS method gives the right shape for the  $p_T$  distribution within an error of 10% for  $p_T < 150$  GeV.

In **b** we give the distribution  $\frac{d\sigma}{dM_{ij}}$  of finding a two jet pair with an invariant mass  $M_{ij} = \sqrt{2p_i \cdot p_j}$ . For this distribution all the approximations give qualitatively the right shape. Notably the MW method is not better than the KS method. The approximations are slightly better for  $n = 6$  than for  $n = 8$ .

When the total cross section rates from table 4.1 are used as a scale factor we find that the largest difference with the exact result for any bin in the  $p_T$  distribution is 2% for the LCA, 8% for the KS method and 7% for the MW method. For the  $M_{ij}$  distribution these numbers are even better, 2%, 3% and 5% for LCA, KS and MW respectively. So the approximations predict the shape of these distributions within an error of say 8%.

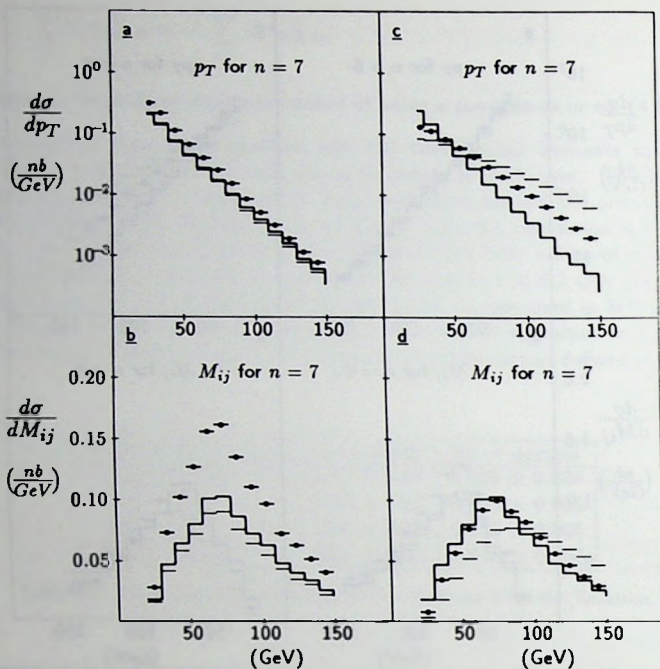


Fig. 4.3. Distributions for the  $n = 7$  process, see text for details.

It is interesting that the peak in the invariant mass distributions is at  $M_{ij} = 70$  GeV for  $n = 6$ ,  $n = 7$  and  $n = 8$ . For Standard Model processes in which a  $W$  decays into jets that have pure QCD backgrounds this is bad. Furthermore we have investigated other distributions, such as

$$\frac{d\sigma}{d\sqrt{s}}, \frac{d\sigma}{d|\eta_i|} \text{ and } \frac{d\sigma}{d\cos\theta_{ij}}.$$

We found that the shapes of these distributions are equally well described by the various approximations, within 10%, the KS method not being worse than the MW method. A more extensive investigation is needed to show whether the approximations give the correct shapes for other distributions.

To illustrate that QCD really matters a comparison is made between the exact matrix element and the pure phase space calculation, normalized to the exact result. Note that a pure phase space calculation does not make much sense in many ways but can be used to examine whether QCD predictions differ from very naive models. In  $c$  the results for

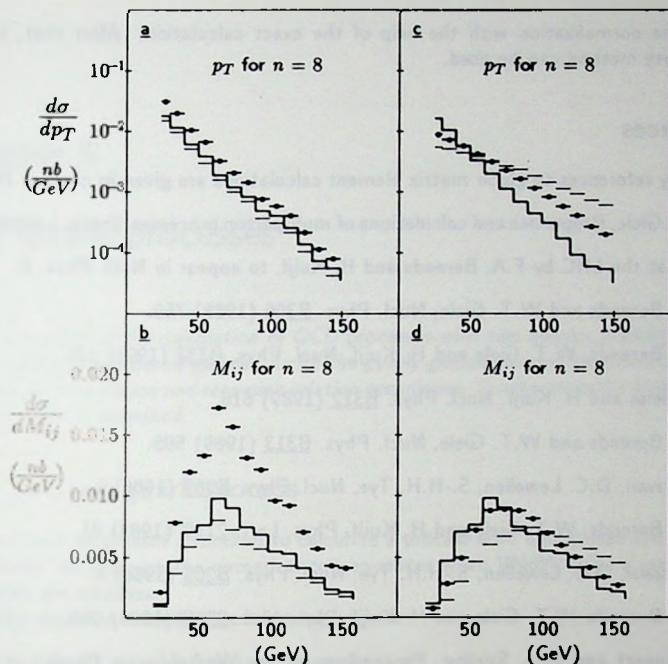


Fig. 4.4. Distributions for the  $n = 8$  process, see text for details.

the  $p_T$  distribution are presented. The continuous line is the exact result copied from a, the normal lines are based on  $\sum_{c,\lambda} |\mathcal{M}_n|^2 \equiv c$ , some constant and the dotted lines are based on  $\sum_{c,\lambda} |\mathcal{M}_n|^2 = (1/\hat{s})^{n-4}$ , with  $\hat{s}$  the parton centre-of-mass energy squared. This last matrix element preserves unitarity and has the same dimension as the exact matrix element. For the  $M_{ij}$  distribution the results are in d. We see that for the  $p_T$  distributions there is a clear difference but that for the  $M_{ij}$  distribution  $\sum_{c,\lambda} |\mathcal{M}_n|^2 = (1/\hat{s})^{n-4}$  gives fair results. This is not strange because the invariant mass distribution scales with  $\sqrt{\hat{s}}$ .

The important lesson is that for many distributions both the KS and the MW methods can very well be used as an approximation to the shape. The MW method is giving somewhat better results for  $n = 6$  but not for  $n = 7$  and  $n = 8$ . The two approximations take about the same computer time.

The exact matrix element squared can be used for determination of the normalization, which is however also sensitive to other influences like the scale choice in the coupling constant and the higher order corrections. Thus in practice an effective strategy would be to establish for a certain approximate calculation the correctness of the distributions

and fix the normalization with the help of the exact calculation. After that, the fast approximate method can be used.

## References

- [1] Many references to gluon matrix element calculations are given in chapter 10.
- [2] W.T.Giele, Properties and calculations of multiparton processes, thesis, Leiden, 1989.
- [3] Jets at the LHC by F.A. Berends and H. Kuijf, to appear in Nucl. Phys. B.
- [4] F.A. Berends and W.T. Giele, Nucl. Phys. B306 (1988) 759.
- [5] F.A. Berends, W.T. Giele and H. Kuijf, Nucl. Phys. B333 (1990) 120.
- [6] R. Kleiss and H. Kuijf, Nucl. Phys. B312 (1989) 616.
- [7] F.A. Berends and W.T. Giele, Nucl. Phys. B313 (1989) 595.
- [8] H. Kawai, D.C. Lewellen, S.-H.H. Tye, Nucl. Phys. B269 (1986) 1.
- [9] F.A. Berends, W.T. Giele and H. Kuijf, Phys. Lett. 211B (1988) 91.
- [10] H. Kawai, D.C. Lewellen, S.-H.H. Tye, Nucl. Phys. B269 (1986) 1.
- [11] F.A. Berends, W.T. Giele and H. Kuijf, Phys. Lett. 232B (1989) 266.
- [12] Z. Kunszt and W.J. Stirling, Proceedings of the Workshop on Physics at Future Accelerators, La Thuile and Geneva, Vol. 2, CERN 87-07, ed. J. H. Mulvey, p. 548.
- [13] C.J. Maxwell, Phys. Lett. B192 (1987) 190.
- [14] D.W. Duke and J.F. Owens, Phys. Rev. D30 (1984) 149.
- [15] M. Mangano and S. Parke, Phys. Rev. D39 (1989) 758.

## Chapter 5

### Two quark processes

*Details are given of the calculation of QCD processes with two quarks, possibly massive, and an arbitrary number of gluons. As for the purely gluonic process the method is based on colour decomposition and recursion relation techniques. Furthermore the leading colour approximation is examined.*

#### 5.1 The two quark process

In this section we present a method to calculate a process with two quarks and  $n$  gluons. In particular we focus on the numerical consequences when WvdW spinors are used and the quarks are massless.

To fix the notation, consider the following process

$$\emptyset \rightarrow q_i(q) + \bar{q}_j(\bar{q}) + g(K_1) + \dots + g(K_n), \quad (5.1.1)$$

where all particles are outgoing, the  $q\bar{q}$ -pair has colours  $i$  and  $j$  and the gluons carry colours  $a_1 \dots a_n$ . The matrix element for process (5.1.1) is given by

$$\mathcal{M}(q; 1 \dots n; \bar{q}) = i g^n \sum_{P(1 \dots n)} (a_1 \dots a_n)_{ij} \mathcal{D}(q; 1 \dots n; \bar{q}). \quad (5.1.2)$$

The decomposition of  $\mathcal{M}$  in the Chan-Paton colour base results in  $n!$  gauge invariant subamplitudes,  $\mathcal{D}(q; 1 \dots n; \bar{q})$ . Note the suggestive notation of  $\mathcal{D}(q; 1 \dots n; \bar{q})$ , the ordering of the particles corresponds with the colour structure. Diagrammatically those Feynman graphs contribute to  $\mathcal{D}(q; 1 \dots n; \bar{q})$  that can be drawn in such a way that the external lines are ordered clockwise as:  $q12 \dots n\bar{q}$ , see section 3.5. Eq. (5.1.2) separates the computation of  $\sum_{c,\lambda} |\mathcal{M}_n|^2$  in two problems. We first present a method to compute the  $\mathcal{D}$ -functions and then indicate how the colour matrix can best be dealt with.

The  $\mathcal{D}$ -functions in eq. (5.1.2) are obtained with a method similar to the way the  $\mathcal{C}$ -functions were computed in chapter 4. Consider a quark-antiquark line with  $n$  on-shell gluons attached to it. The quark is on shell too and has colour  $i$  while the antiquark with colour  $j$  is kept off shell. Summing over all configurations of gluons results in a quark or spinor current,  $\hat{J}_{ij}(q; 1 \dots n)$  where the spinor index is omitted. An antiquark current is

constructed in a similar way and is denoted by  $\hat{J}_{ij}(1 \dots n; \bar{q})$ . Decomposed in the colour base,  $\hat{J}_{ij}(q; 1 \dots n)$  can be written as

$$\hat{J}_{ij}(q; 1 \dots n) = g^n \sum_{P(1 \dots n)} (a_1 \dots a_n)_{ij} J(q; 1 \dots n) \quad (5.1.3)$$

where  $J(q; 1 \dots n)$  no longer contains a colour structure. It is given by [1]

$$J(q; 1 \dots n) = - \sum_{m=0}^{n-1} J(q; 1 \dots m) J(m+1 \dots n) \frac{1}{\not{q} + \not{\epsilon}(1, n) - m_q}. \quad (5.1.4)$$

The vector gluon current  $J_\mu(m+1 \dots n)$  is contracted with a  $\gamma^\mu$  and  $\kappa(1, n)$  is defined in eq. (4.2.3). For  $m=0$  the  $J(q; 1 \dots m) \equiv J(q)$ . It is easy to picture where the various terms in eq. (5.1.4) originate from. A virtual gluon decaying into  $n-m$  gluons is connected at the off-shell side of a quark current that already has  $m$  gluons attached to it. The quark-propagator must be included to get the recursive formulation. The boundary or stopping condition of eq. (5.1.4) reads

$$J(q) = \bar{u}(q), \quad (5.1.5)$$

the spin-state of a free quark. With eqs. (4.2.5)-(4.2.7),  $J(q; 1 \dots n)$  can be computed. For an antiquark current the analogues of eqs. (5.1.3)-(5.1.5) read

$$\hat{J}_{ij}(1 \dots n; \bar{q}) = g^n \sum_{P(1 \dots n)} (a_1 \dots a_n)_{ij} J(1 \dots n; \bar{q}), \quad (5.1.6)$$

$$J(1 \dots n; \bar{q}) = \frac{1}{\not{q} + \not{\epsilon}(1, n) + m_q} \sum_{m=1}^n J(1 \dots m) J(m+1 \dots n; \bar{q}), \quad (5.1.7)$$

and

$$J(\bar{q}) = v(\bar{q}). \quad (5.1.8)$$

The amplitude for a process with a quark pair and  $n$  gluons is obtained from the quark current,  $\hat{J}_{ij}(q; 1 \dots n)$  by contracting it with  $v(\bar{q})$ , an on-shell antiquark and imposing momentum conservation

$$\mathcal{M}(q; 1 \dots n; \bar{q}) = \hat{J}_{ij}(q; 1 \dots n) (-i) [\not{q} + \not{\epsilon}(1, n) - m_q] J(\bar{q}) \Big|_{q+\bar{q}+\kappa(1, n)=0}, \quad (5.1.9)$$

where the factor  $(-i) [\not{q} + \not{\epsilon}(1, n) - m_q]$  removes the unphysical propagator in the quark current. From eqs. (5.1.2) and (5.1.9) follows that

$$\mathcal{D}(q; 1 \dots n; \bar{q}) = -J(q; 1 \dots n) [\not{q} + \not{\epsilon}(1, n) - m_q] J(\bar{q}) \Big|_{q+\bar{q}+\kappa(1, n)=0}. \quad (5.1.10)$$

And the equivalent expression for the antiquark current reads

$$\mathcal{D}(q; 1 \dots n; \bar{q}) = J(q) [\not{q} + \not{\epsilon}(1, n) + m_q] J(1 \dots n; \bar{q}) \Big|_{q+\bar{q}+\kappa(1, n)=0}. \quad (5.1.11)$$

The colour matrix that appears in  $\sum_{c,\lambda} |\mathcal{M}_n|^2$  is a symmetric  $n! \times n!$  matrix. Ordering the permutations as defined in section 4.4, results in the same symmetries, i.e. the complete matrix is obtained from the first  $(n-1)!/2$  rows in a trivial way. The leading order in colour contribution appears on the diagonal of the colour matrix

$$(a_1 \dots a_n)_{ij} (a_1 \dots a_n)_{ij}^* = (a_1 \dots a_n a_n \dots a_1) = \left( \frac{N^2 - 1}{2N} \right)^n. \quad (5.1.12)$$

Like in the zero quark case a factor  $(N^2 - 1)$  is separated in order to get a uniform leading order in colour term for all QCD parton processes, see chapter 8. This leads to

$$\sum_{c,\lambda} |\mathcal{M}(q; 1 \dots n; \bar{q})|^2 = g^{2n} (N^2 - 1) (2N)^{-n} N^{2n-2} \times \quad (5.1.13)$$

$$\sum_{\lambda} \sum_{P(1 \dots n)} \{ |\mathcal{D}(q; 1 \dots n; \bar{q})|^2 + O(N^{-2}) \}. \quad (5.1.14)$$

All other colour products are easily obtained by repeatedly using eq. (3.5.7) which, with the assistance of a symbolic algebra program, does not pose any problem. Discarding all  $O(N^{-2})$  terms corresponds with the leading order in colour approximation (LCA) which is examined in the next section.

We finish this section with a number of remarks that are useful in a numerical situation. In performing the sum over the helicities use should be made of parity conservation

$$\mathcal{D}(q, \lambda_q; 1, \lambda_1 \dots n, \lambda_n; \bar{q}, -\lambda_q) = \mathcal{D}(q, -\lambda_q; 1, -\lambda_1 \dots n, -\lambda_n; \bar{q}, \lambda_q)^*. \quad (5.1.15)$$

and of charge conjugation

$$\mathcal{D}(q, \lambda_q; 1, \lambda_1 \dots n, \lambda_n; \bar{q}, -\lambda_q) = -\mathcal{D}(\bar{q}, \lambda_q; n, -\lambda_n \dots 1, -\lambda_1; q, -\lambda_q)^*. \quad (5.1.16)$$

The latter however does not reduce the amount of work but serves as a numerical check.

The recursion relation can be used to obtain numerical results for scattering processes involving a massive quark pair and  $n$  gluons. With the spin-states as given in eq. (3.3.38) and the  $\gamma$ -matrix representation, eq. (3.3.1), the recursion relation can be expressed in WvdW spinor language. The spinor current  $J(q; 1 \dots n)$  written in components, see eq. (3.3.14), reads

$$J(q; 1 \dots n) = (J_1^A(q; 1 \dots n) \quad J_{2\dot{A}}(q; 1 \dots n)), \quad (5.1.17)$$

and eq. (5.1.4) transforms in

$$\begin{aligned} & (J_1^A(q; 1 \dots n) \quad J_{2\dot{A}}(q; 1 \dots n)) = \quad (5.1.18) \\ & - \frac{1}{(q + \kappa(1, n))^2 - m_q^2} \sum_{m=0}^{n-1} (J_1^C(q; 1 \dots m) \quad J_{2\dot{C}}(q; 1 \dots m)) \times \\ & \begin{pmatrix} 0 & J_{B\dot{C}}(m+1 \dots n) \\ J^{\dot{C}B}(m+1 \dots n) & 0 \end{pmatrix} \begin{pmatrix} m_q \epsilon^A_B & (q + \kappa(1, n))_{A\dot{B}} \\ ((q + \kappa(1, n))^{\dot{B}A}) & m_q \epsilon^{\dot{B}}_{\dot{A}} \end{pmatrix} \end{aligned}$$

The gauge freedom in the gluon polarization vectors and the arbitrariness of  $M$  in eq. (3.3.31) cannot easily be used to simplify the calculation on the numerical level. In case  $m_q = 0$ , eq. (5.1.18) simplifies enormously because the propagator-matrix only contains off-diagonal terms. The recursion relation then effectively becomes one dimensional. For instance with the quark having the + helicity we find

$$J_A(q; 1 \dots n) = - \sum_{m=0}^{n-1} J_C(q; 1 \dots m) J^{CB}(m+1 \dots n) \frac{[q + \kappa(1, n)]_{AB}}{(q + \kappa(1, n))^2}. \quad (5.1.19)$$

This special form shows that the numerical evaluation of the  $\mathcal{D}$ -functions is very easy for massless particles. In chapter 10 analytical results for the  $\mathcal{D}$ -functions are given. Contrary to the massive case compact analytical results in terms of WvdW spinors exist. By cleverly choosing the gauge freedom in the gluon polarization vectors the  $\mathcal{D}$ -functions can be computed for  $n < 5$ . The analytical results are preferable not only for studying the pole structure but most of all in numerical applications. This explains the tremendous difference between the CPU-time needed for the  $n = 4$  and  $n = 5$  cases.

As a last point we note that the sum over all physical parton processes always runs over four fundamentally different processes for all  $n$ . These are

$$q \bar{q} \rightarrow n g \quad (5.1.20)$$

$$q g \rightarrow q (n-1) g \quad (5.1.21)$$

$$g q \rightarrow q (n-1) g \quad (5.1.22)$$

$$g g \rightarrow q \bar{q} (n-2) g \quad (5.1.23)$$

Other parton processes are obtained from the above by means of charge conjugation. Numerically, process (5.1.20) turns out to be of little importance. The three other processes together contribute about the same to the total cross section as the purely gluonic process does, see chapter 8.

## 5.2 The LCA in processes with two quarks

The consequences of neglecting all  $O(1/N^2)$  terms in the colour matrix that occurs in  $\sum_{c,\lambda} |\mathcal{M}_n|^2$  are determined for processes with a quark pair and up to 5 gluons. In section 4.5 the details of the investigation were given.

In the LCA the matrix element squared is given by

$$\sum_{c,\lambda} |\mathcal{M}(q; 1 \dots n; \bar{q})|^2 = g^{2n} \frac{1}{2} (N^2 - 1) \left( \frac{N}{2} \right)^{n-1} \sum_{\lambda} \sum_{P(1 \dots n)} |\mathcal{D}(q; 1 \dots n; \bar{q})|^2. \quad (5.2.1)$$

The ratio LCA/exact for the  $p_T$  and the  $M_{ij}$  distributions is given in fig. 5.1. All two quark processes that contribute to a hadron-hadron collision are included, therefore the deviation from one is the error in the prediction for a collider experiment. The error is small and approximately a constant and thus only affects the normalization of the distributions a little bit. Note that the interference between  $\mathcal{D}$ -functions gives a negative contribution to  $\sum_{c,\lambda} |\mathcal{M}_n|^2$  while for the  $\mathcal{C}$ -functions it was positive.

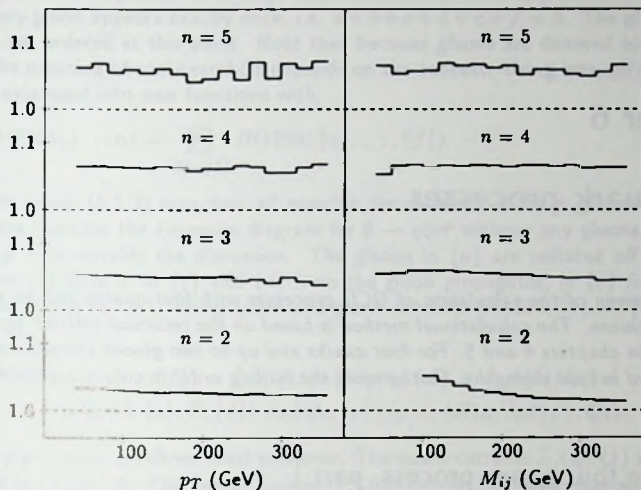


Fig. 5.1. Ratio LCA/exact for the  $p_T$  and  $M_{ij}$  distributions.

## References

- [1] W.T.Giele, Properties and calculations of multiparton processes, thesis, Leiden, 1989;  
 F.A. Berends and W.T. Giele, Nucl. Phys. **B306** (1988) 759.

## Chapter 6

### Four quark processes

*Details are given of the calculation of QCD processes with four quarks and an arbitrary number of gluons. The calculational method is based on the recursion relation techniques introduced in chapters 4 and 5. For four quarks and up to two gluons the subamplitudes are expressed in field strengths. Furthermore the leading order in colour approximation is discussed.*

#### 6.1 The four quark process, part I

The process with four quarks and  $n$  gluons is calculated in two different ways. In this section a method is described to determine the subamplitudes by means of recursion relation techniques. In the next section the subamplitudes are expressed in field strengths. The latter method is more suitable for numerical purposes because it enables us to obtain analytical expressions for the helicity amplitudes in terms of WvdW spinors. However two extra gluons is the limit for this method.

The recursion relations for gluon and quark currents are used to calculate amplitudes with four quarks and  $n$  gluons. Extending the recursive schemes of chapters 4 and 5, only one new ingredient is needed, a recursion relation for an object which consists of two off-shell gluons and a number of on-shell gluons.

With all the particles outgoing the process we consider reads

$$0 \rightarrow q_i(Q_1) + \bar{q}_j(Q_2) + r_k(Q_3) + \bar{r}_l(Q_4) + g(K_1) + \dots + g(K_n) \quad (6.1.1)$$

where  $i, j, k$  and  $l$  are quark colour indices. The gluons carry colour  $a_1 \dots a_n$ . The quark flavours  $q$  and  $r$  need not be the same. The equations in this section are valid for massive quarks too although the quark masses appear nowhere. For ease of notation the  $Q$ 's and  $K$ 's are often omitted. The matrix element for process (6.1.1) can be written as

$$\mathcal{M}(1234; 1 \dots n) = A(1234; 1 \dots n) - \delta_{qr} A(1432; 1 \dots n). \quad (6.1.2)$$

The second  $A(1234; 1 \dots n)$  contributes when  $q$  and  $r$  have the same flavour. The Feynman diagrams contributing to  $A(1234; 1 \dots n)$  are systematically generated and added with a method we now describe. Distribute the  $n$  gluons over six sets  $\{a\}, \{b\}, \dots, \{f\}$ .

Set  $\{a\}$  contains  $a$  gluons,  $a_1$  through  $a_a$ , etc. A set can be empty, the only restriction is that every gluon appears exactly once, i.e.  $a + b + c + d + e + f = n$ . The gluons in a set are not yet ordered at this point. Note that because gluons are denoted by their colour label, the meaning of some symbols depends on the context. Using sets,  $A(1234; 1 \dots n)$  can be expressed into new functions with

$$A(1234; 1 \dots n) = \sum_{\{a\} \dots \{f\}} B(1234; \{a\}, \dots, \{f\}). \quad (6.1.3)$$

The sum in eq. (6.1.3) runs over all possible distributions of the  $n$  gluons over the six sets. Now consider the Feynman diagram for  $\theta \rightarrow q\bar{q}r\bar{r}$  without any gluons and assume that  $q \neq r$  to simplify the discussion. The gluons in  $\{a\}$  are radiated off from  $q$ , the gluons in  $\{b\}$  from  $\bar{q}$ , in  $\{c\}$  and  $\{d\}$  from the gluon propagator, in  $\{e\}$  from  $r$  and in  $\{f\}$  from  $\bar{r}$ , see fig. 6.1. Using quark and gluon currents  $B(1234; \{a\}, \dots, \{f\})$  can be written as

$$B(1234; \{a\}; \dots; \{f\}) = \hat{J}_{im}(Q_1; \{a\}) ig \gamma_\mu (A)_{mn} \hat{J}_{nj}(\{b\}; Q_2) \times \quad (6.1.4) \\ (-i) \hat{J}_{AB}^{\mu\nu}(A; \{c\}; B; \{d\}) \hat{J}_{ko}(Q_3; \{e\}) ig \gamma_\nu (B)_{op} \hat{J}_{pl}(\{f\}; Q_4).$$

$m, n, a, p$  are colour labels we must sum over. The quark currents  $\hat{J}_{ij}(Q; \{a\})$  are described in detail in chapter 5. The tensor current  $\hat{J}_{AB}^{\mu\nu}(A; \{c\}; B; \{d\})$  describes an object with two off-shell and  $c + d$  on-shell gluons. The off-shell gluon with indices  $\mu$  and  $A$  carries momentum  $P_q = Q_1 + Q_2 + \{a\} + \{b\}$ , i.e. the sum of the momenta of the particles at the  $q\bar{q}$  side of the diagram. The other off-shell gluon has indices  $\nu$  and  $B$  and momentum  $P_r = Q_3 + Q_4 + \{e\} + \{f\}$ .

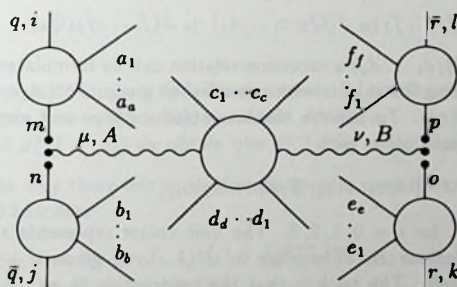


Fig. 6.1. The colour structure decomposition technique applied to a process with four quarks and  $a + b + c + d + e + f = n$  gluons.

The next step is to add those terms in  $B(1234; \{a\}, \dots, \{f\})$  that have the same colour structure. This is accomplished by ordering the gluons inside the sets and using recursion relations or colourless Feynman rules. The colour decomposition techniques applied to the currents that appear in eq. (6.1.4) result in

$$\hat{J}_{ij}(Q; \{a\}) = g^a \sum_{P(a_1 \dots a_a)} (a_1 \dots a_a)_{ij} J(Q; a_1 \dots a_a), \quad (6.1.5)$$

$$\hat{J}_{ij}(\{a\}; Q) = g^a \sum_{P(a_1 \dots a_a)} (a_1 \dots a_a)_{ij} J(a_1 \dots a_a; Q), \quad (6.1.6)$$

and

$$\hat{J}_{AB}^{\mu\nu}(A; \{c\}; B; \{d\}) = 2g^{c+d} \sum_{P(c_1 \dots c_c, B, d_1 \dots d_d)} (Ac_1 \dots c_c B d_1 \dots d_d) J^{\mu\nu}(A; c_1 \dots c_c; B; d_1 \dots d_d). \quad (6.1.7)$$

The  $J^{\mu\nu}(A; c_1 \dots c_c; B; d_1 \dots d_d)$  is a tensor current for an object with two off-shell gluons and  $c + d$  on-shell gluons and the gluons in sets  $\{c\}$  and  $\{d\}$  are ordered as in fig. 6.1. Notice that the off-shell gluon with index  $\nu$  is ordered in between gluons  $c_c$  and  $d_1$ . Now the colour part is separated from the dynamical part, the ordering of the gluons is used to decompose  $B(1234; \{a\}, \dots, \{f\})$  further to make this separation more explicit.

$$B(1234; \{a\}, \dots, \{f\}) = \sum_{P(a), \dots, P(f)} C(1234; a_1 \dots a_a, b_1 \dots b_b, \dots, f_1 \dots f_f), \quad (6.1.8)$$

where  $P(a), \dots, P(f)$  denote the permutations of gluons inside the sets. The  $C$  with indices as in eq. (6.1.8) is diagrammatically depicted in fig. 6.1. Summed over the colour labels,  $m, n, o$  and  $p$  it reads

$$\begin{aligned} C(1234; a_1 \dots a_a, b_1 \dots b_b, \dots, f_1 \dots f_f) &= 2 i g^{2+a+b+c+d+e+f} \quad (6.1.9) \\ &(a_1 \dots a_a b_1 \dots b_b)_{ij} J(Q_1; a_1 \dots a_a) \gamma_\mu J(b_1 \dots b_b; Q_2) \\ &(Ac_1 \dots c_c B d_1 \dots d_d) J^{\mu\nu}(A; c_1 \dots c_c; B; d_1 \dots d_d) \\ &(e_1 \dots e_e B f_1 \dots f_f)_{kl} J(Q_3; e_1 \dots e_e) \gamma_\nu J(f_1 \dots f_f; Q_4) \end{aligned}$$

For  $J^{\mu\nu}(A; c_1 \dots c_c; B; d_1 \dots d_d)$  a recursion relation can be formulated. Since we already have a recursion relation for objects with one off-shell gluon,  $J^{\mu\nu}(A; c_1 \dots c_c; B; d_1 \dots d_d)$  is related to  $J^\mu(1 \dots m)$ . To achieve this we introduce four unit vectors  $u_{i\nu}$  and relate the two currents to each other with

$$J^\mu(1 \dots m) \equiv J^{\mu\nu}(A; c_1 \dots c_c; B; d_1 \dots d_d) u_{i\nu}, \quad (6.1.10)$$

with  $m = c + d + 1$ , for  $i = 0, 1, 2, 3$ . The unit vector represents a gluon that carries momentum  $P_i$  and colour  $B$ . Therefore in  $J^\mu(1 \dots m)$  gluon  $c + 1$  is special in the sense that it is off-shell. The trick is that the contraction in eq. (6.1.10) is reversible. Calculation of  $J^\mu(1 \dots m)$  for every unit vector gives us  $J^{\mu\nu}(A; c_1 \dots c_c; B; d_1 \dots d_d)$ .

The gluon current  $J^\mu(1 \dots m)$  is given by, see also chapter 4

$$J^\mu(1 \dots m) = \frac{1}{\kappa(1, m)^2} \left( \sum_{k=1}^{m-1} [J(1 \dots k), J(k+1 \dots m)]^\mu \right) \quad (6.1.11)$$

$$+ \sum_{k=1}^{m-2} \sum_{l=k+1}^{m-1} \{J(1 \dots k), J(k+1 \dots l), J(l+1 \dots m)\}^\mu, \quad (6.1.12)$$

with

$$[J(1 \dots k), J(k+1 \dots m)]^\mu = \quad (6.1.13)$$

$$+ [2 \kappa(k+1, m) + \kappa(1, k)] \cdot J(1 \dots k) J^\mu(k+1 \dots m) \\ - [\kappa(k+1, m) + 2 \kappa(1, k)] \cdot J(k+1 \dots m) J^\mu(1 \dots k) \\ + J(1 \dots k) \cdot J(k+1 \dots m) [\kappa(1, k) - \kappa(k+1, m)]^\mu,$$

$$\{J(1 \dots k), J(k+1 \dots l), J(l+1 \dots m)\}^\mu = \quad (6.1.14)$$

$$+ 2 J(1 \dots k) \cdot J(l+1 \dots m) J^\mu(k+1 \dots l) \\ - J(1 \dots k) \cdot J(k+1 \dots l) J^\mu(l+1 \dots m) \\ - J(k+1 \dots l) \cdot J(l+1 \dots m) J^\mu(1 \dots k).$$

The boundary conditions read

$$J^\mu(i) = \kappa_i^\mu \quad (i \neq B), \quad J^\mu(B) = u_i^\mu / P_\tau^2, \quad u_i^\mu = \delta_i^\mu, \quad (6.1.15)$$

where the propagator for the internal gluon is included. Furthermore we used that

$$\kappa(1, m) = \sum_{i=1}^m K_i \quad \text{and in particular} \quad \kappa(B, B) = P_\tau \quad (6.1.16)$$

The difference with the original gluonic recursion relation is twofold. Firstly we must use the full three-gluon vertex because gluon  $B$  is off-shell and secondly the polarization vector for the off-shell gluon is artificial and is decomposed in unit vectors. Some properties of the original gluon current still hold, e.g.

$$\sum_{P(1 \dots m)} J^\mu(1 \dots m) = 0. \quad (6.1.17)$$

However,  $J^\mu(1 \dots m)$  is no longer a conserved current. By cutting off the  $u_{i\mu}$  and labeling the indices back again, see eq. (6.1.10), we obtain  $J^{\mu\nu}(A; c_1 \dots c_e; B; d_1 \dots d_d)$ . In other words from the four  $J^\mu(1 \dots m)$  we obtain one  $J^{\mu\nu}(A; c_1 \dots c_e; B; d_1 \dots d_d)$ .

At this point the only thing left to be done is to sum over the colours of the internal gluons. Eq. (6.1.9) becomes

$$C(1234; a_1 \dots a_a, b_1 \dots b_b, \dots, f_1 \dots f_f) = \frac{1}{2} g^{2+n} J(Q_1; a_1 \dots a_a) \gamma_\mu J(b_1 \dots b_b; Q_2) \\ J^{\mu\nu}(A; c_1 \dots c_e; B; d_1 \dots d_d) J(Q_3; e_1 \dots e_e) \gamma_\nu J(f_1 \dots f_f; Q_4) \times \\ [(a_1 \dots a_a c_1 \dots c_e f_1 \dots f_f)_{il} (e_1 \dots e_e d_1 \dots d_d b_1 \dots b_b)_{kj} \\ - \frac{1}{N} (a_1 \dots a_a b_1 \dots b_b)_{ij} (e_1 \dots e_e d_1 \dots d_d c_1 \dots c_e f_1 \dots f_f)_{kl} \\ - \frac{1}{N} (a_1 \dots a_a c_1 \dots c_e d_1 \dots d_d b_1 \dots b_b)_{ij} (e_1 \dots e_e f_1 \dots f_f)_{kl} \\ + \frac{1}{N^2} (a_1 \dots a_a b_1 \dots b_b)_{ij} (c_1 \dots c_e d_1 \dots d_d) (e_1 \dots e_e f_1 \dots f_f)_{kl}], \quad (6.1.18)$$

Substitution of eq. (6.1.18) in eq. (6.1.8) and adding the contributions with the same colour structure leads to a set of subamplitudes. The gauge invariance can be used as a

check on the correctness of the method. The last term in eq. (6.1.18) is special in the sense that we do not expect that colour structure to be present in the final result, i.e. the corresponding subamplitude should be zero. Performing the sum over the permutations, see eqs. (6.1.3) and eq. (6.1.8), and using eq. (6.1.17) shows that this is indeed the case except when both  $\{c\}$  and  $\{d\}$  are empty. Then, with  $Tr(I) = N$  the fourth term cancels the second or the third term.

With the explicit representations for the quark and gluon spin-states, it is possible to compute  $\sum_{c,\lambda} |\mathcal{M}_n|^2$  for any value of  $n$ , using eqs. (6.1.2), (6.1.3), (6.1.8) and (6.1.18). Note that the method described in this section is rather complicated and not very suited for numerical purposes. Nevertheless it can be used to check specific results and the validity of approximations for arbitrary  $n$ .

## 6.2 The four quark process, part II

The method discussed in the previous section is very general and can be extended to processes with more quarks. It allows the quarks to be massive and enables us to calculate  $\sum_{c,\lambda} |\mathcal{M}_n|^2$  for any number of gluons. However it is a complicated method and slow in a numerical application. If possible it is much better to obtain analytical results for the helicity amplitudes that correspond with a base of colour structures. In this section we organize the calculation that way for  $n \leq 2$ . This method resembles previous calculations [1]. In a numerical application we use the results of the previous section for  $n = 3$  only. The colour structures that occur in four quark processes are of the type

$$\frac{-1}{2N} (\{a\})_{ij} (\{b\})_{kl} \quad \text{and} \quad \frac{1}{2} (\{a\})_{ii} (\{b\})_{kj}, \quad (6.2.1)$$

where  $\{a\}$  and  $\{b\}$  represent a set of fundamental representation matrices. Additional colour structures occur for equally flavoured quarks ( $j \leftrightarrow l$ ). The matrix element for process (6.1.1) can be written as

$$\mathcal{M}(1234; 1 \dots n) = ig^{n+2} \sum_{i=1}^{2(n+1)!} e_i \mathcal{E}_i(q, \bar{q}, r, \bar{r}, 1 \dots n). \quad (6.2.2)$$

Note the labelling of the quarks ( $q \leftrightarrow 1$ , etc). The  $e_i$  are colour structures and the  $\mathcal{E}_i$  the corresponding subamplitudes which in principle do not depend on colour. However to minimize the number of different colour structures the explicit  $-1/N$  factor, see eq. (6.2.1), is put in  $\mathcal{E}_i$ . The  $e_i$  are defined as follows. Generate the permutations of gluons with the algorithm of subcyclic permutations, see section 4.4. For each permutation start with putting all the gluons in set  $\{b\}$  and subsequently transfer the foremost gluon to set  $\{a\}$ . This step has to be repeated  $n$  times. This procedure leads to  $(n+1) \times n!$  colour structures. For  $n = 2$  the ordering reads

$$e_1 = \frac{1}{2} \delta_{ij} (a_1 a_2)_{kl}, \quad e_2 = \frac{1}{2} (a_1)_{ij} (a_2)_{kl}, \quad e_3 = \frac{1}{2} (a_1 a_2)_{ij} \delta_{kl},$$

$$e_4 = \frac{1}{2} \delta_{ij} (a_2 a_1)_{kl}, \quad e_5 = \frac{1}{2} (a_2)_{ij} (a_1)_{kl}, \quad e_6 = \frac{1}{2} (a_2 a_1)_{ij} \delta_{kl}.$$

The second  $(n+1)!$  terms have  $j$  and  $l$  interchanged.

The subamplitude  $\mathcal{E}_i$  is either denoted by  $\mathcal{F}_{ab}(1234; \{a\}; \{b\})$  when the colour structure is of the first type in eq. (6.2.1) or by  $\mathcal{E}_{ab}(1234; \{a\}; \{b\})$  when the colour structure is of the second type. The subscript indices denote the number of gluons in sets  $\{a\}$  and  $\{b\}$ . These gluons can be seen to be colour ordered along a quark-antiquark line. In  $\mathcal{F}_{ab}(1234; \{a\}; \{b\})$  the gluons in set  $\{a\}$  are colour ordered along the  $q\bar{q}$  line and thus produce a colour structure  $(a_1 \dots a_n)_{ij}$  and the gluons in set  $\{b\}$  are along the  $r\bar{r}$  line producing a  $(b_1 \dots b_n)_{kl}$  colour chain. Likewise are the gluons in set  $\{a\}$  in  $\mathcal{E}_{ab}(1234; \{a\}; \{b\})$  ordered along the imaginary  $q\bar{r}$  line.

A number of symmetries exist for  $\mathcal{E}_{ab}$  and  $\mathcal{F}_{ab}$ . Interchanging  $1 \leftrightarrow 3$  and  $2 \leftrightarrow 4$  results in

$$\mathcal{E}_{ab}(1234; a_1 \dots a_n; b_1 \dots b_n) = \mathcal{E}_{ba}(3412; b_1 \dots b_n; a_1 \dots a_n), \quad (6.2.3)$$

and likewise for  $\mathcal{F}_{ab}$ . Charge conjugation combined with  $1 \leftrightarrow 2$ ,  $3 \leftrightarrow 4$  leads to

$$\mathcal{E}_{ab}(1234; a_1 \dots a_n; b_1 \dots b_n) = \mathcal{E}_{ba}(2143; b_n \dots b_1; a_n \dots a_1), \quad (6.2.4)$$

$$\mathcal{F}_{ab}(1234; a_1 \dots a_n; b_1 \dots b_n) = \mathcal{F}_{ab}(2143; a_n \dots a_1; b_n \dots b_1). \quad (6.2.5)$$

The subamplitudes can be calculated for all possible helicity combinations by direct methods. A more elegant way is to express them first in terms of field strengths. For  $n \leq 2$  the results read

$$\mathcal{F}_{00}(1234; ; ) = \frac{-1}{N} J_1 \gamma^\mu J_2 \frac{1}{\{1,2\}} J_3 \gamma_\mu J_4 \quad (6.2.6)$$

$$\mathcal{E}_{00}(1234; ; ) = J_1 \gamma^\mu J_2 \frac{1}{\{1,2\}} J_3 \gamma_\mu J_4 \quad (6.2.7)$$

$$\mathcal{F}_{10}(1234; 1; ) = \frac{-1}{N} J_1 \left[ \frac{1}{2} \not{F}_1 \gamma^\mu + \frac{1}{2} \gamma^\mu \not{F}_1 + \frac{4(1 \cdot F_1 \cdot 2)}{\{1, K_1\} \{K_1, 2\}} \right] J_2 \frac{J_3 \gamma_\mu J_4}{\{3,4\}} \quad (6.2.8)$$

$$\mathcal{E}_{10}(1234; 1; ) = +2 \frac{J_1 \gamma^\alpha J_2}{\{1,2\}} \frac{J_3 \gamma^\beta J_4}{\{3,4\}} \times \quad (6.2.9)$$

$$\frac{\{F_{1\alpha\beta} - g_{\alpha\beta} (4 \cdot F_1 \cdot 1) (\{1,2\} + \{3,4\}) - (1 \cdot F_1 \cdot 2) \{4, K_1\} + (4 \cdot F_1 \cdot 3) \{1, K_1\}\}}{\{1, K_1\} \{K_1, 4\}}$$

$$+ \frac{J_1 \not{F}_1 \gamma^\mu J_2}{\{1, K_1\}} \frac{J_3 \gamma_\mu J_4}{\{3,4\}} + \frac{J_1 \gamma^\mu J_2}{\{1,2\}} \frac{J_3 \gamma_\mu \not{F}_1 J_4}{\{K_1, 4\}}$$

$$\mathcal{F}_{20}(1234; 12; ) = \frac{-1}{N} \left[ \frac{J_1 \frac{1}{2} \not{F}_1 \gamma^\mu \frac{1}{2} \not{F}_2 J_2}{\{1, K_1\} \{K_2, 2\}} \frac{J_3 \gamma_\mu J_4}{\{3,4\}} \right. \quad (6.2.10)$$

$$+ J_1 \frac{-\not{F}_1 K_1 \cdot F_2 - 4(1 \cdot F_1 \cdot F_2)}{\{1, K_1\} \{K_1, K_2\}} [I + K_1 + K_2]^{-1} \gamma^\mu J_2 \frac{J_3 \gamma_\mu J_4}{\{3,4\}}$$

$$+ J_1 \gamma^\mu [K_1 + K_2 + 2]^{-1} \frac{K_2 \cdot F_1 \not{F}_2 - 4 F_1 \cdot F_2 \cdot 2}{\{2, K_1\} \{K_1, K_2\}} J_2 \frac{J_3 \gamma_\mu J_4}{\{3,4\}}$$

$$+ J_1 \left[ \frac{4(K_1 \cdot F_2 \cdot 2) \not{F}_1 \gamma^\mu + 4(1 \cdot F_1 \cdot K_2) \gamma^\mu \not{F}_2 - 8(1 \cdot F_1 \cdot F_2 \cdot 2) \gamma^\mu}{\{1, K_1\} \{K_1, K_2\} \{K_2, 2\}} \right] J_2 \frac{J_3 \gamma_\mu J_4}{\{3,4\}}$$

$$\mathcal{F}_{11}(1234; 1; 2) = \frac{-1}{N} J_1 \left[ \frac{\frac{1}{2} \not{F}_1 \gamma^\mu}{\{1, K_1\}} + \frac{\frac{1}{2} \gamma^\mu \not{F}_1}{\{2, K_1\}} + \frac{4(1 \cdot F_1 \cdot 2) \gamma^\mu}{\{1, K_1\} \{K_1, 2\}} \right] J_2 \times \quad (6.2.11)$$

$$\frac{1}{(1+2+K_1)^2} J_3 \left[ \frac{\frac{1}{2} \not{F}_2 \gamma_\mu}{\{3, K_1\}} + \frac{\frac{1}{2} \gamma_\mu \not{F}_2}{\{4, K_1\}} + \frac{4(3 \cdot F_2 \cdot 4) \gamma_\mu}{\{3, K_1\} \{K_1, 4\}} \right] J_4$$

$$\mathcal{E}_{20}(1234; 12; ) = \quad (6.2.12)$$

$$+ J_1 \gamma_\sigma [I + K_1]^{-1} \gamma_\tau [I + K_1 + K_2]^{-1} \gamma^\alpha J_2 \frac{J_3 \gamma_\alpha J_4 - 2(F_1 \cdot F_2)^{\sigma\tau}}{\{3, 4\} \{K_1, K_2\}}$$

$$+ \frac{J_1 \gamma_\alpha J_2}{\{1, 2\}} J_3 \gamma^\alpha [I + K_1 + K_2]^{-1} \gamma_\sigma [\not{I} + K_1]^{-1} \gamma_\tau J_4 \frac{-2(F_1 \cdot F_2)^{\sigma\tau}}{\{K_1, K_2\}}$$

$$+ J_1 \gamma_\sigma [I + K_1]^{-1} \gamma_\alpha J_2 J_3 \gamma^\alpha [I + K_2]^{-1} J_4 \frac{2(F_1 \cdot F_2)^{\sigma\tau}}{(1+2+K_1)^2 \{K_1, K_2\}}$$

$$+ J_1 \gamma_\sigma [I + K_1]^{-1} \gamma_\alpha J_2 \frac{J_3 \gamma^\alpha J_4 4(F_1 \cdot F_2 \cdot (3+4))^\sigma}{\{3, 4\} (1+2+K_1)^2 \{1, 2\}}$$

$$+ \frac{J_1 \gamma_\alpha J_2}{\{1, 2\}} J_3 \gamma^\alpha [I + K_2]^{-1} \gamma_\tau J_4 \frac{4((1+2) \cdot F_1 \cdot F_2)^\tau}{(1+2+K_1)^2 \{K_1, K_2\}}$$

$$+ \frac{J_1 \gamma_\alpha J_2}{\{1, 2\}} \frac{J_3 \gamma^\alpha J_4}{\{3, 4\}} \left\{ \frac{8(1+2) \cdot F_1 \cdot F_2 \cdot (3+4)}{(1+2+K_1)^2 \{K_1, K_2\}} + \frac{2 \text{Tr}(F_1 \cdot F_2)}{\{K_1, K_2\}} \right\}$$

$$+ J_1 \gamma_\sigma [I + K_1]^{-1} \gamma_\beta J_2 \frac{J_3 \gamma_\alpha J_4}{\{3, 4\}} \frac{F_2^{\alpha\beta}}{\{1, 2\}} \left\{ \frac{-2(1+2) \cdot F_1^\beta}{(1+2+K_1)^2} + \frac{2K_2 \cdot F_1^\beta}{\{K_1, K_2\}} \right\}$$

$$+ \frac{J_1 \gamma_\beta J_2}{\{1, 2\}} J_3 \gamma_\alpha [I + K_2]^{-1} \gamma_\sigma J_4 \frac{F_1^{\alpha\beta}}{\{3, 4\}} \left\{ \frac{2(3+4) \cdot F_2^\beta}{(3+4+K_2)^2} - \frac{2K_1 \cdot F_2^\beta}{\{K_1, K_2\}} \right\}$$

$$+ \frac{J_1 \gamma_\alpha J_2}{\{1, 2\}} \frac{J_3 \gamma_\beta J_4}{\{3, 4\}} \left\{ \frac{4(F_2 \cdot F_1)^{\alpha\beta}}{(1+2+K_1)^2} + \frac{4(F_2 \cdot F_1)^{\alpha\beta} - 4(F_1 \cdot F_2)^{\alpha\beta}}{\{K_1, K_2\}} \right\}$$

This expression is easily obtained by rewriting  $\mathcal{M}$  with

$$e_1^\alpha e_2^\beta \mathcal{M}_{\alpha\beta} = \left[ \frac{-K_1^\alpha e_2^\beta \{e_1, K_2\} + K_1^\alpha K_2^\beta \{e_1, e_2\} + e_1^\alpha e_2^\beta \{K_1, K_2\} - e_1^\alpha K_2^\beta \{K_1, e_2\}}{\{K_1, K_2\}} \right] \mathcal{M}_{\alpha\beta}$$

$$= \frac{-(F_1 \cdot F_2)^{\alpha\beta}}{\{K_1, K_2\}} \mathcal{M}_{\alpha\beta}. \quad (6.2.13)$$

$$\mathcal{E}_{11}(1234; 1; 2) = \quad (6.2.14)$$

$$+ \frac{J_1 \frac{1}{2} \not{F}_1 \gamma^\mu \frac{1}{2} \not{F}_2 J_2 J_3 \gamma_\mu J_4}{\{1, K_1\} \{2, K_2\} \{3, 4\}} + \frac{J_1 \frac{1}{2} \not{F}_1 \gamma^\mu J_2 J_3 \gamma_\mu J_4}{\{1, K_1\} \{3, 4\}} \frac{4(3 \cdot F_2 \cdot 2)}{\{3, K_2\} \{K_2, 2\}}$$

$$+ \left\{ \frac{J_1 \frac{1}{2} \not{F}_1 \gamma^\mu J_2}{\{1, K_1\} (1+2+K_1)^2} + \frac{J_1 \gamma_\nu J_2}{\{1, 2\}} \left[ \frac{-4(1 \cdot F_1 \cdot 2) g^{\nu\mu} + 2\{1, K_1\} F_1^{\nu\mu}}{\{1, K_1\} (1+2+K_1)^2} \right] \right\} \times$$

$$J_3 \left[ \frac{\frac{1}{2} \not{F}_2 \gamma_\mu}{\{3, K_2\}} + \frac{4\gamma_\mu (4 \cdot F_2 \cdot 3)}{\{3, 4\} \{3, K_2\}} - \frac{2F_{2\mu\alpha} \gamma^\alpha}{\{3, 4\}} \right] J_4$$

$$\begin{aligned}
& + \frac{J_1 \gamma^\mu J_2}{\{1,2\}} \frac{J_3 \frac{1}{2} \not{F}_2 \gamma_\mu \frac{1}{2} \not{F}_1 J_4}{\{3,K_2\}\{4,K_1\}} - \frac{J_1 \gamma^\mu J_2}{\{1,2\}} \frac{J_3 \gamma_\mu \frac{1}{2} \not{F}_1 J_4}{\{K_1,4\}} \frac{4(2 \cdot F_2 \cdot 3)}{\{2,K_2\}\{K_2,3\}} \\
& + J_1 \left[ \frac{\gamma^\mu \frac{1}{2} \not{F}_2}{\{2,K_2\}} - \frac{2\gamma_\alpha F_2^{\alpha\mu}}{\{1,2\}} - \frac{4\gamma^\mu (1 \cdot F_2 \cdot 2)}{\{1,2\}\{2,K_2\}} \right] J_2 \times \\
& \quad \left\{ \frac{J_3 \gamma_\mu \frac{1}{2} \not{F}_1 J_4}{\{K_1,2\}} + \frac{J_3 \gamma^\nu J_4}{\{3,4\}} \left[ \frac{2F_{1\mu\nu}\{2,K_1\} + 4(2 \cdot F_1 \cdot 3)g_{\mu\nu}}{(1+2+K_2)^2\{2,K_1\}} \right] \right\} \\
& + \frac{J_1 \gamma^\alpha J_2}{\{1,2\}} \frac{J_3 \gamma^\beta J_4}{\{3,4\}} \left[ \frac{8F_{1\beta\alpha}(2 \cdot F_2 \cdot 3)}{\{2,K_2\}\{K_2,3\}} + \frac{8F_{2\alpha\beta}(4 \cdot F_1 \cdot 1)}{\{1,K_1\}\{K_1,4\}} \right] \\
& + \left[ \frac{J_1 \gamma^\mu \frac{1}{2} \not{F}_2 J_2}{\{2,K_2\}\{3,4\}} + \frac{J_1 \gamma^\mu J_2}{\{1,2\}\{3,K_2\}} \frac{J_3 \gamma_\mu J_4}{\{3,4\}} \right] \frac{4(1 \cdot F_1 \cdot 4)}{\{1,K_1\}\{K_1,4\}} \\
& + \frac{J_1 \gamma^\mu J_2}{\{1,2\}} \frac{J_3 \gamma_\mu J_4}{\{3,4\}} \frac{J_1 \gamma^\mu J_2}{\{1,2\}} \frac{J_3 \gamma_\mu J_4}{\{3,4\}} \times \\
& \quad \left[ \frac{8(3 \cdot F_2 \cdot 2)(1 \cdot F_1 \cdot 4)(\{1,2\} + \{3,4\}) + 4(1 \cdot F_1 \cdot 4)(2 \cdot F_2 \cdot 3)\{K_1, K_2\}}{\{1,2\}\{3,4\}\{1,K_1\}\{2,K_2\}\{3,K_2\}\{4,K_1\}} \right. \\
& \quad + 8(3 \cdot F_2 \cdot 4)(2 \cdot F_2 \cdot 3)\{1,K_1\} - 2(2 \cdot F_2 \cdot F_1 \cdot 1)\{3,K_2\}\{4,K_1\} \\
& \quad + 8(2 \cdot F_1 \cdot 1)(3 \cdot F_2 \cdot 2)\{4,K_1\} - 2(2 \cdot F_2 \cdot F_1 \cdot 4)\{3,K_2\}\{1,K_1\} \\
& \quad + 8(1 \cdot F_2 \cdot 2)(4 \cdot F_1 \cdot 1)\{3,K_2\} - 2(3 \cdot F_2 \cdot F_1 \cdot 4)\{2,K_2\}\{1,K_1\} \\
& \quad \left. + 8(4 \cdot F_2 \cdot 3)(1 \cdot F_1 \cdot 4)\{2,K_2\} - 2(3 \cdot F_2 \cdot F_1 \cdot 1)\{2,K_2\}\{4,K_1\} \right]
\end{aligned}$$

In eqs. (6.2.6)-(6.2.14) we used the following abbreviations

$$J_i \equiv J(Q_i), \quad i \equiv Q_i \quad \text{and} \quad \not{F} = \gamma^\mu \gamma^\nu F_{\mu\nu} = \gamma^\mu \gamma^\nu (K_\mu e_\nu - K_\nu e_\mu). \quad (6.2.15)$$

The fact that no explicit gluon polarization vectors are present expresses the gauge invariant nature of the  $\mathcal{E}_i$ . The eqs. (6.2.6)-(6.2.14) are for massless quarks. The following relations are necessary to obtain helicity amplitudes

$$\not{F} = 2K \not{\epsilon}, \quad \not{F}^+ = \begin{pmatrix} 0 & 0 \\ 0 & -2\sqrt{2}k^A k_B \end{pmatrix} \quad \text{and} \quad \not{F}^- = \begin{pmatrix} 2\sqrt{2}k_A k^B & 0 \\ 0 & 0 \end{pmatrix} \quad (6.2.16)$$

from which directly follows that

$$\bar{u}_+(+) \not{F}^- = 0, \quad (6.2.17)$$

$$\not{F}_1^+ \not{F}_2^- = 0, \quad (6.2.18)$$

$$K_1 \not{F}_1 = \not{F}_1 K_1 = 0, \quad (6.2.19)$$

$$\not{F}_1^+ Q \not{F}_2^+ = 0. \quad (6.2.20)$$

In chapter 10 the helicity configurations are given explicitly. The symmetries, eqs. (6.2.3)-(6.2.5), together with parity conservation minimize the calculational effort. For equal flavoured quarks there is a small complication, the  $\mathcal{E}_i$  consist in that case of an  $\mathcal{E}_{ab}$  and an  $\mathcal{F}_{ab}$ . As a last remark we note that for  $n = 2$  the analytical results enable us to compute  $\sum_{c,\lambda} |\mathcal{M}_n|^2$  over 40 times faster than the general method described in the previous section.

### 6.3 The LCA in processes with four quarks

In this section we examine the consequences of neglecting all  $O(1/N)$  terms in the colour matrix for processes with four quarks and up to 3 gluons. This LCA is used in the SPHEL approximation for multiparton matrix elements, see chapter 8.

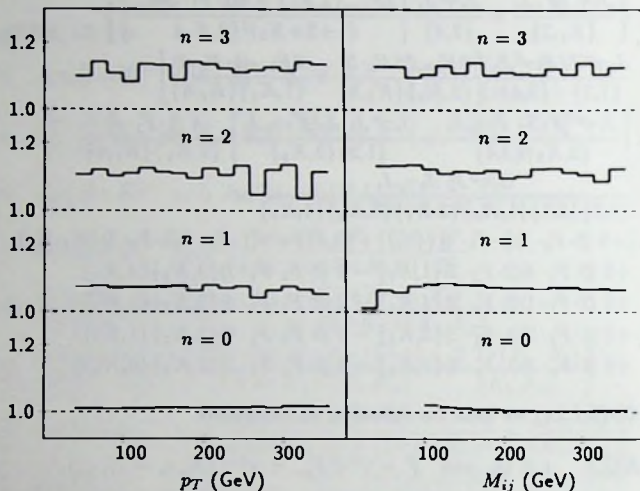


Fig. 6.2. Ratio LCA/exact for the  $p_T$  and  $M_{ij}$  distributions.

We carry out the investigation outlined in section 4.5. The LCA matrix element is

$$\sum_{c,\lambda} |\mathcal{M}(1234; 1 \dots n)|^2 = \frac{1}{4} g^{2n+2} (N^2 - 1) \left( \frac{N}{2} \right)^n \sum_{\lambda, \delta_{13}, \{a\}, \{b\}} |\mathcal{E}_{ab}(1234; \{a\}; \{b\})|^2, \quad (6.3.1)$$

where the sum runs over all helicities and possible distributions of the gluons over the sets  $\{a\}$  and  $\{b\}$ . For equal flavours the sum includes  $1 \leftrightarrow 3$ . The  $(N^2 - 1)$  is introduced to maintain uniformity with LCA for processes with fewer quarks, see eqs. (4.5.1) and (5.2.1). Note further that in the LCA all  $\mathcal{F}_{ab}$  are neglected.

The result for the ratio of exact and LCA in eq. (6.3.1) is given in fig. 6.2. All four quark processes have been included so that the deviation from one is the error caused by the LCA in prediction for collider experiments. The error increases with  $n$  but is not too large. Like for the zero and two quark cases the error caused by the LCA is approximately a constant over the whole  $p_T$  and  $M_{ij}$  domain.

### References

- [1] J.F. Gunion and Z. Kunszt, Phys. Lett. **159B** (1985) 167.

## Chapter 7

### Six quark processes

*Details are given of the calculation of QCD processes with six massless quarks, possibly with extra gluons. The numerical importance of six quark processes relative to processes with fewer quarks is examined.*

#### 7.1 The six quark process

In this section we organize the calculation of the six quark process in such a way that processes with six quarks and  $n$  gluons will be straightforward extensions. The process without gluons has already been dealt with in [1] but there the emphasis lies on the implementation of the calculation in a computer program. The systematic method we use for the calculation is adopted from [2], where processes with four quarks and a vector boson are considered. The six quark process is the only subprocess for which we do not use recursion relations. However we do use colour decomposition techniques, see chapter 3. The contribution of the six quark process to the total cross section is discussed in section 7.3, see also chapter 8.

All the particles are outgoing. The process we consider reads

$$0 \rightarrow q(Q_1) + \bar{q}(Q_2) + r(Q_3) + \bar{r}(Q_4) + s(Q_5) + \bar{s}(Q_6). \quad (7.1.1)$$

Each quark has a flavour  $f_i$  and a colour  $c_i$  ( $i = 1, \dots, 6$ ). The  $q$ ,  $r$  and  $s$  are not necessarily different flavours. For ease of notation the quarks are denoted by their momenta and the  $Q$  is left out, thus 1 stands for  $q(Q_1)$ . The odd numbers represent the quarks and the even numbers the antiquarks. The matrix element for process (7.1.1) is given by

$$\begin{aligned} \mathcal{M}(123456) = & A(123456) - A(123654) + A(163254) \\ & - A(163452) + A(143652) - A(143256), \end{aligned} \quad (7.1.2)$$

in which  $A(123456)$  is given by the seven Feynman diagrams in fig. 7.1.  $A(123456)$  does not contain any permutation of quarks. It consists of a set of  $\delta$ -functions that control the allowed permutations of the quarks, colour structures  $C$  and their corresponding

subamplitudes  $B$ .

$$\begin{aligned}
 A(123456) &= ig^4 \delta_{f_1 f_2} \delta_{f_3 f_4} \delta_{f_5 f_6} \\
 &\times [ C(14; 36; 52) B_1(123456) + C(16; 32; 54) B_2(123456) \\
 &\quad + C(14; 32; 56) B_3(123456) + C(16; 34; 52) B_4(123456) \\
 &\quad + C(12; 36; 54) B_5(123456) + C(12; 34; 56) B_6(123456) ]
 \end{aligned} \tag{7.1.3}$$

with

$$C(12; 34; 56) = \delta_{c_1 c_2} \delta_{c_3 c_4} \delta_{c_5 c_6} \tag{7.1.4}$$

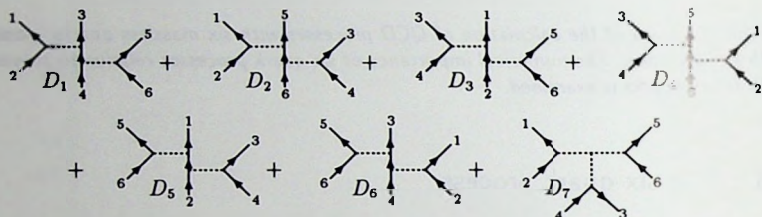


Fig. 7.1. The seven Feynman diagrams contributing to  $A(123456)$ .

The  $B_i(123456)$  are subamplitudes that do not have any colour structure. They can be expressed in the diagrams of fig. 7.1. Application of the Feynman rules gives

$$\begin{aligned}
 D_1(123456) &= -ig^4 (a)_{c_1 c_2} (ab)_{c_3 c_4} (b)_{c_5 c_6} D_A(123456) \\
 D_2(123456) &= -ig^4 (a)_{c_1 c_2} (ab)_{c_5 c_6} (b)_{c_3 c_4} D_A(125634) \\
 D_3(123456) &= -ig^4 (a)_{c_3 c_4} (ab)_{c_1 c_2} (b)_{c_5 c_6} D_A(341256) \\
 D_4(123456) &= -ig^4 (a)_{c_3 c_4} (ab)_{c_5 c_6} (b)_{c_1 c_2} D_A(345612) \\
 D_5(123456) &= -ig^4 (a)_{c_5 c_6} (ab)_{c_1 c_2} (b)_{c_3 c_4} D_A(561234) \\
 D_6(123456) &= -ig^4 (a)_{c_5 c_6} (ab)_{c_3 c_4} (b)_{c_1 c_2} D_A(563412) \\
 D_7(123456) &= -g^4 (a)_{c_1 c_2} (b)_{c_3 c_4} (c)_{c_5 c_6} f^{abc} D_B(123456)
 \end{aligned} \tag{7.1.5}$$

with

$$D_A(123456) = \frac{\bar{u}(1)\gamma_\mu v(2)}{(1+2)^2} \frac{\bar{u}(3)\gamma^\mu(1+2+3)\gamma^\nu v(4)}{(1+2+3)^2} \frac{\bar{u}(5)\gamma_\nu v(6)}{(5+6)^2} \tag{7.1.6}$$

$$\begin{aligned}
 D_B(123456) &= \frac{\bar{u}(1)\gamma_\mu v(2)}{(1+2)^2} \frac{\bar{u}(3)\gamma_\nu v(4)}{(3+4)^2} \frac{\bar{u}(5)\gamma_\alpha v(6)}{(5+6)^2} \\
 &\times [(1+2-3-4)^\alpha g^{\mu\nu} + (3+4-5-6)^\mu g^{\nu\alpha} + (5+6-1-2)^\nu g^{\alpha\mu}].
 \end{aligned} \tag{7.1.7}$$

The quantities  $f^{abc}$  are the structure constants of the  $SU(N)$  colour group, whereas the fundamental representation matrices are abbreviated by  $(a_1 \dots a_n)_{c_1 c_2} \equiv (T^{a_1} \dots T^{a_n})_{c_1 c_2}$ .

Summing over the colours in eqs. (7.1.5) results in the following  $B_i(123456)$

$$\begin{aligned}
 B_1(123456) &= -\frac{1}{4}(D_2 + D_3 + D_6 + D_7)(123456) \\
 B_2(123456) &= -\frac{1}{4}(D_1 + D_4 + D_5 - D_7)(123456) \\
 B_3(123456) &= \frac{1}{4N}(D_1 + D_3 + D_5 + D_6)(123456) \\
 B_4(123456) &= \frac{1}{4N}(D_2 + D_3 + D_4 + D_5)(123456) \\
 B_5(123456) &= \frac{1}{4N}(D_1 + D_2 + D_4 + D_6)(123456) \\
 B_6(123456) &= -\frac{1}{4N^2}(D_1 + D_2 + D_3 + D_4 + D_5 + D_6)(123456)
 \end{aligned} \tag{7.1.8}$$

Organizing the calculation this way it is easy to obtain  $\sum_{c,\lambda} |\mathcal{M}_n|^2$ . By adding the terms from the different  $A$ 's which have the same colour structure we arrive at

$$\begin{aligned}
 \mathcal{M}(123456) &= ig^4 \\
 &\times [ C(14; 36; 52)M_1(123456) + C(16; 32; 54)M_2(123456) \\
 &\quad + C(14; 32; 56)M_3(123456) + C(16; 34; 52)M_4(123456) \\
 &\quad + C(12; 36; 54)M_5(123456) + C(12; 34; 56)M_6(123456) ]
 \end{aligned} \tag{7.1.9}$$

where the  $M_i(123456)$ 's can be constructed from eqs. (7.1.2) and (7.1.3), for instance

$$\begin{aligned}
 M_1(123456) &= \delta_{f_1 f_2} \delta_{f_3 f_4} \delta_{f_5 f_6} B_1(123456) - \delta_{f_1 f_2} \delta_{f_3 f_6} \delta_{f_5 f_4} B_4(123654) \\
 &\quad + \delta_{f_1 f_6} \delta_{f_3 f_2} \delta_{f_5 f_4} B_2(163254) - \delta_{f_1 f_6} \delta_{f_3 f_4} \delta_{f_5 f_2} B_3(163452) \\
 &\quad + \delta_{f_1 f_4} \delta_{f_3 f_6} \delta_{f_5 f_2} B_6(143652) - \delta_{f_1 f_4} \delta_{f_3 f_2} \delta_{f_5 f_6} B_5(143256)
 \end{aligned} \tag{7.1.10}$$

Summing over the helicity states of the quarks gives

$$\sum_{c,\lambda} |\mathcal{M}(123456)|^2 = g^8 \sum_{\lambda} \sum_{i=1,6} \sum_{j=1,6} M_i(123456) C_{ij} M_j^*(123456) \tag{7.1.11}$$

The colour matrix  $C_{ij}$  is obtained by squaring eq. (7.1.9) and summing over the colours, making use of  $\delta_{cc} = N$ . Some remarks need to be made about the helicity configuration sum in eq. (7.1.11). For the six quark process without gluons there are 20 different helicity configurations. In that many ways it is possible to distribute 3 + and 3 - helicities over six particles. At first sight it appears that only 8 different helicity combinations need to be evaluated, because the quarks are massless and the function  $A(123456) = 0$  when, for instance, quarks 1 and 2 have the same helicity. But then  $A(143256)$  need not be zero.

The following procedure is the most efficient one to implement the method described above in a computer program. First determine every  $B_i(123456)$  for the eight different helicity configurations and the six possible permutations of the antiquarks as in eq. (7.1.2). Next determine all the helicity configurations for  $M_i(123456)$  for the five possible flavour combinations of  $q, r$  and  $s$

$$f_1 = f_2, f_3 = f_4, f_5 = f_6 \tag{7.1.12}$$

$$f_1 = f_2 = f_3 = f_4, f_5 = f_6 \tag{7.1.13}$$

$$f_1 = f_2, f_3 = f_4 = f_5 = f_6 \tag{7.1.14}$$

$$f_3 = f_4, f_1 = f_2 = f_5 = f_6 \tag{7.1.15}$$

$$f_1 = f_2 = f_3 = f_4 = f_5 = f_6, \tag{7.1.16}$$

by means of eq. (7.1.10) and the equivalent expressions for  $M_2(123456) - M_6(123456)$ . Finally use eq. (7.1.11) to obtain  $\sum_{c,\lambda} |\mathcal{M}_{n,\lambda}|^2$  for the processes (7.1.12)-(7.1.16). Most of the computer time is needed to evaluate the  $B_i(123456)$  functions, therefore we get the processes (7.1.12)-(7.1.15) at no extra cost when process (7.1.16) is evaluated. This clearly speeds up the sum over all possible physical subprocesses needed in a Monte Carlo simulation.

## 7.2 The six quark process with gluons

The formulae of the previous section are extended to include  $n$  extra gluons. At some places the results will be specifically for the one gluon case because that case is more interesting than the higher  $n$  cases. Eq. (7.1.1) transforms in

$$0 \rightarrow q(Q_1) + \dots + \bar{s}(Q_6) + g_1(K_1) + \dots + g_n(K_n). \quad (7.2.1)$$

where the gluons carry colour  $a_1 \dots a_n$ . The matrix element is again expressed in functions that do not contain permutations of quarks

$$\begin{aligned} \mathcal{M}(123456; 1 \dots n) = & A(123456; 1 \dots n) - A(123654; 1 \dots n) \\ & + A(163254; 1 \dots n) - A(163452; 1 \dots n) \\ & + A(143652; 1 \dots n) - A(143256; 1 \dots n). \end{aligned} \quad (7.2.2)$$

The  $A(123456; 1 \dots n)$ -function is decomposed in the colour base with

$$\begin{aligned} A(123456; 1 \dots n) = & ig^{4+n} \delta_{f_1 f_2} \delta_{f_3 f_4} \delta_{f_5 f_6} \times \sum_{\{a,b,c\}} \\ & [C(1a4; 3b6; 5c2)B_1(123456; a; b; c) + C(1a6; 3b2; 5c4)B_2(123456; a; b; c) \\ & + C(1a4; 3b2; 5c6)B_3(123456; a; b; c) + C(1a6; 3b4; 5c2)B_4(123456; a; b; c) \\ & + C(1a2; 3b6; 5c4)B_5(123456; a; b; c) + C(1a2; 3b4; 5c6)B_6(123456; a; b; c)]. \end{aligned} \quad (7.2.3)$$

In eq. (7.2.3) the  $a, b$  and  $c$  are sets which represent a number of gluons with the restriction that every gluon appears exactly once. Thus  $a, b$  and  $c$  together contain the  $n$  gluons. The ordering of the gluons inside a set is important. An example serves as the definition of the colour structures, see also eq. (7.1.4).

$$C(1a_3 a_1 4; 3a_2 6; 52) \equiv (a_3 a_1)_{c_1 c_4} (a_2)_{c_3 c_6} \delta_{c_5 c_2}. \quad (7.2.4)$$

Setting  $n = 0$  in eq. (7.2.3) transforms it into eq. (7.1.3). The sum in eq. (7.2.3) runs over the distributions of the gluons over  $a, b$  and  $c$ . It contains  $6 \times (n+2)!/2$  terms. The corresponding subamplitudes  $B_i(123456; a; b; c)$  are gauge invariant objects, which provides us with an excellent check on the correctness of the calculation. The number of Feynman diagrams that contribute to  $A(123456; 1 \dots n)$  is a rapidly growing function of  $n$ . For  $n = 1$  it is 64, see chapter 9. The diagrams  $D_1$  through  $D_6$  in fig. 7.1 can have a gluon attached in 9 places while diagram  $D_7$  has 10 places to add the extra gluon. The number of diagrams increases to 727 for  $n = 2$ .

Although  $A(123456; 1 \dots n)$  is very complicated due to the large number of diagrams, the equivalent expressions of eqs. (7.1.5) and (7.1.8) are still manageable. Each of the 64 diagrams in the  $n = 1$  case contribute to at most four different colour structures. The  $B_i(123456; a; b; c)$  are built up from a subset of diagrams just like in eqs. (7.1.8).

The generalization of eqs. (7.1.9)-(7.1.11) to the  $n$  gluon case reads

$$\mathcal{M}(123456; 1 \dots n) = ig^{4+n} \times \sum_{\{a,b,c\}} \quad (7.2.5)$$

$$\begin{aligned} & [ C(1a4; 3b6; 5c2)M_1(123456; a; b; c) + C(1a6; 3b2; 5c4)M_2(123456; a; b; c) \\ & + C(1a4; 3b2; 5c6)M_3(123456; a; b; c) + C(1a6; 3b4; 5c2)M_4(123456; a; b; c) \\ & + C(1a2; 3b6; 5c4)M_5(123456; a; b; c) + C(1a2; 3b4; 5c6)M_6(123456; a; b; c) ], \end{aligned}$$

with for instance,

$$M_1(123456; a; b; c) = \quad (7.2.6)$$

$$\begin{aligned} & \delta_{f_1 f_2} \delta_{f_3 f_4} \delta_{f_5 f_6} B_1(123456; a; b; c) - \delta_{f_1 f_2} \delta_{f_3 f_4} \delta_{f_5 f_6} B_4(123654; a; b; c) \\ & + \delta_{f_1 f_2} \delta_{f_3 f_4} \delta_{f_5 f_6} B_2(163254; a; b; c) - \delta_{f_1 f_6} \delta_{f_3 f_4} \delta_{f_5 f_2} B_3(163452; a; b; c) \\ & + \delta_{f_1 f_4} \delta_{f_3 f_6} \delta_{f_5 f_2} B_6(143652; a; b; c) - \delta_{f_1 f_4} \delta_{f_3 f_2} \delta_{f_5 f_6} B_5(143256; a; b; c). \end{aligned}$$

Summing over the helicity states of the quarks and gluons leads to

$$\sum_{c, \lambda} |\mathcal{M}_n|^2 = g^{8+2n} \sum_{\lambda, i, j, \{a; b; c\}} M_i(123456; a; b; c) C_{ij} M_j^*(123456; a; b; c) \quad (7.2.7)$$

with  $C_{ij}$  a  $3(n+2)! \times 3(n+2)!$  colour matrix.

An excellent check on the correctness of the calculation is taking the soft gluon limit. This limit relates the subamplitudes  $B_i(123456; a; b; c)$  for different number of gluons as follows. Consider that the gluon with index  $j$  is soft. If the fundamental representation matrix ( $a_j$ ) is set to unity, every colour structure of the process with the gluon transforms into one of the colour structures of the process without that gluon. For example

$$C(1aa_1 a_2 b_4; 3c6; 5d2) \rightarrow C(1aa_1 a_2 b_4; 3c6; 5d2). \quad (7.2.8)$$

The corresponding subamplitudes are then related by

$$B_i(123456; aa_1 a_2 b; c; d) = s_{1j2} B_i(123456; aa_1 a_2 b; c; d) \quad (7.2.9)$$

with

$$s_{1j2}^+ = \sqrt{2} \frac{\langle k_1 k_2 \rangle}{\langle k_1 j \rangle \langle j k_2 \rangle} \quad \text{and} \quad s_{1j2}^- = \sqrt{2} \frac{\langle k_1 k_2 \rangle^*}{\langle k_1 j \rangle^* \langle j k_2 \rangle^*} \quad (7.2.10)$$

for + and - helicity of gluon- $j$  respectively. In eq. (7.2.10) Weyl-van der Waerden spinors have been introduced. For the definitions and the properties of these spinors we refer to chapter 3. When a process with more than one gluon is considered one can also take two gluons soft at the same time. Relations like eq. (7.2.9) still hold but the soft factor gets more complicated [3]. In the case of six quarks and one gluon we explicitly verified eq. (7.2.9) numerically.

We conclude with some remarks on the implementation of the calculation in a computer program for  $n = 1$ . There is an exponential growth in complexity compared to the  $n = 0$  case. Twice as many helicity configurations and three times as many subamplitudes which are also more complex by themselves. Furthermore the number of subprocesses that contribute to one event on the hadron level increases from 11 to 19.

It is feasible to repeat the calculation for six quarks and two gluons. For more than one gluon a recursive scheme can be developed to obtain numerical results. However it may be easier to extend the calculational method of section 7.2 to  $n = 2$ . Moreover, in view of its expected numerical insignificance, see section 7.3, and the amount of computer time needed to evaluate one event, extrapolated from the numbers given in appendix A, it is a waste of time to calculate the  $n = 2$  case.

### 7.3 Six quark processes and experiment

We restrict ourselves to a qualitative analysis of the six quark process. In particular for four and five jet production the importance of the six quark process relative to the purely gluonic process is examined.

For the four hadron colliders introduced in section 2.4 we determine the cross sections using the cuts given in table 2.2. Furthermore we take  $n_F = 5$  and assume that the hadrons do not contain bottom quarks. The Duke and Owens set I is used for the structure function [4]. For the scale  $Q$  we take the average  $p_T$ . The results for the different subprocesses are given in table 7.1. In the first 11 subprocesses the  $(g)$  indicates the extra particle in the 5 jet case ( $m$  denotes the number of jets). Where appropriate we summed over the quark  $\leftrightarrow$  antiquark processes as well, for instance the result given for the  $gq$  initial state also contains the  $g\bar{q}$  initial state. To indicate the statistical errors we include both the  $gq$  (gluon from proton) and the  $qg$  (quark from proton) subprocesses. That they do not give the same result shows that the numbers in the table are indicative values only. The numbers for the total cross sections are given to show the relative importance of the six quark subprocess. For four jet production at CERN our results agree with [5]. However the authors counted one subprocess twice, processes 22 and 23 in table 1 in [5] are the same.

The process with six quarks is found to be negligible in the four jet case, contributing about 0.5% to the total cross section. Adding an extra gluon increases its importance for five jet production to 1-5%. The weight of the six quark processes is such that approximations for multijet cross sections can neglect contributions coming from processes with six quarks. The importance of the six quark processes changes only little when the experimental methods improve to the point where the primary parton of a jet can be identified. For instance when one bottom quark pair is identified the  $\sigma_{6q}/\sigma_{tot}$  goes up from 0.69% to 3.2% for the four jet cross section at the Tevatron collider.

| Subprocess                                  | SpS    |       | Tevatron |       | LHC   |       | SSC   |       |
|---------------------------------------------|--------|-------|----------|-------|-------|-------|-------|-------|
|                                             | $m=4$  | $m=5$ | $m=4$    | $m=5$ | $m=4$ | $m=5$ | $m=4$ | $m=5$ |
| $q\bar{q} \rightarrow q\bar{q} q\bar{q}(g)$ | 95     | 52    | 29       | 12    | 1.6   | 0.53  | 0.68  | 0.22  |
| $q\bar{q} \rightarrow q\bar{q} r\bar{r}(g)$ | 390    | 190   | 97       | 51    | 6.5   | 2.3   | 2.9   | 0.70  |
| $q\bar{q} \rightarrow r\bar{r} r\bar{r}(g)$ | 4.9    | 1.9   | 0.98     | 0.33  | 0.11  | 0.03  | 0.04  | 0.01  |
| $q\bar{q} \rightarrow r\bar{r} s\bar{s}(g)$ | 14     | 5.6   | 2.8      | 0.96  | 0.30  | 0.08  | 0.12  | 0.03  |
| $q\bar{q} \rightarrow q\bar{q} q\bar{q}(g)$ | 15     | 3.7   | 5.7      | 1.7   | 2.2   | 0.91  | 0.80  | 0.31  |
| $q\bar{q} \rightarrow q\bar{q} r\bar{r}(g)$ | 59     | 15    | 22       | 6.7   | 8.5   | 3.7   | 3.2   | 1.3   |
| $q\bar{r} \rightarrow q\bar{r} q\bar{q}(g)$ | 35     | 10    | 14       | 4.2   | 4.6   | 1.6   | 1.9   | 0.55  |
| $q\bar{r} \rightarrow q\bar{r} s\bar{s}(g)$ | 110    | 27    | 38       | 15    | 14    | 5.3   | 5.8   | 1.5   |
| $q\bar{t} \rightarrow q\bar{t} q\bar{q}(g)$ | 99     | 49    | 33       | 11    | 4.1   | 1.3   | 1.8   | 0.50  |
| $q\bar{t} \rightarrow q\bar{t} r\bar{r}(g)$ | 100    | 44    | 31       | 13    | 4.0   | 1.5   | 1.7   | 0.54  |
| $q\bar{t} \rightarrow q\bar{t} s\bar{s}(g)$ | 310    | 120   | 85       | 41    | 12    | 4.3   | 5.5   | 1.3   |
| $gq \rightarrow q q\bar{q} q\bar{q}$        |        | 1.0   |          | 0.30  |       | 0.12  |       | 0.05  |
| $gq \rightarrow q q\bar{q} r\bar{r}$        |        | 8.1   |          | 2.3   |       | 0.99  |       | 0.38  |
| $gq \rightarrow q r\bar{r} r\bar{r}$        |        | 3.6   |          | 1.1   |       | 0.49  |       | 0.18  |
| $gq \rightarrow q r\bar{r} s\bar{s}$        |        | 11    |          | 3.7   |       | 1.5   |       | 0.56  |
| $qg \rightarrow q q\bar{q} q\bar{q}$        |        | 1.2   |          | 0.31  |       | 0.11  |       | 0.05  |
| $qg \rightarrow q q\bar{q} r\bar{r}$        |        | 10    |          | 2.8   |       | 0.88  |       | 0.41  |
| $qg \rightarrow q r\bar{r} r\bar{r}$        |        | 6.2   |          | 1.3   |       | 0.42  |       | 0.20  |
| $qg \rightarrow q r\bar{r} s\bar{s}$        |        | 13    |          | 4.4   |       | 1.3   |       | 0.60  |
| Total 6 quarks                              | 1230   | 590   | 360      | 170   | 58    | 27    | 24    | 9.3   |
| Cross section                               | 150000 | 12000 | 52000    | 3500  | 24000 | 3600  | 13000 | 1000  |

Table 7.1. Cross sections in pb for processes with six quarks.

## References

- [1] J.F. Gunion and Z. Kunszt, Phys. Lett. **B176** (1986) 163.
- [2] F.A. Berends, W.T. Giele and H. Kuijf, Nucl. Phys. **B321** (1989) 91.
- [3] F.A. Berends and W.T. Giele, Nucl. Phys. **B313** (1989) 595.
- [4] D.W. Duke and J.F. Owens, Phys. Rev. **D30** (1984) 149.
- [5] Z. Kunszt and W.J. Stirling, Phys. Lett. **B171** (1986) 307.

## Chapter 8

### QCD and experiment

*A comparison of QCD predictions with experiment is made for the  $S\bar{p}\bar{p}S$  collider at CERN. A detailed study of jet production is made for the LHC, where special attention is paid to approximations that are proposed to replace the exact calculation. Furthermore jet cross sections are given for the hadron colliders introduced in section 2.4.*

#### 8.1 Introduction

The calculational methods of chapters 2-7 enable us to write a Monte Carlo program to examine jet production at hadron colliders. In this chapter we present results obtained with our Monte Carlo program NJETS. The predictions of NJETS are compared with collider experiments at CERN, in section 8.2. Four jet production is studied in detail but for five jet production the statistics still is too low. A study of jet production at the LHC is made in section 8.3. The main point of that section is to find out to what extent approximations can be used to replace the exact calculation. In section 8.4 we give the total jet cross sections for four hadron colliders. These are the  $S\bar{p}\bar{p}S$ , the Tevatron, the planned LHC and the proposed SSC. In particular the influence of various parton density functions and the contribution of different parton processes with  $l$  quark pairs to the total cross section, is studied.

#### 8.2 Four jets at the CERN collider

As an example of how well the QCD predictions fit the experimental data we look at four jet production at the CERN collider. The theoretical predictions are based on the exact matrix elements as described in this thesis, but the actual comparison with the experimental data has been carried out by Pasquale Lubrano of the UA2 group [1].

The theoretical input parameters for the CERN collider are:  $\sqrt{s} = 630$  GeV,  $\alpha_S(Q^2)$  with 5 flavours and the maximum  $p_T$  for  $Q$ . The parton density function used is Duke and Owens (set I) [2]. The phase space cuts are

$$p_{T_i} > 12 \text{ GeV.} \quad (8.2.1)$$

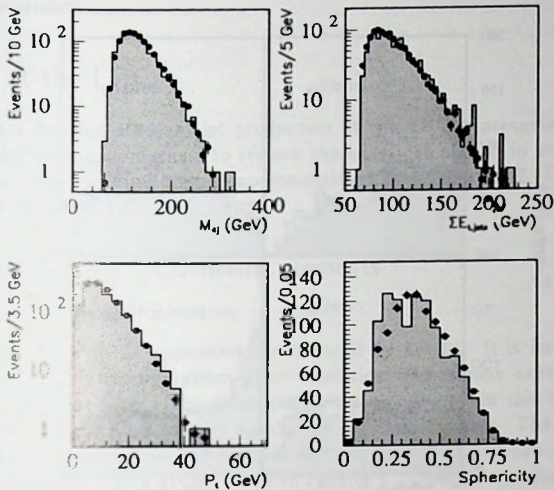


Fig. 8.1. Comparing theory with experiment for 4-jet production at the CERN collider. The quantities are defined in the text.

$$|\eta_i| < 2.5 \quad (8.2.2)$$

$$\theta_{ij} > 30^\circ \quad (8.2.3)$$

In an analysis these cuts only mimic the detector properties and the theoretical cross section based on these cuts is certainly not the measured one. Besides the parton level cuts there is a fragmentation model and a full simulation of the detector. We restrict ourselves to a global discussion of the results. For the details of the analysis see [3].

The data contains 10000 four jet events. With an integrated luminosity of  $7.6 \text{ pb}^{-1}$  this corresponds to a measured cross section of

$$\sigma_4(\text{data}) \simeq 1.30 \text{ nb.} \quad (8.2.4)$$

while the Monte Carlo result based on NJETS is

$$\sigma_4(\text{theory}) \simeq 1.28 \text{ nb.} \quad (8.2.5)$$

The errors are left out but are much larger than the difference between the two  $\sigma$ 's. They originate from two sources. The first one is the measurement of the events themselves. There are uncertainties in the calorimeter energy scale (13%), in the underlying event reconstruction (21%) and in the calorimeter response (20%). The second source is

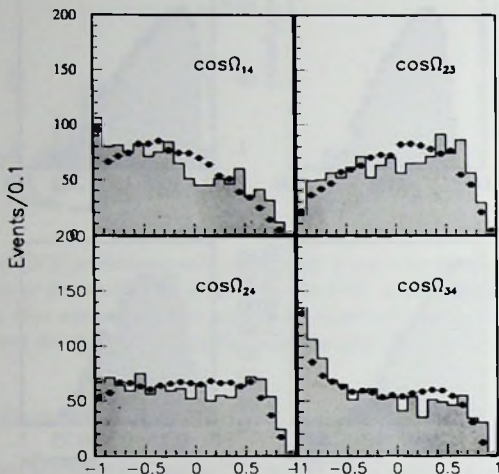


Fig. 8.2. Comparing theory with experiment for 4-jet production at the CERN collider. The angles are defined in the text.

the choice for the QCD scale  $Q$  and the parametrization of the parton density function one uses. It is difficult to estimate the corresponding errors but 50% for each of them appears to be a reasonable estimate. Therefore the cross section comparison only gives an indication that the theory agrees with experiment. It is better to look at the distributions. Some of them are displayed in figure 8.1. The black points are data points and the histograms are the theoretical predictions normalized to the data. In the plots  $M_{4j}$  is the invariant mass of the four-jet system or the parton centre of mass energy. The  $\sum E_{t,jets}$  is the sum of the transverse energies. The quantity  $P_T = |\sum \vec{p}_{T,i}|$  is the missing transverse momentum. Notice that the theoretical prediction for  $P_T$  is a  $\delta$ -peak at  $P_T = 0$ , because of momentum conservation. The fact that the  $P_T$  distribution has a large contribution for  $P_T > 0$  shows that the influence of the detector response is substantial. The sphericity is a measurement of the behaviour of the hadrons in the jets, see [4]. In fig. 8.2,  $\Omega_{14}$ ,  $\Omega_{23}$ ,  $\Omega_{24}$  and  $\Omega_{34}$  are the angles in the lab-frame between the jets ordered according to the  $p_T$ . In fig. 1.1 we have already shown the inclusive  $p_T$  spectrum. From the plots we infer that the agreement between theory and experiment is excellent for all distributions shown. In this respect we add that the theoretical histograms are based on 1250 events only, using a hit or miss Monte Carlo method. Therefore the statistical errors are still notable. Of course we would like to do the same analysis for five jet production but with only 300

events observed the statistics is too low to compare the experimental distributions with the theoretical predictions.

## 8.3 Jets at the LHC

In this section a detailed study of jet production at the LHC is presented. After introducing a number of approximations to replace the exact calculation in section 8.3.1, the exact results are compared with these approximations in section 8.3.2. Our findings are summarized in section 8.3.3.

### 8.3.1 Approximating QCD matrix elements

#### 8.3.1.1 Special helicity approximation

Most attention is paid to an approximation denoted by SPHEL. It is based on the fact that for certain helicity configurations short analytical expressions exist for  $K_F(P)$  in eq. (3.5.12). Together with a simplification of the colour matrix this leads to an approximation that can be used for any number of massless partons. The special helicity configurations are the ones where all but two partons have the same helicity when all the momenta are outgoing. Using SPHEL one can rewrite  $\sum_{c,\lambda} |\mathcal{M}_n|^2$  as follows

$$\sum_{c,\lambda} |\mathcal{M}_k^l(q_1 \bar{q}_1; \dots; q_l \bar{q}_l; g_1 \dots g_k)|^2 = \quad (8.3.1)$$

$$a_k^l S_k^l C_k^l(N) A_k^l(q_1 \bar{q}_1; \dots; q_l \bar{q}_l; g_1 \dots g_k).$$

In the following we explain the contents of eq. (8.3.1) and discuss its assumptions. SPHEL approximates the matrix elements with  $l$  quark pairs and  $k$  gluons by a sum over the special helicities. The event kinematics are contained in  $A_k^l$  which is a function of the momenta but not of the colours. Reduction of the colour matrix to the leading order contribution  $C_k^l(N)$  leads to factorization. The colour parts and the dynamical parts become independent and there is no interference between the  $K_F(P)$ . The two other parameters in eq. (8.3.1) are  $S_k^l$ , a combinatorial factor to account for the uncalculated helicity amplitudes, and  $a_k^l$ , which serves as an additional freedom. It enables us to give different weights to processes with a different number of quarks.

SPHEL contains two assumptions. The first one is that the special helicity configurations are assumed to be typical for all possible configurations. Earlier investigations [5] showed that for the purely gluonic subprocess this assumption is valid provided one considers the shape of distributions. However it fails when the total cross section is evaluated. SPHEL with  $l = 0$  gives results for the total cross section at the Tevatron collider energy which are greater than those of the EXACT, a factor of 1.4 for  $n = 7$ . This can be corrected by setting  $a_7^0 = 0.7$ , but as will be shown in the next section the precise value of  $a_k^l$  depends on both the collider energy and on the phase space cuts applied. Therefore it appears that we cannot expect SPHEL to give good results for the total cross section unless we tune the weight factors  $a_k^l$ . This is a cumbersome procedure and probably not

worth the trouble. Instead SPHEL aims to get the shape of the distributions right rather than their normalization. Note that this is not too serious because there are anyhow great uncertainties. Altogether they can easily account for a factor of 2. However in ratios of cross sections many of the uncertainties cancel. Therefore we have verified that the tune factors  $a_k^l$  of SPHEL do grow slowly with  $n$ .

The second assumption of SPHEL is that one can neglect the non leading order colour contribution. For the gluonic subprocess the error was found to be very small, for  $n = 6$  it is about 1% and for  $n = 7$  about 5%, and depended only slightly on the cuts [5]. However for processes with more quarks the error is substantially larger, for  $l = 1$  it can amount to 10%, but the shape of the distribution does not change much. The difference in the error introduced by the colour approximation is a reason to introduce different  $a_k^l$  for different  $l$ -values. We note that the error caused by the LCA is not very sensitive to changes in the collider energy.

The precise expression for SPHEL depends on the number of quarks present. We first introduce the notation and then distinguish between different values for  $l$ . The quark momenta are denoted by  $q, r$  and  $s$ . This improves the clarity. Permutations of identical partons are denoted by  $P(\dots)$ . In the following we omit the normalization freedom  $a_k^l$ , in the experimental section it is always set to 1.

$$l = 0$$

The  $l = 0$  part of SPHEL has first been proposed by Kunszt and Stirling in [6]. The combinatorial factor uses the property that the subamplitudes are zero when less than two gluons have a helicity opposite to the helicity of the other gluons. Note that for  $k = 4$  there is double counting in  $A_4^0$ , which is corrected by  $S_4^0 = 1/2$ . For  $k \leq 5$  SPHEL coincides with the EXACT result.

$$A_k^0 = 2 \sum_{1 \leq i < j \leq k} (i \cdot j)^4 \sum_{P(2 \dots k)} \frac{1}{(1 \cdot 2)(2 \cdot 3) \dots (k \cdot 1)}, \quad (8.3.2)$$

$$S_k^0 = \frac{2^k - 2(k+1)}{k(k-1)}, \quad (8.3.3)$$

$$C_k^0 = 4(N/2)^{k-2} (N^2 - 1). \quad (8.3.4)$$

$$l = 1$$

The  $l = 1$  case is based on the general form of the subamplitude as given in [7]. The colour part is cast in the same form as for  $l = 0$  and the combinatorial factor is adjusted to exclude the helicity configurations which are zero. Those are the combinations where all the gluons have the same helicity state. Again  $S_2^1 = 1/2$  corrects for the double counting in  $A_2^1$ .

$$A_k^1 = 2 \sum_{i=1}^k \left[ (q \cdot i)^3 (\bar{q} \cdot i) + (q \cdot i)(\bar{q} \cdot i)^3 \right] \quad (8.3.5)$$

$$\sum_{P(1 \dots k)} \frac{1}{(\bar{q} \cdot q)(q \cdot 1)(1 \cdot 2)(2 \cdot 3) \dots (k \cdot \bar{q})}$$

$$S_k^1 = \frac{2^k - 2}{2k}, \quad (8.3.6)$$

$$C_k^1 = 2(N/2)^{k-1}(N^2 - 1). \quad (8.3.7)$$

$l=2$

Ignoring all the  $O(1/N)$  terms we take

$$A_k^2 = 2 \sum_{P(q\bar{r})} \frac{(q \cdot r)^2 + (\bar{q} \cdot \bar{r})^2 + (q \cdot \bar{r})^2 + (r \cdot \bar{q})^2}{(q \cdot \bar{q})(r \cdot \bar{r})} \quad (8.3.8)$$

$$\sum_{P(1 \dots k)} \sum_{t=0}^k \left\{ \frac{(q \cdot \bar{r})}{(q \cdot 1) \dots (t \cdot \bar{r})} \frac{(r \cdot \bar{q})}{(r \cdot t + 1) \dots (k \cdot \bar{q})} \right\}$$

$$S_k^2 = 2^{k-1} \quad (8.3.9)$$

$$C_k^2 = (N/2)^k (N^2 - 1). \quad (8.3.10)$$

The first summation in eq. (8.3.8) should be carried out when the quarks have the same flavour. For different flavours it should be omitted. Eq. (8.3.8) is based on the helicity amplitude where all the gluons have the same helicity [8], see also chapter 10.

$l > 2$

There are no nonzero special helicity configurations with more than two massless quark pairs. SPHEL ignores the subprocesses with  $l > 2$ . This is justified since the dominant subprocess is given by the purely gluonic one ( $l = 0$ ). Moreover for increasing  $l$  the parton subprocesses become less important.

In section 8.3.1.4 a method is sketched how the SPHEL equations can be efficiently evaluated.

### 8.3.1.2 Effective structure function approximation

In this section we discuss the so called effective structure function approximation denoted by ESFA. It assumes that all matrix elements give rise to the same shape for any distribution. The cross sections for any initial state are essentially similar functions which are proportional to the colour charges of the incoming partons. It assumes that the relative weight of the various subprocesses can be attributed to the different parton density functions rather than to the different numbers obtained for  $\sum_{c,\lambda} |\mathcal{M}_n|^2$  [9]. So instead of evaluating all the parton subprocesses we take a limited set and adjust  $f_i^H(x, Q^2)$  in eq. (2.1.1) to account for the other subprocesses. ESFA aims to have both the normalization and the shape of the distributions right. Which matrix elements one should evaluate is a matter of taste and of trial and error. We discuss two choices.

The first approach is based on the multigluon matrix element, also called ESFA<sub>G</sub> or the UA1 structure function. The sum in eq. (2.1.1) is limited to one term only, the  $i = j = g$  term and both the structure functions are replaced by

$$f_{e'f'j}^H(x, Q^2) = f_g^H(x, Q^2) + 4/9 \sum_q [f_q^H(x, Q^2) + f_{\bar{q}}^H(x, Q^2)]. \quad (8.3.11)$$

The sum runs over the quark flavours  $u, d, s$  and  $c$ . The factor  $4/9$  is a naive colour factor which is based on the replacement of a pair of gluons by a pair of quarks and on  $N = 3$ . The  $4/9$  contains a factor  $(N^2 - 1)/N$  from colour averaging and a factor  $1/(2N)$  from the different colour matrix, see also the  $C_k^l$  ratios in the SPHEL method. The only  $\sum_{e,\lambda} |\mathcal{M}_n|^2$  to be evaluated is the one for  $n$ -gluon scattering. Processes like  $gg \rightarrow q\bar{q}(n-4)g$  are omitted because they are numerically unimportant.

The second choice is the application of the ESFA to processes with a quark and antiquark, of different flavour, in the initial state. This approximation is called ESFAQ. The parton subprocess is given by:  $q\bar{r} \rightarrow q\bar{r} + (n-4)g$ . We should also include processes with more quark pairs like  $q\bar{r} \rightarrow q\bar{r}s\bar{s} + (n-6)g$  but these can be neglected because they are numerically very small. The effective structure function becomes

$$f_{e'f'j}^H(x, Q^2) = 9/4 f_g^H(x, Q^2) + \sum_q [f_q^H(x, Q^2) + f_{\bar{q}}^H(x, Q^2)]. \quad (8.3.12)$$

Note that ESFAQ will be less useful than ESFAG because the underlying quark-antiquark subprocess requires much more computer time than the multigluon matrix element, see appendix A.

At this point we summarize the main differences between the SPHEL and ESFA approximations. The first one allows for different distributions of the various subprocesses or different  $l$ -values. Such differences are known to exist. The ESFA is justified from the experimental observation that such differences are not yet important in view of the experimental precision. Priority is given here to predict the absolute rates as good as is possible.

### 8.3.1.3 Other approximations

As mentioned above one drawback of SPHEL is that we do not obtain the correct normalization of the distributions. Two other approximations which we will now discuss try to avoid this problem. However they both have serious disadvantages compared to SPHEL and ESFA. For both cases so far no detailed numerical comparison with the exact calculation has been made. The observations of the next paragraph are based on findings while trying out the various approximations.

SPHEL uses a special helicity configuration which turns out to be too large to represent the average helicity configuration. A possible improvement is to apply the Monte Carlo technique to the helicity configurations. Instead of the complete calculation of  $\sum_{e,\lambda} |\mathcal{M}_n|^2$  we evaluate just one, random, helicity combination and multiply the result by  $n_H$ , the total number of helicity configurations. This Monte Carlo method (MCHL) is much slower than SPHEL because the latter uses a particular helicity configuration for which a short expression exist. However MCHL gets the normalization right and the gain factor on EXACT could in principle be  $n_H$ . In practice it is much lower, since parity conservation makes the actual number of helicity amplitudes to be evaluated smaller. Also not all the helicity configurations are evaluated equally fast. The disadvantages of

a helicity Monte Carlo are twofold. Firstly, in processes with more than one quark pair it is a problem how to handle forbidden helicity combinations that arise when identical quarks are interchanged. Secondly, the statistical errors in a Monte Carlo integration over helicities are larger because not all the helicity configurations are included. The error on the average of  $N$  different helicity combinations is generally smaller than  $N$  times the error on one of them. So more events are needed to get the same accuracy. This disadvantage also exist for SPHEL but in this case it is more than made up by the fact that it is a very fast method. We found that in most cases the MCHL method is not significantly more efficient than the EXACT calculation.

Another attempt to get the normalization right was made in [10] but for the gluonic process only. The matrix element for  $n$ -gluon scattering is approximated by a reduction scheme in which the pair of the most collinear gluons is replaced by a single on shell gluon and a collinearity factor. This procedure continues until only five gluons are left over for which the exact expression is used (SPHEL with  $l = 0$  and  $k = 5$ ). This method is the same as SPHEL but with the difference that the factor  $a_k^0(k > 5)$  in eq. (8.3.1) depends on the momenta of the event instead of being constant. It was shown that the normalization indeed gets better, for instance in [5]. The reduction scheme is not easily applicable to processes with a quark pair [11]. Even more difficulties arise when more quark pairs are involved. Since we do want to include the quark processes, the reduction scheme cannot replace SPHEL. When one is willing to omit quark processes it is conceivable that the reduction method for the gluonic part in conjunction with an effective structure function approximation gives reasonable results for both the distributions and the total cross section.

#### 8.3.1.4 SPHEL in a numerical application

In this section we examine how to evaluate the SPHEL expressions, eqs. (8.3.2)-(8.3.10), most efficiently. The difficulty lies in the permutation sum. To simplify the problem define

$$A_n \equiv \sum_{P(1 \dots n)} f(L, 1, \dots, n, R) \quad (8.3.13)$$

with

$$f(L, 1, \dots, n, R) = \frac{1}{(L \cdot 1)(1 \cdot 2) \dots (n \cdot R)}, \quad (8.3.14)$$

where  $L$  and  $R$  are arbitrary momenta. Because  $A_n$  has to be evaluated many times it is necessary to do it efficiently. The evaluation of eq. (8.3.13) consists of the generation of all the permutations of the indices  $1 \dots n$ . Algorithms to generate permutations are known to be time consuming [5, 16] and if it is possible it is best to generate them once and store them. However this will limit the maximum value of  $n$  considerably due to a limit on the available memory, to  $n = 7$ . The evaluation of eq. (8.3.14) consists of  $n + 1$  multiplications, given the inner products of the momenta. Clearly evaluation of every  $f$  separately leads to many duplicated operations. An interesting property of  $f$  is that the ratio of two  $f$ 's related to each other by a *swap*, i.e. with two neighbouring indices interchanged, is a simple function:

$$\frac{f(L, 1, \dots, a, b, c, d, \dots, n, R)}{f(L, 1, \dots, a, c, b, d, \dots, n, R)} = \frac{(a \cdot c)(b \cdot d)}{(a \cdot b)(c \cdot d)} \quad (8.3.15)$$

If the ordering of the permutations is such that two successive permutations are related to each other by a swap, the evaluation of eq. (8.3.14) simplifies significantly. Based on these requirements we generate all  $n!$  permutations of the indices 1 through  $n$  with the following algorithm.

**Algorithm:** Start with the permutation  $(1, 2, \dots, n)$  and introduce a swap direction for every index. This direction is initially with the left neighbour. Apply the following step recursively: Swap index  $i$  one time unless a) there are no indices in the swap direction, or b) the index to change places with is higher. If the swap was not successful then reverse the swap direction of index  $i$  and apply the recursion step to index  $i - 1$ . If the swap was successful continue the step with index  $n$ . The recursion is started with  $i = n$  and stops when an attempt is made to swap with  $i = 1$ .

An example, for  $n = 3$  the algorithm produces the following list of permutations:  $(1, 2, 3)$ ,  $(1, 3, 2)$ ,  $(3, 1, 2)$ ,  $(3, 2, 1)$ ,  $(2, 3, 1)$  and  $(2, 1, 3)$ . It is easy to prove that after  $n!$  swaps all the permutations are generated. Notice that executing the swap with index 1 restores the original permutation. If the recursion is stopped when an attempt is made to swap with  $i = 2$ , one has exactly those elements where the 2 is to the right of index 1. This is a useful property when  $L = R$ .

| $n$ | Method I | Method II |
|-----|----------|-----------|
| 3   | 0.94     | 1.00      |
| 4   | 1.81     | 1.92      |
| 5   | 5.37     | 5.16      |
| 6   | 27.2     | 23.0      |
| 7   | 207      | 147       |
| 8   | —        | 1160      |
| 9   | —        | 10300     |

Table 8.1. Speed of two different methods to evaluate the SPHEL equations

The algorithm described above allows an efficient evaluation of eqs. (8.3.13) and (8.3.14) for all values of  $n$ . In table 8.1 we compare two different methods. Method I uses storage of the permutations and straightforward evaluation of  $f$ . Method II is the one described above. Furthermore  $n + 1$  corresponds to the number of particles in a physical process and the numbers are normalized to have the  $n = 3$  Method II result equal to 1 unit of time. From the table we conclude that method II is faster for large  $n$ -values and more importantly it works for  $n > 7$ . One can read off the approximate increase in computer time when an extra final state particle is included.

### 8.3.2 Multijets at the LHC

In this section multijet production is studied at the LHC. In particular we are interested whether the approximations can replace the exact calculation. Using realistic input parameters we first determine the multijet production rates. Having thus determined their normalization, the distributions are examined with respect to a number of quantities. We focus on four and five jet production.

For  $\sqrt{s} = 16$  TeV the cuts must be rather stringent in order to stay in the perturbative safe region. If the cuts are set too loose we integrate over those parts of phase space where the events have soft or collinear partons. In that case higher order corrections would be needed to get reliable results. Our choice for the cuts is

$$p_{T_i} > 60 \text{ GeV}, \quad (8.3.16)$$

$$|\eta_i| < 2.0, \quad (8.3.17)$$

$$\theta_{ij} > 40^\circ \quad (8.3.18)$$

for each pair of outgoing partons  $i$  and  $j$ . Here  $p_{T_i}$  is the transverse momentum of parton  $i$ ,  $\eta_i$  the rapidity and  $\theta_{ij}$  is the angle between partons  $i$  and  $j$ . We opt to do an extensive study with this set of cuts only. This last restriction is a necessity since we had to spend the equivalent of 100 hours of CRAY time to get the results of this section. The other parameters are chosen as follows: the parton density function are those of Duke and Owens with  $\Lambda = 0.2$  GeV [2],  $\alpha_S(Q^2)$  is used in first order with  $n_f = 5$  and for the QCD scale  $Q$  we take the maximum  $p_T$  of the event. It is open to debate whether one can still use the Duke and Owens set I (DO I) for the LHC. For two jet production the mean value of  $x_i$  is about  $1.0 \cdot 10^{-2}$  which lies on the boundary of the validity region for most parton density functions. For more jets the mean value of  $x_i$  goes up to  $5.0 \cdot 10^{-2}$  for five jets. As we will show the parametrization of DO I does not deviate much from more recent parametrizations for the quantities under consideration. Therefore it can serve our present purposes.

#### 8.3.2.1 Cross section $\sigma_m$

The cross sections for the multijet final states with the cuts as defined in eqs. (8.3.16)-(8.3.18) are shown in table 8.2. One can see that the two and three jet rates are very large. For LHC, with an expected integrated luminosity of  $10^4 - 10^5 \text{ pb}^{-1}$  one expects in the order of  $10^{10}$  two jet events per  $10^7$  seconds. Clearly an impossible amount to be measured. More important is the expected number of multijet events. With millions of five jet events one can foresee an excellent opportunity to test perturbative QCD. As far as the approximations are concerned we see that ESFAQ gives the best results. The ESFAQ is not only lower but the ratio  $\sigma_{EXACT}/\sigma_{ESFAQ}$  varies between 1.2 and 1.8. This behaviour more or less rules out ESFAQ in favour of ESFAQ. SPHEL has the same problems as ESFAQ but with the error being 20% for five jets it is still reasonable.

We also included in table 8.2 the available fraction of phase space,  $V_m$  which remained after application of the phase space cuts in eqs. (8.3.16)-(8.3.18) for that value of  $\hat{s}$ , the

| nr. of jets | EXACT | SPHEL | ESFAG | ESFAQ | $V_m$ (%) |
|-------------|-------|-------|-------|-------|-----------|
| $m = 2$     | 7400  | 7500  | 7300  | 6400  | 67        |
| $m = 3$     | 250   | 260   | 240   | 190   | 38        |
| $m = 4$     | 19.9  | 22.6  | 19.1  | 12.5  | 21        |
| $m = 5$     | 1.42  | 1.77  | 1.40  | 0.80  | 11        |

Table 8.2. Comparison of the cross section (in nb) for the EXACT and for the proposed approximations at the LHC. Parameters and cuts are defined in the text.

| nr. of jets | EXACT      |                  |                    | SPHEL      |                  |                    |
|-------------|------------|------------------|--------------------|------------|------------------|--------------------|
|             | $\sigma_m$ | $\bar{\sigma}_m$ | $\tilde{\sigma}_m$ | $\sigma_m$ | $\bar{\sigma}_m$ | $\tilde{\sigma}_m$ |
| $m = 2$     | 7400       | -                | -                  | 7500       | -                | -                  |
| $m = 3$     | 250        | 550              | -                  | 260        | 553              | -                  |
| $m = 4$     | 19.9       | 17.9             | 8.5                | 22.6       | 18.7             | 9.0                |
| $m = 5$     | 1.42       | 1.35             | 1.58               | 1.77       | 1.54             | 2.04               |
| $m = 6$     | -          | 0.10             | 0.10               | -          | 0.13             | 0.14               |

Table 8.3. Estimating  $\sigma_6$  from  $\sigma_m$  with  $m < 6$ . Cross sections in nb.

parton level centre of mass energy squared, where the largest contribution to  $\sigma_m$  is coming from. With the results of table 8.2 we can predict the cross section for cases with more jets. There are two different ways to predict  $\sigma_6$ .

The first method proceeds as follows. Together with  $\alpha_S = 0.13$  taken at  $Q = 120$  GeV, we predict  $\sigma_m$  from  $\sigma_{m-1}$  using

$$\bar{\sigma}_m = \alpha_S \sigma_{m-1} V_m / V_{m-1}. \quad (8.3.19)$$

The results for  $\bar{\sigma}_m$  are presented in table 8.3. The agreement gets better for higher  $m$  values. The explanation is that for higher  $n$ -values the kinematic pole structure of the matrix elements do not change much and the shrinking of the available phase space together with the extra  $\alpha_S$  in eq. (8.3.19) become the most important reduction factors. Eq. (8.3.19) should of course only be used as a rule of thumb. For the LHC the prediction is  $\sigma_6 = 100$  pb. A clear drawback of eq. (8.3.19) is that one needs to know  $V_m$ ,  $V_6 \simeq 6\%$ .

The second method uses ratios of cross sections,

$$\tilde{\sigma}_m = (\sigma_{m-1})^2 / \sigma_{m-2} \quad (8.3.20)$$

The results are again in table 8.3. The rules eq. (8.3.19) and eq. (8.3.20) give the same results for  $\sigma_6$ . Therefore with a brief investigation of the exact multijet production rates we can predict  $\sigma_6$  without extensive calculations. The predictions for SPHEL are  $\bar{\sigma}_6 = 130$  pb and  $\tilde{\sigma}_6 = 140$  pb while  $\sigma_6 = 120 \pm 5$  pb is the Monte Carlo result based on SPHEL.

The influence of the parton density function on  $\sigma_m$  is revealed in table 8.4. Using the SPHEL approximation we have calculated  $\sigma_m$  for the following parametrizations. DO

| $\sigma_m$              | $\sigma_{DO I}$ | $\sigma_{DO II}$ | $\sigma_{EHLQ}$ | $\sigma_{GHR}$ | $\sigma_{EMC}$ | $\sigma_{BCDMS}$ |
|-------------------------|-----------------|------------------|-----------------|----------------|----------------|------------------|
| $m = 2$                 | 7500            | 10410            | 8100            | 9100           | 5400           | 7000             |
| $m = 3$                 | 260             | 340              | 290             | 350            | 190            | 250              |
| $m = 4$                 | 22.6            | 31.8             | 25.4            | 33.5           | 16.5           | 22.3             |
| $m = 5$                 | 1.8             | 2.8              | 2.1             | 3.1            | 1.32           | 1.8              |
| $\sigma_{m-1}/\sigma_m$ |                 |                  |                 |                |                |                  |
| $m = 3$                 | 28.8            | 30.6             | 27.9            | 26.0           | 28.4           | 28.0             |
| $m = 4$                 | 11.5            | 10.7             | 11.4            | 10.4           | 11.5           | 11.2             |
| $m = 5$                 | 12.6            | 11.4             | 12.1            | 10.8           | 12.5           | 12.4             |

Table 8.4. Comparison of different parton density functions.  $\sigma_m$  in nb.

set I and set II [2], EHLQ [12], GHR [13] and EMC and BCDMS [14]. As expected the differences in  $\sigma_m$  are considerable. The ratios  $\sigma_{m-1}/\sigma_m$  are in good agreement with each other. This indicates that uncertainties in the parton density function tend to cancel in ratios of quantities.

| $p_T, \theta$       | 12,30 | 12,35 | 12,40 | 15,30 | 15,35 | 15,40 | 20,30 | 20,35 | 20,40 |
|---------------------|-------|-------|-------|-------|-------|-------|-------|-------|-------|
| $\sigma_4$ (nb)     | 106   | 86    | 73    | 23    | 19    | 16    | 2.6   | 2.1   | 1.8   |
| $\sigma_4/\sigma_5$ | 14.3  | 16.2  | 20.3  | 19.0  | 21.1  | 24.6  | 27.7  | 30.9  | 38.5  |
| $\sigma_5/\sigma_6$ | 13.9  | 18.3  | 18.9  | 18.9  | 20.4  | 23.3  | 25.6  | 35.2  | 42.7  |

Table 8.5.  $\sigma_4$  and cross section ratios at the CERN SpP5 energy.

Although the ratio of cross sections is insensitive to the parton density function used it is not a quantity that can be determined without further experimental details. It is difficult to implement the exact detector properties. We make a comparison of  $\sigma_{m-1}/\sigma_m$  with the CERN collider results as reported in [3]. They observed 10000, 300 and 10 events with 4, 5 and 6 jets respectively. Together with an integrated luminosity of 7.6  $\text{pb}^{-1}$  this corresponds to  $\sigma_4 = 1.3$  nb,  $\sigma_4/\sigma_5 = 33$  and  $\sigma_5/\sigma_6 = 30$ . Taking  $\sqrt{s} = 630$  GeV, we varied the constraints in eq. (8.3.16) and eq. (8.3.18) a little bit. The constraint eq. (8.3.17) is kept fixed at  $|\eta_i| < 2.0$ . The cut parameters are denoted by  $p_T, \theta$ . For SPHEL the results can be found in table 8.5. We observe that the ratios are compatible with the measurements as soon as the cuts are tuned such that  $\sigma_4$  is more or less right. Therefore one could use  $p_{T_i} > 20$  and  $\theta_{ij} > 35^\circ$  as an effective set of cuts as far as the total cross section is concerned. We realise that this way of simulating detector properties and fragmentation of partons into jets is rather dangerous.

Next we look at the individual contribution of each parton subprocess to  $\sigma_m$ . For  $n = 6$  and  $n = 7$  the results are presented in the tables 8.6 and 8.7. We compare the EXACT with the SPHEL approximation. First a few remarks to clarify the contents of the tables. We list the parton subprocesses according to the number of quark pairs, the quarks

| nr. of jets | $\sigma_{SPHEL}/\sigma_{EXACT}$ |           |           |
|-------------|---------------------------------|-----------|-----------|
|             | two gluons                      | one gluon | no gluons |
| $m = 2$     | 1.00                            | 1.00      | 1.03      |
| $m = 3$     | 1.02                            | 1.02      | 1.06      |
| $m = 4$     | 1.11                            | 1.19      | 1.25      |
| $m = 5$     | 1.10                            | 1.39      | 1.26      |

Table 8.8. Cross section ratio of SPHEL and EXACT for different numbers of gluons in the initial state.

and  $l > 1$ . The second property is the number of initial state gluons because of the relative importance of  $f_g$  at low  $x$ -values. This property is especially important for the supercolliders. A third property is whether there exists a two particle propagator with an initial and final state particle. The rapidity cut is more loose than the  $\theta_{ij}$  cut. Therefore the process  $q\bar{q} \rightarrow q\bar{q}gg$  is more important than  $q\bar{q} \rightarrow r\bar{r}gg$ . Taking all these properties into account the contribution of  $q\bar{q} \rightarrow (n-2)g$  is still very low compared to the other processes with two quarks. For this we have no satisfactory explanation. Note that  $\sigma_m$  is largely determined by just 4 processes, namely  $gg \rightarrow (n-2)g, gg \rightarrow q(n-3)g, q\bar{q} \rightarrow q(n-3)g$  and  $gg \rightarrow q\bar{q}(n-4)g$ , making up 91% of  $\sigma_4$  and 87% for  $\sigma_5$ .

The comparison of EXACT with SPHEL shows that the latter is mostly higher but that the ratio  $R$  of the two seems to depend on just two things: on the number of gluons and on the spin of the incoming particles. We have no clear understanding why  $R$  behaves like this. Especially the difference in  $R$ -values for  $l = 1$  is striking. To complicate matters further, it is not always true that if  $R > 1$  for  $m = 4$  then also  $R > 1$  for  $m = 5$  (see  $gg \rightarrow q\bar{q}r\bar{r}g$ ). From tables 8.6 and 8.7 we can infer values for  $a_k^l$ , for example taking  $a_k^l = 1.2$  for  $m = 5$  would improve the normalization of the distribution at the LHC. This is not very important.

In table 8.8 a comparison is made between EXACT and SPHEL accordingly to the number of gluons in the initial state. The ratio of cross sections is compatible for the three possible cases. However for higher  $m$ -values the fluctuations become larger.

We stress once again that considered the importance of the  $gg$  initial process it is important to have reliable parton density functions for the gluon for low  $x$ -values. A first attempt has already been made in [15].

### 8.3.2.2 Distributions

As mentioned before it is not important for an approximation to predict  $\sigma_m$  very accurately. A better test is to see whether the shape of distributions resemble the EXACT ones. In fig. 8.3 we start by showing the  $p_T$  distribution for  $m$ -jet production. The normalization is  $m\sigma_m$ , each jet in an event is used for the histogram. The shapes obtained for EXACT, SPHEL and ESFAG are identical but for ESFAQ we see that the shapes are somewhat flatter for 4 and 5 jet production. This indicates that quarks are harder, i.e. they have more chance to be produced with a high  $p_T$ , than gluons.

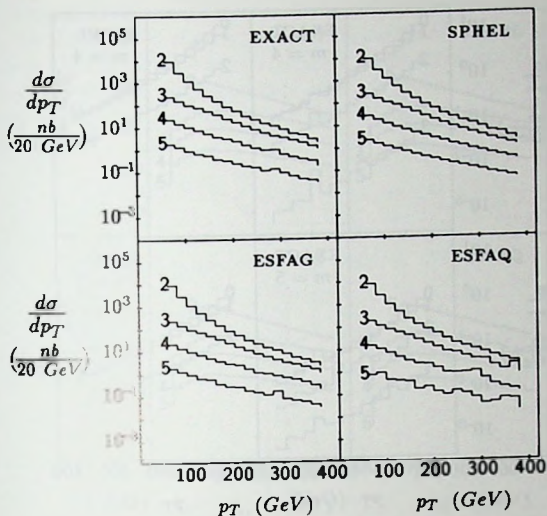


Fig. 8.3. The  $p_T$  distribution for 2,3,4 and 5 jet production.

For ESFAQ the statistical errors are much larger. Still for each  $m$ -value the same amount of events was used to make the plots for ESFAG and ESFAQ. In the latter the four quark process is harder to handle in a Monte Carlo because it contains a more complicated pole structure. In fig. 8.4 we subdivided the EXACT and SPHEL according to the number of quark pairs. One sees that the individual shapes are reproduced by SPHEL. One might suspect that because of the differences between  $l=0$  and  $l=1$ , ESFAG can not be very good but looking at fig. 8.3 in greater detail, i.e. beyond the experimental precision, shows that this is not the case and that ESFAG is very good over the whole  $p_T$  range.

In fig. 8.5 we plot the distribution for  $M_{ij} = \sqrt{2p_i \cdot p_j}$ . The normalization of this distribution is  $\sigma_m m(m-1)/2$ . In fig. 8.6 a detailed comparison is made between EXACT and SPHEL. The agreement is very good for  $m=4$ . For  $m=5$  the statistics are poorer but with some imagination the ratio can be regarded as a constant.

Looking once again at the figures one notices that as far as the distributions are concerned both SPHEL and ESFAG can be used to replace the exact calculation. SPHEL is slightly preferable because a lower statistical error can be reached. As a final remark, distributions evaluated with a constant matrix element are quite different, examples can be found in chapter 4.

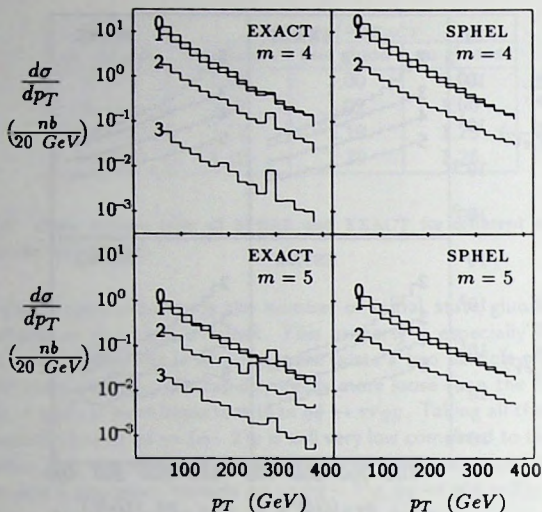


Fig. 8.4. A detailed comparison of the  $p_T$  distributions for EXACT and SPHEL for 4 and 5 jets. A distinction is made according to the number of quark pairs  $l$ .

### 8.3.3 Summary, conclusions and outlook

In the first place this section gave results for multijet production at the LHC using the exact matrix elements. Secondly we have shown that the exact calculation of eq. (2.1.1) can be replaced by two reasonable approximations. SPHEL is the numerically faster method while ESFAG predicts  $\sigma_m$  slightly better. Both approximations do not only describe the distributions very well but also give sufficiently good results for the total cross section considering the problems mentioned in the introduction. At first sight this should lead to the conclusion that both approximations are usable. However we think that SPHEL is the approximation one should use in Monte Carlo simulations. There are three arguments for this: The first one is that SPHEL is much faster in a numerical application. The second one is that it allows for differences between multigluon and multiquark distributions. Although this is not relevant right now it might be in the future when some type of quark jets may be tagged. And a third argument is that ESFAG cannot be used for  $m \geq 5$  unless we replace the exact matrix element by the  $l = 0$  part of SPHEL, but then  $\sigma_m$  will come out too large.

The results shown are for one particular collider energy and with one set of cuts. It is our experience that the approximations also work for other collider energies and other types of cuts. The normalization error of SPHEL varies, for the CERN collider we found

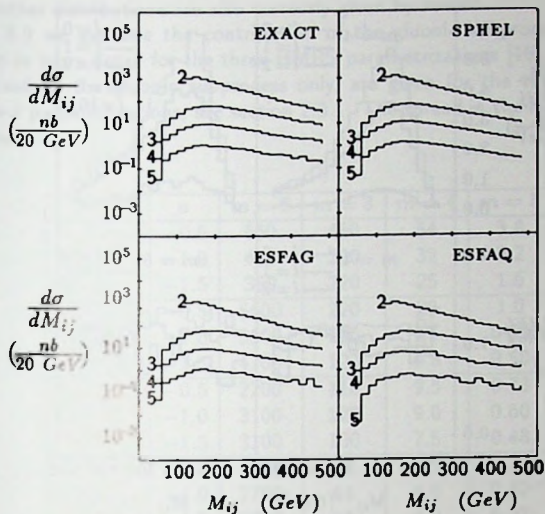


Fig. 8.5. The  $M_{ij}$  distribution for 2,3,4 and 5 jet production.

an overestimation of 30%.

Detailed studies of the jet decay modes of new physics processes should settle whether multijet physics can help in finding the top quark and the Higgs particle. This depends heavily on the ability of jet tagging for bottom quarks and on improvements in jet energy measurements.

## 8.4 Jet cross sections

Jet cross sections are examined for the hadron colliders described in section 2.4, with the cuts as defined in table 2.2,  $\alpha_S(Q^2)$  based on 5 flavours and for  $Q$  we take the average  $p_T$ . For four different parametrizations of the parton density function, [2, 13, 14], the 2, 3, 4 and 5 jet cross sections are in tables 8.10-8.13. We start with a brief description of the entries. The  $\sigma$  in entry  $\sigma/I/P$  refers to the total cross section  $\sigma_m$ , with  $m$  the number of jets, based on the exact matrix elements, or to the cross section  $\sigma_m^{pp}$  based on the SPHEL approximation. The  $I$  refers to the three possible initial states,  $gg$ ,  $gq$  or  $qq$ , where the  $q$  denotes a quark or an antiquark. The  $P$  corresponds to the entry  $0/2/4q$  and denotes the number of quarks present in the subprocess. The numbers for the cross sections are given in nb, the subdivisions are in percentages of the total cross section, i.e. they contain relative contributions. The many sources of uncertainty were already

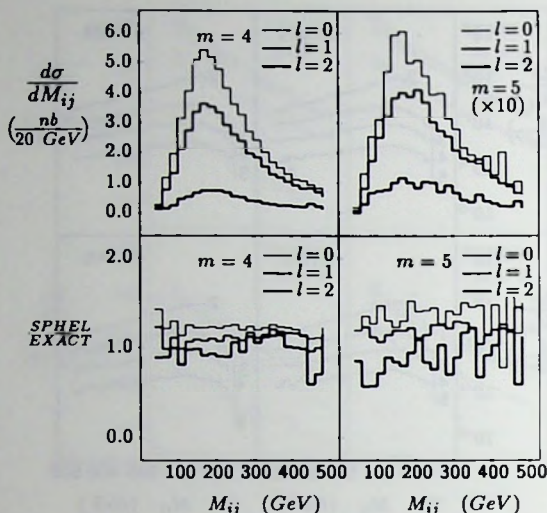


Fig. 8.6. Detailed comparison of EXACT with SPHEL for 4 and 5 jets. In the upper plots we used the EXACT matrix elements. In the lower plots the ratio of the two is plotted.

indicated in chapter 2. The statistical errors in the Monte Carlo integration alone are approximately 0.5, 1.0, 3.0 and 10% for 2, 3, 4 and 5 jets respectively. In this respect we note that some errors are larger, e.g. for the 2q and the 4q entries and some are smaller, e.g. for  $\sigma_m^{app}$ . The Monte Carlo errors depend only little of the particular collider. In spite of the relatively small errors the numbers should be seen as indicative values in view of the additional uncertainties.

Studying the table contents leads to the following conclusions. The particular parton density function used does not alter the relative contributions much. This indicates that the parton density function influences the normalization of the distributions rather than their shape, see also section 8.3. It may eventually be possible to compare absolute predictions with experiment and rule out some of the parton density functions because there is a rather large spread in the predictions. The tables show once again that it is important to have a correct understanding of the low  $x$  behaviour of the parton density function for the gluon. The contribution of processes decreases when the amount of quarks is increased. The SPHEL approximation assumes this behaviour. The results for SPHEL are in fair agreement with the predictions based on the exact matrix elements, indicating that for jet production the SPHEL approximation can be used to replace the exact calculation. Of course a more detailed study, like the one in section 8.3 is necessary

to settle whether distributions are also correctly given by SPHEL.

In table 8.9 we examine the contribution of the gluonic subprocesses to the total cross section in more detail for the three HMRS parametrizations [15]. The  $m$ -jet cross sections, based on the gluonic subprocess only, are given for the three fundamentally different low- $x$  parametrizations, see section 2.3.1. The spread in the results confirms the remarks above.

|          | $a$  | $m = 2$ | $m = 3$ | $m = 4$ | $m = 5$ |
|----------|------|---------|---------|---------|---------|
| SppS     | -0.5 | 660     | 450     | 54      | 3.8     |
|          | -1.0 | 460     | 290     | 32      | 2.2     |
|          | -1.5 | 360     | 220     | 25      | 1.6     |
| Tevatron | -0.5 | 5600    | 220     | 20      | 1.0     |
|          | -1.0 | 5500    | 160     | 13      | 0.65    |
|          | -1.5 | 4700    | 120     | 9.8     | 0.50    |
| LHC      | -0.5 | 2200    | 110     | 9.5     | 0.73    |
|          | -1.0 | 3100    | 120     | 9.0     | 0.60    |
|          | -1.5 | 3100    | 100     | 7.5     | 0.48    |
| SSC      | -0.5 | 1100    | 52      | 4.5     | 0.35    |
|          | -1.0 | 1700    | 61      | 4.6     | 0.32    |
|          | -1.5 | 1700    | 55      | 4.0     | 0.27    |

Table 8.9. Cross sections in nb, based on the gluon subprocess only, for the three HMRS-parametrizations of the gluon density function.

## References

- [1] Private communications, results are to be published by the UA2 group.
- [2] D.W. Duke and J.F. Owens, Phys. Rev. **D30** (1984) 49.
- [3] Jet Physics with UA2, talk presented by P. Lubrano in La Thuile 1990.
- [4] J.D. Bjorken and S.J. Brodsky, Phys. Rev. **D1** (1970) 1416;  
E. Farhi, Phys. Rev. Lett. **39** (1977) 1587.
- [5] F.A. Berends, W.T. Giele and H. Kuijf, Nucl. Phys. **B333** (1990) 120.
- [6] Z. Kunszt and W.J. Stirling, Proceedings of the Workshop on Physics at Future Accelerators, La Thuile and Geneva, ed. J.H. Mulvey, (CERN 87-07), Vol. 2, p. 548.
- [7] W.T. Giele, Properties and calculations of multiparton processes, thesis, Leiden, 1989.
- [8] M. Mangano, Nucl. Phys. **B309** (1988) 461.

| $\sigma/l/P$    | DO I         | GHR          | EMC          | BCDMS        |
|-----------------|--------------|--------------|--------------|--------------|
| $\sigma_2$      | 1430         | 1940         | 1210         | 1350         |
| $\sigma_2^{pp}$ | 1440         | 1960         | 1220         | 1380         |
| $gg/gq/qq$      | 39/48/13     | 42/46/12     | 42/46/11     | 36/49/15     |
| 0/2/4q          | 38/49/12     | 40/49/11     | 41/49/11     | 35/51/14     |
| $\sigma_3$      | 1110         | 1870         | 810          | 1030         |
| $\sigma_3^{pp}$ | 1140         | 1890         | 820          | 1060         |
| $gg/gq/qq$      | 42/46/12     | 44/45/11     | 44/45/11     | 38/47/14     |
| 0/2/4q          | 37/48/15     | 39/47/14     | 40/47/13     | 34/49/17     |
| $\sigma_4$      | 150          | 310          | 100          | 140          |
| $\sigma_4^{pp}$ | 185          | 386          | 116          | 170          |
| $gg/gq/qq$      | 41/46/13     | 44/45/12     | 44/45/11     | 37/47/15     |
| 0/2/4/6q        | 33/47/19/0.8 | 35/47/17/0.7 | 35/47/17/0.7 | 30/48/21/1.0 |
| $\sigma_5$      | 12           | 32           | 7.2          | 11           |
| $\sigma_5^{pp}$ | 18           | 46           | 10.3         | 17           |
| $gg/gq/qq$      | 38/46/16     | 42/45/14     | 41/45/14     | 35/47/19     |
| 0/2/4/6q        | 27/48/21/4.2 | 30/48/19/3.6 | 29/48/19/3.6 | 24/48/23/4.6 |

Table 8.10. Cross sections in nb for the SppS collider.

| $\sigma/l/P$    | DO I         | GHR          | EMC          | BCDMS        |
|-----------------|--------------|--------------|--------------|--------------|
| $\sigma_2$      | 14650        | 18580        | 11510        | 14000        |
| $\sigma_2^{pp}$ | 14800        | 18600        | 11700        | 14100        |
| $gg/gq/qq$      | 52/41/6      | 54/40/6      | 55/39/6      | 50/43/7      |
| 0/2/4q          | 51/43/6      | 52/42/6      | 53/41/6      | 48/45/7      |
| $\sigma_3$      | 540          | 830          | 410          | 510          |
| $\sigma_3^{pp}$ | 550          | 860          | 420          | 530          |
| $gg/gq/qq$      | 42/47/11     | 46/45/10     | 46/45/10     | 40/48/12     |
| 0/2/4q          | 37/49/14     | 41/47/12     | 41/47/12     | 35/50/15     |
| $\sigma_4$      | 51           | 97           | 37           | 48           |
| $\sigma_4^{pp}$ | 62           | 102          | 44           | 59           |
| $gg/gq/qq$      | 38/49/12     | 42/47/11     | 43/46/10     | 36/50/14     |
| 0/2/4/6q        | 31/50/18/0.7 | 34/48/16/0.6 | 35/48/16/0.6 | 29/51/20/0.8 |
| $\sigma_5$      | 3.5          | 7.9          | 2.4          | 3.3          |
| $\sigma_5^{pp}$ | 5.4          | 12.4         | 3.6          | 5.5          |
| $gg/gq/qq$      | 35/47/18     | 37/48/15     | 38/48/15     | 31/49/20     |
| 0/2/4/6q        | 29/41/26/4.5 | 33/41/23/3.8 | 34/41/22/3.6 | 28/40/27/4.9 |

Table 8.11. Cross sections in nb for the Tevatron collider.

| $\sigma/l/P$                          | DO I        | GHR         | EMC         | BCDMS       |
|---------------------------------------|-------------|-------------|-------------|-------------|
| $\sigma_2$                            | 7390        | 9010        | 5320        | 7000        |
| $\sigma_2^{pp}$                       | 7460        | 9100        | 5370        | 7040        |
| $\mathbb{E}\mathbb{E}/\mathbb{E}q/qq$ | 70/27/2.6   | 74/24/1.9   | 72/27/2.2   | 70/27/2.6   |
| 0/2/4q                                | 68/30/2.5   | 71/27/1.9   | 70/28/2.2   | 67/30/2.6   |
| $\sigma_3$                            | 290         | 390         | 210         | 280         |
| $\sigma_3^{pp}$                       | 295         | 395         | 220         | 285         |
| $\mathbb{E}\mathbb{E}/\mathbb{E}q/qq$ | 66/30/3.6   | 69/28/2.9   | 69/28/2.9   | 65/31/3.7   |
| 0/2/4q                                | 59/36/5.4   | 62/34/4.6   | 61/34/4.6   | 58/36/5.5   |
| $\sigma_4$                            | 24          | 36          | 17          | 24          |
| $\sigma_4^{pp}$                       | 28          | 42          | 20          | 27          |
| $\mathbb{E}\mathbb{E}/\mathbb{E}q/qq$ | 65/31/4.0   | 67/29/3.3   | 68/28/3.2   | 65/31/4.0   |
| 0/2/4/6q                              | 53/38/8/0.2 | 55/37/7/0.2 | 56/37/7/0.2 | 54/38/8/0.2 |
| $\sigma_5$                            | 1.8         | 3.1         | 1.2         | 1.9         |
| $\sigma_5^{pp}$                       | 2.5         | 4.3         | 1.6         | 2.4         |
| $\mathbb{E}\mathbb{E}/\mathbb{E}q/qq$ | 77/19/4.6   | 79/18/3.7   | 79/18/3.7   | 76/19/4.7   |
| 0/2/4/6q                              | 67/24/8/0.6 | 69/23/7/0.5 | 69/24/7/0.5 | 67/24/8/0.6 |

Table 8.12. Cross sections in nb for the LHC.

| $\sigma/l/P$                          | DO I        | GHR         | EMC         | BCDMS       |
|---------------------------------------|-------------|-------------|-------------|-------------|
| $\sigma_2$                            | 4140        | 5130        | 2790        | 3730        |
| $\sigma_2^{pp}$                       | 4160        | 5190        | 2820        | 3840        |
| $\mathbb{E}\mathbb{E}/\mathbb{E}q/qq$ | 73/25/2.0   | 77./21/1.5  | 75/24/1.8   | 73/25/2.1   |
| 0/2/4q                                | 70/28/2.0   | 74/24/1.4   | 72/27/1.8   | 70/28/2.1   |
| $\sigma_3$                            | 150         | 210         | 108         | 140         |
| $\sigma_3^{pp}$                       | 152         | 220         | 109         | 145         |
| $\mathbb{E}\mathbb{E}/\mathbb{E}q/qq$ | 69/28/2.9   | 74/24/2.0   | 72/26/2.4   | 69/28/2.8   |
| 0/2/4q                                | 61/34/4.5   | 66/31/3.5   | 64/32/3.9   | 62/34/4.4   |
| $\sigma_4$                            | 13          | 19          | 8.9         | 12          |
| $\sigma_4^{pp}$                       | 14          | 21          | 9.9         | 14          |
| $\mathbb{E}\mathbb{E}/\mathbb{E}q/qq$ | 68/28/3.4   | 72/26/2.6   | 71/26/2.7   | 68/28/3.4   |
| 0/2/4/6q                              | 56/36/7/0.2 | 59/35/6/0.2 | 59/35/6/0.2 | 57/36/7/0.2 |
| $\sigma_5$                            | 1.0         | 1.6         | 0.66        | 0.94        |
| $\sigma_5^{pp}$                       | 1.3         | 2.0         | 0.85        | 1.24        |
| $\mathbb{E}\mathbb{E}/\mathbb{E}q/qq$ | 71/26/3.4   | 74/23/2.7   | 74/23/2.7   | 71/25/3.4   |
| 0/2/4/6q                              | 57/34/8/0.7 | 60/33/7/0.6 | 59/33/7/0.6 | 58/33/8/0.7 |

Table 8.13. Cross sections in nb for the SSC.

- [9] B. L. Combridge and C. J. Maxwell, Nucl. Phys. **B239** (1984) 429; Phys. Lett. **151B** (185) 299.  
F. Halzen and P. Hoyer, Phys. Lett. **130B** (1983) 326.
- [10] C.J. Maxwell, Phys. Lett. **192B** (1987) 190.
- [11] M. Mangano and S. Parke, Phys. Rev. **D39** (1989) 758;  
C.J. Maxwell, Nucl. Phys. **B316** (1989) 321.
- [12] E.J. Eichten, I. Hinchliffe, C. Quigg and K.D. Lane, Rev. Mod. Phys. **56** (1984) 579;  
Erratum: **58** (1986) 1065.
- [13] M. Glück, E. Hoffmann and E. Reya, Zeit. Phys. **C13** (1982) 119.
- [14] A.D. Martin, R.G. Roberts and W.J. Stirling, Phys. Lett. **206B** (1988) 327.
- [15] P.N. Harriman, A.D.Martin, R.G.Roberts and W.J.Stirling, Phys. Lett. **248B** (1990) 421.
- [16] *The art of computer programming*, D.E. Knuth, Addison Wesley, 1968.

## Chapter 9

# Enumeration techniques

*The Feynman diagrams that contribute to a matrix element are enumerated for a number of interaction theories. For QCD the number of parton subprocesses that contribute to one event on the hadron level is determined.*

### 9.1 Enumeration of externally labelled tree graphs

We enumerate a special class of trees, called labelled trees. This is done by formulating a recursion relation in two variables, the number of internal lines,  $i$ , and the number of external lines,  $n$ , for these trees, and subsequently solving it. The solution is discussed in detail. In particular we consider the case where  $n$  becomes large, summing over  $i$ . The labelled trees considered correspond to the Feynman diagrams one encounters in perturbation theories for fundamental forces, involving one type of particle which self-interacts.

#### 9.1.1 Introduction and problem

We begin by defining the notion of an externally labelled tree. An externally labelled tree is a connected graph without cycles, of which the external branches are labelled. Here, an external branch is understood to be a line arriving in a point in which no other lines arrive. The lines in the graph which are not external will be called "internal branches". Internal and external branches are connected at given points, called vertices. The minimum number of branches that can come together in a vertex is three, the maximum number is  $m$  ( $\geq 3$ ), an adjustable integer valued parameter. Both the internal branches and the vertices are unlabelled. External branches connected to the same vertex can be interchanged without producing a different externally labelled tree. We point out that for a given externally labelled tree, letting  $N_k$  denote the number of vertices where  $k$  branches ( $k = 3, \dots, m$ ) come together,  $n$  the number of external branches, and  $i$  the number of internal ones, one has

$$\sum_{k=3}^m N_k = i + 1, \quad (9.1.1)$$

and

$$\sum_{k=3}^m kN_k = n + 2i. \quad (9.1.2)$$

The problem we shall address is to calculate how many different externally labelled trees there exist for given, but general,  $m$  and  $n$ . The number of internal branches  $i$  at given, fixed,  $m$  and  $n$  is allowed to vary. To our knowledge, this question of enumeration has not been studied before in the literature, for general  $m$ . The cases  $m = 3$  and  $m = 4$  have already received some attention from other authors [1, 2]. For some interesting general texts on graph theory see, e.g., [3, 4].

The problem of enumerating externally labelled trees is of some physical relevance from the point of view of high energy physics. This is because externally labelled trees as defined above are just the Feynman diagrams one encounters in a perturbation theory for fundamental forces, involving only one type of particle that self-interacts. There, in order to calculate a scattering process of  $n$  of these particles, one needs to have all the diagrams with  $n$  external branches. It is thus important to know how many of them exist. The parameter  $m$  introduced above, controls the degree of self-interaction, and basically determines which theory one is studying. For example,  $m = 3$  corresponds to  $\Phi^3$ -theory,  $m = 4$  to Yang-Mills theory, whereas the limit  $m \rightarrow \infty$  corresponds to so-called linearized gravitation. In fact, these three cases are the most important ones from the point of view of high energy physics, since theories corresponding to other  $m$ -values are not known as yet. Therefore we shall pay special attention to them in the following. In practical calculations performed up till now,  $n$  has always been less than 10. The record for the largest number of diagrams calculated presently lies at 34300, being the case  $m = 4$  and  $n = 8$  [5].

The outline is as follows. We first formulate recursion relations, expressing the number of externally labelled trees with  $n$  external and  $i$  internal branches in the number of externally labelled trees with lesser branches. Then, these recursion relations are solved, leading to a formal solution of the problem stated above. The solution is subsequently studied in more detail. In particular, we address the question as to how the number of externally labelled trees grows with  $n$ , at fixed  $m$ , as  $n$  becomes large, thus indicating the impossible task one faces when trying to calculate all Feynman diagrams for larger  $n$ .

## 9.1.2 Enumeration

### 9.1.2.1 Recursion relations and solution

Let  $D_n^{(m)}$  denote the number of externally labelled trees, with  $n$  external branches, there exist when allowing 3, 4, ...,  $m$ -point vertices to be present. With  $D_{n,i}^{(m)}(N_3, \dots, N_m)$  denoting the number of these trees with  $i$  internal lines and exactly  $N_3$  3-point vertices,  $N_4$  4-point vertices, up to and including  $N_m$   $m$ -point vertices, we can write

$$D_n^{(m)} = \sum_{i=0}^{\infty} \sum_{N_3=0}^{\infty} \dots \sum_{N_m=0}^{\infty} D_{n,i}^{(m)}(N_3, \dots, N_m). \quad (9.1.3)$$

For given  $n$ , the right-hand side in (9.1.3) converges, since  $D_{n,i}^{(m)}$  only differs from zero if conditions (9.1.1) and (9.1.2) are fulfilled. It is easy to write down a recursion relation for  $D_{n,i}^{(m)}(N_3, \dots, N_m)$ , valid for  $n \geq 4$  and  $i \geq 1$ :

$$D_{n,i}^{(m)}(N_3, \dots, N_m) = (n+i-2)D_{n-1,i-1}^{(m)}(N_3-1, N_4, \dots, N_m) + \sum_{k=3}^{m-1} (N_k+1)D_{n-1,i}^{(m)}(N_3, \dots, N_k+1, N_{k+1}-1, \dots, N_m). \quad (9.1.4)$$

This is so because an externally labelled tree with  $n$  external and  $i$  internal branches can be formed in two different ways. Namely, by taking an externally labelled tree with  $(n-1)$  external and  $(i-1)$  internal branches, then choosing a point on any one of the already existing in- or external branches and attaching the new external branch to it. This creates a new 3-vertex (first term in r.h.s. of (9.1.4)). Or by taking an externally labelled tree with  $(n-1)$  external and  $i$  internal branches, attaching the new external branch to an already existing vertex (second term in r.h.s. of (9.1.4)). In the procedure described here, every externally labelled tree one can think of can be constructed. Also it is easy to convince oneself that there is no double counting. This is because, due to the fact that the external branches are labelled, the procedure itself has a tree structure. One can see this remarking that for a given externally labelled tree one can find its predecessor by just removing the external branch with the highest number, so that its predecessor is unique. Therefore the solution of (9.1.4) is indeed what we are looking for. However, in order for  $D_{n,i}^{(m)}$  to be uniquely determined for all  $n$  and  $i$ , the recursion relation (9.1.4) must be supplemented with boundary conditions. We have

$$D_{3,0}^{(m)}(1, 0, \dots, 0) = 1, \\ D_{3,i}^{(m)}(N_3, \dots, N_m) = 0 \text{ otherwise,} \quad (9.1.5)$$

expressing that there is only one externally labelled tree having three external branches and no internal ones, and, for  $j = 3, \dots, m$ ,

$$D_{j,0}^{(m)}(0, \dots, 0, N_j = 1, 0, \dots, 0) = 1, \quad (9.1.6)$$

expressing that a  $j$ -vertex is unique. The solution for  $D_{n,i}^{(m)}(N_3, \dots, N_m)$  then reads

$$D_{n,i}^{(m)}(N_3, \dots, N_m) = \frac{(\sum_{k=3}^m (k-1)N_k)!}{\prod_{k=3}^m [((k-1)!)^{N_k} N_k!]} \delta_{n-2, \sum_{j=3}^m (j-2)N_j} \delta_{i+1, \sum_{j=3}^m N_j}, \quad (9.1.7)$$

as can be verified by a direct substitution in (9.1.4). It is easy to check that the boundary conditions (9.1.5) and (9.1.6) are indeed fulfilled. Substituting (9.1.7) in (9.1.3), the sum on  $i$  can be performed, yielding

$$D_n^{(m)} = \sum_{N_3=0}^{\infty} \dots \sum_{N_m=0}^{\infty} \frac{(n-2 + \sum_{k=3}^m N_k)!}{\prod_{k=3}^m [((k-1)!)^{N_k} N_k!]} \delta_{n-2, \sum_{j=3}^m (j-2)N_j}. \quad (9.1.8)$$

This, then, is the formal solution to the problem. However, since it still involves  $(m-2)$  sums, it is not very transparent what it implies. In the following we shall therefore study some aspects of it more closely for some special cases. In particular, we shall study the growth factor  $\Xi^{(m)}$ , defined as

$$\Xi^{(m)} = \lim_{n \rightarrow \infty} \frac{D_n^{(m)}}{n D_{n-1}^{(m)}}, \quad (9.1.9)$$

and show that it is finite for all  $m$ . The implications of the finiteness of  $\Xi^{(m)}$  for  $D_n^{(m)}$  itself will be discussed later.

### 9.1.2.2 The case $m = 3$

For  $m = 3$ , the sum in (9.1.8) in fact only consists of one nonzero term, and we find

$$\begin{aligned} D_n^{(3)} &= (2n-5)!!, \quad \text{all } n \geq 3, \\ &\simeq \frac{\sqrt{2}}{e^2} \left(\frac{2n}{e}\right)^{n-2}, \quad n \rightarrow \infty, \end{aligned} \quad (9.1.10)$$

in accordance with [1]. From this one obtains

$$\Xi^{(3)} = 2. \quad (9.1.11)$$

### 9.1.2.3 The case $m = 4$

Performing the sum on  $N_3$  in (9.1.8) we arrive at

$$D_n^{(4)} = \sum_{N_4=0}^{\text{int}(\frac{n}{2}-1)} \frac{(2n - N_4 - 4)!}{2^{n-2-2N_4} (n - 2N_4 - 2)! 6^{N_4} N_4!}, \quad n \geq 3, \quad (9.1.12)$$

where "int" stands for "integer part of". Let us write  $N_4 = \alpha n$ , thus introducing the new variable  $\alpha$ . Then we have

$$D_n^{(4)} = \sum_{\alpha} \frac{[(2-\alpha)n-4]!}{2^{(1-2\alpha)n-2} [(1-2\alpha)n-2]! 6^{\alpha n} (\alpha n)!}, \quad (9.1.13)$$

where  $\alpha$  now takes the values  $0, \frac{1}{n}, \dots, \frac{1}{n} \text{int}(\frac{n}{2}-1)$ . In order to evaluate this sum asymptotically, we use Stirling's formula in the form

$$(an+b)! \simeq \sqrt{2\pi an} (an)^{an+b} e^{-an}, \quad (9.1.14)$$

for the factorials in the summand, and note that  $\frac{1}{n} \sum_{\alpha} \rightarrow \int_0^{\frac{1}{2}} d\alpha$  as  $n \rightarrow \infty$ . We then obtain

$$D_n^{(4)} \simeq n^{n-\frac{3}{2}} \int_0^{\frac{1}{2}} d\alpha f(\alpha) [g(\alpha)]^n, \quad (9.1.15)$$

with

$$f(\alpha) = \frac{4(1-2\alpha)^{\frac{3}{2}}}{(2\pi\alpha)^{\frac{1}{2}}(2-\alpha)^{\frac{3}{2}}} \quad (9.1.16)$$

and

$$g(\alpha) = \frac{(2-\alpha)^{2-\alpha}}{2^{1-2\alpha}(1-2\alpha)^{1-2\alpha}6^\alpha\alpha^\alpha e}. \quad (9.1.17)$$

By considering  $\ln g(\alpha)$  one easily shows that  $g(\alpha)$  has a maximum on  $[0, \frac{1}{2}]$  for  $\alpha = \alpha_0 = \frac{1}{11}(7-3\sqrt{3})$ , the value at the maximum being  $g(\alpha_0) = \frac{3}{11}e(4+3\sqrt{3})$ . Taylor expanding the integrand in (9.1.15) around  $\alpha_0$  and then introducing a new variable  $x$  according to  $\alpha = \alpha_0 + \frac{x}{\sqrt{n}}$  we find

$$D_n^{(4)} \simeq f(\alpha_0) \sqrt{\frac{2\pi g(\alpha_0)}{-g''(\alpha_0)}} [g(\alpha_0)]^n n^{n-2}. \quad (9.1.18)$$

Now,

$$-\frac{g''(\alpha_0)}{g(\alpha_0)} = -\left[\frac{d^2}{d\alpha^2} \ln g(\alpha)\right]_{\alpha_0} = \frac{1}{\alpha_0} - \frac{1}{2-\alpha_0} + \frac{4}{1-2\alpha_0} = 4 + \frac{13}{\sqrt{3}}, \quad (9.1.19)$$

so that one ultimately gets

$$\begin{aligned} D_n^{(4)} &\simeq \frac{1}{e} \sqrt{\frac{g(\alpha_0)}{e\sqrt{3}}} [g(\alpha_0)]^n n^{n-2} \\ &= (0.16285\dots)[0.92265\dots n]^{n-2}. \end{aligned} \quad (9.1.20)$$

The growth factor as defined in (9.1.9) is given by

$$\Xi^{(4)} = e g(\alpha_0) = \frac{3}{11}(4+3\sqrt{3}) = 2.5080416\dots \quad (9.1.21)$$

#### 9.1.2.4 The general case

Finding an asymptotic expression for  $D_n^{(m)}$  as  $n \rightarrow \infty$  in this case, would amount to starting with (9.1.8), then performing, e.g., the sum on  $N_3$  to get rid of the Kronecker delta, and subsequently applying the method of steepest descent on an  $(m-3)$ -fold integral. A procedure which is very similar to the one sketched above for the case  $m=4$ . However, as it turns out, it is already reasonably difficult to find where the maximum used in the method of steepest descent is located. Therefore, we shall at first content ourselves with calculating  $\Xi^{(m)}$ , since here a knowledge of the maximum itself suffices, as we have already seen in the case  $m=4$ . To do so we return to (9.1.7) which we rewrite as

$$D_{n,i}^{(m)}(N_3, \dots, N_m) = \frac{(n+i-1)!}{\prod_{k=3}^m [(k-1)!^{N_k} N_k!]} \delta_{n-2, \sum_{j=3}^m (j-2)N_j} \delta_{i+1, \sum_{j=3}^m N_j} \quad (9.1.22)$$

Obviously, what we are looking for are the values of  $i$  and  $N_3, \dots, N_m$  which maximize  $(n+i-1)!/\prod_{k=3}^m [(k-1)!^{N_k} N_k!]$ , in a space restricted by conditions (9.1.1) and (9.1.2). With this in mind we write

$$i = \gamma n, \quad N_k = \beta_k n, \quad (9.1.23)$$

so that, using (9.1.14), we arrive at

$$\frac{(n+i-1)!}{\prod_{k=3}^m [(k-1)!^{N_k} N_k!]} \approx \frac{f(\gamma, \{\beta_k\})}{n^{(m+1)/2}} [g(\gamma, \{\beta_k\}) n]^m. \quad (9.1.24)$$

Here

$$g(\gamma, \{\beta_k\}) = \frac{(1+\gamma)^{1+\gamma}}{e \prod_{k=3}^m [(k-1)! \beta_k]^{\beta_k}}, \quad (9.1.25)$$

while the expression for  $f(\gamma, \{\beta_k\})$  will not be given, since it is not important for our purposes. Thus, we must maximize  $g(\gamma, \{\beta_k\})$ , or what is easier but amounts to the same,  $\ln g(\gamma, \{\beta_k\})$ , subject to the conditions:

$$\sum_{j=3}^m \beta_j = \gamma, \quad (9.1.26a)$$

$$\sum_{j=3}^m j \beta_j = 2\gamma + 1, \quad (9.1.26b)$$

following from (9.1.1) and (9.1.2) when using the scaling (9.1.23) and taking  $n \rightarrow \infty$  at fixed  $\gamma$  and  $\beta_k$ . Therefore we consider

$$\Lambda_{\lambda, \mu}(\gamma, \{\beta_k\}) = \ln g(\gamma, \{\beta_k\}) - \lambda \left[ \sum_{j=3}^m \beta_j - \gamma \right] - \mu \left[ \sum_{j=3}^m j \beta_j - 2\gamma - 1 \right], \quad (9.1.27)$$

where  $\lambda$  and  $\mu$  are Lagrange multipliers, and we shall want to extremize this expression. Solving

$$\frac{\partial}{\partial \gamma} \Lambda_{\lambda, \mu} = \frac{\partial}{\partial \beta_k} \Lambda_{\lambda, \mu} = 0, \quad \text{for all } k, \quad (9.1.28)$$

one finds

$$\beta_k^0 = \frac{e^{\lambda + \mu k - 1}}{(k-1)!}, \quad (9.1.29a)$$

$$\gamma^0 = e^{\lambda + 2\mu - 1} - 1, \quad (9.1.29b)$$

which expresses  $\gamma^0$  and  $\beta_k^0$ , the values at the extremum, in terms of  $\lambda$  and  $\mu$ . The values of  $\lambda$  and  $\mu$  themselves are obtained by substituting (9.1.29a) and (9.1.29b) back into (9.1.26a) and (9.1.26b), solving the resulting equations for  $\lambda$  and  $\mu$ . In particular, we find that

$$\sum_{k=1}^{m-2} \frac{e^{\mu k}}{k!} = 1, \quad (9.1.30a)$$

$$\sum_{k=1}^{m-2} \frac{e^{\mu k}}{(k+1)!} = \frac{\gamma^0}{1 + \gamma^0}, \quad (9.1.30b)$$

implicitly giving the values of  $\mu$  and  $\gamma^0$ . The growth factor  $\Xi^{(m)}$  is found to be given by

$$\Xi^{(m)} = e g(\gamma^0, \{\beta_k^0\}) = (1 + \gamma^0) e^{-\mu} = \left[ 2e^\mu - 1 - \frac{e^{\mu(m-1)}}{(m-1)!} \right]^{-1}, \quad (9.1.31)$$

where the different equalities can be established using the definition (9.1.9) of  $\Xi^{(m)}$  and formulas (9.1.24)–(9.1.30b). It is directly determined by that solution of (9.1.30a) for which  $e^\mu \in [0, 1]$ . For example, we find

$$\begin{aligned} \Xi^{(3)} &= 2 \\ \Xi^{(4)} &= \frac{3}{11}(4 + 3\sqrt{3}) = 2.508\dots \\ \Xi^{(5)} &= [2x - 1 - \frac{x^4}{24}]^{-1} \text{ with } x = (5 + \sqrt{26})^{\frac{1}{2}} - (5 + \sqrt{26})^{-\frac{1}{2}} - 1 \\ &= 2.578\dots \\ \Xi^{(\infty)} &= \frac{1}{2 \ln 2 - 1} = 2.588\dots \end{aligned} \quad (9.1.32)$$

Also, using (9.1.30a) and (9.1.31), it is not hard to show that  $\Xi^{(\infty)}$  is approached as

$$\Xi^{(\infty)} - \Xi^{(m)} \simeq \frac{\sum_{k=m}^{\infty} \frac{(\ln 2)^k}{k!}}{(2 \ln 2 - 1)^2}, \quad m \rightarrow \infty. \quad (9.1.33)$$

The existence of  $\Xi^{(m)}$  implies that asymptotically, i.e., for  $n \rightarrow \infty$ ,

$$D_n^{(m)} \simeq H_m(n) \left( \Xi^{(m)} \right)^n n!, \quad (9.1.34)$$

where  $H_m(n)$  has the property that  $\lim_{n \rightarrow \infty} H_m(n+1)/H_m(n) = 1$ . Therefore we see that the number of externally labelled trees for fixed  $m$  and  $n \rightarrow \infty$  grows factorially fast. However, we can even do better than this: we can find the  $n$ -dependence of  $H_m(n)$  quite easily. The only thing one has to do is to follow the procedure outlined at the beginning of this section for calculating  $D_n^{(m)}$  asymptotically, keeping track of powers of  $n$ . We stress that it is not necessary to do the whole actual calculation itself. It is not hard to convince oneself that one finds

$$D_n^{(m)} \sim n^{n-2} \quad (9.1.35)$$

as  $n \rightarrow \infty$ , for all  $m$ . Therefore we obtain

$$D_n^{(m)} \simeq C_m \left( \Xi^{(m)} \frac{n}{e} \right)^{n-2}, \quad n \rightarrow \infty, \text{ all } m, \quad (9.1.36)$$

where  $C_m$  is an  $m$ -dependent constant. It is amusing to remark here that the number of ways in which one can join  $n$  labelled points to form a tree (also allowing only two lines to arrive in a given labelled point) is given exactly by  $n^{n-2}$  [6]. The result (9.1.36) is compatible with (9.1.34). One may check that the results (9.1.10) and (9.1.20) for the cases  $m = 3$  and  $m = 4$ , respectively, are indeed of the form (9.1.36). Also, there, the constants  $C_3$  and  $C_4$  can be read off. The corrections to (9.1.36) are of relative order  $1/n$ . Because of this one can actually calculate  $\Xi_n^{(m)} \equiv D_n^{(m)}/nD_{n-1}^{(m)}$ , up to first order in  $1/n$  using (9.1.36), since the corrections to (9.1.36) only contribute to second and higher orders in the large- $n$  expansion of  $\Xi_n^{(m)}$ . We find

$$\Xi_n^{(m)} = \Xi^{(m)} \left[ 1 - \frac{5}{2n} + \dots \right]. \quad (9.1.37)$$

The coefficient of the  $1/n$  term in the expansion of  $\Xi_n^{(m)}/\Xi^{(m)}$  in powers of  $1/n$  thus does not depend on  $m$ . This, however, is no longer true for the higher order terms. For the case  $m = 3$  there are in fact no higher order terms, as can be seen from the exact result in (9.1.10) valid for all  $n \geq 3$ . But a numerical evaluation of  $\Xi_n^{(m)}/\Xi^{(m)}$  for the cases  $m = 4$  and  $m = \infty$  yields that then there are indeed higher order corrections. They are equal to  $k_m/n^2 + l_m/n^3 + \dots$ , say, and we find numerically

$$\begin{aligned} k_4 &= 0.0159860861860\dots, & l_4 &= 0.05227131\dots \\ k_\infty &= 0.0160955983798\dots, & l_\infty &= 0.05633459\dots \end{aligned} \quad (9.1.38)$$

Because these coefficients are so small, one might expect that the approximation to  $\Xi_n^{(m)}$  one obtains when neglecting the terms represented by the dots in (9.1.37), is already quite good for fairly small  $n$ . We have for  $m = 4$  and  $m = \infty$  explicitly verified that this is indeed the case.

Finally we remark that the case  $m = \infty$  can in principle be tackled more directly. Here, namely, one can immediately write down a recursion relation for  $E_n(i)$ , the number of externally labelled trees with  $n$  external and  $i$  internal branches, since all types of vertices are allowed. It reads

$$E_n(i) = (n + i - 2)E_{n-1}(i - 1) + (i + 1)E_{n-1}(i), \quad n \geq 4, \quad i \geq 1, \quad (9.1.39)$$

with boundary conditions

$$E_3(i) = \delta_{i,0}, \quad E_n(0) = 1, \quad n \geq 3. \quad (9.1.40)$$

The first term in the right-hand side of (9.1.39) originates from creating a new vertex in an externally labelled tree with  $n - 1$  external and  $i - 1$  internal branches, and attaching the  $n^{\text{th}}$  external branch to it. The second term comes from adding the new external branch to an already existing vertex in an externally labelled tree with  $n - 1$  external and  $i$  internal branches. Unfortunately, we have not been able to solve (9.1.39) with boundary conditions (9.1.40) directly. However, from the point of view of a numerical evaluation, it is much easier to obtain values for  $D_n^{(\infty)} = \sum_{i=0}^{n-3} E_n(i)$  using (9.1.39) than using (9.1.4). Also, starting from (9.1.39), one may show that

| $n$      | $m = 3$ | $m = 4$  | $m \rightarrow \infty$ |
|----------|---------|----------|------------------------|
| 3        | 1       | 1        | 1                      |
| 4        | 3       | 4        | 4                      |
| 5        | 15      | 25       | 26                     |
| 6        | 105     | 220      | 236                    |
| 7        | 945     | 2485     | 2752                   |
| 8        | 10395   | 34300    | 39208                  |
| 9        | 135135  | 559405   | 660032                 |
| 10       | 2027025 | 10525900 | 12818912               |
| $n(1\%)$ | 250     | 250      | 250                    |

Table 9.1. The number of Feynman diagrams for different values of  $n$  and  $m$ . Furthermore  $n(1\%)$  denotes the lowest  $n$ -value for which  $\Xi/\Xi^{(m)} > 0.99$

$$\Xi_n^{(\infty)} = 1 + 2 \frac{\sum_i i E_{n-1}(i)}{n \sum_i E_{n-1}(i)} \equiv 1 + 2 \frac{\langle i \rangle_{n-1}}{n} . \quad (9.1.41)$$

This implies that as  $n \rightarrow \infty$  the growth factor  $\Xi^{(\infty)}$  is directly determined by the position of the maximum of  $E_n(i)$  as a function of  $i$ . Since  $0 < \langle i \rangle_{n-1}/n < 1$  one immediately sees that  $\Xi^{(\infty)} \in (1, 3)$ , compatible with (9.1.32).

## 9.2 Enumeration in QCD

In this section a variety of quantities in QCD is enumerated. Among them are the Feynman diagrams for any QCD tree level matrix element and the hard parton scattering processes that contribute to a process on the hadron level.

With the results of the previous section it is easy to count the number of Feynman diagrams for theories with one kind of particle and at most  $m$ -points vertices. In tabel 9.1 the results for  $m = 3, 4$  and  $m \rightarrow \infty$  are listed. The table also contains the value for the number of external particles  $n$  for which the growth factor  $\Xi$  is within 1% of the large  $n$  growth factor  $\Xi^{(m)}$ . The 1% limit is reached for exactly the same value of  $n$  for all  $m$ . This confirms eq. (9.1.37).

To count the Feynman diagrams for a general QCD matrix element with  $l$  quark pairs we use recursion in the number of gluons starting with  $l$  quark pairs. One arrives at the following recursion relation:

$$D_{n;l}(Q_1, \dots, Q_l, N_3, N_4) = \quad (9.2.1)$$

$$+ \sum_{i=1}^l Q_i D_{n-1;l}(Q_1, \dots, Q_i - 1, \dots, Q_l, N_3, N_4)$$

$$+ ((n-1) + (l-1) + (N_3-1) + N_4) D_{n-1;l}(Q_1, \dots, Q_l, N_3-1, N_4)$$

$$+ (N_3+1) D_{n-1;l}(Q_1, \dots, Q_l, N_3+1, N_4-1),$$

where  $n$  denotes the number of gluons,  $l$  the number of quark pairs,  $Q_i$  the number of quark-gluon vertices on the quark-line  $i$ ,  $N_3$  the number of three-gluon vertices and  $N_4$  the number of four-gluon vertices. The first term in eq. (9.2.1) originates from adding the extra gluon to quark line  $i$  directly. The second term adds the gluon to a gluon-propagator or to an existing external gluon.

| $D_{n;0}(N_3, N_4)$   | $D_{n;1}(Q_1, N_3, N_4)$ | $D_{n;2}(Q_1, Q_2, N_3, N_4)$ | $D_{n;3}(Q_1, Q_2, Q_3, N_3, N_4)$ |                       |     |                          |    |
|-----------------------|--------------------------|-------------------------------|------------------------------------|-----------------------|-----|--------------------------|----|
| $D_{3;0}(1, 0)$       | 1                        | $D_{1;1}(1, 0, 0)$            | 1                                  | $D_{0;2}(1, 1, 0, 0)$ | 1   | $D_{0;3}(2, 1, 1, 0, 0)$ | 2  |
| $\Rightarrow D_{3;0}$ | 1                        | $\Rightarrow D_{1;1}$         | 1                                  | $\Rightarrow D_{0;2}$ | 1   | $D_{0;3}(1, 2, 1, 0, 0)$ | 2  |
| $\Rightarrow D_{4;0}$ | 4                        | $\Rightarrow D_{2;1}$         | 3                                  | $\Rightarrow D_{1;2}$ | 5   | $D_{0;3}(1, 1, 2, 0, 0)$ | 2  |
| $\Rightarrow D_{5;0}$ | 25                       | $\Rightarrow D_{3;1}$         | 16                                 | $\Rightarrow D_{2;2}$ | 32  | $D_{0;3}(1, 1, 1, 1, 0)$ | 1  |
| $\Rightarrow D_{6;0}$ | 220                      | $\Rightarrow D_{4;1}$         | 123                                | $\Rightarrow D_{3;2}$ | 301 | $\Rightarrow D_{0;3}$    | 7  |
| $\Rightarrow D_{7;0}$ | 2485                     | $\Rightarrow D_{5;1}$         | 1240                               |                       |     | $\Rightarrow D_{1;3}$    | 64 |

Table 9.2. Counting Feynman diagrams using the recursion relation in eq. (9.2.1). The boundary conditions are described in the text.

Finally the third term appends the extra gluon to a three-gluon vertex. The boundary conditions for eq. (9.2.1) are not as easy to formulate as for the  $l = 0$  case. Clearly all  $D_{n;i}(Q_1, \dots, Q_l, N_3, N_4)$  with  $Q_i \leq 0$  or  $N_3 < 0$  or  $N_4 < 0$  must be zero. The non-zero elements can most easily be obtained by drawing all the Feynman diagrams with  $l$  quark pairs with different flavour and simply calculate the  $Q_i$ 's,  $N_3$ ,  $N_4$  of every diagram. In table 9.2 we list the results of solving eq. (9.2.1) with the boundary condition listed as  $D_{n;i}(Q_1, \dots, Q_l, N_3, N_4)$ , for that value of  $n$  for which at least 3 partons are present. The number of Feynman diagrams for a given scattering amplitude with  $l$  different flavoured quarks to is defined as

$$D_{n;l} = \sum_{Q_1, \dots, Q_l, N_3, N_4} D_{n;i}(Q_1, \dots, Q_l, N_3, N_4). \quad (9.2.2)$$

The sum runs over all possible values of the set  $\{Q_1, \dots, Q_l, N_3, N_4\}$ . Note that the results for  $D_{n;0}$  are in table 9.1 too.

The QCD hard parton scattering subprocesses contributing to  $m$ -parton production are enumerated in table 9.3. The results are listed for up to five final state partons. A few remarks will clarify the contents of the table. Firstly, the number of diagrams ( $D$ ) is taken from table 9.2. In case there are  $m$  identical quark pairs this number has to be multiplied with  $m!$ . The number of parton scattering processes ( $P$ ) is based on four initial and five final state flavours, i.e. the incoming hadrons do not contain any bottom quarks. Note that although the number of subprocesses is impressive for every  $m$ , the major contribution to the total cross section for the hadron scattering, is always coming from just one process, the purely gluonic one.

| m = 4                           |   |            | m = 5                            |    |            | m = 6                                   |     |            | m = 7                                    |      |            |
|---------------------------------|---|------------|----------------------------------|----|------------|-----------------------------------------|-----|------------|------------------------------------------|------|------------|
| process                         | D | P          | process                          | D  | P          | process                                 | D   | P          | process                                  | D    | P          |
| $gg \rightarrow gg$             | 4 | 1          | $gg \rightarrow ggg$             | 25 | 1          | $gg \rightarrow gggg$                   | 220 | 1          | $gg \rightarrow ggggg$                   | 2485 | 1          |
| $q\bar{q} \rightarrow gg$       | 3 | 8          | $q\bar{q} \rightarrow ggg$       | 16 | 8          | $q\bar{q} \rightarrow gggg$             | 123 | 8          | $q\bar{q} \rightarrow ggggg$             | 1240 | 8          |
| $qg \rightarrow qg$             | 3 | 8          | $qg \rightarrow qgg$             | 16 | 8          | $qg \rightarrow qggg$                   | 123 | 8          | $qg \rightarrow qgggg$                   | 1240 | 8          |
| $gq \rightarrow qg$             | 3 | 8          | $gq \rightarrow qgg$             | 16 | 8          | $gq \rightarrow qggg$                   | 123 | 8          | $gq \rightarrow qgggg$                   | 1240 | 8          |
| $gg \rightarrow q\bar{q}$       | 3 | 5          | $gg \rightarrow q\bar{q}g$       | 16 | 5          | $gg \rightarrow q\bar{q}gg$             | 123 | 5          | $gg \rightarrow q\bar{q}ggg$             | 1240 | 5          |
| $q\bar{q} \rightarrow q\bar{q}$ | 2 | 8          | $q\bar{q} \rightarrow q\bar{q}g$ | 10 | 8          | $q\bar{q} \rightarrow q\bar{q}gg$       | 64  | 8          | $q\bar{q} \rightarrow q\bar{q}ggg$       | 602  | 8          |
| $q\bar{q} \rightarrow r\bar{r}$ | 1 | 32         | $q\bar{q} \rightarrow r\bar{r}g$ | 5  | 32         | $q\bar{q} \rightarrow r\bar{r}gg$       | 32  | 32         | $q\bar{q} \rightarrow r\bar{r}ggg$       | 301  | 32         |
| $qq \rightarrow qq$             | 2 | 8          | $qq \rightarrow qqg$             | 10 | 8          | $qq \rightarrow qqgg$                   | 64  | 8          | $qq \rightarrow qqggg$                   | 602  | 8          |
| $q\bar{r} \rightarrow q\bar{r}$ | 1 | 24         | $q\bar{r} \rightarrow q\bar{r}g$ | 5  | 24         | $q\bar{r} \rightarrow q\bar{r}gg$       | 32  | 24         | $q\bar{r} \rightarrow q\bar{r}ggg$       | 301  | 24         |
| $qr \rightarrow qr$             | 1 | 24         | $qr \rightarrow qrg$             | 5  | 24         | $qr \rightarrow qr gg$                  | 32  | 24         | $qr \rightarrow qr ggg$                  | 301  | 24         |
|                                 |   |            | $qg \rightarrow q\bar{q}q$       | 10 | 8          | $qg \rightarrow q\bar{q}qg$             | 64  | 8          | $qg \rightarrow q\bar{q}qgg$             | 602  | 8          |
|                                 |   |            | $qg \rightarrow r\bar{r}q$       | 5  | 32         | $qg \rightarrow r\bar{r}qg$             | 32  | 32         | $qg \rightarrow r\bar{r}qgg$             | 301  | 32         |
|                                 |   |            | $gq \rightarrow q\bar{q}q$       | 10 | 8          | $gq \rightarrow q\bar{q}qg$             | 64  | 8          | $gq \rightarrow q\bar{q}qgg$             | 602  | 8          |
|                                 |   |            | $gq \rightarrow r\bar{r}q$       | 5  | 32         | $gq \rightarrow r\bar{r}qg$             | 32  | 32         | $gq \rightarrow r\bar{r}qgg$             | 301  | 32         |
|                                 |   |            |                                  |    |            | $gg \rightarrow q\bar{q}q\bar{q}$       | 64  | 5          | $gg \rightarrow q\bar{q}q\bar{q}g$       | 602  | 5          |
|                                 |   |            |                                  |    |            | $gg \rightarrow q\bar{q}r\bar{r}$       | 32  | 10         | $gg \rightarrow q\bar{q}r\bar{r}g$       | 301  | 10         |
|                                 |   |            |                                  |    |            | $q\bar{q} \rightarrow q\bar{q}q\bar{q}$ | 42  | 8          | $q\bar{q} \rightarrow q\bar{q}q\bar{q}g$ | 384  | 8          |
|                                 |   |            |                                  |    |            | $q\bar{q} \rightarrow q\bar{q}r\bar{r}$ | 14  | 32         | $q\bar{q} \rightarrow q\bar{q}r\bar{r}g$ | 128  | 32         |
|                                 |   |            |                                  |    |            | $q\bar{q} \rightarrow r\bar{r}r\bar{r}$ | 14  | 32         | $q\bar{q} \rightarrow r\bar{r}r\bar{r}g$ | 128  | 32         |
|                                 |   |            |                                  |    |            | $q\bar{q} \rightarrow r\bar{r}s\bar{s}$ | 7   | 48         | $q\bar{q} \rightarrow r\bar{r}s\bar{s}g$ | 64   | 48         |
|                                 |   |            |                                  |    |            | $qq \rightarrow qq\bar{q}\bar{q}$       | 42  | 8          | $qq \rightarrow qq\bar{q}\bar{q}g$       | 384  | 8          |
|                                 |   |            |                                  |    |            | $qq \rightarrow qq\bar{r}\bar{r}$       | 14  | 32         | $qq \rightarrow qq\bar{r}\bar{r}g$       | 128  | 32         |
|                                 |   |            |                                  |    |            | $qr \rightarrow qr\bar{q}\bar{q}$       | 14  | 24         | $qr \rightarrow qr\bar{q}\bar{q}g$       | 128  | 24         |
|                                 |   |            |                                  |    |            | $qr \rightarrow qr\bar{s}\bar{s}$       | 7   | 72         | $qr \rightarrow qr\bar{s}\bar{s}g$       | 64   | 72         |
|                                 |   |            |                                  |    |            | $q\bar{r} \rightarrow q\bar{r}q\bar{q}$ | 14  | 24         | $q\bar{r} \rightarrow q\bar{r}q\bar{q}g$ | 128  | 24         |
|                                 |   |            |                                  |    |            | $q\bar{r} \rightarrow q\bar{r}r\bar{r}$ | 14  | 24         | $q\bar{r} \rightarrow q\bar{r}r\bar{r}g$ | 128  | 24         |
|                                 |   |            |                                  |    |            | $q\bar{r} \rightarrow q\bar{r}s\bar{s}$ | 14  | 72         | $q\bar{r} \rightarrow q\bar{r}s\bar{s}g$ | 128  | 72         |
|                                 |   |            |                                  |    |            | $gq \rightarrow q\bar{q}q\bar{q}q$      |     |            | 384                                      | 8    |            |
|                                 |   |            |                                  |    |            | $gq \rightarrow q\bar{q}r\bar{r}q$      |     |            | 128                                      | 32   |            |
|                                 |   |            |                                  |    |            | $gq \rightarrow r\bar{r}r\bar{r}q$      |     |            | 128                                      | 32   |            |
|                                 |   |            |                                  |    |            | $gq \rightarrow r\bar{r}s\bar{s}q$      |     |            | 128                                      | 48   |            |
|                                 |   |            |                                  |    |            | $qg \rightarrow q\bar{q}q\bar{q}q$      |     |            | 384                                      | 8    |            |
|                                 |   |            |                                  |    |            | $qg \rightarrow q\bar{q}r\bar{r}q$      |     |            | 128                                      | 32   |            |
|                                 |   |            |                                  |    |            | $qg \rightarrow r\bar{r}r\bar{r}q$      |     |            | 128                                      | 32   |            |
|                                 |   |            |                                  |    |            | $qg \rightarrow r\bar{r}s\bar{s}q$      |     |            | 64                                       | 48   |            |
| <b>TOTAL</b>                    |   | <b>126</b> | <b>TOTAL</b>                     |    | <b>206</b> | <b>TOTAL</b>                            |     | <b>597</b> | <b>TOTAL</b>                             |      | <b>839</b> |

Table 9.3. The number of Feynman diagrams (D) and the number of subprocesses (P) based on four initial and five final state flavours. The process prototype includes the charge conjugated one when there are quarks in the initial state. The number of final state partons is denoted by  $m$ .

## References

- [1] R. Kleiss and H. Kuijf, Nucl. Phys. **B312** (1989) 616.
- [2] J. Küblbeck, Master thesis, sept. 1989, Würzburg University.
- [3] *Graph Theory and Theoretical Physics*, ed. F. Harary, Academic Press, London, 1967.
- [4] *Graph Theory 1736-1936*, N.L. Biggs, E.K. Lloyd and R.J. Wilson, Clarendon press, 1976.
- [5] F.A. Berends, W.T. Giele and H. Kuijf, Phys. Lett. **232B** (1989) 266.
- [6] A. Cayley, Quart. J. Pure Appl. Math. **23** (1889) 376.

## Chapter 10

### QCD matrix elements

*Analytical expressions for tree level QCD matrix elements are given in the notation used in previous chapters. Many details relevant for numerical applications are given.*

#### 10.1 Introduction

In the past decade all tree level QCD matrix elements with up to seven partons have been calculated. In addition to this the first order correction on most four parton processes was established. In this chapter we present expressions for the tree level matrix elements that are analytically known. Details of the calculation can be found in chapters 4-7.

The matrix element squared, spin and colour summed reads, see eq. (3.5.12),

$$\sum_{c,\lambda} |\mathcal{M}_n(P)|^2 = g^{2n-4} \sum_{c,\lambda} \left| \sum_{\text{perms}} F(T^a, i, N) K_F(P) \right|^2 \quad (10.1.1)$$

which, with the colour sum evaluated, reads

$$\sum_{c,\lambda} |\mathcal{M}_n|^2 = g^{2n-4} \sum_{\lambda} \sum_{i,j} K_i(P) A^{ij} K_j^*(P). \quad (10.1.2)$$

The sum runs over the permutations of gluons and quarks and  $A^{ij}$  is the colour matrix resulting from  $F^i \times F^{*j}$ . Notice that the type of partons in  $\sum_{c,\lambda} |\mathcal{M}_n|^2$  is implicitly understood. A number of conventions are used to describe the subamplitudes  $K_F(P)$  and the permutation sums.

- All particles our outgoing, i.e. are created out of nothing.
- The gluons are denoted by digits and the quarks by  $q, r$  and  $s$ .
- Helicity configurations are denoted by replacing particle indices by helicities.
- The notational conventions of WvdW spinor language are used, see chapter 3. However both the momentum spinors and the momenta are denoted by the same symbol. In those cases where this leads to confusion the momenta will be denoted by capitals and the spinors by lower case characters. Furthermore we use

$$\{1, 2\} = (1+2)^2 = \langle 12 \rangle \langle 12 \rangle^* \text{ and } \langle 1|2+3|4 \rangle = \langle 12 \rangle^* \langle 42 \rangle + \langle 13 \rangle^* \langle 43 \rangle. \quad (10.1.3)$$

- $P_n$  denotes all the permutations of  $(1 \dots n)$ .  $P_n^*$  has the extra condition that index 1 is on the first spot, i.e. the permutations of  $(2 \dots n)$ .  $P_n^*$  has on top of that the condition that the index on the second place is less than the index on place  $n$ .  $P_n^{\dagger}$  denotes all permutations of  $(3 \dots n)$ .
- The mapping of permutations on to integers is described in section 4.4.
- For the colour structures the notation of section 3.5 is used.

In the case of gluonic amplitudes the  $\mathcal{C}$ -functions are not linearly independent, see section 4.3. This dependence can be used to reduce the colour matrix in size. Using the reflective property of  $\mathcal{C}$ -functions, see eq. (4.3.2), in eq. (10.1.2) results in a  $(n-1)!/2 \times (n-1)!/2$  colour-matrix  $c_n^{ij}$ ,

$$\sum_{c,\lambda} |\mathcal{M}_n|^2 = g^{2n-4} \sum_{\lambda} \sum_{i,j=1}^{(n-1)!/2} c_n^{ij} C_i C_j^* \quad (10.1.4)$$

with

$$c_n^{ij} = \sum_{\text{colours } a} \left( (P_n^{*i}) + (-1)^n (P_n^{*iT}) \right) \times \left( (P_n^{*j}) + (-1)^n (P_n^{*jT}) \right)^* \quad (10.1.5)$$

where  $P_n^{*iT}$  is the reflected permutation of  $P_n^{*i}$ . In eq. (10.1.5) the  $P_n^*$  should be seen as a permutation of  $(a_1 \dots a_n)$ .

Now there are two ways to proceed. The first one is to use the dependence of the  $\mathcal{C}$ -functions to simplify  $c_n^{ij}$  and rewrite eq. (10.1.4) into

$$\sum_{c,\lambda} |\mathcal{M}_n|^2 = g^{2n-4} \sum_{\lambda} \sum_{i,j=1}^{(n-1)!/2} \bar{c}_n^{ij} C_i C_j^* \quad (10.1.6)$$

By definition  $\bar{c}_n^{ij}$  is the matrix that contains the largest number of zeros. For  $n = 4, 5$  it turns out to be a diagonal matrix. The second way is to use the relations between  $\mathcal{C}$ -functions to reduce the size of  $c_n^{ij}$ . This leads to

$$\sum_{c,\lambda} |\mathcal{M}_n|^2 = g^{2n-4} \sum_{\lambda} \sum_{i,j=1}^{(n-2)!} \bar{\bar{c}}_n^{ij} C_i C_j^* \quad (10.1.7)$$

The  $\bar{\bar{c}}_n^{ij}$  is substantially smaller in size than  $\bar{c}_n^{ij}$  and also has a unique form. However, as we will show, it is not always preferable to use  $\bar{\bar{c}}_n^{ij}$  rather than  $\bar{c}_n^{ij}$ . Note that the sum over permutations in eq. (10.1.4) is denoted by  $P_n^*$  and by  $P_n^{\dagger}$  in eq. (10.1.7).

This chapter subsequently deals with the four, five, six and seven parton matrix elements. In the last section the so-called special helicity combinations are given for an arbitrary number of partons. The SPHEL approximation described in chapter 8 is based on these combinations.

## 10.2 Four parton matrix elements

### 10.2.1 $\emptyset \rightarrow gggg$

The four gluon process was first calculated in [1]. In our notation it is given by

$$\sum_{c,\lambda} |\mathcal{M}_4|^2 = g^4 \sum_{\lambda} \left| \sum_{P_4^*} 2 (a_1 a_2 a_3 a_4) \mathcal{C}(1234) \right|^2. \quad (10.2.1)$$

The non-zero  $\mathcal{C}$ -functions are the ones with two + and two - helicities. With gluons  $i$  and  $j$  having the - helicity they read

$$\mathcal{C}(1234) = \frac{(\sqrt{2})^4}{2} \frac{\langle ij \rangle^4}{\langle 12 \rangle \langle 23 \rangle \langle 34 \rangle \langle 41 \rangle}. \quad (10.2.2)$$

The colour matrices in eqs. (10.1.6) and (10.1.7) become

$$\bar{c}_4^{ij} = 2 \left( \frac{N}{2} \right)^2 (N^2 - 1) \delta^{ij} \quad (10.2.3)$$

and

$$\bar{c}_4 = 2 \left( \frac{N}{2} \right)^2 (N^2 - 1) \begin{pmatrix} 2 & 1 \\ 1 & 2 \end{pmatrix}. \quad (10.2.4)$$

With  $s = (1+2)^2$ ,  $t = (1+3)^2$ ,  $u = (1+4)^2$  and  $N = 3$  we find

$$\sum_{c,\lambda} |\mathcal{M}_4|^2 = 288 g^4 \left( \frac{1}{s^2 t^2} + \frac{1}{s^2 u^2} + \frac{1}{t^2 u^2} \right) (s^4 + t^4 + u^4). \quad (10.2.5)$$

### 10.2.2 $\emptyset \rightarrow q\bar{q}gg$

The matrix element for two quarks and two gluons reads

$$\sum_{c,\lambda} |\mathcal{M}_4|^2 = g^4 \sum_{c,\lambda} \left| \sum_{P_2} (a_1 a_2)_{ij} \mathcal{D}(q; 12; \bar{q}) \right|^2. \quad (10.2.6)$$

The non-zero  $\mathcal{D}$ -functions, with gluon  $i$  the - and the other gluon the + helicity, read

$$\mathcal{D}(+; 12; -) = (\sqrt{2})^2 \frac{\langle \bar{q}i \rangle^3 \langle qi \rangle}{\langle q1 \rangle \langle 12 \rangle \langle 2\bar{q} \rangle \langle \bar{q}q \rangle}. \quad (10.2.7)$$

with the mass of the quark  $m_q = 0$ . The colour matrix in eq. (10.1.2) is given by

$$\bar{d}^{ij} = \frac{1}{4} \frac{N^2 - 1}{N} \begin{pmatrix} N^2 - 1 & -1 \\ -1 & N^2 - 1 \end{pmatrix} \text{ with } \mathcal{D}_i = \begin{pmatrix} \mathcal{D}(q; 12; \bar{q}) \\ \mathcal{D}(q; 21; \bar{q}) \end{pmatrix}. \quad (10.2.8)$$

For massive quarks the result is

$$\sum_{c,\lambda} |\mathcal{M}_4|^2 = 2g^4 (N^2 - 1) \left( \frac{-1}{N} + N \left( 1 - \frac{2tu}{s^2} \right) \right) \left( \frac{t}{u} + \frac{u}{t} + \frac{4m_q^2 s}{tu} \left( 1 - \frac{m_q^2 s}{tu} \right) \right) \quad (10.2.9)$$

with  $s = (1+2)^2$ ,  $t = 2Q \cdot 1$ ,  $u = 2Q \cdot 2$ .

### 10.2.3 $\emptyset \rightarrow q\bar{q}r\bar{r}$

The four quark matrix element for a quark pair  $q$  with mass  $m_q$  and a quark pair  $r$  with mass  $m_r$  reads

$$\sum_{c,\lambda} |\mathcal{M}_4|^2 = g^4 (R_1(q, \bar{q}, r, \bar{r}) + \delta_{qr} R_2(q, \bar{q}, r, \bar{r})) \quad (10.2.10)$$

where  $\delta_{qr} = 1(0)$  for identical (different) flavoured quarks and

$$R_1(q, \bar{q}, r, \bar{r}) = 2(N^2 - 1) \frac{(q \cdot r)(\bar{q} \cdot \bar{r}) + (q \cdot \bar{r})(\bar{q} \cdot r) + m_q^2(r \cdot \bar{r}) + m_r^2(q \cdot \bar{q}) + 2m_q^2 m_r^2}{((q \cdot \bar{q}) + m_q^2)^2},$$

$$R_2(q, \bar{q}, r, \bar{r}) = R_1(q, \bar{r}, r, \bar{q}) - \frac{2(N^2 - 1)}{N} \times \frac{2(q \cdot r)(\bar{q} \cdot \bar{r}) + 2m^4 + m^2((q \cdot \bar{q}) + (r \cdot \bar{r}) - (q \cdot r) + (q \cdot \bar{r}) + (\bar{q} \cdot r) - (\bar{q} \cdot \bar{r}))}{((q \cdot \bar{q}) + m^2)((q \cdot \bar{r}) + m^2)},$$

with  $m_q = m_r = m$  for equal flavours. In the case of massless quarks the expressions simplify to

$$\sum_{c,\lambda} |\mathcal{M}_4|^2 = 2g^4 \left( (N^2 - 1) \frac{t^2 + u^2}{s^2} + \delta_{qr} (N^2 - 1) \left( \frac{s^2 + t^2}{u^2} - \frac{2}{N} \frac{t^2}{su} \right) \right) \quad (10.2.11)$$

with  $s = (q + \bar{q})^2$ ,  $t = (q + r)^2$  and  $u = (q + \bar{r})^2$ .

## 10.3 Five parton matrix elements

### 10.3.1 $\emptyset \rightarrow ggggg$

The five gluon process was first calculated with the standard Feynman diagram techniques in [3]. Compact results were obtained in [4]. In analogy with section 10.2 we find

$$\sum_{c,\lambda} |\mathcal{M}_5|^2 = g^6 \sum_{\lambda} \left| \sum_{P_5^*} 2 (a_1 a_2 a_3 a_4 a_5) \mathcal{C}(12345) \right|^2. \quad (10.3.1)$$

When only gluons  $i$  and  $j$  have the  $-$  helicity the  $\mathcal{C}$ -functions are

$$\mathcal{C}(12345) = \frac{(\sqrt{2})^5}{2} \frac{\langle ij \rangle^4}{\langle 12 \rangle \langle 23 \rangle \langle 34 \rangle \langle 45 \rangle \langle 51 \rangle}. \quad (10.3.2)$$

Other helicity combinations can either be obtained by complex conjugation or are zero. The colour matrices of eqs. (10.1.6) and (10.1.7) are

$$\bar{c}_s^{ij} = 2 \left( \frac{N}{2} \right)^3 (N^2 - 1) \delta^{ij}. \quad (10.3.3)$$

and

$$\bar{c}_5 = 2 \left( \frac{N}{2} \right)^3 (N^2 - 1) \begin{pmatrix} 4 & 2 & 1 & 2 & 1 & 0 \\ 2 & 4 & 0 & 1 & 2 & 1 \\ 1 & 0 & 4 & 2 & 1 & 2 \\ 2 & 1 & 2 & 4 & 0 & 1 \\ 1 & 2 & 1 & 0 & 4 & 2 \\ 0 & 1 & 2 & 1 & 2 & 4 \end{pmatrix}. \quad (10.3.4)$$

With  $s_{ij} = (i \cdot j)$  and  $N = 3$  the matrix element squared reads

$$\sum_{c,\lambda} |\mathcal{M}_5|^2 = 432 g^6 \left( \sum_{1 \leq i < j \leq 5} s_{ij}^4 \right) \times \left( \sum_{P_5} \frac{1}{s_{12}s_{23}s_{34}s_{45}s_{51}} \right). \quad (10.3.5)$$

### 10.3.2 $\bar{q} \rightarrow q \bar{q} g g g$

The two quark plus three gluon process is given by

$$\sum_{c,\lambda} |\mathcal{M}_5|^2 = g^6 \sum_{c,\lambda} \left| \sum_{P_3} (a_1 a_2 a_3)_{ij} \mathcal{D}(q; 123; \bar{q}) \right|^2. \quad (10.3.6)$$

The non-zero  $\mathcal{D}$ -functions, with gluon  $i$  the  $-$  and the other gluons the  $+$  helicity, read

$$\mathcal{D}(+; 123; -) = (\sqrt{2})^3 \frac{\langle \bar{q} i \rangle^3 \langle q i \rangle}{\langle q 1 \rangle \langle 1 2 \rangle \langle 2 3 \rangle \langle 3 \bar{q} \rangle \langle \bar{q} q \rangle}, \quad (10.3.7)$$

where the mass of the quarks is set to zero. The colour matrix in eq. (10.1.2) is given by

$$d^{ij} = \frac{1}{8} \frac{N^2 - 1}{N^2} \begin{pmatrix} d_1 & d_2 & d_3 & d_2 & d_3 & d_4 \\ d_2 & d_1 & d_4 & d_3 & d_2 & d_3 \\ d_3 & d_4 & d_1 & d_2 & d_3 & d_2 \\ d_2 & d_3 & d_2 & d_1 & d_4 & d_3 \\ d_3 & d_2 & d_3 & d_4 & d_1 & d_2 \\ d_4 & d_3 & d_2 & d_3 & d_2 & d_1 \end{pmatrix} \quad \text{with } \mathcal{D}_i = \begin{pmatrix} \mathcal{D}(q; 123; \bar{q}) \\ \mathcal{D}(q; 132; \bar{q}) \\ \mathcal{D}(q; 231; \bar{q}) \\ \mathcal{D}(q; 213; \bar{q}) \\ \mathcal{D}(q; 312; \bar{q}) \\ \mathcal{D}(q; 321; \bar{q}) \end{pmatrix} \quad (10.3.8)$$

with  $d_1 = N^4 - 2N^2 + 1$ ,  $d_2 = -N^2 + 1$ ,  $d_3 = 1$ ,  $d_4 = N^2 + 1$ . Analytical evaluation of eq. (10.3.6) leads to the following compact form for  $\sum_{c,\lambda} |\mathcal{M}_5|^2$  [4] ( $n_q$  is the number of quarks crossed to the initial state).

$$\sum_{c,\lambda} |\mathcal{M}_5|^2 = g^6 (-1)^{n_q} \frac{N^2 - 1}{N^2} \left( \sum_{i=1}^3 \frac{(q \cdot i)^3 (\bar{q} \cdot i) + (q \cdot i) (\bar{q} \cdot i)^3}{(q \cdot 1)(q \cdot 2)(q \cdot 3)(\bar{q} \cdot 1)(\bar{q} \cdot 2)(\bar{q} \cdot 3)} \right) \times \quad (10.3.9)$$

$$\left\{ (q \cdot \bar{q}) + N^2 \left( (q \cdot \bar{q}) - \sum_{P_3} \frac{(q \cdot 1)(\bar{q} \cdot 2)}{(1 \cdot 2)} \right) + \frac{N^4}{(q \cdot \bar{q})} \sum_{P_3} \frac{(q \cdot 1)(\bar{q} \cdot 1)(q \cdot 2)(\bar{q} \cdot 3)}{(2 \cdot 1)(1 \cdot 3)} \right\}$$

### 10.3.3 $\emptyset \rightarrow q\bar{q}r\bar{r}g$

The matrix element squared for processes with four quarks and a gluon reads

$$\sum_{c,\lambda} |\mathcal{M}_S|^2 = g^6 \sum_{\lambda} \sum_{i,j=1}^4 e^{ij} \mathcal{E}_i \mathcal{E}_j^*, \quad (10.3.10)$$

where the subamplitudes  $\mathcal{E}_i$  and  $e^{ij}$  correspond to the following structures,

$$\mathcal{E}_i \Leftrightarrow \begin{pmatrix} \mathcal{F}_{01} \\ \mathcal{F}_{10} \\ \mathcal{E}_{01} \\ \mathcal{E}_{10} \end{pmatrix} \Leftrightarrow \frac{1}{2} \begin{pmatrix} \delta_{c_1 c_2} (a_1)_{c_3 c_4} \\ (a_1)_{c_1 c_2} \delta_{c_3 c_4} \\ \delta_{c_1 c_4} (a_1)_{c_3 c_2} \\ (a_1)_{c_1 c_4} \delta_{c_3 c_2} \end{pmatrix} \text{ and } e^{ij} = \frac{1}{8} (N^2 - 1) \begin{pmatrix} N & 0 & 1 & 1 \\ 0 & N & 1 & 1 \\ 1 & 1 & N & 0 \\ 1 & 1 & 0 & N \end{pmatrix}.$$

The  $\mathcal{F}_{01}, \dots$  are defined in chapter 6. The colour assignment is  $(q, c_1), (\bar{q}, c_2), (r, c_3)$  and  $(\bar{r}, c_4)$ . For equal flavours the  $\mathcal{E}_i(q, \bar{q}, r, \bar{r}; 1)$  must be replaced by

$$\mathcal{E}_i(q, \bar{q}, r, \bar{r}) - \mathcal{E}_i(q, \bar{r}, r, \bar{q}).$$

Although the  $\mathcal{E}_i$ 's in principle do not depend on  $N$ , they do in eq. (10.3.10) because we reduced the amount of possible colour structures by a factor of two by putting the explicit  $1/N$  dependence in  $\mathcal{E}_i$ . The helicity amplitudes are given by

$$\mathcal{E}_i(q, \bar{q}, r, \bar{r}) = \mathcal{E}_i^* \times \frac{A(\lambda_q, \lambda_r)}{\langle q\bar{q} \rangle \langle r\bar{r} \rangle} \quad (10.3.11)$$

with

$$\mathcal{E}_1^* = \frac{-\sqrt{2}}{N} \frac{\langle q\bar{q} \rangle}{\langle q1 \rangle \langle 1\bar{q} \rangle}, \mathcal{E}_2^* = \frac{-\sqrt{2}}{N} \frac{\langle r\bar{r} \rangle}{\langle r1 \rangle \langle 1\bar{r} \rangle}, \mathcal{E}_3^* = \sqrt{2} \frac{\langle q\bar{r} \rangle}{\langle q1 \rangle \langle 1\bar{r} \rangle}, \mathcal{E}_4^* = \sqrt{2} \frac{\langle r\bar{q} \rangle}{\langle r1 \rangle \langle 1\bar{q} \rangle}$$

and

$$A(+,+) = \langle \bar{q}\bar{r} \rangle^2, A(+,-) = -\langle \bar{q}r \rangle^2, A(-,+) = -\langle q\bar{r} \rangle^2, A(-,-) = \langle qr \rangle^2$$

Evaluating eq. (10.3.10) analytically leads to compact expressions in terms of Minkowski inner products [4]. When the quark pair  $r$  has a mass  $m_r$ , the resulting expression for  $\sum_{c,\lambda} |\mathcal{M}_n|^2$  consists of 650 terms. However this result was obtained by standard Feynman diagram techniques and computer algebra. No attempt was made to simplify the expression.

## 10.4 Six parton matrix elements

### 10.4.1 $\emptyset \rightarrow gggggg$

The process with six gluons has been calculated four times in the past seven years. The first calculations [5] used the Feynman diagram technique in a straightforward way. Using spinor calculus [6] and the colour basis  $(a_1 \dots a_6)$  compact expressions were obtained. The matrix element squared for the six gluon process reads

|             |                                                                                                                                                |
|-------------|------------------------------------------------------------------------------------------------------------------------------------------------|
| $C(++++++)$ | no $M_i \neq 0$                                                                                                                                |
| $C(+++++-)$ | no $M_i \neq 0$                                                                                                                                |
| $C(++++--)$ | $M_4 = \langle 56 \rangle^4 \langle 12 \rangle \langle 23 \rangle \langle 34 \rangle \langle 45 \rangle \langle 56 \rangle \langle 61 \rangle$ |
| $C(++++-+)$ | $M_4 = \langle 46 \rangle^4 \langle 12 \rangle \langle 23 \rangle \langle 34 \rangle \langle 45 \rangle \langle 56 \rangle \langle 61 \rangle$ |
| $C(++++--)$ | $M_4 = \langle 36 \rangle^4 \langle 12 \rangle \langle 23 \rangle \langle 34 \rangle \langle 45 \rangle \langle 56 \rangle \langle 61 \rangle$ |
| $C(++++--)$ | $M_2 = \langle 56 \rangle \langle 23 \rangle \langle 1 2+3 4 \rangle$                                                                          |
|             | $M_3 = \langle 45 \rangle \langle 12 \rangle \langle 3 1+2 6 \rangle$                                                                          |
|             | $M_4 = M_2 M_3 (1+2+3)^2$                                                                                                                      |
| $C(++++--)$ | $M_1 = \langle 46 \rangle \langle 12 \rangle \langle 5 1+2 3 \rangle$                                                                          |
|             | $M_2 = \langle 34 \rangle \langle 15 \rangle \langle 2 3+4 6 \rangle$                                                                          |
|             | $M_3 = \langle 34 \rangle \langle 12 \rangle \langle 5 3+4 6 \rangle$                                                                          |
|             | $M_4 = M_1 M_2 (1+2+3)^2 + M_1 M_3 (2+3+4)^2 + M_2 M_3 (1+2+3)^2$                                                                              |
| $C(++++--)$ | $M_1 = \langle 64 \rangle \langle 13 \rangle \langle 5 4+6 2 \rangle$                                                                          |
|             | $M_2 = \langle 42 \rangle \langle 51 \rangle \langle 3 2+4 6 \rangle$                                                                          |
|             | $M_3 = \langle 26 \rangle \langle 35 \rangle \langle 1 6+2 4 \rangle$                                                                          |
|             | $M_4 = M_1 M_2 (1+2+3)^2 + M_1 M_3 (2+3+4)^2 + M_2 M_3 (1+2+3)^2$                                                                              |

Table 10.1. The non-zero  $M$ 's for the  $C$ -functions. Add a factor  $(\sqrt{2})^6/2$ .

$$\sum_{c,\lambda} |\mathcal{M}_6|^2 = g^8 \sum_{\lambda} \left| \sum_{P_6^c} 2 (a_1 a_2 a_3 a_4 a_5 a_6) C(123456) \right|^2. \quad (10.4.1)$$

Using parity and the various relations between  $C$ -functions, see section 4.3, it suffices to calculate just a few out of the 128 helicity configurations. The pole structure of  $C(123456)$  reads

$$C(123456) = \frac{M_1 M_1}{\{1,2\}(1+2+3)^2 \{2,3\} \{4,5\} \{5,6\}} + \frac{M_2 M_2}{\{2,3\}(2+3+4)^2 \{3,4\} \{5,6\} \{6,1\}} \\ + \frac{M_3 M_3}{\{1,2\} \{3,4\} (3+4+5)^2 \{4,5\} \{6,1\}} + \frac{M_4}{\{1,2\} \{2,3\} \{3,4\} \{4,5\} \{5,6\} \{6,1\}} \quad (10.4.2)$$

The expressions for  $M_1$  through  $M_4$  are listed in table 10.1.

We rewrite  $c_6^{ij}$  in such a way that it contains as many zeros as possible. As the best solution the following expression was found [6, 7]

$$\sum_{c,\lambda} |\mathcal{M}_6|^2 = 2g^8 (N/2)^4 (N^2 - 1) \sum_{\lambda} \sum_{P_6^c} C(123456) \times \quad (10.4.3) \\ \left[ C(123456) + 2/N^2 (C(135264) + C(142635) + C(136425)) \right]^2.$$

The colour matrix,  $\tilde{c}_6^{ij}$  contains 240 non-zero terms of which 180 are non-leading order in colour. By expressing all  $C$ -functions in the 1,2-basis we obtain  $\tilde{c}_6^{ij}$ , see eq. (10.1.7), with the new colour matrix given in table 10.2. Only the first row of the matrix, i.e. the terms of the form  $(123456) \times (12x_1 x_2 x_3 x_4)$  are given. The linear labeling of the permutations is included in the table. We note that there are more than 240 non-zero elements in  $\tilde{c}_6^{ij}$ .

|            |         |             |             |             |             |
|------------|---------|-------------|-------------|-------------|-------------|
| (1234) = 1 | $48N^2$ | (2413) = 9  | $6N^2$      | (3241) = 17 | 0           |
| (1243) = 2 | $24N^2$ | (2431) = 10 | 0           | (3214) = 18 | 0           |
| (1342) = 3 | $12N^2$ | (2134) = 11 | $24N^2$     | (4123) = 19 | $6N^2$      |
| (1324) = 4 | $24N^2$ | (2143) = 12 | $12N^2$     | (4132) = 20 | 0           |
| (1423) = 5 | $12N^2$ | (3412) = 13 | $12N^2$     | (4231) = 21 | 0           |
| (1432) = 6 | 0       | (3421) = 14 | $6N^2 + 24$ | (4213) = 22 | 0           |
| (2341) = 7 | $6N^2$  | (3124) = 15 | $12N^2$     | (4312) = 23 | $6N^2 + 24$ |
| (2314) = 8 | $12N^2$ | (3142) = 16 | $6N^2$      | (4321) = 24 | $6N^2 + 24$ |

Table 10.2. The first row of the colour matrix  $\bar{c}_g^{ij}$ . Add a factor  $N^2(N^2 - 1)2^{-4}$ .

so eq. (10.4.3) appears to be the best method. However careful study of the LO and NLO contributions shows that the best method is a mixture. Take the LO terms from eq. (10.4.3) and the NLO terms from eq. (10.1.7) to arrive at the following expression.

$$\sum_{c,\lambda} |\mathcal{M}_6|^2 = g^8 2(N/2)^4 (N^2 - 1) \sum_{\lambda} 2 \sum_{P_g^*} C(123456) C(123456)^* \quad (10.4.4)$$

$$+ g^8 6(N/2)^2 (N^2 - 1) \sum_{\lambda} \sum_{P_g^*} C(123456) \times [ + C(125634) + C(125643) + C(126453) + C(126534) + C(126543) ]^* \quad (10.4.5)$$

#### 10.4.2 $\emptyset \rightarrow q\bar{q}gggg$

The process with a massless quark pair and four gluons has first been calculated in [8] by making use of supersymmetry and the results for the six gluon process. The expressions for the helicity amplitudes have been verified using the techniques described in this thesis. The matrix element squared for the process  $\emptyset \rightarrow q\bar{q}gggg$  reads

$$\sum_{c,\lambda} |\mathcal{M}_6|^2 = g^8 \sum_{c,\lambda} \left| \sum_{P_4} (a_1 a_2 a_3 a_4)_{ij} \mathcal{D}(q; 1234; \bar{q}) \right|^2. \quad (10.4.6)$$

Ten different helicity configurations need to be evaluated. In contrast with [8] our expressions for the helicity amplitudes manifestly have the charge conjugation symmetry. The pole structure of  $\mathcal{D}(q; 1234; \bar{q})$  reads

$$\begin{aligned} \mathcal{D}(q; 1234; \bar{q}) = & \frac{M_1}{\{1,2\}(1+2+3)^2\{2,3\}\{2,3\}\{4,q\}\{q,\bar{q}\}} \quad (10.4.7) \\ & + \frac{M_2}{\{q,1\}\{1,2\}\{3,4\}(3+4+\bar{q})^2\{4,\bar{q}\}} + \frac{M_3}{\{q,1\}\{2,3\}(2+3+4)^2\{3,4\}\{\bar{q},q\}} \\ & + \frac{M_4}{\{q,1\}\{1,2\}\{2,3\}\{3,4\}\{4,\bar{q}\}\{\bar{q},q\}}. \end{aligned}$$

The expressions for  $M_1$  through  $M_4$  are listed in table 10.3.

The colour matrix in eq. (10.1.2) is given in terms of  $\sum_c (a_1 a_2 a_3 a_4)_{ij} \times (P(a_1 a_2 a_3 a_4))_i^j$  in table 10.4. The other colour products can be obtained by renumbering.

|                    |                                                                                                                                                                                                                                                                                                                                                                                                                                                                                                                                                                                                                                                                                                                                                                                                                                                                                                                                                                                                                                                                                                                                                                                                                                                                                                                                                                                                                                                               |
|--------------------|---------------------------------------------------------------------------------------------------------------------------------------------------------------------------------------------------------------------------------------------------------------------------------------------------------------------------------------------------------------------------------------------------------------------------------------------------------------------------------------------------------------------------------------------------------------------------------------------------------------------------------------------------------------------------------------------------------------------------------------------------------------------------------------------------------------------------------------------------------------------------------------------------------------------------------------------------------------------------------------------------------------------------------------------------------------------------------------------------------------------------------------------------------------------------------------------------------------------------------------------------------------------------------------------------------------------------------------------------------------------------------------------------------------------------------------------------------------|
| $D(+; + + + +; -)$ | no $M_i \neq 0$                                                                                                                                                                                                                                                                                                                                                                                                                                                                                                                                                                                                                                                                                                                                                                                                                                                                                                                                                                                                                                                                                                                                                                                                                                                                                                                                                                                                                                               |
| $D(+; + + + -; -)$ | $M_4 = \langle 4\bar{q} \rangle^3 \langle 4q \rangle \langle q1 \rangle \langle 12 \rangle \langle 23 \rangle \langle 34 \rangle \langle 4\bar{q} \rangle \langle \bar{q}q \rangle$                                                                                                                                                                                                                                                                                                                                                                                                                                                                                                                                                                                                                                                                                                                                                                                                                                                                                                                                                                                                                                                                                                                                                                                                                                                                           |
| $D(+; + + - +; -)$ | $M_4 = \langle 3\bar{q} \rangle^3 \langle 3q \rangle \langle q1 \rangle \langle 12 \rangle \langle 23 \rangle \langle 34 \rangle \langle 4\bar{q} \rangle \langle \bar{q}q \rangle$                                                                                                                                                                                                                                                                                                                                                                                                                                                                                                                                                                                                                                                                                                                                                                                                                                                                                                                                                                                                                                                                                                                                                                                                                                                                           |
| $D(+; + - + +; -)$ | $M_4 = \langle 2\bar{q} \rangle^3 \langle 2q \rangle \langle q1 \rangle \langle 12 \rangle \langle 23 \rangle \langle 34 \rangle \langle 4\bar{q} \rangle \langle \bar{q}q \rangle$                                                                                                                                                                                                                                                                                                                                                                                                                                                                                                                                                                                                                                                                                                                                                                                                                                                                                                                                                                                                                                                                                                                                                                                                                                                                           |
| $D(+; - + + +; -)$ | $M_4 = \langle 1\bar{q} \rangle^3 \langle 1q \rangle \langle q1 \rangle \langle 12 \rangle \langle 23 \rangle \langle 34 \rangle \langle 4\bar{q} \rangle \langle \bar{q}q \rangle$                                                                                                                                                                                                                                                                                                                                                                                                                                                                                                                                                                                                                                                                                                                                                                                                                                                                                                                                                                                                                                                                                                                                                                                                                                                                           |
| $D(+; + + - -; -)$ | $M_1 = \langle q4 \rangle \langle \bar{q}4 \rangle \langle 12 \rangle^{-2} \langle q \bar{q}+4 3 \rangle^2$<br>$M_3 = -\langle 34 \rangle^2 \langle q1 \rangle \langle \bar{q}1 \rangle \langle 2 q+1 \bar{q} \rangle^2$<br>$M_4 = -\langle \bar{q}4 \rangle \langle 34 \rangle \langle q1 \rangle \langle 12 \rangle \langle (q \bar{q}+4 3) \langle \bar{q} 3+4 q \rangle \langle 2 3+4 \bar{q} \rangle$<br>$+ \{1, 2\} \langle 43 \rangle \langle \bar{q}4 \rangle \langle 2 3+4 \bar{q} \rangle - \{3, 4\} \langle q1 \rangle \langle 12 \rangle \langle q 1+2 3 \rangle$                                                                                                                                                                                                                                                                                                                                                                                                                                                                                                                                                                                                                                                                                                                                                                                                                                                                                 |
| $D(+; + - - -; -)$ | $M_1 = \langle q4 \rangle \langle \bar{q}4 \rangle \langle 13 \rangle^{-2} \langle q \bar{q}+4 2 \rangle^2$<br>$M_2 = -\langle \bar{q}4 \rangle \langle q1 \rangle \langle 1 \bar{q}+3 4 \rangle \langle 3 \bar{q}+4 2 \rangle^2$<br>$M_3 = -\langle 24 \rangle^2 \langle q1 \rangle \langle \bar{q}1 \rangle \langle 3 2+4 \bar{q} \rangle^2$<br>$M_4 = -(1+2+3)^2 \langle 24 \rangle \langle q1 \rangle \langle 1 \bar{q}+3 4 \rangle \langle 3 \bar{q}+4 2 \rangle \langle 3 2+4 \bar{q} \rangle$<br>$+ (q+1+2)^2 \langle 24 \rangle \langle 13 \rangle \langle 1 \bar{q}+3 4 \rangle \langle q \bar{q}+4 2 \rangle \langle 3 2+4 \bar{q} \rangle$<br>$+ (2+3+4)^2 \langle \bar{q}4 \rangle \langle 13 \rangle \langle 1 \bar{q}+3 4 \rangle \langle q \bar{q}+4 2 \rangle \langle 3 \bar{q}+4 2 \rangle$<br>$- \langle 24 \rangle \langle 34 \rangle \langle 12 \rangle \langle 13 \rangle \langle q \bar{q}+4 2 \rangle \langle 3 \bar{q}+4 2 \rangle \langle 3 2+4 \bar{q} \rangle$                                                                                                                                                                                                                                                                                                                                                                                                                                                                     |
| $D(+; + - - +; -)$ | $M_1 = -\langle 23 \rangle^2 \langle q4 \rangle \langle \bar{q}4 \rangle \langle 1 q+4 \bar{q} \rangle^2$<br>$M_2 = -\langle \bar{q}3 \rangle \langle q1 \rangle \langle 1 \bar{q}+4 3 \rangle \langle 4 \bar{q}+3 2 \rangle^2$<br>$M_3 = -\langle 23 \rangle^2 \langle q1 \rangle \langle \bar{q}1 \rangle \langle 4 2+3 \bar{q} \rangle^2$<br>$M_4 = -(1+2+3)^2 \langle \bar{q}3 \rangle \langle 23 \rangle \langle q1 \rangle \langle \bar{q}1 \rangle \langle 4 \bar{q}+3 2 \rangle \langle 4 2+3 \bar{q} \rangle$<br>$+ (q+1+2)^2 \langle 23 \rangle^2 \langle q4 \rangle \langle \bar{q}1 \rangle \langle 1 q+4 \bar{q} \rangle \langle 4 2+3 \bar{q} \rangle$<br>$+ (2+3+4)^2 \langle \bar{q}3 \rangle \langle 23 \rangle \langle q4 \rangle \langle \bar{q}1 \rangle \langle 1 q+4 \bar{q} \rangle \langle 4 \bar{q}+3 2 \rangle$<br>$- \langle 23 \rangle \langle 34 \rangle \langle q\bar{q} \rangle \langle 14 \rangle \langle 1 q+4 \bar{q} \rangle \langle 4 \bar{q}+3 2 \rangle \langle 4 2+3 \bar{q} \rangle$                                                                                                                                                                                                                                                                                                                                                                                                                                  |
| $D(+; - + - +; -)$ | $M_1 = -\langle 13 \rangle^2 \langle q4 \rangle \langle \bar{q}4 \rangle \langle 2 q+4 \bar{q} \rangle^2$<br>$M_2 = -\langle \bar{q}3 \rangle \langle q2 \rangle \langle 2 \bar{q}+4 3 \rangle \langle 4 \bar{q}+3 1 \rangle^2$<br>$M_3 = \langle q1 \rangle \langle \bar{q}1 \rangle \langle 24 \rangle^{-2} \langle q 4+2 3 \rangle^2$<br>$M_4 = \langle q3 \rangle \langle \bar{q}1 \rangle \langle \bar{q}3 \rangle \langle 12 \rangle \langle q\bar{q} \rangle \langle \bar{q}4 \rangle \langle q2 \rangle \langle 24 \rangle \langle 2 q+4 \bar{q} \rangle$<br>$- \langle q\bar{q} \rangle \langle q1 \rangle \langle \bar{q}3 \rangle \langle 13 \rangle \langle q2 \rangle \langle q4 \rangle \langle \bar{q}2 \rangle \langle 34 \rangle \langle q 2+4 3 \rangle$<br>$+ \{q, 1\} \{ \bar{q}, 4 \} \langle 13 \rangle \langle 24 \rangle \langle (\bar{q}1) \langle 24 \rangle \langle q 2+4 3 \rangle$<br>$- \langle 13 \rangle \langle 24 \rangle \langle q 1+3 \bar{q} \rangle + \langle 13 \rangle \langle q4 \rangle \langle 2 1+3 \bar{q} \rangle$<br>$+ \{q, \bar{q}\} \langle 13 \rangle \langle \bar{q}3 \rangle \langle 24 \rangle \langle q2 \rangle$<br>$([\{q, 1\} - \{2, 3\} + \{ \bar{q}, 4 \}] \langle 4 \bar{q}+3 1 \rangle + \{ \bar{q}, 3 \} \langle q1 \rangle \langle q4 \rangle$<br>$- \{q, 2\} \langle \bar{q}1 \rangle \langle \bar{q}4 \rangle + \langle q1 \rangle \langle 4\bar{q} \rangle \langle q 1+3 \bar{q} \rangle)$ |
| $D(+; + + - -; -)$ | $M_1 = -\langle 12 \rangle^2 \langle q4 \rangle \langle \bar{q}4 \rangle \langle 3 q+4 \bar{q} \rangle^2$<br>$M_3 = \langle q1 \rangle \langle \bar{q}1 \rangle \langle 34 \rangle^{-2} \langle q 3+4 2 \rangle^2$<br>$M_4 = -\langle q1 \rangle \langle 12 \rangle \langle \bar{q}4 \rangle \langle 34 \rangle \langle q 3+4 \bar{q} \rangle \langle q 3+4 2 \rangle \langle 3 q+4 \bar{q} \rangle$                                                                                                                                                                                                                                                                                                                                                                                                                                                                                                                                                                                                                                                                                                                                                                                                                                                                                                                                                                                                                                                          |

Table 10.3. The non-zero  $M$ 's for the  $\mathcal{D}$ -functions. Add a factor  $(\sqrt{2})^4$  to  $M_i$ .

|                     |                         |                     |                   |
|---------------------|-------------------------|---------------------|-------------------|
| $(a_1 a_2 a_3 a_4)$ | $N^6 - 3N^4 + 3N^2 - 1$ | $(a_3 a_4 a_1 a_2)$ | $+N^4 - N^2 - 1$  |
| $(a_1 a_2 a_4 a_3)$ | $-N^4 + 2N^2 - 1$       | $(a_3 a_4 a_2 a_1)$ | $+N^4 - 2N^2 - 1$ |
| $(a_1 a_3 a_4 a_2)$ | $N^2 - 1$               | $(a_3 a_1 a_2 a_4)$ | $N^2 - 1$         |
| $(a_1 a_3 a_2 a_4)$ | $-N^4 + 2N^2 - 1$       | $(a_3 a_1 a_4 a_2)$ | $-1$              |
| $(a_1 a_4 a_2 a_3)$ | $N^2 - 1$               | $(a_3 a_2 a_4 a_1)$ | $-N^2 - 1$        |
| $(a_1 a_4 a_3 a_2)$ | $+N^4$                  | $(a_3 a_2 a_1 a_4)$ | $+N^4$            |
| $(a_2 a_3 a_4 a_1)$ | $-1$                    | $(a_4 a_1 a_2 a_3)$ | $-1$              |
| $(a_2 a_3 a_1 a_4)$ | $N^2 - 1$               | $(a_4 a_1 a_3 a_2)$ | $-N^2 - 1$        |
| $(a_2 a_4 a_1 a_3)$ | $-1$                    | $(a_4 a_2 a_3 a_1)$ | $+N^4 - 2N^2 - 1$ |
| $(a_2 a_4 a_3 a_1)$ | $-N^2 - 1$              | $(a_4 a_2 a_1 a_3)$ | $-N^2 - 1$        |
| $(a_2 a_1 a_3 a_4)$ | $-N^4 + 2N^2 - 1$       | $(a_4 a_3 a_1 a_2)$ | $+N^4 - 2N^2 - 1$ |
| $(a_2 a_1 a_4 a_3)$ | $N^2 - 1$               | $(a_4 a_3 a_2 a_1)$ | $-3N^2 - 1$       |

Table 10.4. The colour matrix  $d_6^{ij}$ . A factor  $(N^2 - 1)N^{-3}2^{-4}$  must be added.

### 10.4.3 $\emptyset \rightarrow q\bar{q}r\bar{r}g$

The matrix element squared for processes with four massless quarks and two gluons was first calculated in [9]. In our notation it reads written as

$$\sum_{c,\lambda} |\mathcal{M}_6|^2 = g^6 \sum_{\lambda} \sum_{i,j=1}^{12} e^{ij} \mathcal{E}_i \mathcal{E}_j^* \quad (10.4.8)$$

For remarks about colour dependence and different flavours we refer to the four quark and one gluon process. The subamplitudes  $\mathcal{E}_i$  and the colour matrix  $e^{ij}$  in eq. (10.4.8) are given by

$$\mathcal{E}_i \Leftrightarrow \begin{pmatrix} \mathcal{F}_{02}(q\bar{q}r\bar{r}; 12) \\ \mathcal{F}_{11}(q\bar{q}r\bar{r}; 1; 2) \\ \mathcal{F}_{20}(q\bar{q}r\bar{r}; 12; ) \\ \mathcal{F}_{02}(q\bar{q}r\bar{r}; ; 21) \\ \mathcal{F}_{11}(q\bar{q}r\bar{r}; 2; 1) \\ \mathcal{F}_{20}(q\bar{q}r\bar{r}; 21; ) \\ \mathcal{E}_{02}(q\bar{q}r\bar{r}; 12) \\ \mathcal{E}_{11}(q\bar{q}r\bar{r}; 1; 2) \\ \mathcal{E}_{20}(q\bar{q}r\bar{r}; 12; ) \\ \mathcal{E}_{02}(q\bar{q}r\bar{r}; ; 21) \\ \mathcal{E}_{11}(q\bar{q}r\bar{r}; 2; 1) \\ \mathcal{E}_{20}(q\bar{q}r\bar{r}; 21; ) \end{pmatrix} \Leftrightarrow \frac{1}{2} \begin{pmatrix} \delta_{c_1 c_2} (a_1 a_2)_{c_3 c_4} \\ (a_1)_{c_1 c_2} (a_2)_{c_3 c_4} \\ (a_1 a_2)_{c_1 c_2} \delta_{c_3 c_4} \\ \delta_{c_1 c_2} (a_2 a_1)_{c_3 c_4} \\ (a_2)_{c_1 c_2} (a_1)_{c_3 c_4} \\ (a_2 a_1)_{c_1 c_2} \delta_{c_3 c_4} \\ \delta_{c_1 c_4} (a_1 a_2)_{c_3 c_2} \\ (a_1)_{c_3 c_4} (a_2)_{c_3 c_2} \\ (a_1 a_2)_{c_1 c_4} \delta_{c_3 c_2} \\ \delta_{c_1 c_4} (a_2 a_1)_{c_3 c_2} \\ (a_2)_{c_3 c_4} (a_1)_{c_3 c_2} \\ (a_2 a_1)_{c_1 c_4} \delta_{c_3 c_2} \end{pmatrix} \quad (10.4.9)$$

and

|                  |                                                                                                                                                       |
|------------------|-------------------------------------------------------------------------------------------------------------------------------------------------------|
| +, -, +, -, +, + | $M_3 = -\langle \bar{q}\bar{r} \rangle^2 \langle q1 \rangle^* \langle 12 \rangle^* \langle 2\bar{q} \rangle^* \langle r\bar{r} \rangle^*$             |
| +, -, -, +; +, + | $M_3 = \langle \bar{q}r \rangle^2 \langle q1 \rangle^* \langle 12 \rangle^* \langle 2\bar{q} \rangle^* \langle r\bar{r} \rangle^*$                    |
| -, +, +, -, +, + | $M_3 = \langle q\bar{r} \rangle^2 \langle q1 \rangle^* \langle 12 \rangle^* \langle 2\bar{q} \rangle^* \langle r\bar{r} \rangle^*$                    |
| -, +, -, +; +, + | $M_3 = -\langle qr \rangle^2 \langle q1 \rangle^* \langle 12 \rangle^* \langle 2\bar{q} \rangle^* \langle r\bar{r} \rangle^*$                         |
| +, -, +, -, +; - | $M_1 = \langle \bar{q}2 \rangle^2 \langle 1\bar{q} \rangle^* \langle qr \rangle^* \langle 1 2 + \bar{q} \bar{r} \rangle$                              |
|                  | $M_2 = \langle q1 \rangle^* \langle q2 \rangle \langle \bar{q}\bar{r} \rangle \langle 1q \rangle^* \langle r q + 1 2 \rangle$                         |
|                  | $M_3 = \langle \bar{q}2 \rangle \langle q1 \rangle \langle r q + 1 2 \rangle \langle 1 \bar{q} + 2 \bar{r} \rangle$                                   |
| +, -, -, +; +, - | $M_1 = \langle \bar{q}2 \rangle^2 \langle 1\bar{q} \rangle^* \langle q\bar{r} \rangle^* \langle 1 2 + \bar{q} r \rangle$                              |
|                  | $M_2 = \langle q1 \rangle^* \langle q2 \rangle \langle \bar{q}r \rangle \langle 1q \rangle^* \langle \bar{r} q + 1 2 \rangle$                         |
|                  | $M_3 = \langle \bar{q}2 \rangle \langle q1 \rangle \langle \bar{r} q + 1 2 \rangle \langle 1 \bar{q} + 2 r \rangle$                                   |
| -, +, +, -, +; - | $M_1 = \langle \bar{q}2 \rangle \langle \bar{r}q \rangle \langle 1\bar{q} \rangle^* \langle r 1 + \bar{q} 2 \rangle$                                  |
|                  | $M_2 = \langle q1 \rangle^* \langle q2 \rangle^2 \langle r\bar{q} \rangle^* \langle 1 q + 2 \bar{r} \rangle$                                          |
|                  | $M_3 = \langle \bar{q}2 \rangle \langle q1 \rangle \langle q\bar{r} \rangle \langle q2 \rangle \langle \bar{q}r \rangle^* \langle \bar{q}1 \rangle^*$ |
| -, +, -, +; +, - | $M_1 = \langle \bar{q}2 \rangle \langle rq \rangle \langle 1\bar{q} \rangle^* \langle \bar{r} 1 + \bar{q} 2 \rangle$                                  |
|                  | $M_2 = \langle q1 \rangle^* \langle q2 \rangle^2 \langle \bar{r}\bar{q} \rangle^* \langle 1 q + 2 r \rangle$                                          |
|                  | $M_3 = \langle \bar{q}2 \rangle \langle q1 \rangle \langle qr \rangle \langle q2 \rangle \langle \bar{q}\bar{r} \rangle^* \langle \bar{q}1 \rangle^*$ |

Table 10.5. The  $M_i$ 's of  $\mathcal{F}_{20}$ , see eq. (10.4.11).

|                  |                                                                                                                                                                                      |
|------------------|--------------------------------------------------------------------------------------------------------------------------------------------------------------------------------------|
| +, -, +, -, +, + | $M_2 = -\langle \bar{q}\bar{r} \rangle^2 \langle q1 \rangle^* \langle 1\bar{q} \rangle^* \langle r2 \rangle^* \langle 2\bar{r} \rangle^*$                                            |
| +, -, -, +; +, + | $M_2 = \langle \bar{q}r \rangle^2 \langle q1 \rangle^* \langle 1\bar{q} \rangle^* \langle r2 \rangle^* \langle 2\bar{r} \rangle^*$                                                   |
| -, +, +, -, +, + | $M_2 = \langle q\bar{r} \rangle^2 \langle q1 \rangle^* \langle 1\bar{q} \rangle^* \langle r2 \rangle^* \langle 2\bar{r} \rangle^*$                                                   |
| -, +, -, +; +, + | $M_2 = -\langle qr \rangle^2 \langle q1 \rangle^* \langle 1\bar{q} \rangle^* \langle r2 \rangle^* \langle 2\bar{r} \rangle^*$                                                        |
| +, -, +, -, +; - | $M_1 = \langle q1 \rangle^* \langle 1\bar{q} \rangle^* \langle r2 \rangle^* \langle 2\bar{r} \rangle^* \langle r q + 1 \bar{q} \rangle \langle r 2 + \bar{r} \bar{q} \rangle$        |
| +, -, -, +; +, - | $M_1 = -\langle q1 \rangle^* \langle 1\bar{q} \rangle^* \langle r2 \rangle^* \langle 2\bar{r} \rangle^* \langle \bar{r} q + 1 \bar{q} \rangle \langle \bar{r} 2 + r \bar{q} \rangle$ |
| -, +, +, -, +; - | $M_1 = -\langle q1 \rangle^* \langle 1\bar{q} \rangle^* \langle r2 \rangle^* \langle 2\bar{r} \rangle^* \langle r \bar{q} + 1 q \rangle \langle r 2 + \bar{r} q \rangle$             |
| -, +, -, +; +, - | $M_1 = \langle q1 \rangle^* \langle 1\bar{q} \rangle^* \langle r2 \rangle^* \langle 2\bar{r} \rangle^* \langle \bar{r} \bar{q} + 1 q \rangle \langle \bar{r} 2 + r q \rangle$        |

Table 10.6. The  $M_i$ 's of  $\mathcal{F}_{11}$ , see eq. (10.4.12).

$$e^{ij} = \frac{1}{16}(N^2 - 1) \begin{pmatrix} e_1 & e_2 & e_3 & e_4 & e_2 & e_3 & e_5 & e_6 & e_5 & e_6 & e_5 & e_6 \\ e_2 & e_1 & e_2 & e_2 & e_3 & e_2 & e_6 & e_5 & e_5 & e_5 & e_5 & e_6 \\ e_3 & e_2 & e_1 & e_3 & e_2 & e_4 & e_5 & e_5 & e_5 & e_6 & e_6 & e_6 \\ e_4 & e_2 & e_3 & e_1 & e_2 & e_3 & e_6 & e_5 & e_5 & e_6 & e_5 & e_6 \\ e_2 & e_3 & e_2 & e_2 & e_1 & e_2 & e_5 & e_5 & e_6 & e_6 & e_5 & e_5 \\ e_3 & e_2 & e_4 & e_3 & e_2 & e_1 & e_6 & e_6 & e_6 & e_5 & e_5 & e_5 \\ e_5 & e_6 & e_5 & e_6 & e_5 & e_6 & e_1 & e_2 & e_3 & e_4 & e_2 & e_3 \\ e_6 & e_5 & e_5 & e_5 & e_5 & e_6 & e_2 & e_1 & e_2 & e_2 & e_3 & e_2 \\ e_5 & e_5 & e_5 & e_6 & e_6 & e_6 & e_3 & e_2 & e_1 & e_3 & e_2 & e_4 \\ e_6 & e_5 & e_6 & e_5 & e_6 & e_5 & e_4 & e_2 & e_3 & e_1 & e_2 & e_3 \\ e_5 & e_5 & e_6 & e_6 & e_5 & e_5 & e_2 & e_3 & e_2 & e_2 & e_1 & e_2 \\ e_6 & e_6 & e_6 & e_5 & e_5 & e_5 & e_3 & e_2 & e_4 & e_3 & e_2 & e_1 \end{pmatrix} \quad (10.4.10)$$

|                    |                                                                                                                                                                                   |
|--------------------|-----------------------------------------------------------------------------------------------------------------------------------------------------------------------------------|
| $+, -, +, -, +, +$ | $M_4 = -(q\bar{r})\langle q1 \rangle \langle 12 \rangle \langle 2\bar{r} \rangle \langle \bar{q}\bar{r} \rangle^2 \langle q\bar{q} \rangle \langle r\bar{r} \rangle$              |
| $+, -, -, +, +, +$ | $M_4 = -(q\bar{r})\langle q1 \rangle \langle 12 \rangle \langle 2\bar{r} \rangle \langle \bar{q}\bar{r} \rangle^2 \langle q\bar{q} \rangle \langle \bar{r}\bar{r} \rangle$        |
| $-, +, +, -, +, +$ | $M_4 = -(q\bar{r})\langle q1 \rangle \langle 12 \rangle \langle 2\bar{r} \rangle \langle q\bar{r} \rangle^2 \langle \bar{q}\bar{q} \rangle \langle r\bar{r} \rangle$              |
| $-, +, -, +, +, +$ | $M_4 = -(q\bar{r})\langle q1 \rangle \langle 12 \rangle \langle 2\bar{r} \rangle \langle q\bar{r} \rangle^2 \langle \bar{q}\bar{q} \rangle \langle \bar{r}\bar{r} \rangle$        |
| $+, -, +, -, +, -$ | $M_1 = (2q)\langle q\bar{r} \rangle \langle q1 \rangle^2 \langle r q+1 2 \rangle$                                                                                                 |
|                    | $M_2 = (\bar{r}2)^2 \langle r\bar{q} \rangle \langle 1\bar{r} \rangle \langle 1 \bar{r}+2 \bar{q} \rangle$                                                                        |
|                    | $M_3 = (\bar{r}2)^2 \langle q1 \rangle^2 \langle r \bar{q}+1 q \rangle \langle \bar{r} r+2 \bar{q} \rangle$                                                                       |
|                    | $M_4 = +(\bar{r}2)^2 \langle 2q \rangle \langle q1 \rangle \langle 21 \rangle \langle r\bar{q} \rangle \langle \bar{r} r+2 \bar{q} \rangle$                                       |
|                    | $+ (\bar{r}2)\langle 12 \rangle \langle \bar{q}\bar{r} \rangle \langle q1 \rangle^2 \langle 1\bar{r} \rangle \langle r \bar{q}+1 q \rangle$                                       |
|                    | $- (\bar{q} + q + 1)^2 (\bar{r}2)\langle 2q \rangle \langle \bar{q}\bar{r} \rangle \langle q1 \rangle \langle r\bar{q} \rangle \langle 1\bar{r} \rangle$                          |
| $+, -, -, +, +, -$ | $M_1 = (r\bar{q})\langle q2 \rangle \langle q1 \rangle^2 \langle \bar{r} q+1 2 \rangle$                                                                                           |
|                    | $M_2 = (\bar{q}\bar{r})\langle \bar{r}2 \rangle \langle 1\bar{r} \rangle^2 \langle q \bar{r}+1 2 \rangle$                                                                         |
|                    | $M_3 = (2r)\langle 2\bar{r} \rangle \langle q1 \rangle^2 \langle \bar{r} \bar{q}+1 q \rangle \langle \bar{r} r+2 \bar{q} \rangle$                                                 |
|                    | $M_4 = + (2r)\langle 2\bar{r} \rangle \langle 2q \rangle \langle 21 \rangle \langle q1 \rangle \langle \bar{r}\bar{q} \rangle \langle \bar{r} r+2 \bar{q} \rangle$                |
|                    | $+ (2\bar{r})\langle \bar{q}\bar{r} \rangle \langle 21 \rangle \langle q1 \rangle^2 \langle 1\bar{r} \rangle \langle \bar{r} \bar{q}+1 q \rangle$                                 |
|                    | $+ (\bar{q} + q + 1)^2 \langle 2q \rangle \langle 2\bar{r} \rangle \langle \bar{q}\bar{r} \rangle \langle q1 \rangle \langle \bar{r}\bar{q} \rangle \langle 1\bar{r} \rangle$     |
| $-, +, +, -, +, -$ | $M_1 = (2q)^2 \langle 1q \rangle \langle \bar{q}\bar{r} \rangle \langle 1 q+2 \bar{r} \rangle$                                                                                    |
|                    | $M_2 = (\bar{r}2)^2 \langle \bar{q}\bar{r} \rangle \langle \bar{r}1 \rangle \langle 1 \bar{r}+2 \bar{q} \rangle$                                                                  |
|                    | $M_3 = (\bar{r}2)^2 \langle 1q \rangle \langle 1\bar{q} \rangle \langle \bar{r} r+2 q \rangle \langle r \bar{q}+1 q \rangle$                                                      |
|                    | $M_4 = + \langle 2q \rangle (\bar{r}2)^2 \langle 12 \rangle \langle r\bar{q} \rangle \langle 1q \rangle \langle \bar{r} r+2 \bar{q} \rangle$                                      |
|                    | $+ \langle q\bar{r} \rangle \langle \bar{r}\bar{q} \rangle \langle 12 \rangle \langle 1q \rangle \langle 1\bar{r} \rangle \langle 1\bar{q} \rangle \langle r \bar{q}+1 q \rangle$ |
|                    | $+ (\bar{q} + q + 1)^2 (\bar{r}2)\langle q\bar{r} \rangle \langle 2q \rangle \langle 1q \rangle \langle 1\bar{r} \rangle \langle r\bar{q} \rangle$                                |
| $-, +, -, +, +, -$ | $M_1 = (2q)^2 \langle \bar{r}\bar{q} \rangle \langle q1 \rangle \langle 1 q+2 \bar{r} \rangle$                                                                                    |
|                    | $M_2 = \langle q\bar{r} \rangle \langle \bar{r}2 \rangle \langle \bar{r}1 \rangle^2 \langle \bar{q} \bar{r}+1 2 \rangle$                                                          |
|                    | $M_3 = (\bar{r}2)\langle r2 \rangle \langle \bar{q}1 \rangle \langle q1 \rangle \langle \bar{r} r+2 q \rangle \langle \bar{r} \bar{q}+1 q \rangle$                                |
|                    | $M_4 = + (\bar{r}2)\langle r2 \rangle \langle q2 \rangle \langle 12 \rangle \langle \bar{r}\bar{q} \rangle \langle q1 \rangle \langle \bar{r} r+2 q \rangle$                      |
|                    | $+ (\bar{r}2)\langle r\bar{q} \rangle \langle 12 \rangle \langle q1 \rangle \langle \bar{q}1 \rangle \langle \bar{r}1 \rangle \langle \bar{r} \bar{q}+1 q \rangle$                |
|                    | $+ (\bar{q} + q + 1)^2 \langle q2 \rangle \langle r\bar{q} \rangle \langle \bar{r}2 \rangle \langle q1 \rangle \langle \bar{r}1 \rangle \langle \bar{r}\bar{q} \rangle$           |

Table 10.7. The  $M_i$ 's of  $\mathcal{E}_{20}$ , see eq. (10.4.13).

where  $e_1 = (N^2 - 1)$ ,  $e_2 = 0$ ,  $e_3 = 1$ ,  $e_4 = -1$ ,  $e_5 = N^{-1}$ ,  $e_6 = -N^{-1}$ . Using parity conservation and other symmetries, see chapter 6, the following expressions enable us to evaluate all  $\mathcal{E}_i$  for all possible helicity configurations.

$$\mathcal{F}_{20}(q\bar{q}r\bar{r}; 12;) = -2 * N^{-1} \left[ \frac{M_1}{\{q, 2\}\langle q+2+1 \rangle^2 \{2, 1\}\{\bar{r}, r\}} \right. \quad (10.4.11)$$

$$\left. + \frac{M_2}{\{2, 1\}\langle 2+1+q \rangle^2 \{1, q\}\{\bar{q}, q\}} + \frac{M_3}{\{\bar{q}, 2\}\{2, 1\}\{1, q\}\{\bar{r}, r\}} \right]$$

For eight helicity configurations the expressions for  $\mathcal{F}_{20}$  are in table 10.5

|                  |                                                                                                                                                                                                                                                                                                                                                                                                                                                                                                                                 |
|------------------|---------------------------------------------------------------------------------------------------------------------------------------------------------------------------------------------------------------------------------------------------------------------------------------------------------------------------------------------------------------------------------------------------------------------------------------------------------------------------------------------------------------------------------|
| +, -, +, -; +, + | $M_3 = -\langle 1q \rangle^* \langle q\bar{r} \rangle \langle \bar{r}1 \rangle^* \langle 2r \rangle^* \langle r\bar{q} \rangle \langle \bar{q}2 \rangle^* \langle \bar{q}\bar{r} \rangle^2 \langle q\bar{q} \rangle^* \langle r\bar{r} \rangle^*$                                                                                                                                                                                                                                                                               |
| +, -, -, +; +, + | $M_3 = -\langle 1q \rangle^* \langle q\bar{r} \rangle \langle \bar{r}1 \rangle^* \langle 2r \rangle^* \langle r\bar{q} \rangle \langle \bar{q}2 \rangle^* \langle \bar{q}r \rangle^2 \langle q\bar{q} \rangle^* \langle \bar{r}r \rangle^*$                                                                                                                                                                                                                                                                                     |
| -, +, +, -; +, + | $M_3 = -\langle 1q \rangle^* \langle q\bar{r} \rangle \langle \bar{r}1 \rangle^* \langle 2r \rangle^* \langle r\bar{q} \rangle \langle \bar{q}2 \rangle^* \langle q\bar{r} \rangle^2 \langle q\bar{q} \rangle^* \langle \bar{r}\bar{r} \rangle^*$                                                                                                                                                                                                                                                                               |
| -, +, -, +; +, + | $M_3 = -\langle 1q \rangle^* \langle q\bar{r} \rangle \langle \bar{r}1 \rangle^* \langle 2r \rangle^* \langle r\bar{q} \rangle \langle \bar{q}2 \rangle^* \langle qr \rangle^2 \langle q\bar{q} \rangle^* \langle \bar{r}r \rangle^*$                                                                                                                                                                                                                                                                                           |
| +, -, +, -; +, - | $M_1 = \langle \bar{r}2 \rangle \langle r2 \rangle \langle 1q \rangle^* \langle r \bar{q}+1 q \rangle \langle r q+1 \bar{q} \rangle$<br>$M_2 = \langle \bar{q}2 \rangle^2 \langle 1\bar{r} \rangle^* \langle 1\bar{r} \rangle^* \langle \bar{q} q+2 \bar{r} \rangle \langle q \bar{q}+2 \bar{r} \rangle$<br>$M_3 = \langle 1q \rangle^* \langle q\bar{r} \rangle \langle \bar{r}1 \rangle^* \langle 2r \rangle \langle r\bar{q} \rangle^* \langle \bar{q}2 \rangle \langle r q+1 \bar{q} \rangle \langle q r+1 \bar{r} \rangle$ |
| +, -, +, -; +, - | $M_1 = \langle 2r \rangle^2 \langle q1 \rangle^* \langle r \bar{q}+1 q \rangle \langle \bar{r} q+1 \bar{q} \rangle$<br>$M_2 = \langle \bar{q}2 \rangle^2 \langle 1\bar{r} \rangle^* \langle q \bar{q}+2 r \rangle \langle \bar{q} q+2 \bar{r} \rangle$<br>$M_3 = \langle 1q \rangle^* \langle q\bar{r} \rangle \langle \bar{r}1 \rangle^* \langle 2r \rangle \langle r\bar{q} \rangle^* \langle \bar{q}2 \rangle \langle q \bar{r}+1 r \rangle \langle \bar{r} q+1 \bar{q} \rangle$                                             |
| -, +, +, -; +, - | $M_1 = \langle \bar{r}2 \rangle \langle 2r \rangle \langle 1\bar{q} \rangle^* \langle q1 \rangle^* \langle r \bar{q}+1 q \rangle^2$<br>$M_2 = \langle 2q \rangle \langle 2\bar{q} \rangle \langle 1\bar{r} \rangle^* \langle 1r \rangle^* \langle \bar{q} q+2 \bar{r} \rangle^2$<br>$M_3 = \langle 1q \rangle^* \langle q\bar{r} \rangle \langle \bar{r}1 \rangle^* \langle 2r \rangle \langle r\bar{q} \rangle^* \langle \bar{q}2 \rangle \langle r \bar{q}+1 q \rangle \langle \bar{q} r+1 \bar{r} \rangle$                   |
| -, +, -, +; +, - | $M_1 = \langle r2 \rangle^2 \langle 1q \rangle^* \langle 1\bar{q} \rangle^* \langle r \bar{q}+1 q \rangle \langle \bar{r} \bar{q}+1 \bar{q} \rangle$<br>$M_2 = \langle 2\bar{q} \rangle \langle 2q \rangle \langle 1\bar{r} \rangle^* \langle \bar{q} q+2 r \rangle \langle \bar{q} q+2 \bar{r} \rangle$<br>$M_3 = \langle 1q \rangle^* \langle q\bar{r} \rangle \langle \bar{r}1 \rangle^* \langle 2r \rangle \langle r\bar{q} \rangle^* \langle \bar{q}2 \rangle \langle \bar{r} r+2 q \rangle \langle \bar{q} q+2 r \rangle$ |

Table 10.8. The  $M_i$ 's of  $\mathcal{E}_{11}$ , see eq. (10.4.13).

$$\mathcal{F}_{11}(q\bar{q}r\bar{r}; 1; 2) = -2 * N^{-1} \times \quad (10.4.12)$$

$$\left[ + \frac{M_1}{\{q, 1\} \{1, \bar{q}\} (q + \bar{q} + 1)^2 \{r, 2\} \{2, \bar{r}\}} + \frac{M_2}{\{q, 1\} \{1, \bar{q}\} \{r, 2\} \{2, \bar{r}\}} \right]$$

For eight helicity configurations the expressions for  $\mathcal{F}_{11}$  are in table 10.6

$$\mathcal{E}_{20}(q\bar{q}r\bar{r}; 12; ) = 2 \left[ \frac{M_1}{\{q, 1\} (q+1+2)^2 \{1, 2\} \{\bar{r}, r\}} + \frac{M_2}{\{\bar{q}, q\} \{1, 2\} (1+2+\bar{r})^2 \{2, \bar{r}\}} \right. \\ \left. + \frac{M_3}{\{\bar{q}, q\} (\bar{q}+q+1)^2 \{q, 1\} \{2, \bar{r}\} \{\bar{r}, r\}} + \frac{M_4}{\{\bar{q}, q\} \{q, 1\} \{1, 2\} \{2, \bar{r}\} \{\bar{r}, r\}} \right]$$

For eight helicity configurations the expressions for  $\mathcal{E}_{20}$  are in table 10.8

$$\mathcal{E}_{11}(q\bar{q}r\bar{r}; 1; 2) = 2 \left[ \frac{M_1}{\{\bar{q}, q\} (\bar{q}+q+1)^2 \{q, 1\} \{\bar{r}, r\}} \right. \quad (10.4.13) \\ \left. + \frac{M_2}{\{\bar{q}, q\} \{1, \bar{r}\} (1+\bar{r}+r)^2 \{\bar{r}, r\} \{2, \bar{q}\}} + \frac{M_3}{\{\bar{q}, q\} \{q, 1\} \{1, \bar{r}\} \{\bar{r}, r\} \{r, 2\} \{2, \bar{q}\}} \right]$$

For eight helicity configurations the expressions for  $\mathcal{E}_{11}$  are in table 10.8

#### 10.4.4 $\emptyset \rightarrow q\bar{q}r\bar{r}s\bar{s}$

This process has been dealt with in chapter 7 and in ref. [10].

## 10.5 Seven parton matrix elements

### 10.5.1 $\emptyset \rightarrow ggggggg$

The matrix element squared for the seven gluon process reads [11]

$$\sum_{c,\lambda} |\mathcal{M}_7|^2 = g^{10} \sum_{\lambda} \left| \sum_{P_7^*} 2 (a_1 a_2 a_3 a_4 a_5 a_6 a_7) \mathcal{C}(1234567) \right|^2, \quad (10.5.1)$$

For the seven fundamentally different helicity configurations the  $\mathcal{C}(1234567)$  are as follows. When all or all but one, helicities are the same we have

$$\mathcal{C}(++++++) = 0. \quad (10.5.2)$$

$$\mathcal{C}(+++++-) = 0. \quad (10.5.3)$$

With gluons  $i$  and  $j$  the  $-$  helicity and the other gluons the  $+$  helicity.

$$\mathcal{C}(1234567) = \frac{(\sqrt{2})^7}{2} \frac{(ij)^4}{\langle 12 \rangle \langle 23 \rangle \langle 34 \rangle \langle 45 \rangle \langle 56 \rangle \langle 67 \rangle \langle 71 \rangle} \quad (10.5.4)$$

For three  $+$  and four  $-$  helicities the pole structure of  $\mathcal{C}(1234567)$  is very complicated. Basically there are four different configurations. First we define our choice of the pole structure. It reads

$$\begin{aligned} \mathcal{C}(1234567) = & \quad (10.5.5) \\ & + \frac{M_1}{\{1,2\}(1+2+3)^2\{2,3\}\{4,5\}(4+5+6)^2\{5,6\}\{6,7\}} \\ & + \frac{M_2}{\{1,2\}(1+2+3)^2\{2,3\}\{4,5\}\{5,6\}(5+6+7)^2\{6,7\}} \\ & + \frac{M_3}{\{2,3\}(2+3+4)^2\{3,4\}\{5,6\}(5+6+7)^2\{6,7\}} \\ & + \frac{M_4}{\{2,3\}(2+3+4)^2\{3,4\}\{5,6\}\{6,7\}(6+7+1)^2\{7,1\}} \\ & + \frac{M_5}{\{2,3\}(2+3+4)^2\{3,4\}\{5,6\}\{6,7\}\{7,1\}} \\ & + \frac{M_6}{\{1,2\}\{3,4\}(3+4+5)^2\{4,5\}\{6,7\}(6+7+1)^2\{7,1\}} \\ & + \frac{M_7}{\{3,4\}(3+4+5)^2\{4,5\}\{5,6\}\{7,1\}(7+1+2)^2\{1,2\}} \\ & + \frac{M_8}{\{1,2\}\{3,4\}(3+4+5)^2\{4,5\}\{5,6\}\{6,7\}\{7,1\}} \\ & + \frac{M_9}{\{1,2\}\{2,3\}\{3,4\}\{4,5\}(4+5+6)^2\{5,6\}\{6,7\}\{7,1\}} \end{aligned}$$

$$\begin{aligned}
& + \frac{M_{10}}{\{3,4\}\{4,5\}(4+5+6)^2\{5,6\}\{7,1\}(7+1+2)^2\{1,2\}} \\
& + \frac{M_{11}}{\{1,2\}\{2,3\}\{3,4\}\{4,5\}\{5,6\}(5+6+7)^2\{6,7\}} \\
& + \frac{M_{12}}{\{1,2\}\{2,3\}\{3,4\}\{4,5\}\{5,6\}\{6,7\}(6+7+1)^2\{7,1\}} \\
& + \frac{M_{13}}{\{3,4\}\{4,5\}\{5,6\}\{6,7\}\{7,1\}(7+1+2)^2\{1,2\}} \\
& + \frac{M_{14}}{\{1,2\}\{2,3\}\{3,4\}\{4,5\}\{5,6\}\{6,7\}\{7,1\}}
\end{aligned}$$

C(+ + + - - - -)

$$\begin{aligned}
M_4 & = -(56)(67)(71)(1|6+7|5)A^2 \\
M_6 & = +(12)^*(23)^*(45)^2(67)^2((34)^*(1|6+7|4) + (35)^*(1|6+7|5))\{1,2\} \\
M_7 & = -(34)(45)(56)(3|4+5|6)B^2 \\
M_8 & = -(12)^*(45)^2(56)(67)B((56)^*(3|1+2|6) + (57)^*(3|1+2|7)) \\
M_{12} & = -(23)^*(45)(56)(67)^2A((64)^*(1|2+3|4) + (65)^*(1|2+3|5)) \\
M_{14} & = +(45)(56)(67)AB(1+2+3)^2
\end{aligned}$$

with  $A = (12)^*(1|2+3|4)$  and  $B = (12)^*(3|1+2|7)$ .

C(+ + - + - - -)

$$\begin{aligned}
M_1 & = -(45)(56)(67)(4|5+6|7)A^2 \\
M_4 & = -(56)(67)(71)(1|6+7|5)B^2 \\
M_6 & = -(12)^*(24)^*(35)^2(67)^2((43)^*(1|6+7|3) + (45)^*(1|6+7|5))\{1,2\} \\
M_7 & = +(34)(35)(56)(4|3+5|6)C^2 \\
M_8 & = +(12)^*(35)^2(56)(67)C((56)^*(4|1+2|6) + (57)^*(4|1+2|7)) \\
M_9 & = +(12)^*(34)(56)^2(67) \{+(24)^*(67)^*(23)(4|1+2|7)(4|5+6|7) \\
& \quad + (16)^*(34)^*(17)(4|1+2|3)^2 + (14)^*(34)^*(67)^*(17)(37)(4|1+2|3)\} \\
M_{10} & = -(34)(56)^2(4|5+6|3)C^2 \\
M_{12} & = -(24)^*(56)(67)^2\{1,2\} \{+(16)^*(35)(1|2+4|3)\{4,5\} \\
& \quad + (46)^*(45)(1|2+4|3)(1|6+7|3) - (12)^*(56)^*(23)(35)(1|6+7|5)\} \\
M_{14} & = +(56)(67) \left[ -(35)AC(2+3+4)^2 \right. \\
& \quad \left. - (12)^*B(45)(4|1+2|7)(4|1+2|3) - (12)^*B(35)(4|5+6|7)\{1,2\} \right]
\end{aligned}$$

with  $A = (12)^*(4|1+2|3)$ ,  $B = (24)^*(1|2+4|3)$ ,  $C = (12)^*(4|1+2|7)$ .

C(+ + - - + - -)

$$M_1 = +(45)(46)(67)(5|4+6|7)A^2$$

$$\begin{aligned}
M_2 &= -(45)(67)^2(5|6+7|4)A^2 \\
M_3 &= -(12)^*(15)^*(34)^2(67)^2(2|3+4|1) \\
M_4 &= -(15)^*(25)^*(34)^2(67)^2((23)^*(1|6+7|3) + (24)^*(1|6+7|4))\{5,6\} \\
M_5 &= -(15)^*(34)^2(67)((12)^*(17)(2|3+4|6) - (25)^*(56)(2|3+4|7)) \\
M_6 &= -(12)^*(25)^*(34)^2(67)^2(1|6+7|2) \\
M_7 &= -(34)^2(56)(5|3+4|6)B^2 \\
M_8 &= +(12)^*(34)^2(56)(67) \left[ +(57)^*(5|1+2|7)^2 \right. \\
&\quad \left. + (56)^*(5|1+2|7)(5|1+2|6) - (15)^*(25)^*(56)^*(12)(67) \right] \\
M_9 &= -(12)^*(46)^2(17)(67)A((17)^*(56)^*(37) + (16)^*(5|4+6|3))\{3,4\} \\
&\quad - (12)^*(23)(34)(46)^2B((23)^*(45)^*(37) + (24)^*(5|4+6|7))\{6,7\} \\
M_{10} &= +(34)(46)(56)(5|4+6|3)B^2 \\
M_{11} &= -(12)^*(34)(45)(67)^2 \left[ -(35)^*(5|1+2|3)^2 \right. \\
&\quad \left. - (45)^*(5|1+2|3)(5|1+2|4) + (15)^*(25)^*(45)^*(12)(34) \right] \\
M_{12} &= +(25)^*(34)(67)^2((12)^*(23)(1|6+7|4) - (15)^*(45)(1|6+7|4))\{1,2\}\{5,6\} \\
M_{14} &= -(12)^*(34)(67) \times \\
&\quad \left[ +(15)^*(25)^*(34)(67)\{1,2\}(\{4,5\} + \{5,6\}) \right. \\
&\quad + (15)^*(25)^*(45)(56)(5|1+2|3)(5|1+2|7) \\
&\quad + (12)^*(15)^*(17)(46)\{3,4\}(5|1+2|3) \\
&\quad + (12)^*(56)^*(17)(46)(1|2+5|3)(5|1+2|6) \\
&\quad + (12)^*(25)^*(57)^*(23)(47)(56)(5|1+2|7) \\
&\quad - (12)^*(15)^*(57)^*(17)(34)(56)(5|1+2|7) \\
&\quad + (12)^*(57)^*(17)(46)(1|2+5|3)(5|1+2|7) \\
&\quad \left. + (12)^*(25)^*(23)(46)(5|1+2|7)(\{5,6\} + \{6,7\}) \right. \\
&\quad \left. - (12)^*(15)^*(16)(34)(5|1+2|7)(\{4,5\} + \{5,6\}) \right]
\end{aligned}$$

with  $A = (12)^*(5|1+2|3)$ ,  $B = (12)^*(5|1+2|7)$

C(+ - + - + - -)

$$\begin{aligned}
M_1 &= +(13)^*(45)(46)(67)(5|4+6|7)(5|1+3|2)^2 \\
M_2 &= -(13)^*(45)(67)^2(5|6+7|4)(5|1+3|2)^2 \\
M_3 &= -(13)^*(15)^*(24)^2(67)^2(3|2+4|1) \\
M_4 &= -(15)^*(35)^*(24)^2(67)^2((34)^*(1|6+7|4) + (32)^*(1|6+7|2))\{5,6\} \\
M_5 &= -(15)^*(24)^2(67)((13)^*(17)(3|4+2|6) - (35)^*(56)(3|2+4|7)) \\
M_6 &= -(35)^*(12)(67)^2(1|6+7|2)(1|3+5|4)^2 \\
M_7 &= -(35)^*(67)(12)(27)(1|2+7|6)(1|3+5|4)^2 \\
M_9 &= -(13)^*(67)(46)^2 \left[ +(35)^*(67)^*(27)(23)(5|4+6|7) \right. \\
&\quad \left. - (15)^*(67)^*(17)(27)(5|1+3|2) + (61)^*(17)(5|1+3|2)^2 \right]
\end{aligned}$$

$$\begin{aligned}
M_{10} &= -(13)^*(35)^*(46)^2(27)^2 ((54)^*(1|2+7|4) + (56)^*(1|2+7|6)) \{5,6\} \\
M_{11} &= -(13)^*(45)(67)^2 [-(13)^*(15)^*(45)^*(12)(24)(5|1+3|4) \\
&\quad - (15)^*^2(23)^*(45)^*(12)(24)^2 + (13)^*(35)^*(34)(5|1+3|2)(5|6+7|2)] \\
M_{12} &= -(35)^*^2(67)^2 \{5,6\} \times \\
&\quad [+ (13)^*(12)(23)(1|3+5|4)(1|6+7|4) \\
&\quad + (15)^*(24)(45)(1|6+7|2)\{1,2\}] \\
M_{13} &= +(35)^*^2(27)^2(67) [-(17)^*(46)(1|3+5|4)\{5,6\} \\
&\quad - (57)^*(56)(1|3+5|4)(1|2+7|4) + (13)^*(67)^*(34)(46)(1|2+7|6)] \\
M_{14} &= -(67) \times \\
&\quad [+(13)^*^2(35)^*^2(23)(34)(46)(27)\{6,7\} \\
&\quad + (13)^*(35)^*(17)^*(15)^*(17)(67)(45)(24)(5|1+3|2) \\
&\quad - (13)^*(15)^*^2(35)^*(17)(45)(26)(24)\{1,2\} \\
&\quad + (13)^*(12)^*(15)^*(35)^*^2(17)(23)(45)(26)(24) \\
&\quad - (13)^*(35)^*^2(15)^*(17)(23)(46)(24)(1|3+4|5) \\
&\quad - (13)^*^2(15)^*(35)^*(17)(23)(46)(12)(1|3+5|4) \\
&\quad + (13)^*^2(35)^*^2(17)(23)(46)(34)(1|6+7|2) \\
&\quad - (13)^*(15)^*^2(34)^*(17)(46)(24)(12)(1|3+5|4) \\
&\quad + (15)^*^2(35)^*^2(24)(27)(45)(56)(1+2+3)^2 \\
&\quad - (35)^*^2(13)^*(15)^*(34)(45)(27)(56)(5|1+3|2) \\
&\quad + (35)^*^2(13)^*^2(23)(27)(34)(56)(5|6+7|4)]
\end{aligned}$$

For the colour matrix it turns out to be best to use eq. (10.1.6). Two orders in  $N$  are present. The following expression for the NLO term was found by trial and error and using the uniqueness of  $\tilde{\mathcal{E}}_7^j$ .

$$\begin{aligned}
\sum_{c,\lambda} |\mathcal{M}_7|^2 &= 2g^{10}(N/2)^5(N^2 - 1) \sum_{\lambda} \sum_{P_7^*} \mathcal{C}(1234567) \mathcal{C}(1234567)^* \quad (10.5.6) \\
&\quad - g^{10}(N/2)^3(N^2 - 1) \sum_{\lambda} \sum_{P_7^*} \mathcal{C}(1234567) \times \\
&\quad [+3\mathcal{C}(1235746) + 3\mathcal{C}(1236475) + 3\mathcal{C}(1246357) + 3\mathcal{C}(1253647) \\
&\quad + 3\mathcal{C}(1345726) + 3\mathcal{C}(1356724) + \mathcal{C}(1357246) + 3\mathcal{C}(1352467) \\
&\quad + \mathcal{C}(1357246) + 3\mathcal{C}(1352467) + 3\mathcal{C}(1372456) - 3\mathcal{C}(1372654) \\
&\quad - 3\mathcal{C}(1376524) - \mathcal{C}(1473625) + 3\mathcal{C}(1425367) + 3\mathcal{C}(1572346) \\
&\quad - 3\mathcal{C}(1574326) - 3\mathcal{C}(1543726)]^* .
\end{aligned}$$

This is the most compact for the NLO term we were able to find. Finally we remark that the NLO term in  $\tilde{\mathcal{E}}_7^j$ , see eq. (10.1.7), has 59 non-zero terms per row.

## 10.5.2 Other seven parton processes.

For the other seven parton processes no analytic expressions have been derived. The process  $\emptyset \rightarrow q\bar{q}ggggg$  is described in chapter 5, the process  $\emptyset \rightarrow q\bar{q}r\bar{r}ggg$  is chapter 6 and the process  $\emptyset \rightarrow q\bar{q}r\bar{r}s\bar{s}g$  in chapter 7.

## 10.6 Special helicity configurations

In this section we give analytical expressions for the subamplitudes of eq. (10.1.2) for a special helicity configuration. The expressions are valid for an arbitrary number of gluons and up to two massless quark pairs. They form the basis for the SPHEL approximation in chapter 8. The special helicity configuration is the one where two helicities are different from all the others. We specify this to be two partons with  $-$  helicity and  $n-2$  partons with  $+$  helicity.

For the purely gluonic  $\mathcal{C}$ -function, with gluons  $i$  and  $j$  the  $-$  helicity we have

$$\mathcal{C}(12\dots n) = \frac{(\sqrt{2})^n}{2} \frac{\langle ij \rangle^4}{\langle 12 \rangle \langle 23 \rangle \dots \langle n-1n \rangle \langle n1 \rangle}, \quad (10.6.1)$$

corresponding with the colour structure  $2(a_1 a_2 \dots a_n)$ . The  $\mathcal{D}$ -function for a  $q\bar{q}$ -pair with colours  $c, d$  and gluon  $i$  and the  $\bar{q}$  the  $-$  helicity reads

$$\mathcal{D}(+; 12\dots n-2; -) = (\sqrt{2})^{n-2} \frac{\langle \bar{q}i \rangle^3 \langle qi \rangle}{\langle q1 \rangle \langle 12 \rangle \langle 23 \rangle \dots \langle n-2\bar{q} \rangle \langle \bar{q}q \rangle}, \quad (10.6.2)$$

and it corresponds with the colour structure  $(a_1 a_2 \dots a_{n-2})_{cd}$ . The  $\mathcal{E}$ -function for a  $q\bar{q}r\bar{r} + n_g$  process and all gluons the  $+$  helicity, with the colour assignment,  $(q, c_1), (\bar{q}, c_2), (r, c_3)$  and  $(\bar{r}, c_4)$  reads

$$\mathcal{E}(q\bar{q}r\bar{r}; 1\dots l; l+1\dots n-4) = (\sqrt{2})^{n-4} \frac{A(\lambda_q, \lambda_r)}{\langle q\bar{q} \rangle \langle r\bar{r} \rangle} \frac{\langle q\bar{r} \rangle}{\langle q1 \rangle \dots \langle l\bar{r} \rangle} \frac{\langle r\bar{q} \rangle}{\langle r l+1 \rangle \dots \langle n-4\bar{q} \rangle} \quad (10.6.3)$$

corresponding with the colour-structure  $\frac{1}{2}(a_1 \dots a_l)_{c_1 c_4} (a_{l+1} \dots a_{n-4})_{c_3 c_2}$  and

$$\mathcal{E}(q\bar{q}r\bar{r}; 1\dots l; l+1\dots n-4) = -(\sqrt{2})^{n-4} \frac{A(\lambda_q, \lambda_r)}{N} \frac{\langle q\bar{q} \rangle}{\langle q\bar{q} \rangle \langle r\bar{r} \rangle} \frac{\langle q\bar{r} \rangle}{\langle q1 \rangle \dots \langle l\bar{q} \rangle} \frac{\langle r\bar{r} \rangle}{\langle r l+1 \rangle \dots \langle n-4\bar{r} \rangle} \quad (10.6.4)$$

corresponding with the colour-structure  $\frac{1}{2}(a_1 \dots a_l)_{c_1 c_2} (a_{l+1} \dots a_{n-4})_{c_3 c_4}$ . The  $A(\lambda_q, \lambda_r)$  are given by

$$A(+, +) = \langle q\bar{r} \rangle^2, \quad A(+, -) = -\langle q\bar{r} \rangle^2, \quad A(-, +) = -\langle q\bar{r} \rangle^2, \quad A(-, -) = \langle q\bar{r} \rangle^2.$$

This result was also obtained in [12]. Note that on grounds of  $N=1$  supersymmetry the expressions for the special helicities, eq. (10.6.1)-(10.6.4) can be derived from each other [8, 13].

## References

- [1] B.L. Combridge, J. Kripfganz and J. Ranft, Phys. Lett **70B** (177) 234;  
R. Cutler and D. Sivers, Phys. Rev. **D17** (1978) 196.
- [2] G. Altarelli, M. Diemoz, G. Martinelli and P. Nason, Nucl. Phys. **B308** (1988) 724.
- [3] T. Gottschalk and D. Sivers, Phys. Rev. **D21** (180) 102;  
Z. Kunzst and E. Pietarinen, Nucl. Phys. **B164** (1980) 45.
- [4] F.A. Berends, R. Kleiss, P. de Causmaecker, R. Gastmans and T.T. Wu,  
Phys. Lett. **103B** (1981) 124.
- [5] J. F. Gunion and J. Kalinowski, Phys. Rev. **D34** (1986) 2119.  
S. J. Parke and T. R. Taylor, Nucl. Phys. **B269** (1986) 410.
- [6] F.A. Berends and W.T. Giele, Nucl. Phys. **B294** (1987) 700;  
M. Mangano, S.J. Parke and Z. Xu, Nucl. Phys. **B298** (1988) 653.
- [7] G.J. Oldenborgh, master thesis, Leiden, 1986.
- [8] Z. Kunzst, Nucl. Phys. **B271** (1986) 333.  
S.J. Parke and T. R. Taylor, Phys. Rev. **D35** (1987) 313.
- [9] J.F. Gunion and Z. Kunzst, Phys. Lett. **159B** (1985) 167.
- [10] J.F. Gunion and Z. Kunzst, Phys. Lett. **176B** (1986) 163.
- [11] F.A. Berends, W.T. Giele and H. Kuijf, Nucl. Phys. **B333** (1990) 120.
- [12] M. Mangano, Nucl. Phys. **B309** (1988) 461.
- [13] M. F. Sohnius, Phys. Rep. **128** (1985) 39.

## Appendix A: Matrix elements and computers

In this appendix CPU-time tables are presented for the multiparton matrix elements. Such tables are relevant when one wants to examine whether a certain statistical precision can be obtained in a Monte Carlo simulation with the computer resources one has at hand. The timing was done on a VAX 3500 with the matrix elements from the  $n$ -jet Monte Carlo program NJETS. In a Monte Carlo integration one event on the hadron level represents the sum over all possible subprocesses on the parton level. First we look at the CPU-times for parton scattering amplitudes and count how many times they need to be evaluated in a physical process. Finally we compute the time needed for one collider event in table A.3.

| Method       | nr. jets | 0 quarks | 2 quarks | 4 quarks | 6 quarks |
|--------------|----------|----------|----------|----------|----------|
| EXACT        | 2        | 0.117    | 0.088    | 0.222    | —        |
|              | 3        | 0.34     | 2.61     | 3.16     | —        |
|              | 4        | 78.8     | 103.0    | 67.2     | 43.7     |
|              | 5        | 6300     | 7400     | 6100     | 600      |
| SPHEL        | 2        | 0.36     | 0.32     | 0.9      | —        |
|              | 3        | 0.72     | 0.58     | 1.1      | —        |
|              | 4        | 2.20     | 1.30     | 1.4      | —        |
|              | 5        | 11.0     | 4.50     | 2.1      | —        |
| MCHL         | 2        | 0.117    | 0.088    | 0.222    | —        |
|              | 3        | 0.34     | 2.61     | 3.32     | —        |
|              | 4        | 8.3      | 27.9     | 42.1     | 10.5     |
|              | 5        | 132      | 510      | 1520     | 107      |
| $m_q \neq 0$ | 2        | —        | 10.2     | 18.0     | —        |
|              | 3        | —        | 63.2     | 86.2     | —        |
|              | 4        | —        | 703.0    | 1120     | —        |
|              | 5        | —        | 11750    | 18000    | —        |

Table A.1. CPU-timing of multiparton matrix elements in msec on a VAX 3500

For the parton matrix elements the usual distinction has been made between the matrix elements according to the number of quarks. Table A.1 contains the CPU-time needed for one call to a matrix element, for the exact matrix element as well as for the SPHEL and MCHL approximations. Because of the simple form of the special helicities and the fact that the colour matrix is diagonal SPHEL is by far the fastest method. The SPHEL entry is lacking in the six quark case because then there is no special helicity as we defined it. As an extra entry we included the timing for some massive quark cases. In that case the most general recursion relations have to be used, even for some five parton matrix elements.

The next step is to examine how many times the basic matrix elements have to be

| nr. jets | 0 quarks | 2 quarks | 4 quarks | 6 quarks |
|----------|----------|----------|----------|----------|
| 2        | 1        | 4        | 3        | —        |
| 3        | 1        | 4        | 5        | —        |
| 4        | 1        | 4        | 6        | 3        |
| 5        | 1        | 4        | 6        | 5        |

Table A.2. Number of calls to the basic matrix elements per hadronic event.

used during the evaluation of one hadronic event. The number of times is equivalent with the number of different kinematical situations that can arise in the process. Of course use is made of all kind of symmetries such as flavour changes. The results are listed in table A.2. For example in the case of two quarks and  $n$  gluons we always have four different kinematical situations. Looking at the different initial states we find them to be:  $gg$ ,  $gq$ ,  $q\bar{q}$  respectively  $q\bar{q}$ . A complication is that the matrix elements with four and six quarks have two respectively five different flavour combinations. These combinations are all calculated at the same time.

| Method | nr. jets | 0 quarks | 2 quarks | 4 quarks | 6 quarks | time/event |
|--------|----------|----------|----------|----------|----------|------------|
| EXACT  | 2        | 0.34     | 1.2      | 1.8      | —        | 3.3        |
|        | 3        | 0.56     | 11       | 19       | —        | 31         |
|        | 4        | 80       | 410      | 410      | 120      | 1000       |
|        | 5        | 6300     | 30000    | 36500    | 2500     | 75000      |
| SPHEL  | 2        | 0.61     | 2.1      | 5.8      | —        | 8.5        |
|        | 3        | 1.0      | 3.2      | 6.8      | —        | 11.0       |
|        | 4        | 3.0      | 5.8      | 9.1      | —        | 17.9       |
|        | 5        | 12.0     | 18.7     | 13       | —        | 44         |
| MCHL   | 2        | 0.34     | 1.2      | 1.8      | —        | 3.3        |
|        | 3        | 0.56     | 11       | 19       | —        | 31         |
|        | 4        | 9.8      | 110      | 260      | 28       | 410        |
|        | 5        | 230      | 2150     | 9300     | 330      | 12000      |

Table A.3. CPU-time per event in milliseconds on a VAX 3500.

From tables A.1 and A.2 we establish table A.3 by means of multiplication. For the four and five jet cases the CPU-time needed for the exact matrix elements is really considerable. Note that for the five jet case only the purely gluonic subprocess is analytically known.

From table A.3 we see that SPHEL is very fast compared to the exact expressions. For five jets it is more than 5000 times faster. As a concluding remark we note that it is hard to predict how many events are needed to get reliable results for quantities like the total cross section. The amount of events depends very much on the collider energy and the detector cuts imposed. In general a few thousand events which pass the phase space cuts, are the minimum.

## Samenvatting

De fysica probeert de natuur zo fundamenteel mogelijk te beschrijven. De elementaire deeltjesfysica in het bijzonder houdt zich bezig met de samenstelling van materie in termen van de kleinst mogelijke componenten en met de beschrijving van de krachten die tussen deze elementaire deeltjes bestaan. In dit proefschrift zijn we geïnteresseerd in de sterke kracht die bestaat tussen quarks en gluonen, de bouwstenen van hadronen. Deze bouwstenen worden aangeduid met de term partonen. De theorie van de Quantum Chromo Dynamica (QCD) wordt vanwege haar vele successen gezien als de beste theoretische modellering van de sterke kracht. Vooral de sterke aanwijzingen dat QCD kan verklaren waarom quarks en gluonen niet vrij kunnen voorkomen maakt haar aantrekkelijk. Een groot nadeel van QCD is echter dat het buitengewoon moeilijk is om er overgangswaarschijnlijkheden of matrix elementen van botsingsprocessen mee uit te rekenen. In bepaalde omstandigheden, gerealiseerd in grote deeltjesversnellers zoals de SpS in CERN en het Tevatron in Fermilab, mogen we een storingstheoretische benadering van QCD gebruiken. Met behulp van het partonmodel kunnen we in deze gevallen voorspellingen doen voor hadron-hadron verstrooiingsexperimenten. In dit model zien we de botsing tussen de hadronen als een botsing tussen twee partonen. Voor de beschrijving van dit parton-parton botsingsproces gebruiken we storingstheoretische QCD. Dit is gerechtvaardigd omdat door het hoog-energetische karakter van de botsing de storingsparameter  $\alpha_S$  klein is. In veel gevallen kan zelfs volstaan worden met de laagste orde in  $\alpha_S$ , de zogeheten Born-benadering. Het feit dat experimenteel een bij de botsing ontstaan parton wordt waargenomen als een straal hadronen, aangeduid met de term jet, is een gevolg van het opgesloten zijn van quarks en gluonen binnen hadronen. Bij het doen van voorspellingen laten we dit fragmentatieproces echter achterwege aangezien daarvoor kennis nodig is van de precieze eigenschappen van de detector. De berekening van bovengenoemde laagste orde matrixelementen vormt het hoofdbestanddeel van dit proefschrift.

In hoofdstuk 2 besteden we eerst aandacht aan de bepaling van voorspellingen voor fysische observabelen bij hadron-hadron botsingsprocessen. Aan de hand van een gedetailleerde beschrijving van het partonmodel komen we tot een numerieke bepaling van de totale werkzame doorsnede voor multi-partonproductie. Met behulp van Monte Carlo integratietechnieken worden de daarbij voorkomende integraties over de parton impulsfrakties en over de veel-deeltjes faseruimte uitgevoerd.

De voor de berekening benodigde rekentechnieken worden afgeleid in hoofdstuk 3. De Weyl-van der Waerden-spinoren die we daar introduceren vervangen niet alleen de traditionele Dirac-spinoren maar zijn ook zeer geschikt om de polarisatievectoren van bosonen te representeren. Dit op gelijke voet behandelen van fermionen en bosonen

maakt het mogelijk de aanwezige ijkvrijheid in de polarisatievectoren van bijvoorbeeld gluonen optimaal te gebruiken. Tevens verlost het ons van het uitwerken van sporen van  $\gamma$ -matrices, een vervelende complicatie van de standaard Feynman-diagramtechniek. In een aantal voorbeelden demonstreren we de kracht van het Weyl-van der Waerden spinorformalisme en laten we zien dat ook buiten QCD het formalisme bruikbaar is.

In de hoofdstukken 4 tot en met 7 volgt de berekening van partonprocessen waarin ten hoogste 6 quarks, maar een willekeurig aantal gluonen aanwezig zijn. Door de kleurstructuren in de QCD Feynman-regels te herschrijven in termen van Chan-Paton kleurbasis structuren vereenvoudigt de berekening van de matrixelementen op twee punten. Ten eerste behoort bij elke structuur in de kleurbasis een ijkinvariante subamplitude waar slechts een klein deel van de Feynman-diagrammen toe bijdraagt. En ten tweede is het mogelijk voor deze subamplitudes recursierelaties in het aantal gluonen te formuleren, uitgaande van een bepaalde quarkconfiguratie zonder externe gluonen. Door de partonprocessen te beschouwen met alle deeltjes uitgaand zijn we in staat verschillende fysische partonprocessen met behulp van hetzelfde algoritme uit te rekenen. Dit is belangrijk met het oog op het snel groeiende aantal partonprocessen als er meer partonen bij de botsing geproduceerd worden. De resultaten van hoofdstukken 4 tot en met 7 zijn voldoende om voorspellingen te kunnen doen voor  $m$ -parton productie ( $2 \leq m \leq 5$ ).

Gezien de benodigde computer rekentijd voor de  $m=4$  en  $m=5$  gevallen is het noodzakelijk benaderingen te hebben voor deze multi-partonprocessen. In hoofdstuk 8 beschrijven we er een aantal en vergelijken we ze in detail met de exacte berekeningen. Het blijkt dat SPHEL, een benadering die gebaseerd is op de berekening van een aantal speciale heliceitsamplitudes, voor praktische doeleinden de exacte matrixelementen goed kan vervangen. Dit geldt zeker zolang de experimentele fouten niet onder de 20% komen.

In hoofdstuk 9 bepalen we het aantal Feynman-diagrammen voor theorieën waarin slechts één soort deeltjes voorkomt. De zelfinteractie vindt plaats tussen ten hoogste  $m$  van deze deeltjes. Het blijkt dat, als het aantal externe deeltjes  $n$  groot is, het aantal Feynman-diagrammen zonder lussen groeit als  $(c_m n)^{n-2}$  ( $c_m < 1$ ). Een interessant resultaat gezien het analytisch bekende groeigedrag van het aantal boomdiagrammen met  $n$  knooppunten:  $n^{n-2}$ .

In hoofdstuk 10 geven we de analytisch bekende resultaten voor alle laagste orde processen in QCD met ten hoogste 7 externe deeltjes. De nadruk ligt op het numeriek gebruik ervan en in die context worden veel details vermeld.

De experimentele analyse van multi-jetproductie gaat gepaard met grote moeilijkheden en er is nog maar weinig aan gewerkt. In de hoofdstukken 1 en 8 doen we verslag van een vergelijking van voorspellingen voor vier-partonproductie met de experimentele resultaten van de UA2 groep op CERN. De overeenstemming is zeer goed wat de vorm van distributies betreft. Gezien de nog aanwezige moeilijkheden op zowel theoretisch als experimenteel gebied zal een kwantitatieve analyse nog wel even op zich laten wachten. Hierbij denken we met name aan de nog te bouwen Large Hadron Collider in Zwitserland en de Superconducting Super Collider in Amerika. Waarschijnlijk kan dan ook een begin gemaakt worden met de analyse van vijf en zes partonproductie waarvoor thans de experimentele statistiek onvoldoende is.

## Curriculum vitae

Na het behalen van het V.W.O diploma aan het Chr. Lyceum te Alphen a/d Rijn in 1980, begon ik aan de studie natuurkunde aan de rijksuniversiteit te Leiden. Het kandidaats examen natuurkunde met bijvakken wiskunde en sterrenkunde werd afgelegd in oktober 1983. In december 1986 volgde het doctoraal examen in de theoretische natuurkunde met bijvak wiskunde. Tijdens de doctoraal-fase heb ik een experimentele stage gelopen in de groep Quantumvloeistoffen o.l.v. prof. dr. R. de Bruyn Ouboter. Het afstudeeronderzoek met als onderwerp "Processen in Quantum Gravitatie", stond o.l.v. prof. dr. F.A. Berends. Sinds januari 1986 heb ik met name onderzoek gedaan aan verstrooiingsprocessen binnen het kader van de Quantum Chromo Dynamica. Tijdens deze periode heb ik de vakgroep theoretische natuurkunde vertegenwoordigd in de computercommissie van de afdeling en gaf ik werkcolleges bij het college Veldentheorie en Padintegralen van dr. W. L. van Neerven.

## List of publications

1. Electroweak radiative corrections to  $e^+e^- \rightarrow W^+W^-$ ,  
M. Böhm, A. Denner, T. Sack, W. Beenakker, F. Berends and H. Kuijf,  
Nucl. Phys. B304 (1988) 463.
2. Multigluon cross sections and five jet production at hadron colliders.  
R. Kleiss and H. Kuijf, Nucl. Phys. B312 (1989) 616.
3. QCD corrections to heavy-quark production in  $p\bar{p}$  collisions.  
W. Beenakker, H. Kuijf, W. van Neerven and J. Smith,  
Phys. Rev. D40 (1989) 54.
4. On relations between multigluon and multigraviton scattering.  
F. Berends, W. Giele and H. Kuijf, Phys. Lett. 211B (1988) 91.
5. Exact expressions for processes involving a vectorboson and up to 5 partons.  
F. Berends, W. Giele and H. Kuijf, Nucl. Phys. B321 (1989) 39.
6. Exact and approximate expressions for multigluon scattering.  
F. Berends, W. Giele and H. Kuijf, Nucl. Phys. B333 (1990) 120.
7. Jet production in  $W$  and  $Z$  events at  $p\bar{p}$  colliders.  
F. Berends, W. Giele, R. Kleiss, H. Kuijf and J. Stirling,  
Phys. Lett. 224B (1989) 237.
8. On six jet production at hadron-hadron colliders.  
F. Berends, W. Giele and H. Kuijf, Phys. Lett. 232B (1989) 266.
9. Jets at the LHC.  
F. Berends and H. Kuijf, to be published in Nucl. Phys. B.
10. Four and six quarks in multiparton processes.  
F. Berends, H. Kuijf and B. Tausk, Submitted to Nucl. Phys. B.
11. Enumeration of externally labelled trees.  
M. Brummelhuis and H. Kuijf, to be published in Journal of Physics, A.
12. On the production of a  $W$  and jets at hadron colliders.  
F. Berends, W. Giele, H. Kuijf and B. Tausk, to be published in Nucl. Phys. B.

## STELLINGEN

1. Met behulp van Weyl-van der Waerden spinoren is het eenvoudig om helicitetsvectoren voor massieve spin-1 deeltjes te construeren.

*Hoofdstuk 3 van dit proefschrift.*

2. De bewering dat men door de berekening van hogere orde QCD-correcties een betere keuze kan maken voor de renormalisatieschaal  $\mu$ , is behalve misleidend ook nog onjuist.
3. Om door middel van metingen aan het proces  $e^+e^- \rightarrow W^+W^-$  bij LEP 200 de betrouwbaarheid van het Standaard Model te kunnen toetsen, is het noodzakelijk de waarden voor de massa en de breedte van de vectorbosonen zeer nauwkeurig te kennen. Dit geldt in het bijzonder als men de vorm van de niet-abelse interacties wil controleren aan de hand van dit proces.

*Böhm et al., Nucl. Phys. B304 (1988) 463.*

4. Verstrooiingsprocessen waarbij een leptonisch vervallend  $W$ -boson in combinatie met vier jets geproduceerd wordt, zijn ondanks de geringe experimentele nauwkeurigheid van groot belang voor het vinden van het top quark in hadron-hadron botsingsexperimenten.
5. Voor de berekening van tweede orde begintoestand QED correcties in de 'leading log' benadering op de totale werkzame doorsnede voor Bhabha-verstrooiing onder kleine hoeken, kan men niet volstaan met het slechts bepalen van die correcties die verkregen kunnen worden met behulp van een zgn. fluxfunctie aanpak.
6. Voor de effectieve connectiviteits constante  $\mu_M$ , behorend bij een wandeling op het vierkante rooster, waarbij  $M$  het aantal stappen aangeeft waarna de wandeling weer over een reeds gepasseerd punt mag gaan, vindt men de volgende waarden:

$$\mu_2 = 3$$

$$\mu_4 = 2.831177207208337 \dots$$

$$\mu_6 = 2.775591142350911 \dots$$

$$\mu_8 = 2.744458210180004 \dots$$

$$\mu_{10} = 2.724799017563782 \dots$$

$$\mu_{12} = 2.711252338667630 \dots$$

$$\mu_{14} = 2.701374267979759 \dots$$

Gezien de schatting  $\mu_\infty \equiv \mu = 2.63815 \dots$  voor een SAW op het vierkante rooster is het praktisch onmogelijk op deze manier  $\mu$  nauwkeurig te bepalen.

7. Voor de berekening van speciale heliceitsamplitudes in graviton-graviton verstrooiingsprocessen is het mogelijk recursierelaties in het aantal gravitonen op te stellen en op te lossen. Het is echter niet mogelijk voor het algemene geval recursierelaties te formuleren.

8. De eerste orde correctie van meer dan 100% in het verstrooiingsproces  $gg \rightarrow Q\bar{Q}$  (zware quarkproductie d.m.v. gluon-fusie), betekent niet dat de storingstheoretische benadering faalt voor de berekening van dit proces.

*Beenakker et al., Phys Rev. D39 (1989) 54.*

9. Gegeven  $n$  impulsen  $K_i^\mu, i = 1, \dots, n$  met  $K_1^2 = K_n^2 = 0$ . De stroom

$$L^\mu(1, \dots, n) = \sum_{m=1}^{n-1} \left\{ \left( \sum_{i=1}^m K_i^\mu - \sum_{i=m+1}^n K_i^\mu \right) \prod_{i=2}^m \kappa^2(i, n) \prod_{i=m+1}^{n-1} \kappa^2(1, i) \right\}$$

is behouden, dat wil zeggen

$$L^\mu(1, \dots, n) \kappa_\mu(1, n) = 0.$$

Hierbij is de volgende definitie gebruikt:

$$\kappa^\mu(i, j) = \sum_{m=i}^j K_m^\mu.$$

10. De bewering dat het meenemen van de interferenties tussen Drell-Yan en QCD processen het verschil tussen de voorspelling gebaseerd op Drell-Yan alleen en het experimentele resultaat voor het twee-jet invariante massa spectrum verklaart, is onjuist.

*Bauer, Glover en Martin, CERN-TH 5523/89*

11. Door het sterk gepiekte gedrag van de multi-parton matrixelementen is de "hit or miss" Monte Carlo techniek om de veel-deeltjes faseruimte integralen uit te voeren in de praktijk onbruikbaar.

12. Kasparov is de laatste echte schaakwereldkampioen.

BIBLIOTHEEK  
 INSTITUUT-LORENTZ  
 voor theoretische natuurkunde  
 Postbus 9506 - 3300 RA Leiden  
 Nederland

J.G.M. Kuijf, Leiden, 20 februari 1991.